Strategic Exploitation of NDV-Plasmodium Interaction Axis to Develop Novel Anti-malarials

A Thesis Submitted in Partial Fulfillment of the Requirements for the Degree

of

Doctor of Philosophy

by

Siddharth Neog

186106017

Department of Biosciences and Bioengineering

Indian Institute of Technology Guwahati

Guwahati, Assam, 781039, India

Indian Institute of Technology Guwahati

Department of Biosciences and Bioengineering

Declaration

I, **Siddharth Neog**, declare that the thesis entitled **"Strategic Exploitation of NDV-Plasmodium Interaction Axis to Develop Novel Anti-malarials",** culminating my research efforts regarding of malaria and NDV co-infection represents an original inquiry into understanding the impact of NDV on the malaria parasite. Throughout this research endeavor, I have adhered to the highest standards of academic integrity and ethics. All sources of information, including data, ideas, and concepts, have been duly acknowledged and referenced, following the guidelines provided by my institution. I have not plagiarized or misrepresented the work of others in any form. I affirm that this thesis is the result of my original research work conducted under the guidance of my mentor, Prof. Vishal Trivedi, and in compliance with the regulations of my academic institution, the **Department of Biosciences and Bioengineering, Indian Institute of Technology Guwahati.** I declare that this work has not been submitted for any other degree or examination at any other university or institution.

April 5, 2025

Siddharth Neog

(186106017)

Indian Institute of Technology Guwahati

Department of Biosciences and Bioengineering

Certificate

This is to certify that the thesis entitled **"Strategic Exploitation of NDV-Plasmodium Interaction Axis to Develop Novel Anti-malarials"**, submitted by Siddharth Neog, bearing registration number **186106017**, has been prepared under my supervision and is a record of the original research work carried out by the student. This thesis fulfills the requirements for the Doctor of Philosophy degree at the **Indian Institute of Technology Guwahati.** The findings presented in this thesis are original and contribute to the existing knowledge in the explored area of research. To the best of my knowledge, I certify that this thesis represents original work and has not been submitted for any degree or examination at any other institute or university. The research follows the ethical standards outlined by the Indian Institute of Technology and relevant regulatory bodies. Additionally, we emphasize that the thesis has meticulously acknowledged all research materials obtained from external sources. Moreover, we have diligently cited and attributed any textual content, illustrations, tables, figures, and other elements borrowed from external sources to the best of our knowledge and following scholarly conventions.

April 5, 2025,

Prof. Vishal Trivedi

(Supervisor)

Acknowledgements

Throughout this journey, I have been shaped, guided, and revitalized by the invaluable ideas, critiques, and suggestions from many individuals who have helped me reach this point. While words may fall short in conveying my sincere gratitude, I will attempt to express my appreciation as best I can.

First and foremost, I would like to extend my deepest gratitude to my thesis supervisor, Prof. Vishal Trivedi, for his unwavering guidance, academic support, and the freedom he provided in my research. The training I received in his lab has been invaluable and will undoubtedly aid in my growth as a researcher.

I am also profoundly thankful to the current head of my department, Prof. Rakhi Chaturvedi, and the former heads, Prof. Kannan Pakshirajan and Prof. Latha Rangan, for their support. Additionally, I owe my thanks to my esteemed Doctoral Committee members, Prof. Nitin Chaudhary, Prof. Sachin Kumar, and Prof. Tharmalingam Punniyamurthy, whose guidance and inspiration have been instrumental in my academic journey.

Special thanks are due to all the past and current members of Prof. Trivedi's Lab, including Dr. Sooram Banesh, Dr. Anil Kumar, Dr. Rafi Uz Zama Khan, Mr. Alok Kumar Pandey, Mr. Rajendra Prasad, Mr. Shirish Bhagwan Kathane, Ms. Eena Dodwani, Mr. Pitam Chakrabarty, Mr. Rakesh, Late Ms. Sikha, Mr. Umesh, Mr. Sai, Mr. Shyamji, Ms. Neha, Mr. Sandeep, Mr. Divyanshu, and Ms. Arunima. Their support and companionship have made my Ph.D. journey not only manageable but also memorable. The emotional bonds we forged during this time will stay with me always. I also extend my gratitude to all past and current members of Prof. Sachin Kumar's Lab and Prof. Baskaran Anand for their invaluable support and contributions. I am grateful to my friends—Nikhil, Sahil, Rushikesh, Arman, Alok, Sonia, Seema, and Krishnakant—for the unbreakable bond we share. Despite the distances, they have always ensured that we remain connected, providing much-needed support in times of need.

I owe a debt of gratitude to my lifeline at IITG, whom I consider a family away from home: Nikhil, Rafi Uz Zama Khan, Sonia Ningthoujam, Sahil Dhull, Arman Mohanty, Alok Pandey, Suraj Kumar Panda, Ajit Kumar, Ankush Sontakke, Seema Lokhandwala, Pavan Dev, and Sandeep Reddy. The memories we have created together—during meals, tea breaks, parties, night walks, trips, and endless conversations—are treasures I will carry with me forever.

My heartfelt thanks extend to my dear childhood friends Irshad, Bikash, Pallav, Pranab, Kundan, Nandan, Debabrata, Jyotipom, Amar, Hassan, and Khiroj, whose unwavering support and friendship have been a pillar of strength throughout this journey.

Lastly, I thank the Almighty and my parents and my brother and sisters for unwavering support.

I am also grateful to the Department of Biosciences and Bioengineering and the Central Instrument Facility (CIF) for providing the essential analytical instruments crucial to my research. I am thankful to my institute, the Indian Institute of Technology, Guwahati, for offering me the opportunity to conduct my research and for providing a fellowship during my Ph.D. tenure.

This acknowledgment is a small effort to express my heartfelt thanks to everyone who has been part of this journey, whether directly or indirectly. Thank you all for being with me.

Table of Contents

Chapter VI: Conclusions and Future directions

List of Figures

List of Tables

Abbreviations

AF - Allantoic Fluid

AMA1 - Apical Membrane Antigen 1

BHK-21 - Baby Hamster Kidney 21 Cells

BSA - Bovine Serum Albumin

CD - Circular Dichroism

CM - Cerebral Malaria

CQ - Chloroquine

CR1 - Complement Receptor 1

CsCl - Cesium Chloride

CyRPA - Cysteine-Rich Protective Antigen

DAPI - 4',6-Diamidino-2-Phenylindole

DEV - Duck Enteritis Virus

DLS - Dynamic Light Scattering

DMEM - Dulbecco's Modified Eagle's Medium

EBAs - Erythrocyte-Binding Antigens

F - Fusion Protein

FBS - Fetal Bovine Serum

G6PD - Glucose-6-Phosphate Dehydrogenase

GFP - Green Fluorescent Protein

GPC - Glycophorin C

GPB - Glycophorin B

GRO - Groningen Machine for Chemical Simulations

HA - Hemagglutinin

HAd - Hemadsorption

PfEMP1 - *Plasmodium falciparum* Erythrocytic Membrane Protein 1

MOI - Multiplicity of Infection

MSP1 - Merozoite Surface Protein 1

NDV - Newcastle Disease Virus

PfRh5 - *Plasmodium falciparum* Reticulocyte Binding Protein Homologue 5

PfRhs - *Plasmodium falciparum* Reticulocyte-binding Protein Homologs

PI - Propidium Iodide

PCR - Polymerase Chain Reaction

PFA - Paraformaldehyde

PEG - Polyethylene Glycol

pI - Isoelectric Point

PR8 - Influenza A Virus (strain PR8)

PRBC - Parasite-Infected Red Blood Cell

PRBCs - Parasite-Infected Red Blood Cells

qPCR - Quantitative Polymerase Chain Reaction

RBC - Red Blood Cell

RNA - Ribonucleic Acid

RNP - Ribonucleoprotein

ROS - Reactive Oxygen Species

SDM - Site Directed Mutagenesis

SEM - Scanning Electron Microscopy

SDF - Structure Data File

HBV - Hepatitis B Virus

HCV - Hepatitis C Virus

HN - Hemagglutinin-Neuraminidase

HIA - Hemagglutination Inhibition Assay

IC50 - Half-Maximal Inhibitory Concentration

ITC - Isothermal Titration Calorimetry

JEV - Japanese Encephalitis Virus

MAPK - Mitogen-Activated Protein Kinase

MD - Molecular Dynamics

PfCDPK5 - *Plasmodium falciparum* Calcium-Dependent Protein Kinase 5

SLNs - Solid Lipid Nanoparticles

SPR - Surface Plasmon Resonance

SPF - Specific Pathogen-Free

TBST - Tris-Buffered Saline with Tween

TCA - Trichloroacetic Acid

TEM - Transmission Electron Microscopy

TNF-α - Tumor Necrosis Factor Alpha

VLPs - Virus-Like Particles

Units

Å	Angstrom	**nm**	Nanometer
°C	Degree Celsius	**kcal/mole**	Kilocalorie per mole
%	Percent	**kJ/mole**	Kilojoule per mole
µM	Micro molar	**mg**	Milligram
µW	Microwatt	**kV**	Kilovolt
µg/ml	Microgram per millilitre	**mm**	millimeter
µmole/min	Micromoles per minute	**U/L**	Units per Liter
µl	Micro Liter	**g**	Gram
µg	Micro gram	**mdeg**	Millidegrees
mM	Mill molar	**ml**	Milliliter
mg/ml	Milligram per millilitre	**ps**	Picosecond
		nM	Nano molar
ns	Nanosecond	**cm^{-1}**	Centimetre inverse

Chapter I

Biology of the human malaria parasite, emerging treatment regimens and interaction with other organisms

Summary

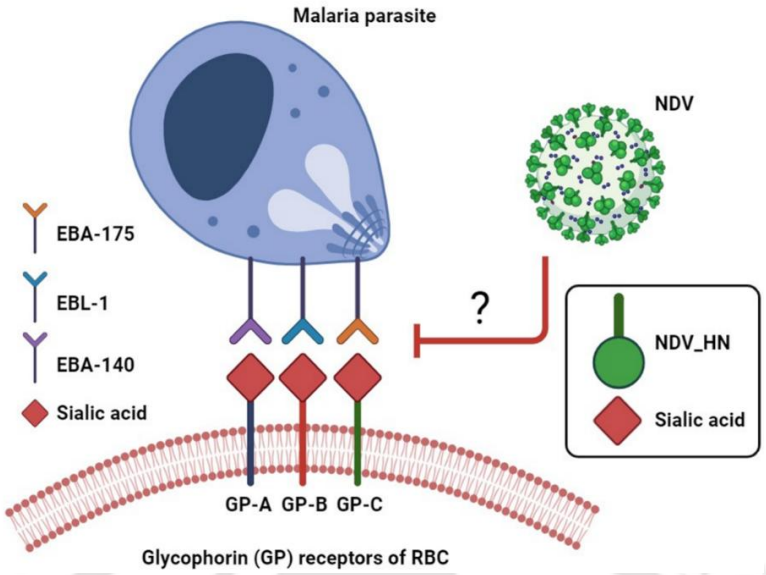

Malaria is a severe protozoan infection that affects around 200 million people annually, with *Plasmodium falciparum* being the major driver of malaria-related mortality. Treatment of the disease mainly relies on antimalarial drugs that target the blood stages of the parasite. However, drug-induced toxicity and the development of resistance pose significant challenges. Independent cases of multi-drug resistance to Artemisinin Combination Therapies (ACTs) have emerged globally, driven by prolonged parasite clearance times, allowing resistant strains to emerge. This underscores the need for novel antimalarial agents and targeted drug delivery approaches. The erythrocytic cycle of the parasite is a key target for both novel therapies and targeted delivery. The ability of the malaria parasite to propagate in blood depends on its interaction with uninfected red blood cells (RBCs). The merozoite, an invasive form of the parasite, must adhere to and invade uninfected RBCs for erythrocytic schizogony. This process involves recognition of sialic acid-rich receptors on the RBC surface, including Glycophorin A, B, C, D, and Band 3, through various parasite antigens like the Erythrocyte-Binding Antigens (EBAs) and rhoptry proteins. Blocking these receptors with specific antibodies and anti-malarial peptides has been shown to disrupt the erythrocytic cycle across multiple parasite strains. The Newcastle Disease Virus (NDV) also targets sialic acid-rich receptors on host cells through its Hemagglutinin Neuraminidase (HN) spike protein. Similar to the malaria parasite, this interaction is vital for viral entry and infection. The affinity of NDV for avian erythrocytes suggests potential implications in co-infection scenarios, where the possible engagement with the RBCs and malaria parasitized RBCs (PRBCs) could be the key to offering a novel therapeutic strategy against human malaria.

1. Introduction

1.1 A Brief History of Malaria

The etymology of "malaria," derived from the Italian phrase mala-aria or "bad air," reflects historical misconceptions about its transmission, tracing back to the mid-18th century [1]. References to malaria-like symptoms could be found in ancient Chinese, Indian, and Greek texts as early as the third millennium before the common era (BCE) [2]. However, the first reliable description of malaria is often attributed to the Roman physician Celsus in the first-century common era (CE) [3]. The true nature of malaria transmission remained elusive until the late nineteenth century when new discoveries fundamentally altered our understanding of the disease. The first major breakthrough came in 1880, when Charles Louis Alphonse Laveran, a French army surgeon stationed in Algeria, observed parasites in the blood of a malaria patient [4, 5]. Laveran identified these parasites as the causative agents of malaria, marking the first time where a microorganism was linked to a specific disease in humans. This discovery was crucial, as it shifted the focus from environmental theories, such as the "miasma" theory, which attributed malaria to bad air or toxic vapours, to a more precise understanding of infectious agents [6, 7].

Building on Laveran's work, British medical officer Ronald Ross made a significant contribution in the 1890s by identifying the mosquito as the vector responsible for transmitting the malaria parasite [8]. While stationed in India, he conducted experiments on the malaria parasite's life cycle and, in 1897, successfully demonstrated that the parasite could be transmitted from infected birds to mosquitoes and then back to healthy birds. This confirmed the role of mosquitoes in the transmission cycle of malaria. The crucial discovery made by Ross was particularly important because it provided conclusive evidence that malaria was spread through the bite of Anopheles mosquitoes rather than through direct human contact or environmental factors.

Today, we know that the most complicated form of human malaria is caused by *Plasmodium falciparum*, which diverged from *P. reichenowi*, a parasite infecting chimpanzees, approximately five to ten million years ago [2]. This divergence is correlated with the evolutionary split between humans and chimpanzees, which further highlights the deep evolutionary roots of the disease [9]. Genetic anthropological studies have revealed that the most recent common ancestor of *P. falciparum* likely existed in tropical Africa around 100,000 years ago. In contrast, other *Plasmodium* species, including *P. vivax*, *P. ovale*, and *P. malariae*,

are believed to have been transmitted from non-human primates to humans through lateral transfer, at the later stages of human evolution (**Figure 1.1**) [10]. This long history of the association between the malaria parasite and the human host proves that the impact of malaria on human populations has been profound, exerting one of the strongest selective pressures on the human genome.

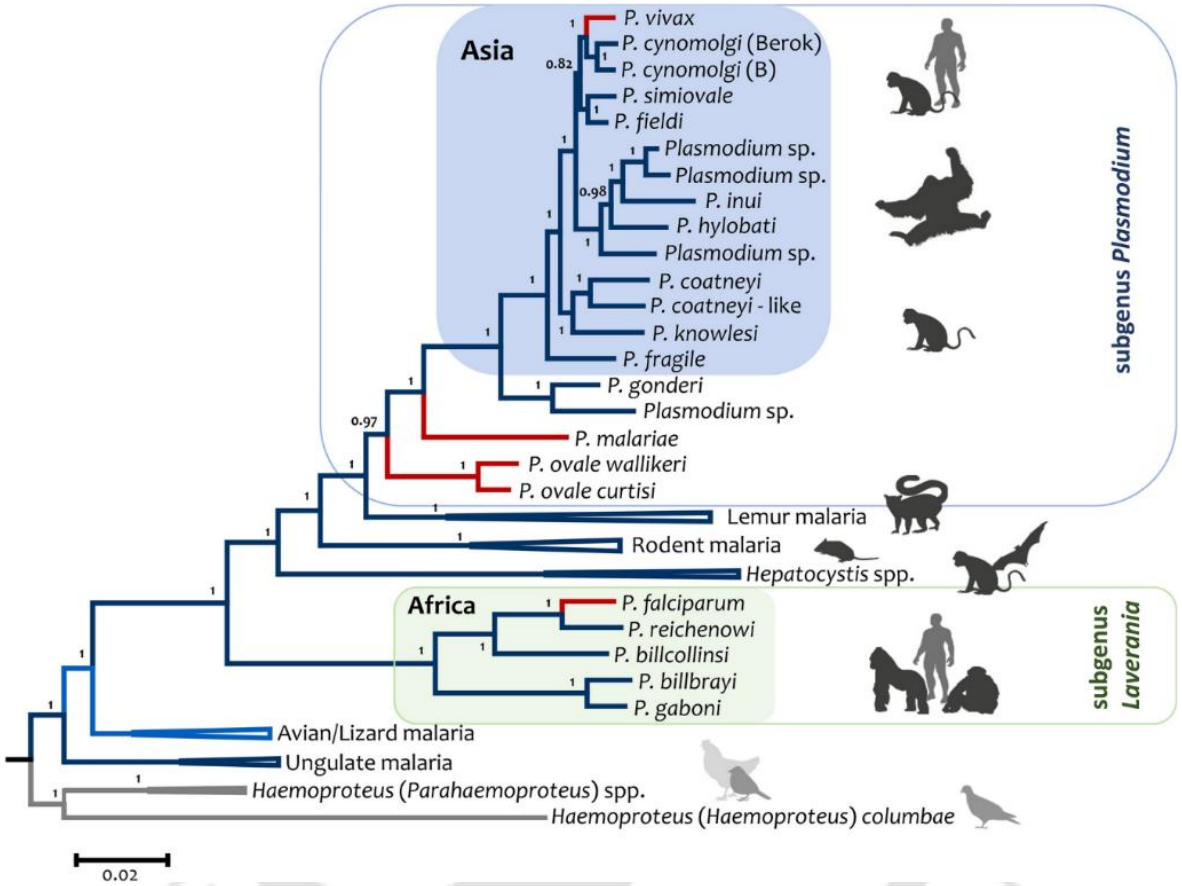

Figure 1.1: Phylogenetic tree of *Plasmodium* spp. based on complete mitochondrial genomes. The analysis of the phylogenetic tree shows distinct origins of the two most important human malaria parasites, *P. falciparum* and *P. vivax*. (Source: Escalante et al. [10])

It is supported by the overwhelming prevalence of genetic adaptations in humans such as sickle-cell trait, thalassemia, and glucose-6-phosphate dehydrogenase deficiency, which although provides some resistance to malaria, cause significant health burdens as well [11-13]. Thus, the malaria parasite is one of the few pathogens that have shown the potential to alter genetic composition of a species through eons of evolutionary arms race.

1.2 The Global Burden of Malaria

In modern times, malaria still remains a significant public health challenge, particularly in tropical and sub-tropical regions where the disease is the most prevalent [14]. The ability of

these parasite to infect and cause disease in humans is linked to the presence of an apical complex, which is a specialized structure that facilitates the entry of the parasite into host cells. They are hence classified under the phylum Apicomplexa which defines this special feature of apicomplexan parasites [15, 16]. Among the five *Plasmodium* species that infect humans, *Plasmodium falciparum* is responsible for the majority of malaria-related morbidity and mortality worldwide [17]. Other species, including *P. vivax*, *P. ovale*, *P. malariae*, and *P. knowlesi*, also contribute to the global burden but typically cause less severe disease and thus leads to lesser number of deaths compared to *P. falciparum* infection [18, 19].

According to the World Health Organization (WHO) report of 2023, an estimated 249 million new cases and approximately 0.4 million deaths were reported in 2022 alone [17]. Children, who are aged less than 5 years were the most vulnerable group affected by malaria and accounted for 67% (272 000) of all malaria deaths worldwide. Nineteen countries in sub-Saharan Africa and India carried almost 85% of the global malaria burden. In Africa, *P. falciparum* alone accounted for 99.7% of the estimated malaria cases (**Figure 1.2**).

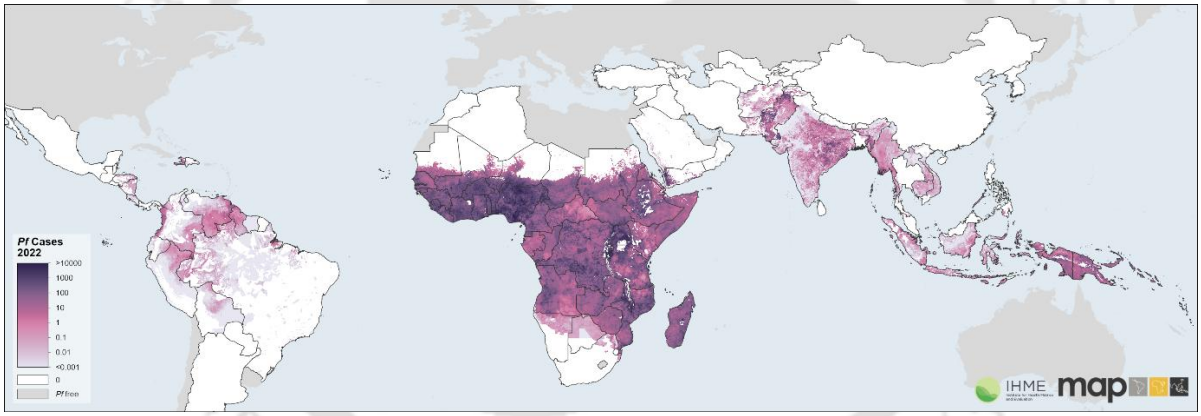

Figure 1.2: Geographical distribution of cases related to *P. falciparum* infection. Areas in a dark hue of purple show a high prevalence of *P. falciparum* infection. The map presents *Plasmodium falciparum-related* cases for all age groups. (Source: Malaria Atlas Project)

Despite substantial efforts and significant progress towards the treatment and control of *P. falciparum* infection, it continues to exert a heavy toll, particularly in developing countries, where it is responsible for over 90% of malaria-related deaths [17]. As of 2022, malaria had claimed about 4,05,000 lives. Sub-Saharan Africa is disproportionately affected, accounting for the vast majority of these fatalities, largely due to the widespread presence of *Plasmodium falciparum*, the deadliest malaria parasite, and highly efficient *Anopheles* mosquito vectors, such as *Anopheles gambiae* (**Figure 1.3**) [20, 21].

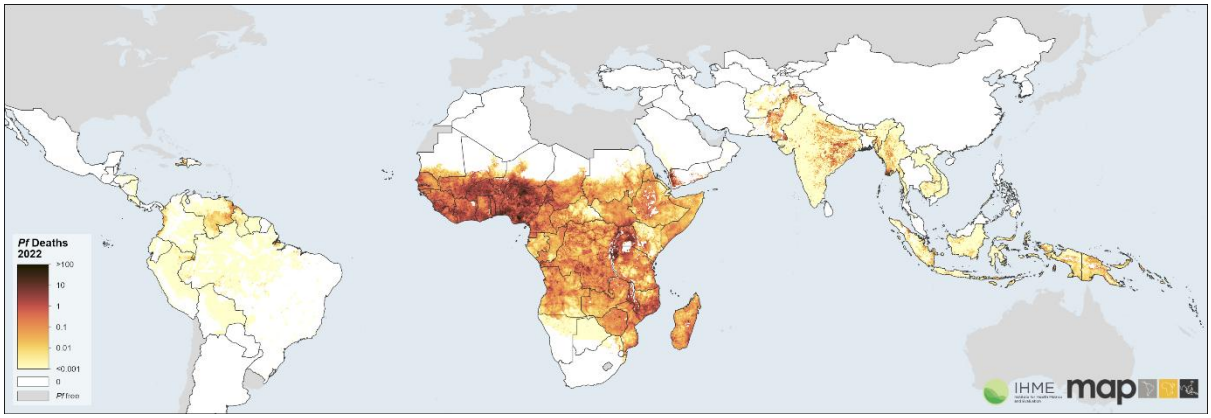

Figure 1.3: *Plasmodium falciparum-related* deaths. Areas in a dark hue of orange show high numbers of mortality due to *P. falciparum* infection. The map presents *Plasmodium falciparum*-related deaths for all age groups (Source: Malaria Atlas Project)

Malaria, as an infectious disease, is also highly influenced by geographical factors. The incidence of the disease is particularly prevalent in regions with environmental conditions that favour the breeding and survival of Anopheles mosquitoes. These regions, which include large parts of Sub-Saharan Africa, Southeast Asia, and parts of Latin America, often coincide with some of the poorest areas of the world [22]. This correlation between malaria incidence and economic development has been well-documented, with numerous studies highlighting how the burden of malaria can negatively impact economic growth and, conversely, how poverty can lead to an increase in malaria transmission [23-26]. For instance, a study in 2018 estimated that the African continent incurs direct economic losses of approximately USD 12 billion annually due to malaria [27]. These losses are attributed to various factors, including healthcare costs, loss of productivity, and the impact of the disease on education and workforce participation. Furthermore, the economic burden of malaria extends beyond its direct costs, as it also hampers long-term economic growth by affecting human capital. Malaria, particularly in its severe forms, such as cerebral malaria (CM) and severe malarial anaemia (SMA), induces long-lasting effects on neurodevelopment, especially in children. Studies have shown that African children who survive these severe forms of malaria often suffer from long-term cognitive impairments and neurodevelopmental deficits [28, 29]. These impairments can lead to learning difficulties, reduced academic achievement, and diminished earning potential in adulthood, creating a cycle of poverty and disease that is difficult to break.

1.3 Plasmodium is a genus of intracellular obligate unicellular parasites

Malaria parasites are obligate unicellular eukaryotic parasites of the genus *Plasmodium*. There are over 200 species of *Plasmodium* that infect a wide range of animal hosts [30]. Four species

of *Plasmodium* are traditionally recognized to be responsible for human malaria: *Plasmodium falciparum*, *P.malariae*, *P.ovale* and *P.vivax*. However, humans can also be infected with various simian species as well, such as *P. cynomolgi*, *P. brasilianum*, *P. schwetzi*, *P. inui*, *P. knowlesi* and *P. simioval* [19, 30, 31]. Despite the overwhelming diversity at the species level, the malaria parasites universally require two hosts for the successful completion of their life cycle, and hence its life cycle is digenetic.

The malaria parasite exhibits a complex life cycle that involves two evolutionarily distinct hosts: the female *Anopheles* mosquito, which acts as a vector, and the vertebrate host, humans [32, 33]. The parasite employs unique defence mechanisms against the host immune system and has acquired great genetic and proteomic diversity during the epochs of the evolutionary arms race [34]. These molecular diversities also translate into the diversity in their cellular structure and physical capabilities. Multiple stages of malaria parasites can be seen during its life cycle adapted for infecting specific organs such as the liver and also asexual expansion in human RBCs through the erythrocytic schizogony. Interestingly, the motility of the malaria parasite through the skin is reported to be ten times faster than the immune cells, that counter such pathogens [35]. They also employ camouflage strategies and modulation of host immune response, metabolism and behaviour for their survival and transmission [36]. Thus, a complex life cycle coupled with a myriad of defence mechanisms makes the parasite particularly suitable for infecting its host and continuing its life cycle.

1.4 The complex life cycle of the Malaria parasite

The digenetic life cycle of the *Plasmodium spp.* can be divided into an exogenous sexual phase (sporogony) in female Anopheles mosquitoes and an endogenous asexual phase (schizogony) in humans (**Figure 1.4**). In humans, the onset of the asexual phase begins when an infected female Anopheles mosquito, harbouring sporozoites in its salivary glands, takes a blood meal and injects the malaria parasite into the dermis of the skin. New evidence suggests that the sporozoites, after being injected into the dermis of the skin, may also remain in the tissue for several hours and are slowly released into blood capillaries [37]. The parasite uses a process called gliding motility to find its way to the capillaries with the help of Trap-like proteins, which appear to be essential for its exit from the dermis [35, 37]. The sporozoites go through the bloodstream and then enter the liver. This process is often termed “traversal” in the liver, where the sporozoites finally establish themselves in the parenchymal cells [38]. This tissue phase, or pre-erythrocytic schizogony, leads to the development of tissue schizonts. These

schizonts contain thousands of merozoites. In *P. falciparum*, this number can be as high as 30,000, while in *P. vivax* and, *P. ovale*, around 10,000 merozoites are formed [33]. The rupture of infected hepatocytes releases thousands of merozoites in parasite-filled vesicles known as merosomes. The merosomes provide a protective barrier and act like camouflage to the host immune system.

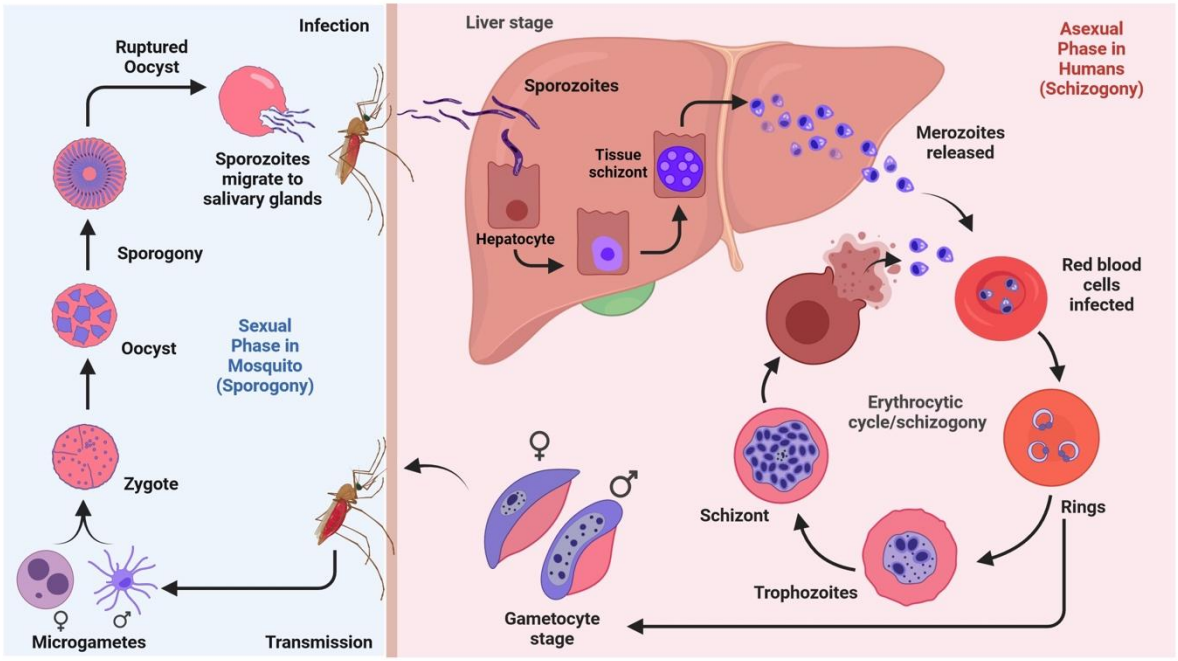

Figure 1.4: The digenetic life cycle of the malaria parasite. The life cycle of the malaria parasite begins when an infected mosquito inoculates sporozoites from its salivary glands into the dermis, during a blood meal (1). Stages 2 to 5 represents the asexual phase (schizogony) in humans. Stages 6 to 7 represents the sexual phase in mosquito (sporogony). (Source: created with BioRender)

The tissue phase ends in this point in the case of *P. falciparum*, while it persists in *P. vivax* and *P. ovale* as hypnozoites. The hypnozoites are the source of malaria relapse in *vivax* and *ovale* malaria. The merozoites released from the liver find their way to the erythrocytes and the process of invasion occurs. While the merozoites are in the bloodstream, prior to RBC entry, the Merozoite Surface Proteins, particularly MSP1, which covers the surface of the merozoites, are responsible for defence against immune activation [36]. The EBLs (Erythrocytic Binding Ligands) and PfRhs (Plasmodium falciparum reticulocyte binding homologs) of the merozoite surface are involved in the binding to the RBC surface through sialic acid-containing surface receptors, particularly the Glycophorins. Initial binding of the merozoites leads to the formation of AMA1-RON complex that marks the reorientation and strong binding phases of invasion. This is followed by activation of the Actino-myosin motor in the apical end of the merozoites where the parasite forces inside the RBC and is an active process. Resealing of the RBC

membrane marks the end of invasion and the formation of parasitophorous vacuole where the parasite undergoes further sequential development from Rings to Trophozoites and ultimately mature blood Schizonts. The parasite must invade new RBCs for the continuation of erythrocytic schizogony [33, 36].

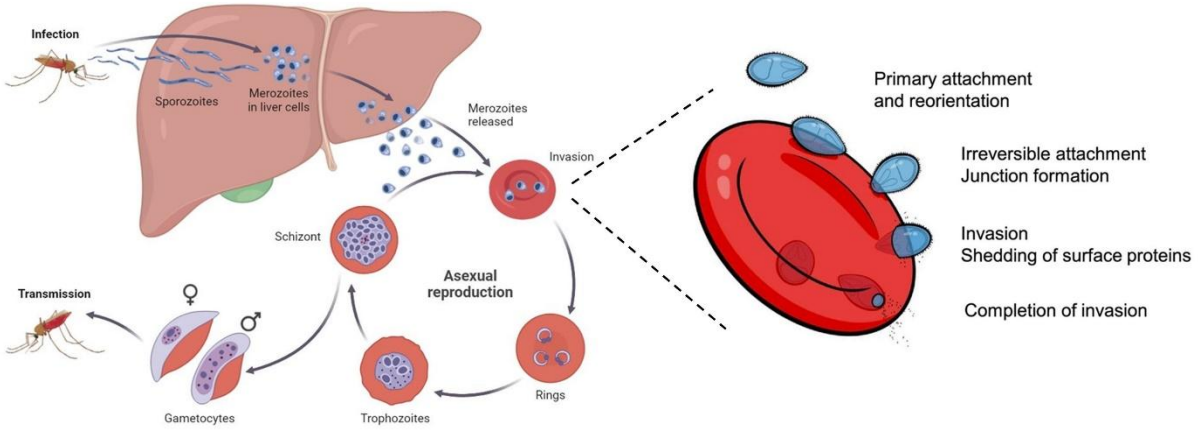

Figure 1.5: Invasion of RBC by merozoites is a multistep process involving specific receptor-ligand interaction. Invasion of merozoite into the uninfected RBC is a multistep process and under tight regulation. (Source: created with BioRender)

During the erythrocytic phase the parasite also remodels the host cell and export hundreds of proteins to the extracellular environment and RBC membrane. One such notable protein is the PfEMP1 (*Plasmodium falciparum* Erythrocytic Membrane Protein-1) which upon display on the RBC membrane surface results in formation of antibodies by the host immune system [39]. This follows to the switch of expression of antigenically distinct isoforms of the protein which results in evasion from immune destruction. Such Antigenic variation or diversifications are processes through which chronic *Plasmodium falciparum* malaria is established [36, 40]. The blood schizonts rupture after being matured and the released merozoites invade new RBCs located in the vicinity and the exponential increase of parasitemia is observed in the individual. The synchronized release of merozoites by rupturing infected RBCs causes the pathogenicity seen in malaria. Some merozoites differentiate into male (microgametocytes) and female (macrogametocytes) which through a blood meal is transferred to the female Anopheles and marks the beginning of the sporogonic phase which ensures the continuation and survival of the malaria parasite [33].

Lethality of *P. falciparum* is multifactorial and some of the basic characteristics that differentiate it from other malarial infection include the following:

(a) The tissue schizonts of *P. falciparum* display almost a three-fold increase numbers of merozoites. Typical *P. falciparum* tissue schizonts contains about 30,000 merozoites as compared to 10,000 in *P. vivax* and *P. ovale* which results in a more aggressive pre-disposition towards the erythrocytic cycle.

(b) Higher average parasitemia level in blood, which is due to its ability to infect RBCs of all ages, is also another factor which leads to elevated severe anaemic condition due to *P. falciparum* malaria.

(c) Induction of host inflammatory responses and cytoadherence due to endothelial activation causes microvascular obstruction. This leads to metabolic acidosis and more importantly local end organ damage mostly in the brain resulting in cerebral malaria.

Comparatively, *P. vivax* malaria show low parasitemia and does not undergo extensive intravascular sequestering due to which complicated malaria cases leading to deaths are fewer as compared to *P. falciparum* infection [41].

1.5 Molecular players involved in invasion of the Merozoite

Historically, it was postulated that the interaction between the merozoite surface protein 1 (MSP1) of *P. falciparum* and specific erythrocyte proteins was indispensable for the successful invasion of red blood cells by the parasite. This assumption was grounded in the critical role MSP1 was believed to play in the invasion process. However, recent studies have challenged this notion, revealing that merozoites which are deficient in surface MSP1 are still capable of invading erythrocytes. This observation suggests that the presence of MSP1 is not an absolute requirement for erythrocyte invasion. In the pre-invasion phase, *P. falciparum* merozoites engage in a complex series of interactions with the host erythrocyte, leading to actomyosin motor-driven deformation of the erythrocyte membrane. This deformation is a crucial step in the invasion process and is mediated predominantly by two families of type-1 membrane proteins, the *P. falciparum* reticulocyte-binding protein homologs (PfRhs) and erythrocyte binding-like proteins (EBLs).

These merozoite surface proteins specifically bind to erythrocyte receptors, such as complement receptor-1 (CR1) and glycophorin A, B, and C, playing a crucial role in both the initial binding and activation of downstream signaling pathways necessary for invasion. Upon egress, merozoites are exposed to the low-potassium ion concentrations present in blood plasma, which leads to a gradual increase in cytosolic calcium levels [42]. This calcium influx triggers the release of erythrocyte binding-like (EBL) family proteins, including EBA-175. The

EBA-175 protein specifically binds to the Glycophorin A receptor on erythrocytes, signaling the release of invasion-related proteins stored in the rhoptry.

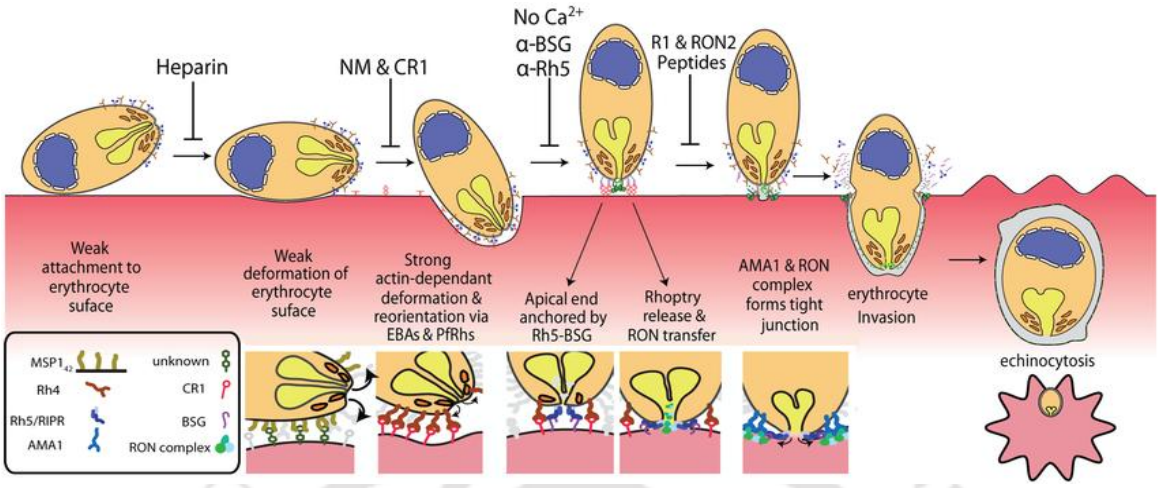

Figure 1.6: Model for the sequence of interactions during P. falciparum invasion of an erythrocyte. The molecular players involved in the different stages of merozoite invasion are described along with their known inhibitors. (Source: Weiss et al. [47])

After the erythrocyte is deformed, the merozoite reorients itself so that its apical end contacts the erythrocyte membrane. In this process, an atypical member of the PfRh family, PfRh5, plays a critical role by forming a complex with CyRPA (cysteine-rich protective antigen) and PfRipr (Rh5-interacting protein) [43]. The binding of PfRh5 to the host receptor basigin is a pivotal event in merozoite invasion, which is closely associated with the influx of Ca^{2+} into the host cell [44, 45]. Additionally, the formation of a tight junction between the erythrocyte and parasite-derived proteins, particularly involving the AMA1 and RON complexes, leads to the irreversible attachment of the erythrocyte and the merozoite. This process involves the deposition of the RON complex in the erythrocyte membrane, where RON2 spans the membrane and binds to AMA1 on the merozoite surface [46]. Once this attachment is secured, the merozoite is propelled into the erythrocyte using force generated by the actomyosin motor of the parasite. During this phase, the parasitophorous vacuole membrane is also formed from the lipid-rich contents of the rhoptries [47].

Once the active invasion phase concludes, the membranes at the posterior end of the merozoite fuse, encasing the parasite within both the parasitophorous vacuole and the erythrocyte. This process triggers echinocytosis, causing the red blood cell to shrink and develop spiky protrusions. Following the successful establishment of infection, the parasite begins to replicate, while going through distinct developmental phases, the Ring, Trophozoite

and Schizont. Schizonts harbour merozoites and upon maturation releases 16-32 merozoites into the bloodstream. These newly released merozoites quickly invade fresh host cells, continuing the cycle of infection. This cyclic process of erythrocytic schizogony requires 48 hours in *Plasmodium falciparum*. Furthermore, the egress of merozoites is also a tightly regulated process involving several protein kinases, including the plant-like calcium-dependent protein kinase PfCDPK5 and the cGMP-dependent protein kinase PfPKG [48]. These kinases play critical roles in controlling the timing of merozoite egress. Additionally, MSP1 is involved in the egress process by facilitating the processing of subtilisin 1 on the merozoite surface, enabling it to bind to the erythrocyte membrane protein spectrin [49]. This cyclical destruction of red blood cells is responsible for the characteristic symptoms of malaria, including fever, chills, anaemia, and splenomegaly, the enlargement of the spleen [50]. The periodic fever patterns termed as tertian or quartan fever corresponds to the synchronous rupture of red blood cells upon the release of the merozoites into the bloodstream [51].

1.6 Antimalarial drugs and development of resistance

The 20th century witnessed the development of a wide array of antimalarial drugs, with Artemisinin and Chloroquine being among the most widely used [52]. These drugs, along with others such as sulfadoxine-pyrimethamine and Artemisinin-based combination therapies (ACTs), remain the cornerstone of current malaria treatment protocols and are regarded as frontline interventions against the disease [53, 54]. However, *Plasmodium falciparum*, the primary causative agent of malaria, has demonstrated a continual ability to develop resistance to these therapeutic agents. Development of resistance against classical and frontline antimalarial drugs poses significant challenges to malaria control and eradication efforts.

1.6.1 Classical anti-malarial drugs used for the treatment of malaria

Classical antimalarial drugs have long played a pivotal role in the treatment of malaria, targeting various stages of the *Plasmodium* life cycle with varying degrees of success. The major classical drugs used for the treatment of malaria are discussed as follows.

(a) Chloroquine is a 4-aminoquinoline, that has historically been the primary treatment for malaria due to its ability to inhibit the heme detoxification process of the parasite. By interfering with the polymerization of heme into hemozoin, chloroquine causes the accumulation of toxic free heme within the parasite, leading to its death. However, the

rise of chloroquine-resistant *Plasmodium falciparum* strains has significantly compromised its effectiveness [55, 56].

(b) Quinine is derived from the bark of the *Cinchona* tree, represents another classical antimalarial with a long history of use. Quinine operates similarly to chloroquine by affecting the heme detoxification process, but it also has a broader spectrum of action [57]. Despite its efficacy, quinine is often associated with adverse effects such as cinchonism, which includes symptoms like tinnitus, headache, and gastrointestinal disturbances. Due to these side effects and the development of resistance, quinine is now primarily reserved for severe cases of malaria and is typically administered intravenously [58-60].

(c) Primaquine which is a quinoline methanol, is utilized specifically for treating the hepatic stages of *Plasmodium vivax* and *Plasmodium ovale*. It targets the hypnozoites, the dormant liver stages responsible for relapses [61]. The ability of this drug to eliminate these dormant forms helps in preventing the recurrence of malaria. However, its use is restricted in individuals with glucose-6-phosphate dehydrogenase (G6PD) deficiency due to the risk of haemolytic anemia, which limits its application in some distinct populations [62, 63].

In response to the challenges caused by drug resistance and the limitations of classical antimalarial treatments, combination therapy has emerged as a crucial strategy in malaria management. Combination therapies aim to enhance therapeutic efficacy of the drugs and mitigate the risk of resistance by using multiple drugs that act through different mechanisms or target different stages of the life cycle of the parasite.

1.6.2 Artemisinin-based Combination Therapies (ACTs)

Artemisinin, extracted from *Artemisia annua*, exhibits rapid and potent activity against malaria parasites. It generates Reactive Oxygen Species (ROS) through the cleavage of its endoperoxide bridge, causing oxidative damage to critical cellular components of the parasite. However, the rapid clearance of parasites by Artemisinin led to the use of a partner drug to provide sustained efficacy and address any residual parasites. Partner drugs such as lumefantrine**,** mefloquine**,** amodiaquine**,** and piperaquine each offer distinct mechanisms of action, complementing artemisinin [53]. For instance, lumefantrine that has a long half-life, is maintained at therapeutic levels in the bloodstream, while mefloquine affects the heme-detoxification process, and piperaquine provides extended antimalarial activity [64]. The use

of ACTs represents a significant advancement in malaria treatment, providing a multifaceted approach that reduces the likelihood of resistance development [65]. By combining artemisinin with other antimalarial drugs, ACTs enhance the overall effectiveness of treatment and ensure comprehensive parasite clearance. The World Health Organization (WHO) endorses ACTs as the first-line treatment for uncomplicated *Plasmodium falciparum* malaria, reflecting their proven efficacy and safety [66].

1.6.3 Emergence of resistance in the malaria parasite

A thorough analysis of the emergence and spread of drug-resistant *P. falciparum* strains reveals that the origins of resistance can be traced back to Myanmar and other hotspots in Southeast Asia [67]. Molecular markers indicative of Artemisinin resistance was detected in P. falciparum populations circulating in regions including Thailand, Myanmar, India, and Bangladesh. These areas reported alarmingly high treatment failure rates with first-line ACTs, with Thailand experiencing a staggering 93% failure rate. Between 2016 and 2018, it was found that 80% of the malaria parasites circulating in north-eastern Thailand and Vietnam were resistant to widely used ACTs [67].

A further complication in the treatment of P. falciparum infections arose with the observed decrease in the sensitivity of parasites to Artemisinin derivatives, particularly in Cambodia. This decreased sensitivity led to an increase in the time required to clear the parasites from patients' bodies, thereby elevating the selective pressure exerted by the drugs and providing greater opportunities for the emergence of new resistant strains [68]. Investigations into the molecular mechanisms underlying Artemisinin resistance identified mutations in the gene encoding the K13 propeller protein as a key factor. These mutations were found to contribute to a multi-genetic defence mechanism within the parasite, which not only resulted in resistance but also prolonged the clearance time of the parasite [69]. Moreover, transcriptional analyses of resistant *P. falciparum* strains isolated from patients with severe malaria revealed that the unfolded protein response was another contributing factor to resistance.

Tracing the geographical origin of various resistant *P. falciparum* strains consistently points to their emergence in Myanmar, Thailand, and the Mekong region of Southeast Asia, from where they gradually spread to other parts of the world [70]. This is a classical pattern observed in the spread of resistant parasite strains across different human populations, as it was for the distribution of resistant parasites against the classical antimalarial drugs [61]. This calls

the need for sustained surveillance and the development of new therapeutic strategies to combat the evolving threat of drug-resistant malaria.

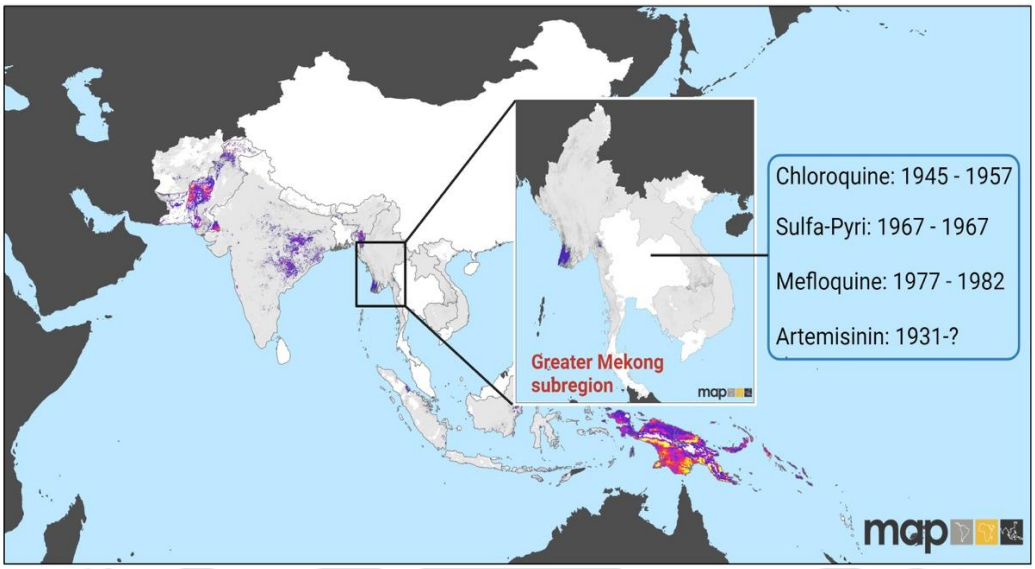

Figure 1.7: Map showing the emergence of resistant parasite strains. Emerging resistance to ACTs and other drugs might lead to widespread distribution of resistant parasites similar to that of chloroquine. (Source: created with BioRender, adapted from: https://doi.org/10.1038/nrd1416)

1.7 Novel therapeutic approaches against malaria

The emergence of drug-resistant strains, particularly in *P. falciparum*, have shown that the development of new treatment strategies to combat the disease effectively is the need of the hour. Recent advances in nanotechnology and targeted drug delivery systems have provided promising avenues for improving the efficacy and safety of antimalarial therapies. Additionally, the search for an effective vaccine for malaria is an ongoing scientific endeavour that has the potential to eradicate the disease. Although, in recent years two vaccines, the RTS, S/AS01 (Mosquirix) and R21/Matrix-M were released for public administration, their limited efficacy and the inability for a broad-spectrum action demands a continuous search for alternative therapeutic interventions [71, 72].

Therapeutic interventions against drug-resistant parasite strains includes the search for new targets in the parasite, synthesis of novel antimalarial drugs, efficient platforms for targeted drug delivery and an anti-malarial vaccine. However, the search for new targets in the parasite poses significant challenges including the limited knowledge of the parasite proteome and signaling pathways and also the risk of off-target toxicity. Additionally, both the classical and the modern antimalarial drugs have shown to induce drug toxicity. It is therefore eminent

that any modified versions of the existing drugs could carry the limitations of the previously used small molecules. The malaria parasite also has a history of developing novel and effective ways to tackle these small molecules, primarily through their efficient drug efflux machinery [73].

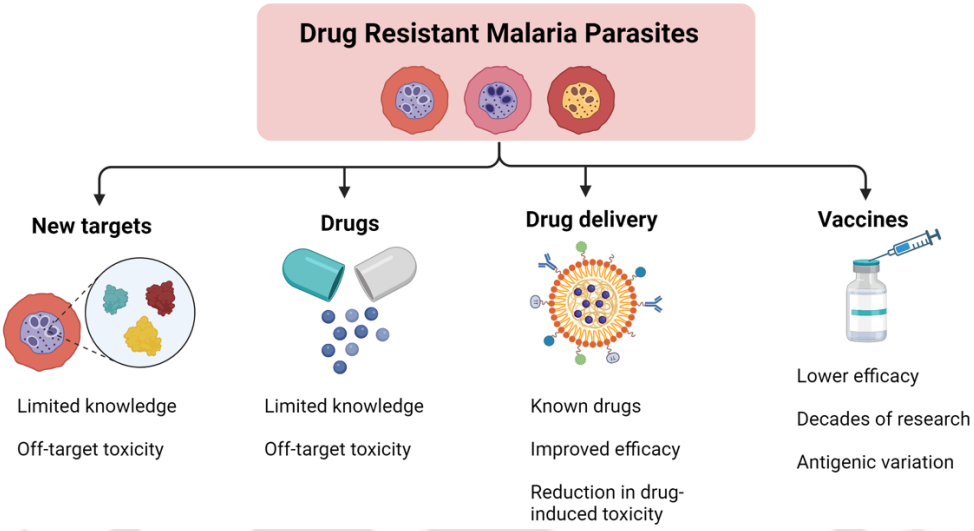

Figure 1.8: Novel therapeutic strategies against malaria. The targeted drug delivery (highlighted with green dotted line of known antimalarial drugs represents the optimal choice against drug resistant parasite strains. Vaccines against malaria (highlighted with blue dotted line) represents long-term solution against drug resistant malaria. (Source: Created with BioRender)

Thus, the targeted delivery of existing antimalarial drugs is an attractive avenue to explore as it has the potential to improve the efficacy of the drug while also minimizing their off-target toxicity. Developing efficient vehicles for targeted delivery is also a less-time consuming process compared to finding a new target or developing new drugs. In the scenario, where the emergence of resistant parasite strains is only a matter of time, the drug delivery approach seems to be the most rational. Furthermore, the continuous search for an effective vaccine against the malaria parasite is required as an effective vaccine could provide the advantage of a long-term therapeutic solution and also opens the avenue for complete elimination of the disease.

1.7.1 Passive Drug Delivery of Antimalarial Drugs

1.7.1.1 Liposomes

Liposomes are spherical vesicles consisting of one or more phospholipid bilayers, which can encapsulate hydrophilic and hydrophobic drugs. They have been extensively studied as drug

carriers due to their biocompatibility, ability to encapsulate diverse drug molecules, and potential for surface modification to enhance targeting [74].

In the context of malaria treatment, liposomal formulations have shown promise in improving the pharmacokinetics and therapeutic efficacy of antimalarial drugs. For instance, earlier reports by Peeters et al. have already demonstrated that liposomal encapsulation of chloroquine significantly enhanced its antimalarial activity against *Plasmodium berghei* in mice, resulting in improved survival rates compared to non-encapsulated chloroquine [75]. Similarly, a comprehensive review on liposomal formulations of artemisinin derivatives discusses that liposomal formulations could enhance drug stability and bioavailability, reducing the required dose and minimizing side effects [76].

1.7.1.2 PEGylated Liposomes

PEGylation involves the attachment of polyethylene glycol (PEG) chains to the surface of liposomes, which imparts "stealth" properties, reducing recognition and clearance by the reticuloendothelial system [77]. This modification prolongs the circulation time of liposomes in the bloodstream, allowing for more sustained drug release and better targeting of infected tissues. In a study by Ma YLu T and group, PEGylated liposomes loaded with artemether-lumefantrine exhibited prolonged circulation time and enhanced antimalarial efficacy in a mouse model of *P.berghei*. The PEGylated formulation resulted in higher drug concentrations in the bloodstream and more effective parasite clearance compared to non-PEGylated liposomes [78].

1.7.1.3 Solid Lipid Nanoparticles (SLNs)

Solid lipid nanoparticles (SLNs) are composed of a solid lipid core that can encapsulate lipophilic drugs, offering protection from degradation and controlled drug release. SLNs have gained attention as carriers for antimalarial drugs due to their stability, biocompatibility, and ability to improve drug solubility and bioavailability [79]. Studies into the use of Solid Lipid Nanoparticles (SLNs) for oral delivery of arteether has demonstrated notable benefits. In these studies, arteether was encapsulated within SLNs, which effectively shielded the drug from degradation in the acidic environment of the gastrointestinal tract. This protection resulted in a high entrapment efficiency of approximately 69%, significantly reducing the drug's premature breakdown and delaying its metabolism in vivo [80]. Additionally, a separate investigation focused on combining artemether and lumefantrine within SLNs. The results from in vivo

studies showed that this combination achieved substantial reduction in parasitemia after a 14-day oral administration period [79].

1.7.1.4 Nanoemulsions

Nanoemulsions are colloidal dispersions of oil and water stabilized by surfactants, with droplet sizes typically in the nanometer range. They offer advantages such as high drug loading capacity, improved solubility of hydrophobic drugs, and enhanced bioavailability. In the context of malaria treatment, Nanoemulsions have been explored as carriers for artemisinin derivatives. Oral Dihydroartemisinin formulations solubilized in surface modified lipid Nanoemulsions showed enhanced activity against murine malaria [81]. The Nanoemulsions enhanced drug absorption and prolonged circulation time, leading to more effective parasite clearance.

1.7.1.5 Nanocapsules

Nanocapsules are vesicular systems with a drug-containing core surrounded by a polymeric shell. They offer controlled drug release, protection from degradation, and the ability to target specific cells or tissues. A study from Michels and group explores how the surface characteristics of polymeric nanocapsules affect the pharmacokinetics and efficacy of quinine, an antimalarial drug. The study demonstrated that cationic nanocapsules modified the pharmacology of quinine, presenting a potential alternative for malaria treatment [82]. Another study deals with the optimization of Curcuma Oil/Quinine-Loaded Nanocapsules where they reported significant antimalarial activity and improved bio-efficacy of Quinine loaded on the Nanocapsules [83].

1.7.2 Targeted Drug Delivery to PRBCs

1.7.2.1 PSP-Liposomes

Phosphatidylserine-targeted liposomes (PSP-liposomes) represent a novel strategy for targeting parasitized red blood cells (PRBCs). During malaria infection, the membrane of infected RBCs becomes altered, exposing phosphatidylserine (PS) on the outer leaflet. PSP-liposomes are designed to specifically bind to these exposed PS molecules, ensuring targeted delivery of antimalarial drugs to PRBCs. Study evaluating PSP-conjugated liposomes using a model system of malaria-infected erythrocytes indicated that PSP-liposomes could effectively target and bind to malaria-infected erythrocytes, suggesting their potential as a novel drug

delivery system for malaria treatment. Although the nanocarriers could deliver a higher quantity of drugs to the PRBC, they were found to cause RBC eryptosis [84].

1.7.2.2 Antibody-Coupled Nanoparticles

Antibody-coupled nanoparticles represent a cutting-edge approach for targeted drug delivery to PRBCs. In this strategy, nanoparticles are conjugated with antibodies that specifically recognize antigens expressed on the surface of infected RBCs, such as P. falciparum erythrocyte membrane protein 1 (PfEMP1). The study by Moles and group investigated the use of immunoliposomes for targeted drug delivery of weak basic drugs chloroquine (CQ) and primaquine to both *Plasmodium*-infected and non-infected red blood cells. The immunoliposomes significantly improved the delivery of antimalarial drugs to the target cells, enhancing the efficacy of the treatment. Additionally, by specifically targeting red blood cells, the immunoliposomes reduced the systemic toxicity of the antimalarial drugs [85]. Another study by Marques and group extensively investigated the potential of targeted delivery using immunoliposome-mediated release of new lipid-based antimalarials. The study demonstrated that nanocarriers could be adapted to deliver various antimalarial drugs effectively, addressing different stages of the life cycle of the malaria parasite including in humans and mosquitoes [86].

1.7.3 Vaccines against malaria

Vaccine development against malaria has been a major focus of research, with most efforts targeting the erythrocytic stage of the life cycle of the parasite, responsible for the symptomatic phase of the disease. RTS, S/AS01, also known as Mosquirix, is the first malaria vaccine to receive a recommendation from the World Health Organization (WHO) for widespread use. Developed by GlaxoSmithKline (GSK) in partnership with the PATH Malaria Vaccine [87]. It consists of a recombinant protein that includes part of the *P. falciparum* circumsporozoite protein (CSP) fused with the hepatitis B surface antigen (HBsAg) to enhance immune response. The vaccine is formulated with the AS01 adjuvant, which contains monophosphoryl lipid A (MPL) and QS-21, both of which enhance the immune response by promoting strong antibody and T-cell production [88, 89]. Upon vaccination, the immune system generates CSP-specific antibodies that neutralize sporozoites, preventing them from invading liver cells. Additionally, cytotoxic CD8+ T cells are activated to recognize and destroy any liver cells infected by the parasite. This dual humoral and cellular response effectively reduces the parasite's ability to

cause symptomatic malaria [90]. Although the vaccine provides significant protection, its efficacy decreases over time, necessitating booster doses to maintain immunity [91].

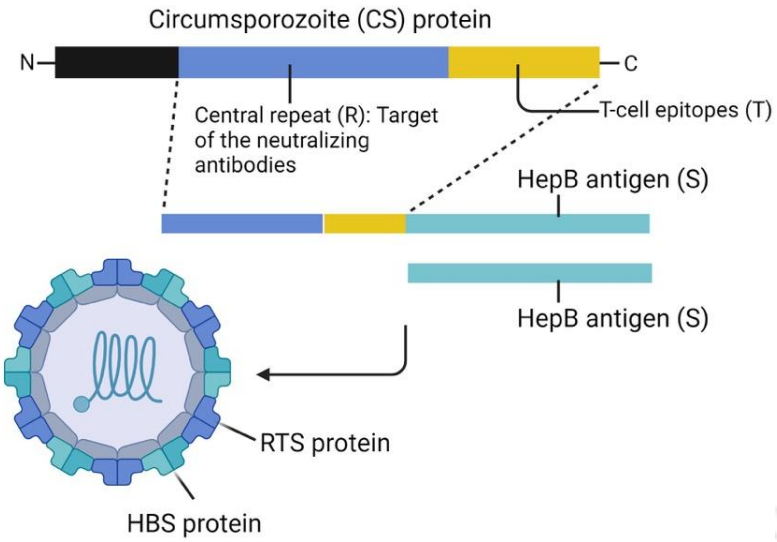

Figure 1.9: The RTS, S vaccine. The vaccine consists of a recombinant protein that includes part of the *P. falciparum* circumsporozoite protein (CSP) fused with the hepatitis B surface antigen (HBsAg) to enhance immune response. (Source: created with BioRender, adapted from: http://ema.europa.eu/en/documents/outside-eu-assessment-report/mosquirix-public-assessment report_en.pdf)

Clinical trials have shown that RTS, S/AS01 can reduce the incidence of malaria by about 40% and severe malaria by about 30% in children under five years old. The vaccine has been implemented in pilot programs in Ghana, Kenya, and Malawi, reaching nearly 2 million children and resulting in a significant reduction in severe malaria cases and child mortality [92, 93]. The R21/Matrix-M malaria vaccine is a promising new candidate that targets the pre-erythrocytic stage of *Plasmodium falciparum*, aiming to prevent the parasite from developing in the liver. Similar to the RTS, S vaccine, R21 includes a fusion protein composed of part of the circumsporozoite protein (CSP) of P. falciparum. However, R21 differs by containing a higher proportion of CSP without the hepatitis B surface antigen (HBsAg) fusion, which may enhance its immunogenicity. The Matrix-M adjuvant, composed of saponin-based nanoparticles, significantly boosts the immune response by enhancing antigen presentation and stimulating a robust production of both antibodies and T-cells [94-96]. The R21 antigen is taken up by antigen-presenting cells, leading to the generation of high titters of CSP-specific antibodies that target the sporozoite stage of the parasite. These antibodies neutralize the sporozoites, preventing them from invading liver cells. Simultaneously, the vaccine induces a strong T-cell response, particularly cytotoxic CD8+ T cells, which recognize and destroy

infected liver cells. This dual action of blocking liver cell invasion and killing of the infected cells aims to provide high levels of protection against malaria. Preliminary results indicate that R21/Matrix-M can prevent around 75% of malaria episodes when given seasonally in areas with highly seasonal transmission [97-99].

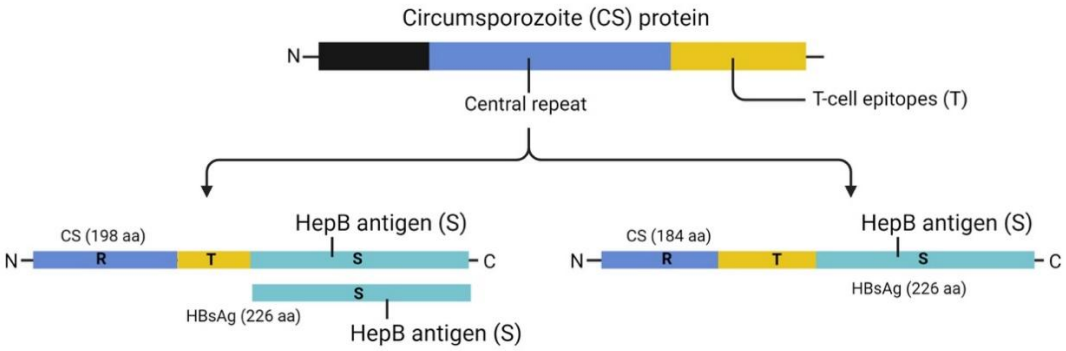

Figure 1.10: The R21/Matrix-M vaccine is a successor of the RTS, S. (Source: created with BioRender, adapted from: doi:10.1038/srep46621)

Other vaccine candidates target different antigens expressed during the erythrocytic stage, such as merozoite surface proteins (MSPs), apical membrane antigen 1 (AMA1), and reticulocyte-binding protein homolog 5 (PfRh5). These vaccines aim to block the invasion of RBCs by the malaria parasite, thereby preventing the establishment of blood-stage infection and reducing the severity of the disease. For example, a vaccine candidate targeting PfRh5 has shown promise in preclinical studies, inducing strong immune responses that block merozoite invasion of RBCs. Another candidate, targeting AMA1, has demonstrated partial protection in clinical trials, with immune responses correlated with reduced parasite burden [100]. Despite the progress in vaccine development, several limitations remain that limit their widespread use and effectiveness. One major challenge is the genetic diversity of *P. falciparum* populations, which leads to antigenic variation and immune evasion. The high degree of polymorphism in vaccine target antigens, such as CSP and MSPs, can result in reduced vaccine efficacy against different parasite strains circulating in endemic regions. Another limitation is the complexity of the malaria parasite's life cycle, which involves multiple stages and antigenic targets. Developing a vaccine that provides comprehensive protection across all stages of the parasite's life cycle is challenging.

1.8 The malaria parasite interacts with various other pathogens within the human host

While extensive research has been conducted on the pathogenesis, treatment, and prevention of malaria, the interaction between *Plasmodium* species and other pathogens during co-

infections has garnered increasing scientific interest. Co-infections, where malaria parasites coexist with other pathogens, can significantly impact disease outcomes, immune responses, and treatment efficacy.

1.8.1 Co-Infections with Bacterial Pathogens

1.8.1.1 Salmonella spp.

Co-infection of malaria with *Salmonella* species, particularly non-typhoidal *Salmonella* (NTS), is a well-documented phenomenon, especially in sub-Saharan Africa. Studies have shown that children with malaria are at a significantly increased risk of developing invasive NTS infections. This increased susceptibility is partly due to malaria-induced hemolysis, which releases haemoglobin and heme into the bloodstream, providing a nutrient-rich environment for Salmonella proliferation [101]. Additionally, malaria-induced immune dysregulation, particularly the impairment of phagocytic function and the suppression of pro-inflammatory cytokine responses, further predisposes individuals to bacterial infections [102]. The result of this co-infection is often severe, leading to increased morbidity and mortality. For instance, Salmonella co-infection in malaria patients is associated with a higher risk of bacteremia, septicemia, and death compared to patients infected with either pathogen alone [103].

1.8.1.2 Escherichia coli and Other Enterobacteriaceae

Co-infections of malaria with *Escherichia coli* and other members of the *Enterobacteriaceae* family, although less studied than *Salmonella*, also pose significant clinical challenges. The interaction between malaria and these bacterial pathogens often results in exacerbated disease symptoms, including severe gastrointestinal disturbances, dehydration, and increased likelihood of developing systemic infections [104]. The inflammatory response triggered by Plasmodium infection may disrupt the gut mucosal barrier, facilitating the translocation of these bacteria from the gut into the bloodstream. This can lead to bacteremia and septic shock, conditions that require prompt and aggressive treatment [105].

1.8.2 Co-Infections with Parasitic Pathogens

1.8.2.1 Schistosomiasis

Co-infection of malaria with schistosomiasis, caused by *Schistosoma* species, is common in endemic regions where both parasites coexist. The interaction between these two parasitic infections can result in complex immunological and pathological outcomes. Schistosomiasis is

known to induce a strong Th2-type immune response characterized by elevated levels of IgE and eosinophilia, which contrasts with the Th1-type response typically associated with malaria. This immune modulation can affect the host's ability to control *Plasmodium* infection, potentially leading to altered malaria pathogenesis [106, 107]. For instance, studies have shown that co-infected individuals may experience more severe anemia and higher parasite loads compared to those infected with malaria alone [108]. The presence of schistosome eggs in the liver and spleen may also exacerbate organ damage during malaria infection, complicating the clinical management of co-infected patients.

1.8.2.2 Helminths

Helminth co-infections, particularly with soil-transmitted helminths such as Ascaris lumbricoides and Hookworm species, are frequently observed alongside malaria in endemic regions [109]. Helminth infections are known to modulate the host immune response through mechanisms such as the induction of regulatory T cells and the secretion of anti-inflammatory cytokines like IL-10 and TGF-β. This immunomodulation can have both protective and detrimental effects on malaria outcomes [110, 111]. On one hand, the anti-inflammatory environment created by helminths may reduce the severity of malaria-induced inflammation, potentially lowering the risk of severe malaria syndromes such as cerebral malaria. On the other hand, the dampened immune response may impair the ability of the host to clear *Plasmodium* parasites, leading to chronic infection and increased transmission potential [112]. Additionally, the nutritional deficiencies associated with helminth infections, particularly anemia due to hookworm, can compound the haematological complications of malaria, leading to severe anemia and increased morbidity [113].

1.8.2.3 Leishmaniasis

Co-infection with Leishmania species, the causative agents of leishmaniasis, and Plasmodium can result in a complex interplay between the two protozoan parasites. Both diseases share overlapping endemic regions, particularly in South Asia and parts of Africa. The immune response to Leishmania infection is predominantly cell-mediated, involving macrophage activation and the production of IFN-γ, which contrasts with the humoral response typically observed in malaria [114]. This dichotomy in immune responses can influence the clinical outcomes of co-infected individuals. Co-infection with Leishmania and malaria can alter the progression and severity of both diseases. For example, a study found that co-infection with *Leishmania braziliensis* and *Plasmodium yoelii* resulted in lower malaria parasitemia,

suggesting a protective effect of Leishmania co-infection on malaria progression. Conversely, co-infection with *Leishmania amazonensis* increased malaria parasitemia and mortality [115]. The immune response to co-infection can also vary depending on the Leishmania species involved. Previous study mentioned that the above observed different cytokine profiles and T-cell responses in co-infected mice, indicating that the immune modulation depends on the specific Leishmania species [115]. Additionally, the co-infection can lead to diagnostic challenges, as the symptoms of leishmaniasis, such as fever and hepatosplenomegaly, can mimic those of malaria. Clinically, patients co-infected with both parasites may experience more severe disease manifestations, including prolonged fever, severe anemia, and increased risk of secondary infections [116].

1.8.2.4 Trypanosomiasis

Trypanosomiasis, caused by Trypanosoma species, particularly *T. brucei* in Africa and *T. cruzi* in Latin America, can also co-occur with malaria, leading to complicated disease dynamics. The immune response to trypanosomiasis involves strong polyclonal B cell activation and the production of high levels of non-specific antibodies, which can interfere with the immune response to *Plasmodium* [117]. This may result in increased susceptibility to malaria or exacerbation of malaria symptoms in co-infected individuals. Moreover, the chronic nature of trypanosomiasis, characterized by prolonged parasitemia and immune evasion strategies employed by Trypanosoma spp., can lead to sustained immune activation and inflammation, which may aggravate malaria pathogenesis [118].

1.8.3 Co-Infections with Viral Pathogens

1.8.3.1 Human Immunodeficiency Virus (HIV)

The co-infection of malaria with Human Immunodeficiency Virus (HIV) presents a complex interplay between two of the most devastating infections affecting global public health. HIV-positive individuals are at an increased risk of severe malaria due to the immunosuppressive nature of HIV, which diminishes the ability of the host to mount an effective immune response against *Plasmodium infection* [119]. A meta-analysis found that co-infection with malaria and HIV increases the severity and mortality rates of both diseases. The study reported that patients with co-infection had significantly higher odds of severe malaria compared to those with malaria alone. This was particularly pronounced in children, who showed a much higher risk of severe malaria when co-infected with HIV [120]. Co-infection can also exacerbate immune suppression, making individuals more susceptible to both infections. Asymptomatic malaria

parasitemia in HIV-infected individuals was associated with abnormal hematological outcomes, suggesting that the immune suppression caused by HIV can alter the course of malaria infection [119]. Additionally, the interactions between anti-retroviral (ARV) and antimalarial drugs can complicate treatment. Some studies have reported reduced efficacy of these drugs when used concurrently, raising concerns about optimal treatment strategies for co-infected patients [121]. The geographical distribution of malaria and HIV infections also overlaps significantly, particularly in sub-Saharan Africa. This overlap leads to a high prevalence of co-infection, which leads to severe P. falciparum malaria in adults [122].

1.8.3.2 Hepatitis B and C Viruses

Co-infections of malaria with Hepatitis B (HBV) and Hepatitis C (HCV) viruses are particularly concerning in regions where these infections are endemic. Malaria can exacerbate liver damage in patients co-infected with HBV or HCV due to the additional hepatic burden imposed by the parasite [123]. The hepatotropic nature of *Plasmodium spp*., which involves the liver stage of the parasite's lifecycle, can worsen pre-existing liver conditions caused by HBV or HCV. Moreover, the immune response to malaria infection, particularly the production of pro-inflammatory cytokines, may trigger viral reactivation in patients with chronic HBV or HCV infections, leading to acute hepatitis and liver failure [124]. Clinically, co-infected patients may present with jaundice, elevated liver enzymes, and a higher risk of developing cirrhosis and hepatocellular carcinoma. Such co-infection scenario calls for a careful approach to managing both malaria and viral hepatitis, considering the potential for drug-induced hepatotoxicity and the need for liver-protective therapies.

1.8.3.3 Newcastle Disease Virus

Co-infections of malaria parasites with Newcastle Disease Virus (NDV), an avian virus, have not been reported in either avian species or humans. However, studies exploring the use of NDV as an immunomodulatory agent have shown that the virus can inhibit the growth of *Plasmodium berghei* in mice and *P. gallinaceum* in chickens. In mice, NDV was found to be a potent inducer of interferons, providing dose-dependent protection against P. berghei infection [125]. Conversely, while NDV did not provide *in ovo* protection against *P. gallinaceum* in chickens, it was still able to reduce parasite growth in chicks through interferon induction [126].

1.9 The curious case of viruses with hemagglutinin activity

Hemagglutinin activity is a characteristic feature of several viruses, particularly those belonging to the Orthomyxoviridae and Paramyxoviridae families [127, 128]. This activity refers to the ability of viral surface proteins, such as hemagglutinin (HA) or hemagglutinin-neuraminidase (HN), to bind to sialic acid residues on the surface of host cells, facilitating viral attachment and subsequent entry. NDV, which belongs to the Paramyxoviridae family display dedicated lectins (HN) in their coat for binding to sialic acids and consequently show strong affinity towards sialic acid rich RBCs [129].

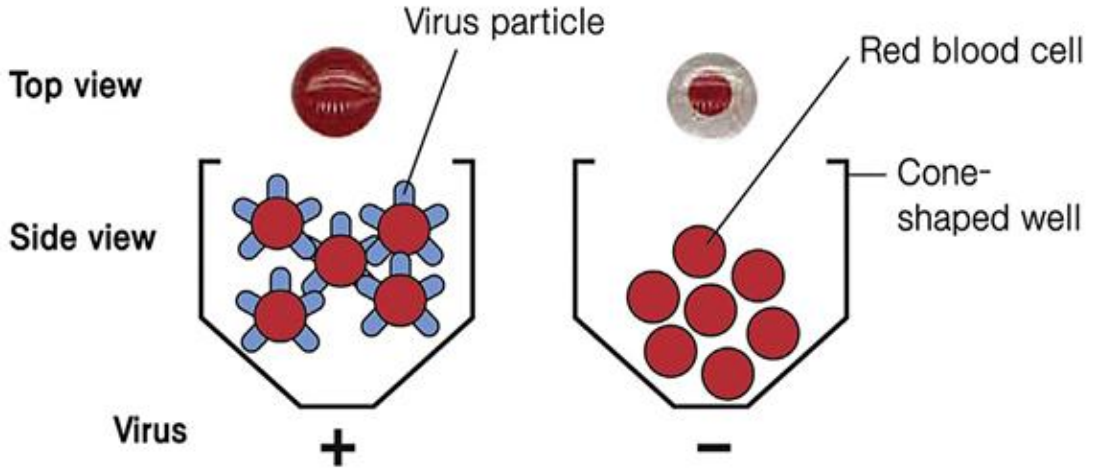

Figure 1.11: The Hemagglutination Assay. Several avian viruses show high affinity towards erythrocytes which forms lattices of RBCs. (Source: created with BioRender, adapted from: https://doi.org/10.1016/B978-0-12-800838-6.00004-7)

This property of the virus is routinely used for its detection, quantification and identification through the Hemagglutination assay (HA) and the Hemagglutination Inhibition assay (HIA). Interestingly, NDV show exceptional affinity for the avian RBCs that are used for the assays. As described earlier in section 1.8.3.3, the Newcastle Disease Virus (NDV), exhibited potent ant-plasmodial activity against murine malaria and to a degree against avian malaria as well. Although the virus was primarily utilized as an immunomodulatory agent against the malaria parasite, we began to consider whether its RBC-binding property might also have an impact on malaria outcomes.

Within its host cell or RBC, the survival of the malaria parasite relies on critical signaling pathways involving cyclic nucleotides, ATP, and calcium, which are essential for its development, egress, and invasion. Host cell-dependent pathways, such as the MAPK pathway, and the coordinated release of intracellular calcium are crucial for the parasite to progress

through its complex developmental stages. These signaling pathways also play a key role in extensively modifying the red cell cytoplasm and membrane. Therefore, an agent that strongly interacts with RBCs or PRBCs could carry the potential to disrupt these intricate yet vital processes necessary for the malaria parasite's survival. In this context, the natural affinity of Newcastle Disease Virus (NDV) for engaging with avian erythrocytes was particularly intriguing.

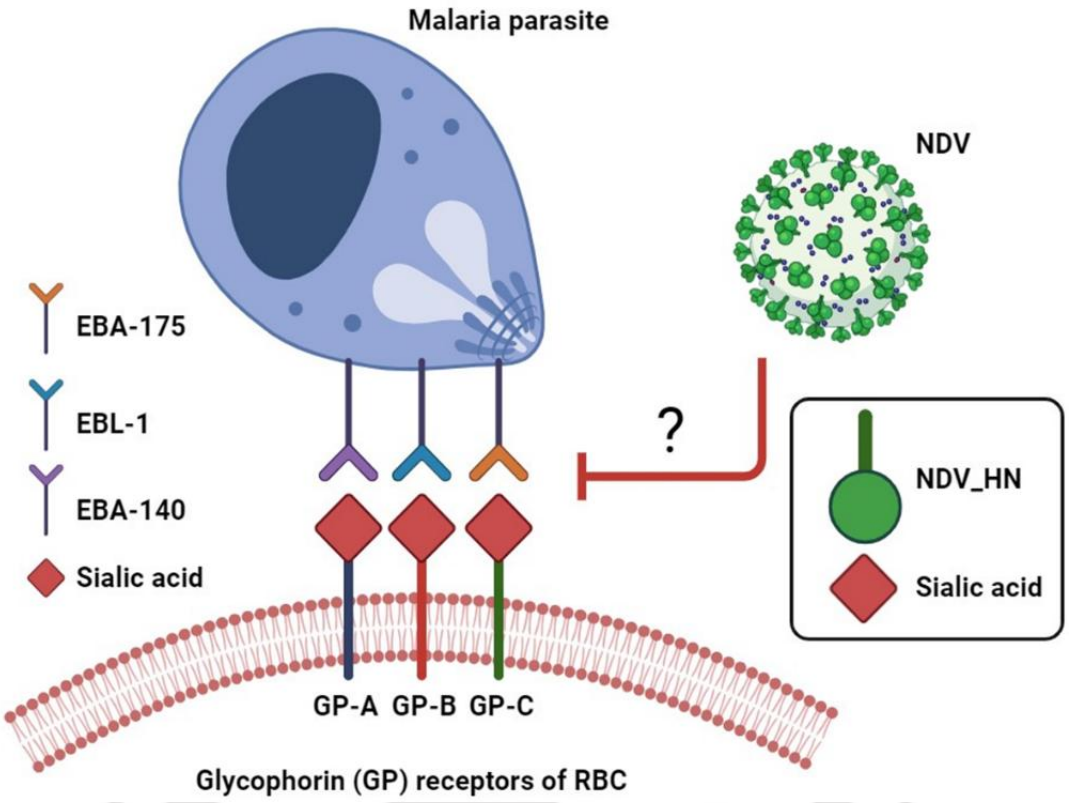

Figure 1.12: A graphical representation of the central idea formulated for the study. The malaria parasite and NDV, both display affinity towards sialic acid rich erythrocyte surface. (Source: created with BioRender)

1.10 Biology of NDV and molecular mechanism involved in cellular recognition

NDV is a pleomorphic enveloped virus and ranges from 200-300 nm in diameter. It belongs to the Paramyxoviridae family of the order Mononegavirales. It carries a non-segmented, negative sense, single stranded RNA genome [129].

1.10.1 Structure and Genomic Composition of NDV

NDV is an enveloped virus with a pleomorphic shape, typically spherical or filamentous, and measures approximately 200-300 nm in diameter [130]. The viral envelope is derived from the host cell membrane and contains two critical glycoproteins: the hemagglutinin-neuraminidase (HN) and fusion (F) proteins. These proteins are essential for virus attachment and entry into

the host cell. NDV has a single-stranded, negative-sense RNA genome that is approximately 15.2 kb in length. The genome is non-segmented and encodes six major structural proteins in the following order: nucleoprotein (N), phosphoprotein (P), matrix protein (M), fusion protein (F), hemagglutinin-neuraminidase (HN), and large polymerase protein (L) [127]. Additionally, two non-structural proteins, V and W, are produced by RNA editing during P gene transcription [129].

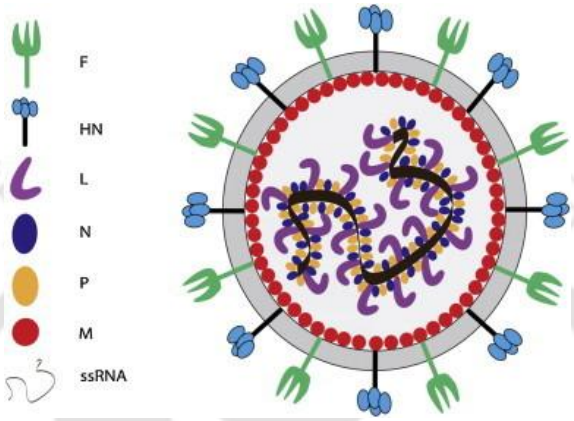

Figure 1.13: Diagrammatic representation of the structure of the Newcastle Disease Virus (NDV). (Source: Ganar et al., 2014 [127])

The function of the different proteins of NDV are discussed below:

N protein: The N-protein encapsidates the viral RNA to form the ribonucleoprotein (RNP) complex, which is crucial for maintaining the integrity of the viral genome and for the transcription and replication processes.

Phosphoprotein (P): The P protein serves as a cofactor for the RNA-dependent RNA polymerase (RdRp) and is involved in the formation of the RNA polymerase complex along with the L protein.

Matrix Protein (M): The M protein is located underneath the viral envelope and plays a central role in virus assembly and budding. It interacts with the cytoplasmic tails of the glycoproteins and the RNP complex to facilitate the packaging of viral components into new virions.

F-protein: The F protein mediates the fusion of the viral envelope with the host cell membrane, a critical step for viral entry. The F protein is synthesized as an inactive precursor (F0), which is cleaved by host proteases into two subunits, F1 and F2, to become active.

Hemagglutinin-Neuraminidase Protein (HN): The HN protein is responsible for virus attachment to the host cell by binding to sialic acid receptors on the cell surface. It also possesses neuraminidase activity, which facilitates the release of progeny virions from the host cell by cleaving sialic acid residues.

Large Polymerase Protein (L): The L protein is the catalytic subunit of the viral RNA polymerase complex and is responsible for RNA synthesis, including both transcription of viral mRNAs and replication of the viral genome [127].

1.10.2 Mechanism of NDV replication

The process of virus attachment and entry is a critical initial step in the life cycle of Newcastle Disease Virus (NDV), dictating its ability to infect host cells and propagate infection. NDV, like other members of the Paramyxoviridae family, employs a complex and highly coordinated mechanism involving viral surface glycoproteins and host cell receptors to achieve successful entry [131]. NDV has two key surface glycoproteins that mediate the processes of attachment and membrane fusion: the hemagglutinin-neuraminidase (HN) protein and the fusion (F) protein. These proteins are integral to the viral envelope and are essential for the virus to establish infection in host cells.

The initial step in the NDV life cycle is the attachment of the virus to the host cell surface. This is mediated by the HN protein, which specifically recognizes and binds to sialic acid-containing receptors on the host cell membrane. It is a type II integral membrane protein that forms tetramers on the viral surface. The HN protein binds to sialic acid residues through its receptor-binding domain (RBD) [132]. Studies show that the HN protein could target both the α2,3-linked and α2,3-linked sialic acids [133]. The HN protein also possesses neuraminidase activity, which is critical for cleaving sialic acid residues during the release of new virions, preventing self-aggregation and facilitating the spread of the virus [134].

Upon binding to the sialic acid receptor, the HN protein undergoes conformational changes that are critical for subsequent steps in the entry process (**Figure 1.14**). These changes are thought to facilitate the activation of the F protein, preparing it for the fusion event. The F protein mediates the fusion of the viral envelope with the host cell membrane. The F protein is initially synthesized as an inactive precursor (F0). Cleavage of F0 into the active F1 and F2 subunits is required for membrane fusion. This cleavage is typically performed by host cell proteases, which can be either extracellular or intracellular, depending on the virus strain. The cleavage site of the F protein contains multiple basic amino acids in virulent strains, making it susceptible to cleavage by ubiquitous proteases such as furin [135]. The cleavage of F0 exposes the fusion peptide located at the N-terminus of the F1 subunit. The fusion peptide is highly hydrophobic and plays a critical role in the fusion of the viral and host cell membranes. This

insertion of the hydrophobic peptide into the host cell membrane creates a connection between the viral envelope and the host cell. The F protein facilitates the merging of the viral and host cell membranes, forming a fusion pore. This pore expands, allowing the viral RNP complex to pass through and enter the host cell cytoplasm. The energy required for this process is derived from the conformational changes in the F protein, which transition from a metastable prefusion state to a highly stable post-fusion state [136].

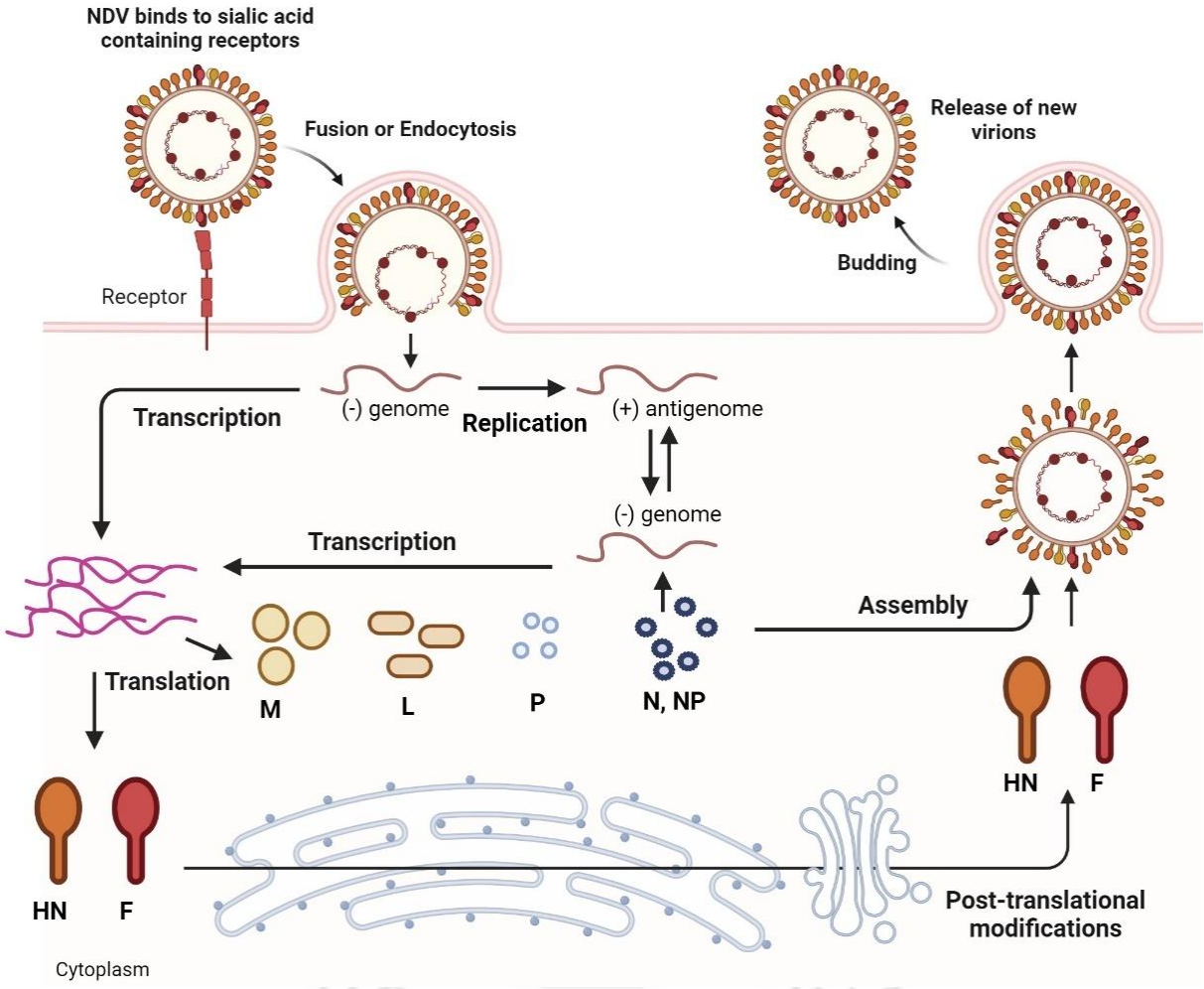

Figure 1.14: Schematic representation of the life cycle of paramyxoviruses. NDV transfers its genome into the cell cytoplasm where the transcription (facilitated by the viral RNA-dependent RNA polymerase), translation (mediated by host ribosomes) and replication of the viral genome and proteome takes place. Following this, the newly produced viral components are transported to specific regions of the infected cell's plasma membrane, where they undergo assembly and the budding of new virus particles. (Source: created with BioRender)

Once the viral and host membranes have fused, the viral RNP complex, consisting of the RNA genome encapsidated by the nucleoprotein (N), along with associated proteins (P and L), is released into the host cell cytoplasm. The fusion pore facilitates the direct release of the RNP complex into the cytoplasm. NDV can delivers its genetic material directly into the cytoplasm

or enter the cell through caveolae-mediated endocytosis [137]. The transcription and replication of the viral genome occur within the cytoplasm, driven by the viral RNA-dependent RNA polymerase. Host-ribosome mediated translation leads to the synthesis of the viral proteins. Once these viral components are synthesized, they are directed to specific regions of the plasma membrane of the infected cell. The final stage of the NDV life cycle is the release of progeny virions from the host cell. The newly formed virions are released into the extracellular environment, where they can infect neighbouring cells and continue the cycle of infection. The release process is facilitated by the HN protein, which cleaves sialic acid residues on the host cell surface, preventing the aggregation of virions and ensuring efficient release of the virus [129].

1.10.3 NDV is a well-established oncolytic virus and a vector for vaccine delivery

Newcastle Disease Virus (NDV) is increasingly recognized as a potent oncolytic agent due to its ability to selectively replicate in cancer cells while causing minimal infectivity in normal tissues. This selective tropism is largely attributed to the inherent defects in the interferon signaling pathways of the tumor cells, which fails to elicit an effective antiviral response, thereby allowing NDV to replicate preferentially within these cells [138]. Upon replication, NDV induces direct oncolysis through the destruction of infected cancer cells. Moreover, the virus triggers immunogenic cell death, characterized by the release of tumor antigens that stimulate a robust anti-tumor immune response. NDV also modulates the tumor microenvironment by enhancing the infiltration and activation of immune cells, including dendritic cells and cytotoxic T lymphocytes, which further amplify the anti-tumor response. Clinical trials have demonstrated the safety and efficacy of NDV in various cancers, such as glioblastoma, melanoma, and breast cancer, showing promising results in terms of tumor regression and prolonged patient survival [139]. Additionally, NDV has been engineered to express therapeutic genes or to enhance its oncolytic properties, making it a versatile tool in cancer therapy [140]. NDV is also an attractive platform to develop it as a vector for delivery of sub-unit vaccines. The virus shows many desirable characteristics as a potential vaccine vector platform which are listed below.

(a) High titres of NDV can be grown in embryonated chicken eggs and in cell cultures of both avian and non-avian species NDV
(b) NDV has the ability to induce both local and systemic immune response. It can also induce cell-mediated as well as humoral immune response.

(c) Engineering of the NDV genome is also easy as it harbours only six essential and two accessory genes.
(d) The genome of NDV does not integrate with the host genome and replicate in the host cell cytoplasm.
(e) Genetic recombination in NDV is also very low.
(f) Stable expression of the inserted foreign gene can be achieved in both in-vitro and in-vivo settings.

The ability to attenuate NDV while achieving high immunogenicity is also a desirable quality that can be achieved by developing deletion mutants and alteration of F-protein cleavage sites. Apart from these innate abilities, recombinant NDV is safe to be administered in humans as it is non-pathogenic and attenuates due to natural host range restriction. In brief, its safety, efficacy and cost effectiveness qualities make it a potential candidate for the development of a viral vectored vaccine in humans. The development of NDV as a potential viral vector for vaccine delivery is not a new concept but has been extensively developed mainly to treat human viral infections. Its oncolytic properties have also been utilized for therapeutic interventions in a wide range of human cancers. However, there are no reports of NDV to be used as a vaccine delivery vector in protozoan infections.

Table 1.1: NDV is used as a vaccine delivery vector for various viral pathogens in humans. The virus efficiently delivers sub-unit antigens of pathogenic viruses for triggering an immune response in the host.

Antigen	Reference
Human influenza virus hemagglutinin protein	DiNapoli et al., 2010 [141]; Ge et al., 2007 [142]
HIV and SIV Gag protein	Lawrence et al., 2013 [143] ; Nakaya et al., 2004 [144]
HIV glycoproteins	Khattar et al., 2011, 2013 [145] [146]
F glycoprotein of human respiratory syncytial virus	Martinez-Sobrido et al., 2006 [147]
HN protein of human parainfluenza virus 3	Bukreyev et al., 2005 [148]
Spike glycoprotein of SARS-CoV	DiNapoli et al., 2007 [149]

Thus, given the clinical significance of NDV as oncolytic agents and a viral vector, the virus was selected for our study where the its potential to be used as an anti-malarial agent was explored. From our study, we aim to show that viruses like NDV could also be used as active therapeutic agents against the malaria parasite, rather than their limited application as vectors for vaccine delivery.

1.11 Aims and Objectives formulated for the study

1. In-depth study of the impact of NDV on the erythrocytic schizogony of the malaria parasite of *Plasmodium falciparum*.

1.1 Study the effects of NDV on the erythrocytic cycle of the malaria parasite.

1.2 Decipher the mechanism of anti-plasmodial action of NDV.

1.3 Explore the potential of NDV against murine parasite strain.

2. Study the involvement of receptor ligand interaction

2.1 Binding studies of NDV to RBC/PRBC under different experimental conditions.

2.2 Study the role of HN: sialic acid interaction in the anti-plasmodial activity of NDV.

2.3 Explore the potential of purified HN protein in disrupting malaria parasite growth.

3. Modulation of sialic acid binding by specific mutations in the binding pocket of HN

3.1 Study the sialic acid binding pocket of the NDV HN protein.

3.2 In silico mutagenesis, docking and MD simulation of selected mutants.

3.3 Compare the sialic acid binding affinity of wild-type HN and the mutants.

3.4 Test and compare the activity of mutant against the malaria parasite.

1.12 Significance of the study

The significance of this study lies in its innovative approach of leveraging the Newcastle Disease Virus (NDV) and its HN spike protein for exploring novel therapeutic approaches against the malaria parasite. The study explores the innate anti-plasmodial activity of NDV. To the best of our knowledge, there are no reports that have explored this virus in the context of human malaria. The study also highlights two possible therapeutic applications of the virus. Firstly, the NDV-HN protein or NDV virus-like particles (VLPs) could be used for the development of targeted delivery vehicles, carrying antimalarial drugs. Current drug delivery systems, such as liposomes and PEGylated liposomes, have demonstrated efficacy in passive drug delivery. However, these systems often face challenges such as non-specific binding or toxicity. The study proposes that coupling NDV-HN protein with nanocarriers could enhance specificity and efficiency in targeting Plasmodium-infected red blood cells (PRBCs). This approach could potentially reduce drug dosages while increasing therapeutic efficacy, addressing the limitations of existing drug delivery methods. Secondly, the study underscores the potential of NDV-HN protein in developing novel antimalarial peptides. While viruses typically do not produce antimicrobial peptides, this study demonstrates that functional peptides derived from NDV-HN protein exhibit significant inhibitory effects on malaria parasites. This finding opens new avenues for designing peptide-based therapies, which could be produced efficiently in prokaryotic systems and may offer a targeted approach to blocking parasite invasion of red blood cells. We envision that the innate anti-plasmodial activity of the virus coupled with the potential of targeted drug delivery could provide a dual mechanism of action against the malaria parasite.

1.13 References

1. Reiter, P., From Shakespeare to Defoe: malaria in England in the Little Ice Age. Emerging infectious diseases, 2000. 6(1): p. 1.

2. Sallares, R., A. Bouwman, and C. Anderung, The spread of malaria to Southern Europe in antiquity: new approaches to old problems. Medical history, 2004. 48(3): p. 311-328.

3. Celsus, A.C., Aur. Corn. Celsi de medicina libri octo. Vol. 1. 1746: apud Joh. Arn. Langerak.

4. Bruce-Chwatt, L.J., Alphonse Laveran's discovery 100 years ago and today's global fight against malaria. Journal of the Royal Society of Medicine, 1981. 74(7): p. 531-536.

5. Jarcho, S., Laveran's discovery in the retrospect of a century. Bulletin of the History of Medicine, 1984. 58(2): p. 215-224.

6. Kannadan, A., History of the miasma theory of disease. Essai, 2018. 16(1): p. 18.

7. Lalchhandama, K., The making of modern malariology: from miasma to mosquito-malaria theory. Science Vision, 2014. 14(1): p. 3-17.

8. Guillemin, J., Choosing scientific patrimony: Sir Ronald Ross, Alphonse Laveran, and the mosquito-vector hypothesis for malaria. Journal of the history of medicine and allied sciences, 2002. 57(4): p. 385-409.

9. Conway, D.J., et al., Origin of Plasmodium falciparum malaria is traced by mitochondrial DNA. Molecular and biochemical parasitology, 2000. 111(1): p. 163-171.

10. Escalante, A.A., A.S. Cepeda, and M.A. Pacheco, Why Plasmodium vivax and Plasmodium falciparum are so different? A tale of two clades and their species diversities. Malaria Journal, 2022. 21(1): p. 139.

11. Aidoo, M., et al., Protective effects of the sickle cell gene against malaria morbidity and mortality. The Lancet, 2002. 359(9314): p. 1311-1312.

12. Allen, S., et al., α+-Thalassemia protects children against disease caused by other infections as well as malaria. Proceedings of the National Academy of Sciences, 1997. 94(26): p. 14736-14741.

13. Martin, S., et al., Severe malaria and glucose-6-phosphate-dehydrogenase deficiency: a reappraisal of the malaria/G-6-PD hypothesis. The Lancet, 1979. 313(8115): p. 524-526.

14. Guerra, C.A., et al., Assembling a global database of malaria parasite prevalence for the Malaria Atlas Project. Malaria journal, 2007. 6: p. 1-13.

15. Kalanon, M. and G.I. McFadden, Malaria, Plasmodium falciparum and its apicoplast. Biochemical Society Transactions, 2010. 38(3): p. 775-782.

16. Escalante, A.A. and F.J. Ayala, Evolutionary origin of Plasmodium and other Apicomplexa based on rRNA genes. Proceedings of the National Academy of Sciences, 1995. 92(13): p. 5793-5797.

17. Organization, W.H., World malaria report 2023. 2023: World Health Organization.

18. Mayxay, M., et al., Mixed-species malaria infections in humans. Trends in parasitology, 2004. 20(5): p. 233-240.

19. Kantele, A. and T.S. Jokiranta, Review of cases with the emerging fifth human malaria parasite, Plasmodium knowlesi. Clinical infectious diseases, 2011. 52(11): p. 1356-1362.

20. Lehmann, T., et al., Population structure of Anopheles gambiae in Africa. Journal of Heredity, 2003. 94(2): p. 133-147.

21. White, G., Anopheles gambiae complex and disease transmission in Africa. Transactions of the Royal Society of Tropical Medicine and hygiene, 1974. 68(4): p. 278-298.

22. Worrall, E., S. Basu, and K. Hanson, Is malaria a disease of poverty? A review of the literature. Tropical Medicine & International Health, 2005. 10(10): p. 1047-1059.

23. Tusting, L.S., et al., Why is malaria associated with poverty? Findings from a cohort study in rural Uganda. Infectious diseases of poverty, 2016. 5(04): p. 45-55.

24. Wafula, S.T., et al., What are the pathways between poverty and malaria in sub-Saharan Africa? A systematic review of mediation studies. Infectious Diseases of Poverty, 2023. 12(03): p. 13-30.

25. Bi, Y. and S. Tong, Poverty and malaria in the Yunnan province, China. Infectious Diseases of Poverty, 2014. 3: p. 1-4.

26. Humphreys, M., Malaria: poverty, race, and public health in the United States. 2001: JHU Press.

27. Gallup, J.L. and J.D. Sachs, The economic burden of malaria. CID Working Paper Series, 2000.

28. Monteiro, M.C., et al., Neurological and behavioral manifestations of cerebral malaria: An update. World Journal of Translational Medicine, 2014. 3(1): p. 9-16.

29. Idro, R., N.E. Jenkins, and C.R. Newton, Pathogenesis, clinical features, and neurological outcome of cerebral malaria. The Lancet Neurology, 2005. 4(12): p. 827-840.

30. Sato, S., Plasmodium—a brief introduction to the parasites causing human malaria and their basic biology. Journal of physiological anthropology, 2021. 40(1): p. 1.

31. Bruce, M.C., et al., Cross-species interactions between malaria parasites in humans. Science, 2000. 287(5454): p. 845-848.

32. Fujioka, H. and M. Aikawa, The malaria parasite and its lifecycle. Malaria: molecular and clinical aspects. First edition. Amsterdam: Harwood Academic Publishers, 1999: p. 21-36.

33. Antinori, S., et al., Biology of human malaria plasmodia including Plasmodium knowlesi. Mediterranean journal of hematology and infectious diseases, 2012. 4(1).

34. Rougeron, V., et al., A population genetic perspective on the origin, spread and adaptation of the human malaria agents Plasmodium falciparum and Plasmodium vivax. FEMS Microbiology Reviews, 2022. 46(1): p. fuab047.

35. Douglas, R.G., et al., Inter-subunit interactions drive divergent dynamics in mammalian and Plasmodium actin filaments. PLoS biology, 2018. 16(7): p. e2005345.

36. Cowman, A.F., et al., Malaria: biology and disease. Cell, 2016. 167(3): p. 610-624.

37. Ejigiri, I. and P. Sinnis, Plasmodium sporozoite–host interactions from the dermis to the hepatocyte. Current opinion in microbiology, 2009. 12(4): p. 401-407.

38. Tavares, J., et al., Role of host cell traversal by the malaria sporozoite during liver infection. The Journal of experimental medicine, 2013. 210(5): p. 905.

39. Pasternak, N.D. and R. Dzikowski, PfEMP1: an antigen that plays a key role in the pathogenicity and immune evasion of the malaria parasite Plasmodium falciparum. The international journal of biochemistry & cell biology, 2009. 41(7): p. 1463-1466.

40. Gomes, P.S., et al., Immune escape strategies of malaria parasites. Frontiers in microbiology, 2016. 7: p. 1617.

41. Gomes, A.P., et al., Severe Plasmodium falciparum malaria. Revista brasileira de terapia intensiva, 2011. 23: p. 358-369.

42. Gao, X., et al., Triggers of key calcium signals during erythrocyte invasion by Plasmodium falciparum. Nature communications, 2013. 4(1): p. 2862.

43. Crosnier, C., et al., Basigin is a receptor essential for erythrocyte invasion by Plasmodium falciparum. Nature, 2011. 480(7378): p. 534-537.

44. Volz, J.C., et al., Essential role of the PfRh5/PfRipr/CyRPA complex during Plasmodium falciparum invasion of erythrocytes. Cell host & microbe, 2016. 20(1): p. 60-71.

45. Weiss, G.E., et al., Revealing the sequence and resulting cellular morphology of receptor-ligand interactions during Plasmodium falciparum invasion of erythrocytes. PLoS pathogens, 2015. 11(2): p. e1004670.

46. Besteiro, S., J.F. Dubremetz, and M. Lebrun, The moving junction of apicomplexan parasites: a key structure for invasion. Cellular microbiology, 2011. 13(6): p. 797-805.

47. Riglar, D.T., et al., Super-resolution dissection of coordinated events during malaria parasite invasion of the human erythrocyte. Cell host & microbe, 2011. 9(1): p. 9-20.

48. Collins, C.R., et al., Malaria parasite cGMP-dependent protein kinase regulates blood stage merozoite secretory organelle discharge and egress. PLoS pathogens, 2013. 9(5): p. e1003344.

49. Das, S., et al., Processing of Plasmodium falciparum merozoite surface protein MSP1 activates a spectrin-binding function enabling parasite egress from RBCs. Cell host & microbe, 2015. 18(4): p. 433-444.

50. Warrell, D.A., Clinical features of malaria, in Essential Malariology, 4Ed. 2017, CRC Press. p. 191-205.

51. Garcia, C.R., R.P. Markus, and L. Madeira, Tertian and quartan fevers: temporal regulation in malarial infection. Journal of biological rhythms, 2001. 16(5): p. 436-443.

52. Rathore, D., et al., Antimalarial drugs: current status and new developments. Expert opinion on investigational drugs, 2005. 14(7): p. 871-883.

53. Cui, L. and X.-z. Su, Discovery, mechanisms of action and combination therapy of artemisinin. Expert review of anti-infective therapy, 2009. 7(8): p. 999-1013.

54. Eastman, R.T. and D.A. Fidock, Artemisinin-based combination therapies: a vital tool in efforts to eliminate malaria. Nature Reviews Microbiology, 2009. 7(12): p. 864-874.

55. Chinappi, M., et al., On the mechanism of chloroquine resistance in Plasmodium falciparum. PloS one, 2010. 5(11): p. e14064.

56. Krogstad, D.J., et al., Efflux of chloroquine from Plasmodium falciparum: mechanism of chloroquine resistance. Science, 1987. 238(4831): p. 1283-1285.

57. Achan, J., et al., Quinine, an old anti-malarial drug in a modern world: role in the treatment of malaria. Malaria journal, 2011. 10: p. 1-12.

58. Bateman, D. and E. Dyson, Quinine toxicity. Adverse drug reactions and acute poisoning reviews, 1986. 5(4): p. 215-233.

59. Okombo, J., et al., Update on genetic markers of quinine resistance in Plasmodium falciparum. Molecular and biochemical parasitology, 2011. 177(2): p. 77-82.

60. Sidhu, A.B.S., S.G. Valderramos, and D.A. Fidock, pfmdr1 mutations contribute to quinine resistance and enhance mefloquine and artemisinin sensitivity in Plasmodium falciparum. Molecular microbiology, 2005. 57(4): p. 913-926.

61. Ashley, E.A., J. Recht, and N.J. White, Primaquine: the risks and the benefits. Malaria journal, 2014. 13: p. 1-7.

62. Vale, N., R. Moreira, and P. Gomes, Primaquine revisited six decades after its discovery. European journal of medicinal chemistry, 2009. 44(3): p. 937-953.

63. Howes, R.E., et al., G6PD deficiency: global distribution, genetic variants and primaquine therapy. Advances in parasitology, 2013. 81: p. 133-201.

64. Nsanzabana, C., Resistance to artemisinin combination therapies (ACTs): do not forget the partner drug! Tropical medicine and infectious disease, 2019. 4(1): p. 26.

65. van der Pluijm, R.W., et al., Triple artemisinin-based combination therapies for malaria–a new paradigm? Trends in parasitology, 2021. 37(1): p. 15-24.

66. Organization, W.H., Artemisinin and artemisinin-based combination therapy resistance: status report, 2016, World Health Organization.

67. Hamilton, W.L., et al., Evolution and expansion of multidrug-resistant malaria in southeast Asia: a genomic epidemiology study. The Lancet Infectious Diseases, 2019. 19(9): p. 943-951.

68. Bannister-Tyrrell, M., et al., Forest goers and multidrug-resistant malaria in Cambodia: an ethnographic study. The American journal of tropical medicine and hygiene, 2019. 100(5): p. 1170.

69. Chhibber-Goel, J. and A. Sharma, Profiles of Kelch mutations in Plasmodium falciparum across South Asia and their implications for tracking drug resistance. International Journal for Parasitology: Drugs and Drug Resistance, 2019. 11: p. 49-58.

70. Molina-Cruz, A. and C. Barillas-Mury, The remarkable journey of adaptation of the Plasmodium falciparum malaria parasite to New World anopheline mosquitoes. Memórias do Instituto Oswaldo Cruz, 2014. 109: p. 662-667.

71. Duffy, P.E. and J. Patrick Gorres, Malaria vaccines since 2000: progress, priorities, products. npj Vaccines, 2020. 5(1): p. 48.

72. Skwarczynski, M., et al., Progress in the development of subunit vaccines against malaria. Vaccines, 2020. 8(3): p. 373.

73. Valderramos, S.G. and D.A. Fidock, Transporters involved in resistance to antimalarial drugs. Trends in pharmacological sciences, 2006. 27(11): p. 594-601.

74. Sharma, A. and U.S. Sharma, Liposomes in drug delivery: progress and limitations. International journal of pharmaceutics, 1997. 154(2): p. 123-140.

75. Peeters, P.A., et al., Chloroquine blood levels after administration of the liposome-encapsulated drug in relation to therapy of murine malaria. Pharmaceutical research, 1989. 6: p. 787-793.

76. Aderibigbe, B.A., Design of drug delivery systems containing artemisinin and its derivatives. Molecules, 2017. 22(2): p. 323.

77. Veronese, F.M. and G. Pasut, PEGylation, successful approach to drug delivery. Drug discovery today, 2005. 10(21): p. 1451-1458.

78. Ma, Y., et al., Enhanced antimalarial activity by a novel artemether-lumefantrine lipid emulsion for parenteral administration. Antimicrobial Agents and chemotherapy, 2014. 58(10): p. 5658-5665.

79. Attama, A.A., et al., Solid lipid nanoparticles encapsulating a fluorescent marker (coumarin 6) and antimalarials–artemether and lumefantrine: evaluation of cellular uptake and antimalarial activity. European Journal of Nanomedicine, 2016. 8(3): p. 129-138.

80. Dwivedi, P., et al., Preparation and characterization of solid lipid nanoparticles of antimalarial drug arteether for oral administration. Journal of biomaterials and tissue engineering, 2014. 4(2): p. 133-137.

81. Umeyor, C.E., et al., Development insights of surface modified lipid nanoemulsions of dihydroartemisinin for malaria chemotherapy: characterization, and in vivo antimalarial evaluation. Recent Patents on Biotechnology, 2019. 13(2): p. 149-165.

82. Michels, L.R., et al., Effects of surface characteristics of polymeric nanocapsules on the pharmacokinetics and efficacy of antimalarial quinine. International Journal of Nanomedicine, 2019: p. 10165-10178.

83. Gomes, G.S., et al., Optimization of curcuma oil/quinine-loaded nanocapsules for malaria treatment. AAPS PharmSciTech, 2018. 19: p. 551-564.

84. Tagami, T., et al., Evaluation of phosphatidylserine-specific peptide-conjugated liposomes using a model system of malaria-infected erythrocytes. Biological and Pharmaceutical Bulletin, 2015. 38(10): p. 1649-1651.

85. Moles, E., et al., Immunoliposome-mediated drug delivery to Plasmodium-infected and non-infected red blood cells as a dual therapeutic/prophylactic antimalarial strategy. Journal of Controlled Release, 2015. 210: p. 217-229.

86. Marques, J., Exploration of sulfated polysaccharides as antimalarials and as targeting molecules for nanovector-mediated drug delivery to Plasmodium-infected cells. 2015.

87. Cohen, J., et al., From the circumsporozoite protein to the RTS, S/AS candidate vaccine. Human vaccines, 2010. 6(1): p. 90-96.

88. Moorthy, V.S. and W.R. Ballou, Immunological mechanisms underlying protection mediated by RTS, S: a review of the available data. Malaria journal, 2009. 8: p. 1-7.

89. Casares, S., T.-D. Brumeanu, and T.L. Richie, The RTS, S malaria vaccine. Vaccine, 2010. 28(31): p. 4880-4894.

90. Kurtovic, L., et al., Antibody mechanisms of protection against malaria in RTS, S-vaccinated children: a post-hoc serological analysis of phase 2 trial. The Lancet Microbe, 2024.

91. Nadeem, A.Y., et al., Mosquirix™ RTS, S/AS01 vaccine development, immunogenicity, and efficacy. Vaccines, 2022. 10(5): p. 713.

92. Penny, M.A., et al., Public health impact and cost-effectiveness of the RTS, S/AS01 malaria vaccine: a systematic comparison of predictions from four mathematical models. The Lancet, 2016. 387(10016): p. 367-375.

93. Zavala, F., RTS, S: the first malaria vaccine. The Journal of clinical investigation, 2022. 132(1).

94. Hammershaimb, E.A. and A.A. Berry, Pre-erythrocytic malaria vaccines: RTS, S, R21, and beyond. Expert Review of Vaccines, 2024. 23(1): p. 49-52.

95. Datoo, M.S., et al., Safety and efficacy of malaria vaccine candidate R21/Matrix-M in African children: a multicentre, double-blind, randomised, phase 3 trial. The Lancet, 2024. 403(10426): p. 533-544.

96. Schmit, N., et al., The public health impact and cost-effectiveness of the R21/Matrix-M malaria vaccine: a mathematical modelling study. The Lancet Infectious Diseases, 2024. 24(5): p. 465-475.

97. Laurens, M.B., RTS, S/AS01 vaccine (Mosquirix™): an overview. Human vaccines & immunotherapeutics, 2020. 16(3): p. 480-489.

98. Arunachalam, P.S., et al., A comparative immunological assessment of multiple clinical-stage adjuvants for the R21 malaria vaccine in nonhuman primates. Science Translational Medicine, 2024. 16(758): p. eadn6605.

99. Datoo, M.S., et al., Efficacy of a low-dose candidate malaria vaccine, R21 in adjuvant Matrix-M, with seasonal administration to children in Burkina Faso: a randomised controlled trial. The Lancet, 2021. 397(10287): p. 1809-1818.

100. Graves, P.M., H. Gelband, and C.I.D. Group, Vaccines for preventing malaria. Cochrane Database of Systematic Reviews, 1996. 2006(3).

101. Mabey, D., A. Brown, and B. Greenwood, Plasmodium falciparum malaria and Salmonella infections in Gambian children. The Journal of infectious diseases, 1987. 155(6): p. 1319-1321.

102. Mackenzie, G., et al., A decline in the incidence of invasive non-typhoidal Salmonella infection in The Gambia temporally associated with a decline in malaria infection. PloS one, 2010. 5(5): p. e10568.

103. Wilairatana, P., et al., The prevalence of malaria and bacteremia co-infections among febrile patients: a systematic review and meta-analysis. Tropical medicine and infectious disease, 2022. 7(9): p. 243.

104. Cunnington, A.J., et al., Identification and management of co-infections in people with malaria. bmj, 2024. 384.

105. Salam, N., et al., Global prevalence and distribution of coinfection of malaria, dengue and chikungunya: a systematic review. BMC public health, 2018. 18: p. 1-20.

106. Cummings, L.A., B.L. Deatherage, and B.T. Cookson, Adaptive immune responses during Salmonella infection. EcoSal Plus, 2009. 3(2): p. 10.1128/ecosalplus. 8.8. 11.

107. Long, C.A. and F. Zavala, Immune responses in malaria. Cold Spring Harbor perspectives in medicine, 2017. 7(8): p. a025577.

108. Dassah, S.D., et al., Co-infection of Plasmodium falciparum and Schistosoma mansoni is associated with anaemia. Malaria Journal, 2023. 22(1): p. 272.

109. Afolabi, M.O., et al., Prevalence and distribution pattern of malaria and soil-transmitted helminth co-endemicity in sub-Saharan Africa, 2000–2018: A geospatial analysis. PLoS neglected tropical diseases, 2022. 16(9): p. e0010321.

110. Motran, C.C., et al., Helminth infections: recognition and modulation of the immune response by innate immune cells. Frontiers in immunology, 2018. 9: p. 664.

111. Lee, S.C. and O.O. Oyesola, Effects of helminths on the human immune response and the microbiome. Mucosal Immunology, 2022. 15(6): p. 1224-1233.

112. Costa-da-Silva, A.C., et al., Immune responses in leishmaniasis: an overview. Tropical medicine and infectious disease, 2022. 7(4): p. 54.

113. Pinna, R.A., et al., Malaria-cutaneous leishmaniasis co-infection: influence on disease outcomes and immune response. Frontiers in Microbiology, 2016. 7: p. 982.

114. Ghimire, P.G., et al., A case report of visceral leishmaniasis and malaria co-infection with pancytopenia and splenomegaly-a diagnostic challenge. BMC Infectious Diseases, 2019. 19: p. 1-3.

115. Onyilagha, C. and J.E. Uzonna, Host immune responses and immune evasion strategies in African trypanosomiasis. Frontiers in immunology, 2019. 10: p. 2738.

116. Kotepui, K.U., et al., Prevalence and outcomes of malaria as co-infection among patients with human African trypanosomiasis: a systematic review and meta-analysis. Scientific reports, 2021. 11(1): p. 23777.

117. Roberds, A., et al., Longitudinal impact of asymptomatic malaria/HIV-1 co-infection on Plasmodium falciparum gametocyte transcript expression and transmission to Anopheles mosquitoes. Frontiers in Cellular and Infection Microbiology, 2022. 12: p. 934641.

118. Mahittikorn, A., et al., A meta-analysis on the prevalence and characteristics of severe malaria in patients with Plasmodium spp. and HIV co-infection. Scientific Reports, 2021. 11(1): p. 16655.

119. Figueroa-Romero, A., et al., Uncovering HIV and malaria interactions: the latest evidence and knowledge gaps. The Lancet HIV, 2024.

120. Grimwade, K., et al., HIV infection as a cofactor for severe falciparum malaria in adults living in a region of unstable malaria transmission in South Africa. Aids, 2004. 18(3): p. 547-554.

121. Nasir, I.A., S.a. Yakubu, and J.O. Mustapha, Epidemiology and synergistic hepatopathology of malaria and hepatitis C virus coinfection. Virology: Research and Treatment, 2017. 8: p. 1178122X17724411.

122. Anabire, N.G., et al., Impact of malaria and hepatitis B co-infection on clinical and cytokine profiles among pregnant women. PloS one, 2019. 14(4): p. e0215550.

123. Jahiel, R.I., et al., Anti-malarial effect of interferon inducers at different stages of development of Plasmodium berghei in the mouse. Nature, 1968. 220(5168): p. 710-711.

124. Herman, R., T. Shiroishi, and C.E. Buckler, Viral interference with exoerythrocytic forms of malaria (Plasmodium gallinaceum) in ovo. Journal of Infectious Diseases, 1973. 128(2): p. 148-155.

125. Wagner, R., M. Matrosovich, and H.D. Klenk, Functional balance between haemagglutinin and neuraminidase in influenza virus infections. Reviews in medical virology, 2002. 12(3): p. 159-166.

126. Aguilar, H.C., et al., Paramyxovirus glycoproteins and the membrane fusion process. Current clinical microbiology reports, 2016. 3: p. 142-154.

127. Ganar, K., et al., Newcastle disease virus: current status and our understanding. Virus research, 2014. 184: p. 71-81.

128. Merino, R., et al., Comparison of the virulence of pathogenic Newcastle disease viruses belonging to the same or different genotypes. Int J Poult Sci, 2011. 10(9): p. 713-20.

129. Gravel, K.A. and T.G. Morrison, Interacting domains of the HN and F proteins of Newcastle disease virus. Journal of Virology, 2003. 77(20): p. 11040-11049.

130. Huang, Z., et al., The hemagglutinin-neuraminidase protein of Newcastle disease virus determines tropism and virulence. Journal of virology, 2004. 78(8): p. 4176-4184.

131. Sánchez-Felipe, L., E. Villar, and I. Muñoz-Barroso, α2-3-and α2-6-N-linked sialic acids allow efficient interaction of Newcastle Disease Virus with target cells. Glycoconjugate journal, 2012. 29: p. 539-549.

132. Iorio, R.M., et al., Structural and functional relationship between the receptor recognition and neuraminidase activities of the Newcastle disease virus hemagglutinin-neuraminidase protein: receptor recognition is dependent on neuraminidase activity. Journal of virology, 2001. 75(4): p. 1918-1927.

133. Yuan, P., et al., Structure of the Newcastle disease virus hemagglutinin-neuraminidase (HN) ectodomain reveals a four-helix bundle stalk. Proceedings of the National Academy of Sciences, 2011. 108(36): p. 14920-14925.

134. Swanson, K., et al., Structure of the Newcastle disease virus F protein in the post-fusion conformation. Virology, 2010. 402(2): p. 372-379.

135. Cantin, C., et al., Newcastle disease virus may enter cells by caveolae-mediated endocytosis. Journal of general virology, 2007. 88(2): p. 559-569.

136. Schirrmacher, V., Molecular mechanisms of anti-neoplastic and immune stimulatory properties of oncolytic Newcastle disease virus. Biomedicines, 2022. 10(3): p. 562.

137. Sinkovics, J.G. and J.C. Horvath, Newcastle disease virus (NDV): brief history of its oncolytic strains. Journal of clinical virology, 2000. 16(1): p. 1-15.

138. Tayeb, S., Z. Zakay-Rones, and A. Panet, Therapeutic potential of oncolytic Newcastle disease virus: a critical review. Oncolytic virotherapy, 2015: p. 49-62.

139. DiNapoli, J.M., et al., Respiratory tract immunization of non-human primates with a Newcastle disease virus-vectored vaccine candidate against Ebola virus elicits a neutralizing antibody response. Vaccine, 2010. 29(1): p. 17-25.

140. Ge, J., et al., Newcastle disease virus-based live attenuated vaccine completely protects chickens and mice from lethal challenge of homologous and heterologous H5N1 avian influenza viruses. Journal of virology, 2007. 81(1): p. 150-158.

141. Lawrence, T.M., et al., Comparison of heterologous prime-boost strategies against human immunodeficiency virus type 1 Gag using negative stranded RNA viruses. PloS one, 2013. 8(6): p. e67123.

142. Nakaya, Y., et al., Induction of cellular immune responses to simian immunodeficiency virus gag by two recombinant negative-strand RNA virus vectors. Journal of virology, 2004. 78(17): p. 9366-9375.

143. Khattar, S.K., et al., Evaluation of humoral, mucosal, and cellular immune responses following co-immunization of HIV-1 Gag and Env proteins expressed by Newcastle disease virus. Human Vaccines & Immunotherapeutics, 2015. 11(2): p. 504-515.

144. Khattar, S.K., et al., Comparative immunogenicity of HIV-1 gp160, gp140 and gp120 expressed by live attenuated newcastle disease virus vector. PloS one, 2013. 8(10): p. e78521.

145. Martinez-Sobrido, L., et al., Protection against respiratory syncytial virus by a recombinant Newcastle disease virus vector. Journal of virology, 2006. 80(3): p. 1130-1139.

146. Bukreyev, A., et al., Recombinant Newcastle disease virus expressing a foreign viral antigen is attenuated and highly immunogenic in primates. Journal of virology, 2005. 79(21): p. 13275-13284.

147. DiNapoli, J.M., et al., Newcastle disease virus, a host range-restricted virus, as a vaccine vector for intranasal immunization against emerging pathogens. Proceedings of the National Academy of Sciences, 2007. 104(23): p. 9788-9793.

Chapter 2

Purification of NDV particles from culture lysate using Anion Exchange Chromatography

*The contents of this chapter are published as "**Neog, S., Kumar, S., & Trivedi, V.** (2023). **Isolation and characterization of Newcastle disease virus from biological fluids using column chromatography.** Biomedical Chromatography, 37(1), e5527."

Summary

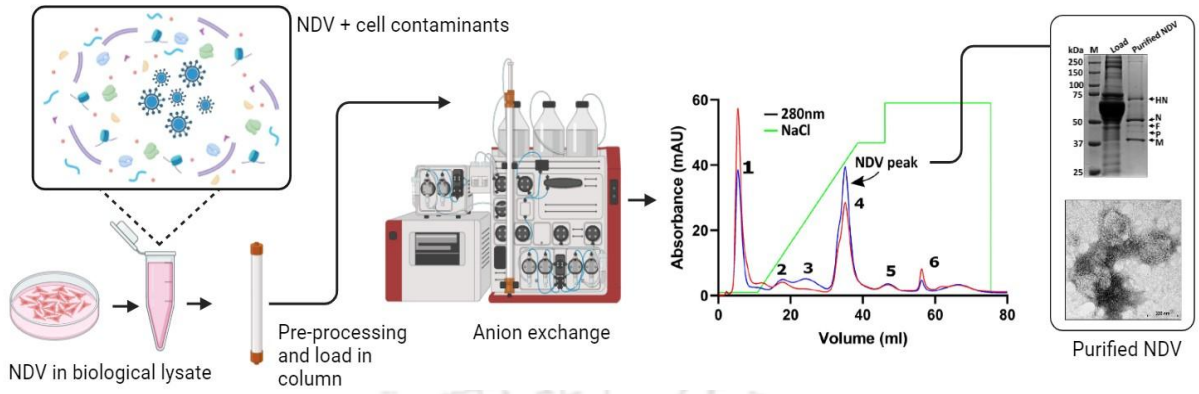

Newcastle disease virus (NDV), classified within the avian orthoavulavirus 1 species, genus Orthoavulavirus, and family Paramyxoviridae, causes Newcastle disease in various avian species. Apart from its pathogenic effects, NDV has garnered attention for its potential applications in oncolytic therapy and as a vector for vaccine delivery. In our study, the virus was used for co-infection studies with *Plasmodium falciparum*, which demanded a very high purity of the virus, devoid of cellular contaminants. Traditionally, NDV is purified from infected biological sera with the help of density gradient ultracentrifugation. However, it has several drawbacks such as a longer processing time and limited sample capacity. We employed a column chromatography method for a simpler single-step purification of the virus from infected cell lysate while preventing the addition of any added contaminants. Native agarose gel electrophoresis and dynamic light scattering (DLS) revealed that the virus carried a net negative surface charge. Thus, we employed a HiTrap Q Sepharose Fast Flow (QFF) anion exchange column with salt elution to purify the virus. Hemagglutination assay (HA) and plaque assay highlighted the efficacy of this approach which yields high-purity NDV particles with over 80% recovery. Confirmation of virus purity was achieved through sodium dodecyl sulfate-polyacrylamide gel electrophoresis (SDS-PAGE) and Western blot analysis. The hydrodynamic volume and 'dry state' diameter measurements with dynamic light scattering and transmission electron microscopy suggested that the purified virus was physically intact. Infectivity of the purified virus was also tested with *in ovo* studies and was found to be similar to the crude virus. Furthermore, detection of the virus genome was done by amplifying a 423-bp region using a reverse transcription-polymerase chain reaction. Our findings offer a simple but efficient procedure for isolating pure NDV from infected biological fluid for further experimentation.

2.1 Introduction

High-purity virus particles must be obtained to mitigate the effect of any host cellular impurities in the viral preparations before testing the Newcastle disease virus (NDV) against the malaria parasite. NDV is propagated in mammalian cells or allantoic fluid and is typically purified with ultracentrifugation involving a density gradient of sucrose [1]. NDV-enriched allantoic fluid or cell lysate is initially pre-cleared from cell debris by low-speed centrifugation, followed by single or multiple rounds of gradient ultracentrifugation to concentrate and purify the virus. Studies have shown that chromatographic methods offer a simpler but efficient way to isolate viruses from host contaminants as an alternative to classical methods of virus purification. Burova and Iofee have reviewed both the classical methods, such as density gradient centrifugation, and chromatographic methods, such as anion exchange, gravity-flow columns, affinity columns, and others for purification of recombinant adenoviral and adeno-associated viral vectors [2]. Purification of adeno-associated virus using metal affinity chromatography was described by James et al. (2016). Hydrophobic interaction chromatography was used successfully for influenza A and B viruses and foot and mouth disease viruses [3, 4]. Tavern and Wildy showed the purification of the herpes simplex virus using calcium phosphate columns [5]. Wolff et al. described the purification of modified vaccinia ankara virus using pseudo-affinity membrane adsorbers and hydrophobic interaction chromatography [6]. In addition, size exclusion chromatography has been used as a standalone or supplemental step during viral purification [7, 8]. However, there is limited literature on the use of column chromatography for the purification of NDV.

We tested anion exchange chromatography as a single-step protocol for separating NDV from host cellular contaminants. Initially, virus preparations from the host cells were subjected to native agarose gel electrophoresis followed by electroelution, where the NDV particles were detected with the help of hemagglutination assay (HA) and hemagglutination inhibition assay (HIA). The virus particles showed strong mobility towards the positive electrode, which suggested that they carried a net negative charge. Considering this observation, NDV was purified with a HiTrap QFF anion exchange column and eluted with a gradient of NaCl. The viral peak in the chromatogram was identified with the help of HA and plaque assay. Over 80% of the virus particles that were loaded in the column were found to be recovered. SDS-PAGE and western blot analysis showed that the virus particles obtained were of very high purity. To verify the physical integrity of the purified virus particles, the hydrodynamic volume and charge were calculated with the help of Dynamic Light Scattering

(DLS). The hydrodynamic volume was found to be around 350 nm, while the particles were found to carry a net negative charge. Transmission Electron Microscopy (TEM) was used to calculate the dry-state diameter and physical integrity of the purified virus particles. The purified NDV was found to be within the range of 200-300 nm in diameter, as previously described [9]. The replicative potential of the purified virus was also tested by allowing it to proliferate in the allantoic fluid. Both the crude and purified NDV showed similar infectivity in allantoic fluid and hence deduced to be functionally active. Finally, a diagnostic PCR test was run to confirm that the viruses packaged a viable genome. As a result, anion exchange chromatography was found to be very effective in isolating NDV particles from the host cellular contaminants.

2.2 Experimental procedures

2.2.1 Cells and Viruses

NDV Lasota vaccination strain, procured from Indoma Marine Private Ltd, Guwahati, Assam (Indovax Pvt. Ltd. Hissar, Haryana, India), and NDV R_2B was grown in baby hamster kidney (BHK-21) cells, maintained in Dulbecco's Modified Eagle's Medium (DMEM, Gibco, 12100-061, NY, USA), supplemented with 10% fetal bovine serum (FBS) (Himedia, RM9955-500ML, Mumbai, India) and antibiotics at 37°C under 5% CO_2. Post-infection, the virus from the infected cells was harvested with the freeze and thaw method followed by passing the lysate through a narrow-gauze syringe several times, to ensure complete lysis of the cells. The viral titer in the lysates was quantified by HA and plaque assay, and stored at -80°C for further analysis.

2.2.2 Chicken red blood cells

Chicken whole blood was collected in tubes with Ethylenediaminetetraacetic acid (EDTA) and centrifuged at 1500 rpm for 10 min. The plasma and the buffy layer were carefully removed using Pasteur pipettes followed by extensive washing of the RBCs with PBS. For HA, a 1% RBC solution was obtained by suspending the pelleted RBCs in PBS at the appropriate volume.

2.2.3 Embryonated chicken eggs

Nine-day specified pathogen-free (SPF) embryonated chicken eggs were purchased from Lotus Chicks' Hatchery, Guwahati, Assam, India and maintained at 37°C and 60% humidity. The eggs were candled to ensure that the embryos were in a viable state. The air sac was located, and the chorioallantoic membrane was outlined. The position of the head of the embryo was

noted, and an injection point opposite to it was marked for each egg. The eggs were then used for propagating different viral fractions in the allantoic fluid.

2.2.4 Agarose gel electrophoresis of NDV

NDV-enriched BHK-21 lysate (200 µl) was incubated with 0.5 µg/ml of EtBr for 1 h and loaded onto a 0.5% agarose gel slab run at 100 V for 1 h. The contents of the lanes were electro-eluted from the excised gel blocks in separate dialysis bags containing 1 ml of PBS for 1 h at 100 V. HA, hemagglutination inhibition assay (HIA), and plaque assay were performed to detect the presence of the virus.

2.2.5 Anion exchange chromatography

Cell lysate (1 ml) containing the virus was loaded on a HiTrap QFF (5 ml) column connected to an FPLC system (AKTA pure, GE Healthcare, Chicago, IL, USA). The flow rate was maintained at 0.5 ml/min for all the operations, and absorbance at 260 and 280 nm was recorded. The column was washed and equilibrated with 10 ml or two column volumes of PBS (pH 7.4). After the sample was injected, the column was washed with 10 ml or two column volumes of PBS (pH 7.4) to remove the unbound fraction. An initial NaCl gradient (0 - 0.7 M) was used to elute the bound fraction. It was followed by 1 M NaCl elution to remove any proteins interacting very strongly with the matrix. Fractions of 1 ml were collected from the injection point to the end point of elution. All the fractions were tested for the virus using HA. Fractions showing HA activity were subsequently analyzed using plaque assay.

2.2.6 HA and HIA

HA was performed to confirm the presence of NDV, as described previously [10] . Briefly, a two-fold serial dilution of the analyte (50 µl) and the controls was prepared with PBS across the wells, and 50 µl of chicken RBCs (1%) was pipetted into each well to make a 100 µl reaction volume. The plate was left undisturbed for 15–30 min and checked for hemagglutination. The viral titer was expressed as HA units. For HIA, the mouse monoclonal anti-HN antibody (Santa Cruz Biotechnology, sc-53562, Texas, USA) was used. A two-fold dilution of the antibody starting from 1:25 (antibody: PBS) was prepared across a V-bottom plate and incubated with 4 HA units of the crude and purified virus. The HIA titer of the antibody was expressed as the highest dilution at which hemagglutination of the two fractions was inhibited.

2.2.7 Plaque assay

A monolayer of BHK 21 cells was used for plaque assay, as described previously [11]. Briefly, BHK 21 cells were seeded on a 12-well cell culture plate at a confluency of 80–90% and kept overnight for adhesion, followed by incubation with 0.4 ml of NDV dilutions in DMEM with 10% FBS for 1 h. The plates were gently rocked every 15 min to ensure proper spread over the monolayer. The infection media was removed, and the cells were washed thrice with PBS and gently overlaid with a pre-warmed solid medium (0.3% agarose plaque media). The cells were incubated at 37°C and 5% CO_2 for 48 h and fixed with 10% paraformaldehyde (PFA) for 30 min by directly overlaying it in the solid media. The solid agarose layer was removed using forceps, and the fixing solution was drained. The cells were washed with PBS and stained with 1% crystal violet solution for 15 min. The excess stain was then washed off, and the wells were allowed to dry before the visible plaques were counted.

2.2.8 Detection of NDV in fractions using immunoblotting

The crude NDV, load, and purified fractions of the virus, each 30 µl, were resolved in a 10% polyacrylamide gel at constant voltage, 80 V, for 2 h 30 min under denaturing conditions. The gel was stained with Coomassie Brilliant Blue R-250 (MB153-25G, Himedia, Mumbai, India), and the protein bands were visualized and captured using an imaging station (Chemidoc™ MP Imaging system, Bio-Rad, California, USA). In a separate 10% polyacrylamide gel, 40 µl of each load and the purified NDV fractions were resolved and stained with Coomassie to visualize the bands. An identical gel was used to transfer the identified proteins onto a polyvinylidene fluoride (PVDF) membrane using a Trans-BlotR Turbo™ (Bio-Rad, Singapore) system, blocked with 5% bovine serum albumin (BSA), probed with chicken polyclonal anti-NDV antibody (raised in-house) [12] at a dilution of 1: 20,000, and detected with goat anti-chicken horseradish peroxidase (HRP) (Southern Biotech, 6100-05, Birmingham, Alabama, USA) with 1: 5000 dilutions. Chemiluminescence was recorded using a ChemiDoc (Bio-Rad) imaging station.

2.2.9 Dynamic light scattering

The hydrodynamic size and the zeta potential of NDV were calculated for both the crude and purified NDV fractions using a DLS instrument (Zetasizer Nano ZS90, Malvern Instruments, Malvern, UK). Both the samples were precleared by centrifuging at 1500 g for 30 min to remove any cellular debris or aggregates and diluted with PBS to avoid multiple scattering. The particle size was recorded by the detection of the scattering light from a 632.8 nm laser

passing through the sample in a quartz cuvette at 175°. The zeta potential was measured by loading 0.9 ml of the diluted samples in a DTS1070 cuvette. The average value of five runs for each sample and the controls was calculated as the hydrodynamic size and zeta potential.

2.2.10 Transmission electron microscopy

Carbon-coated copper TEM grids were treated with 0.01% Poly-L lysine to render them hydrophilic. Anion exchange–purified NDV particles were adsorbed onto the dark side of the grids for 20 min. Any excess sample was blotted out. The grid was immediately stained with 0.2% uranyl acetate for 20 seconds, and the extra stain was blotted out. The grids were allowed to air-dry and later transferred to a desiccator and kept until analysis. Images were obtained using a JEOL-2100F field emission transmission electron microscope.

2.2.11 *In ovo* proliferation of purified NDV

Nine-day SPF eggs were prepared, as discussed earlier in Section 2.2.3. One group of eggs was inoculated with the purified NDV, and the other group was injected with the crude virus. A hole was made by punching the egg with a sterile needle at the point marked for injection earlier. It was used to inject both the crude and purified NDV with a 31-gauge needle and sealed with glue. The eggs were incubated at 37°C, and allantoic fluid was collected at 24, 48, and 72 h from each group, respectively. To collect the allantoic fluid, the apical end of the eggs was sterilized, and the eggshell was broken apart using a pair of sterile forceps. The chorioallantoic membrane was removed, and the allantoic fluid was collected using serological pipettes in 15-ml falcons, precleared by centrifuging at 1500 g for 20 min and then stored at –80°C for further analysis.

2.2.12 Diagnostic PCR test

To confirm that the purified virus grown in the allantoic fluid is NDV and carries a viable genome, a diagnostic PCR was performed using NDV-specific primers. RNA was isolated using Trizol, where 300 µl of allantoic fluid containing the virus was mixed with 1 ml of Trizol and agitated. The mixture was treated with 200 µl of ice-cold chloroform, mixed vigorously for 30 s, and incubated at room temperature for 2–3 min. The solution was centrifuged at 12,000 rpm for 10 min, and the aqueous phase was collected, followed by the addition of an equal volume of chloroform. The step was repeated four to five times, and the final aqueous phase was treated with an equal volume of isopropanol. The mixture was agitated gently for 10–15 seconds, incubated at room temperature for 10–15 min, and centrifuged at 12,000 rpm for 15

min. The pellet was washed with 75% ethanol at 14,000 rpm for 5 min. The ethanol was discarded, and the pellet was air-dried. It was suspended with 20 µl of nuclease-free water and then quantified with a nanodrop. The isolated RNA was used for complementary DNA (cDNA) synthesis using random hexamers. The cDNA obtained was used for amplifying a 423-bp NDV-specific product with the following primers: forward 5'-GCAGCTGCAGGGATTGTGGT-3' and reverse 5'-GGATGTTGGCRGCATTYTGGTTGGC-3'. Separate PCRs with primers for influenza (PR8) and JEV were also set up with the cDNA from the purified virus as controls to further confirm that the purified virus obtained was NDV and that no cross-contamination had occurred.

2.3 Results

2.3.1 The surface of NDV is negatively charged

To assess the overall surface charge of NDV particles, BHK-21 lysate containing the virus was subjected to electrophoresis on a 0.5% agarose gel, as outlined in section 2.2.4. The agarose gel was excised into three zones, as shown in **Figure 2.1 A**, after the run was completed. The agarose blocks were further subjected to electro-elution separately by packaging in dialysis bags containing 1 ml PBS. Upon HA analysis, NDV was detected in the zone corresponding to the second block out of the three gel sections that were excised (**Figure 2.1 A, B**). The HA titer of the NDV recovered from this process was determined to be 4 HA units, in contrast to the 32 HA units of the initially loaded virus, as indicated in **Figure 2.1 B**. The depletion in viral titer in the recovered sample could be because of two major factors. Firstly, the virus was electro-eluted in a greater volume (1 ml of PBS) as compared to the load (200 µl) and hence diluted. Second, a fraction of NDV could still be trapped inside the gel matrix, which did not get eluted from the gel during electro-elution.

To further validate that the electro-eluted fraction exhibiting HA activity is indeed comprised of NDV particles, an HIA was conducted using a specific monoclonal anti-HN antibody. As seen in **Figure 2.1 C**, the HA activity of both the crude and electro-eluted viruses was inhibited up to the 1:200 dilutions of the anti-HN antibody. The HIA result thus confirms that the electro-eluted virus was NDV. Since the virus migrates towards the positive electrode during electrophoresis, we hypothesized that the virus could carry a net negative charge which was further confirmed with the help of DLS analysis.

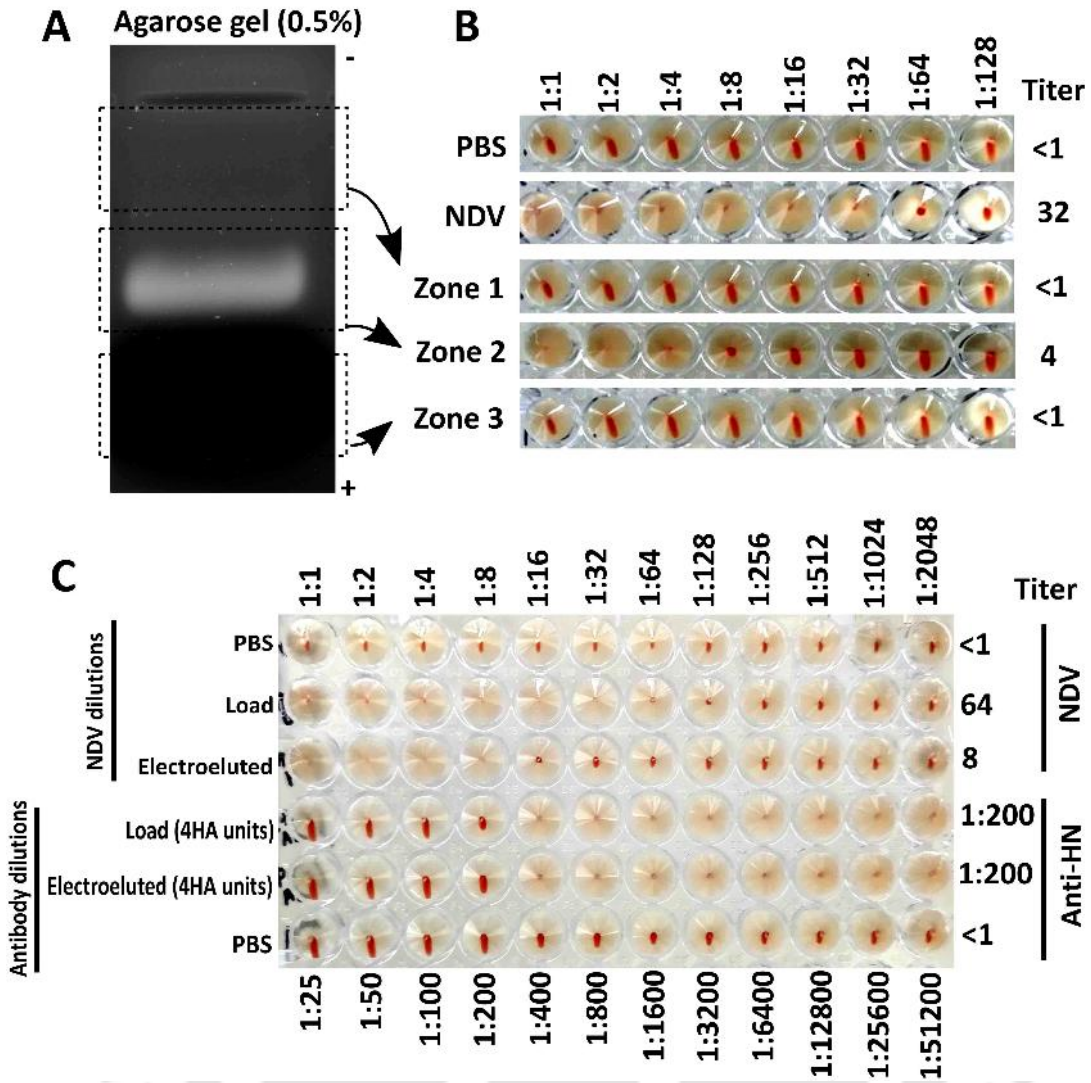

Figure 2.1: Agarose gel electrophoresis of NDV (Newcastle disease virus) particles shows that they carry an overall negative charge. (A) Agarose gel (0.5%) was cut into three zones (1, 2, and 3) and subjected to electro-elution separately. (B) HA (Hemagglutination Assay) showing NDV titers of the eluted fractions of the three zones. NDV was detected in zone 2. (C) HIA (Hemagglutination Inhibition Assay) of electro-eluted fraction from zone 2 of a separate gel, showed that the anti-HN antibody was able to inhibit hemagglutination of the virus up to 1:200 dilutions in both the crude and purified fractions. It can be concluded that the electro-eluted virus showing similar HIA titer with the control (crude NDV) is the NDV.

2.3.2 NDV can be effectively purified using an anion exchange column

Given the results from native agarose gel electrophoresis that the virus carried a negative surface charge, we employed the HiTrap QFF anion exchange column for the purification of NDV. BHK lysate containing NDV was pre-cleared with low-speed centrifugation as described previously and passed through a 0.22 µm syringe filter to remove any remaining cell debris. 1 ml of the lysate was loaded onto the anion exchange column. The unbound fraction was

collected for further analysis. The virus was eluted in a linear gradient of NaCl, from 0 mM to 700 mM M NaCl in 25 ml (rate of increase in NaCl gradient = 28 mM/ml). Following that, the column was washed with 700 mM NaCl for an additional two column volumes. A final elution step with 1 M NaCl was performed to elute any proteins that were strongly bound to the column. Several peaks from 0 to 30 ml were observed in the chromatogram, representing various cellular proteins separated from the viral fraction (**Figure 2.2 A**). Upon HA analysis of the peaks from 0 to 30 ml, they did not show any HA activity confirming that the virus was absent in these fractions. The HA analysis of the remaining fractions (30 to 80 ml) showed that the NDV particles were eluted in the fractions corresponding to peak 4 (**Figure 2.2 B**).

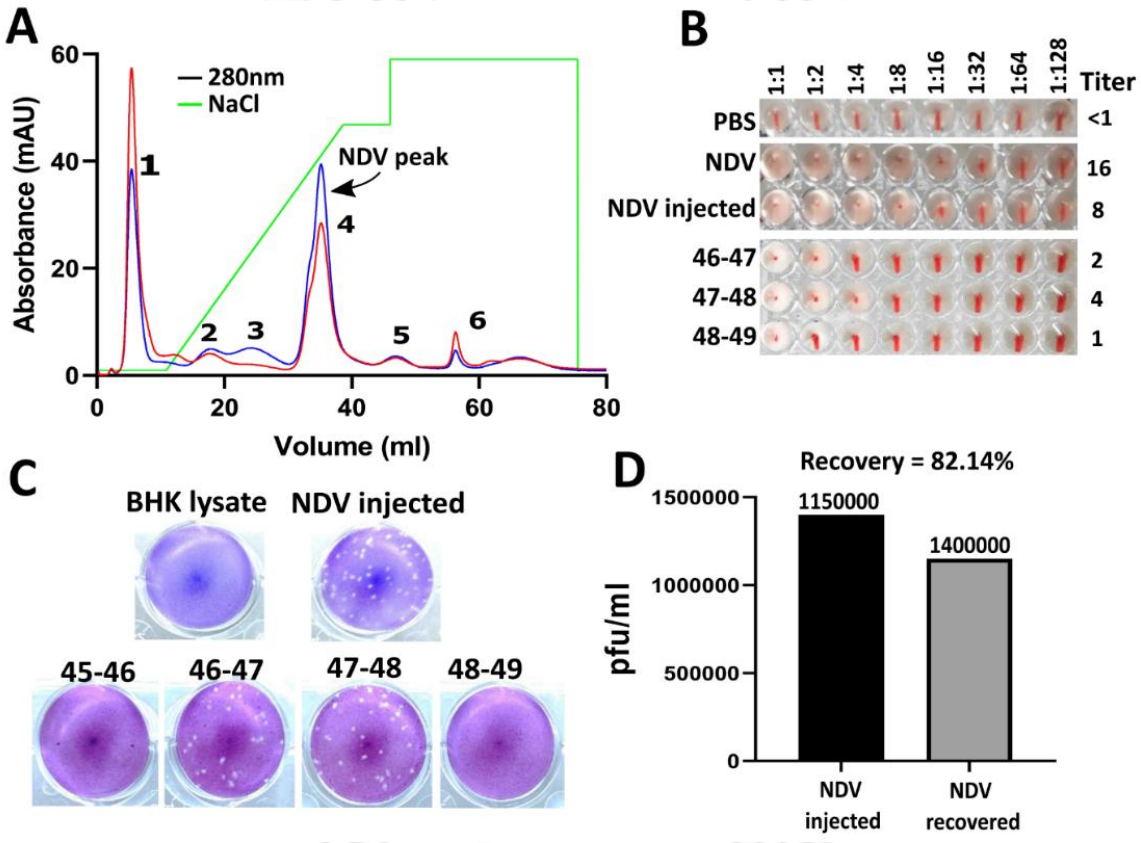

Figure 2.2: Purification of NDV with anion exchange chromatography. (A) Chromatogram showing that Peak 4 corresponds to the elution of NDV in a total 3 ml volume (fractions from 46 to 49 ml). (B) HA assay showing the hemagglutination pattern of the fractions of peak 4. (C) Plaque assay of the fractions where HA was detected. (D) Recovery (%) of the NDV was calculated from the titers observed in the plaque assay.

The fractions that showed HA activity were used to perform plaque assay for calculating the virus titer. Both the crude and the purified viral fractions of the same dilutions (10^{-5}) were used for the assay. As depicted in **Figures 2.2 C and D**, the analysis conducted through the plaque assay showed that 82.14% of the virus that was loaded in the column was recovered. The assay not only provided insights into the efficiency of NDV recovery but also served as an indication

that the anion exchange-purified NDV particles retained their infectivity potential as they could form plaques in monolayers of cells. However, further *in ovo* experiments were conducted to validate the observation.

2.3.3 NDV obtained after anion exchange chromatography were of high purity

To evaluate the purity of the virus particles, the fractions containing NDV were analyzed with SDS-PAGE and western blotting with specific antibodies.

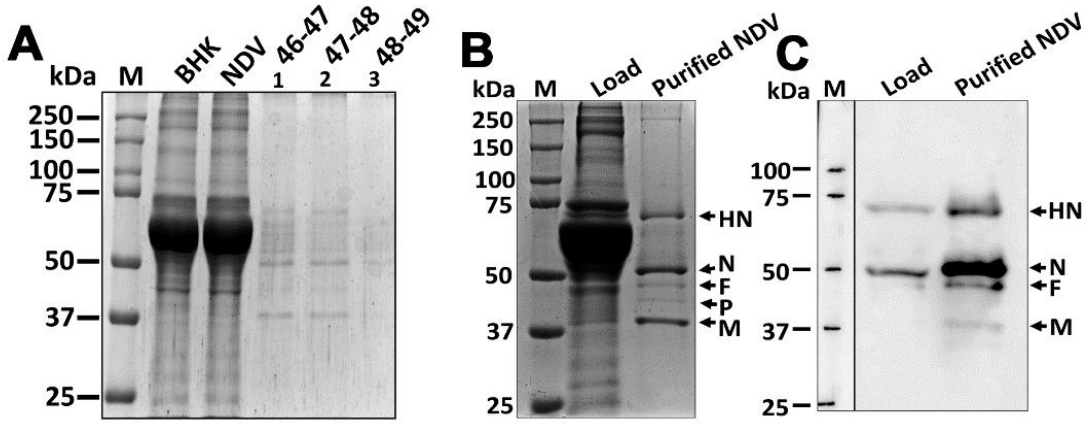

Figure 2.3: SDS-PAGE analysis and western blotting of purified NDV. (A and B) SDS-PAGE analysis of the purified virus fractions shows the five major NDV proteins: HN (72 kDa), N (55 kDa), F (52 k Da), P (42 kDa), and M (40 kDa). (C) Western blot detection of viral proteins with anti-NDV antibody shows that the purified virus is the NDV, and all the major bands observed in SDS-PAGE were of viral origin.

The fractions showing HA activity (46–49) were resolved on a 10% polyacrylamide gel under denaturing conditions (**Figure 2.3 A**). The SDS-PAGE analysis revealed that the virus fractions obtained after anion exchange chromatography were devoid of contaminating proteins from the cell lysate as the five major NDV proteins, namely HN (72 kDa), N (55 kDa), F (52 kDa), P (42 kDa), and M (40 kDa) were observed in the fractions (**Figure 2.3 B**). To validate the identity of these proteins, a western blot analysis of the fraction 47-48 was performed with the help of polyclonal anti-NDV antibody (**Figure 2.3 C**). It confirmed that the major bands seen in the SDS-PAGE were the NDV HN, N, F, and M proteins. Notably, no significant band other than those corresponding to NDV proteins was observed, thereby affirming the purity of the viral fractions.

2.3.4 The physical parameters of the purified virus particles were conserved

The interaction between NDV and the solid matrix of the anion exchange column and subsequent elution with high salt concentration might affect the physical integrity of the virus

particles. The purified viruses were therefore characterized using DLS and TEM. The hydrodynamic diameter of the precleared cell lysate without the virus was calculated to be 71.88 nm (**Figure 2.4 A**). The hydrodynamic diameter of the crude and purified NDV was found to be 395.8 nm and 353.2 nm, respectively (**Figure 2.4 A, ii, and iii**). However, it should be noted that the hydrodynamic diameter is a measurement of the solvated particles, and thus, the size of the virus particles might appear to be larger. To obtain the "dry state" measurement of the diameter of the particles, purified NDV was visualized and analyzed with the help of TEM.

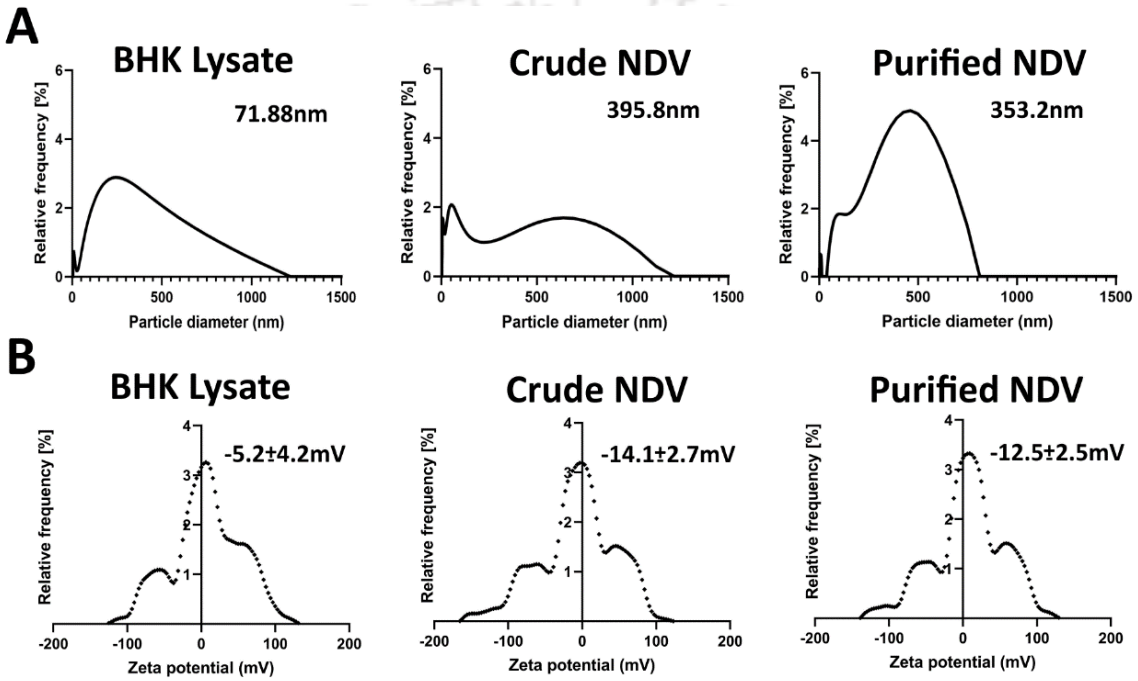

Figure 2.4: Hydrodynamic diameter and zeta potential of purified NDV were calculated using DLS. The hydrodynamic diameter is plotted as particle diameter (nm) versus relative frequency (%) of BHK lysate (A, i), crude NDV (A, ii), and purified NDV (A, iii). The zeta potential of the particles, plotted as zeta potential (mV) versus relative frequency (%), of BHK lysate (B, i), crude NDV (B, ii), and purified NDV (B, iii).

The zeta potential and electrophoretic mobility of NDV particles were also determined using DLS. It is widely accepted that particles with zeta potential values falling within the range of (-) 10 to (+) 10 mV are considered to be electrically neutral. Our findings revealed that the zeta potential of NDV particles before and after purification was (-) 14.1 ± 2.7 mV and (-) 12.5 ± 2.5 mV, respectively, indicating a weakly anionic character of the NDV particles (**Figure 2.4 B, ii and iii**). Additionally, the electrophoretic mobility of NDV particles before and after purification was calculated to be (-) $1x10^4$ cm^2/Vs and (-) $8.8x10^5$ cm^2/Vs, respectively. The results suggest that during electrophoresis, the NDV particles would migrate toward the

positive electrode. This migration behaviour was indeed observed in the native agarose gel electrophoresis of the virus. These findings collectively provide insights into the electro-kinetic properties of NDV particles and their behaviour under electric fields. Electron micrographs of the purified virus particles showed that the physical integrity of NDV was conserved after purification. We also measured the diameter of the particles from the micrographs which ranged from 200 to 300 nm (**Figure 2.5 A and B**). The majority of the particles observed were found to be intact, with a few disrupted virions associated with the nucleocapsid released from the particles (**Figure 2.5 C**). However, the majority of the virus particles were found to be intact in our TEM analysis. Overall, it suggests that the anion exchange–purified NDV particles were physically intact and pleomorphic as previously described. Considering these observations, the functional characteristics of the purified virus, such as its infective and replicative potential, are analysed as discussed hereafter.

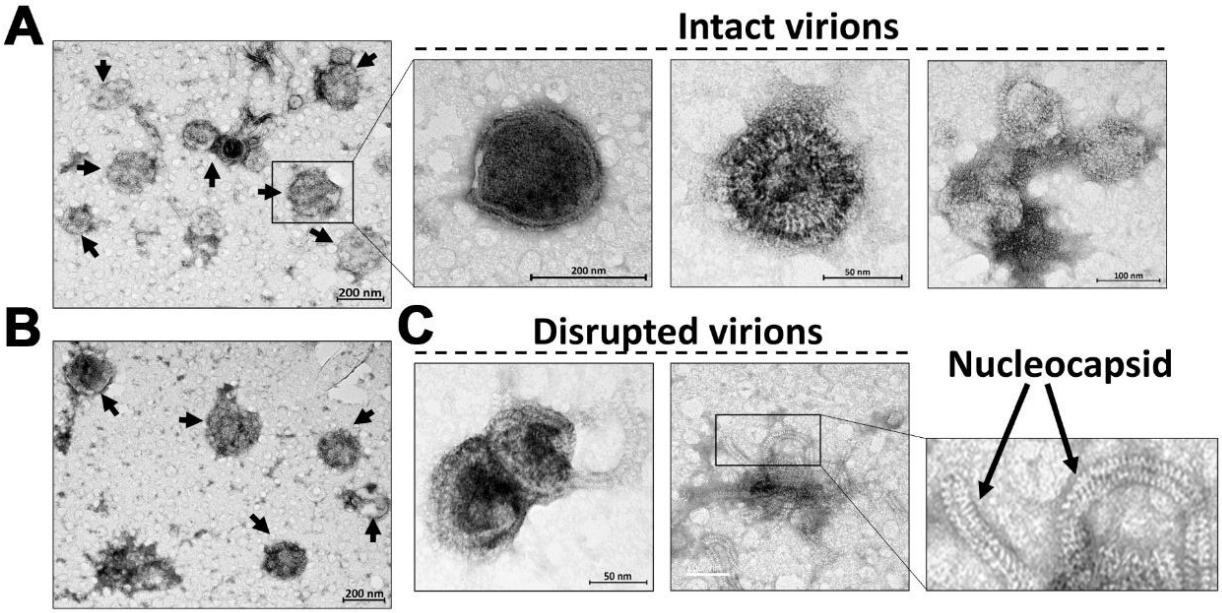

Figure 2.5: TEM (Transmission Electron Microscopy) images of the purified NDV particles. (A and B) Intact virions with their diameter within the range of 200–300 nm. (C) Disrupted virions showing the release of the nucleocapsid.

2.3.5 Purified NDV is functionally active for experimentation

To confirm that the replicative potential of the virus was conserved and carried a viable genome, the purified NDV particles were inoculated in the allantoic fluid of SPF-embryonated chicken eggs and allowed to propagate. Their genome was also detected with the help of PCR using viral-specific primers after the preparation of their cDNA. As described in Section 2.2.3,

both the purified and crude NDV were injected into 9-day-old embryonated chicken eggs and monitored for growth in the allantoic fluid (**Figure 2.6 A**).

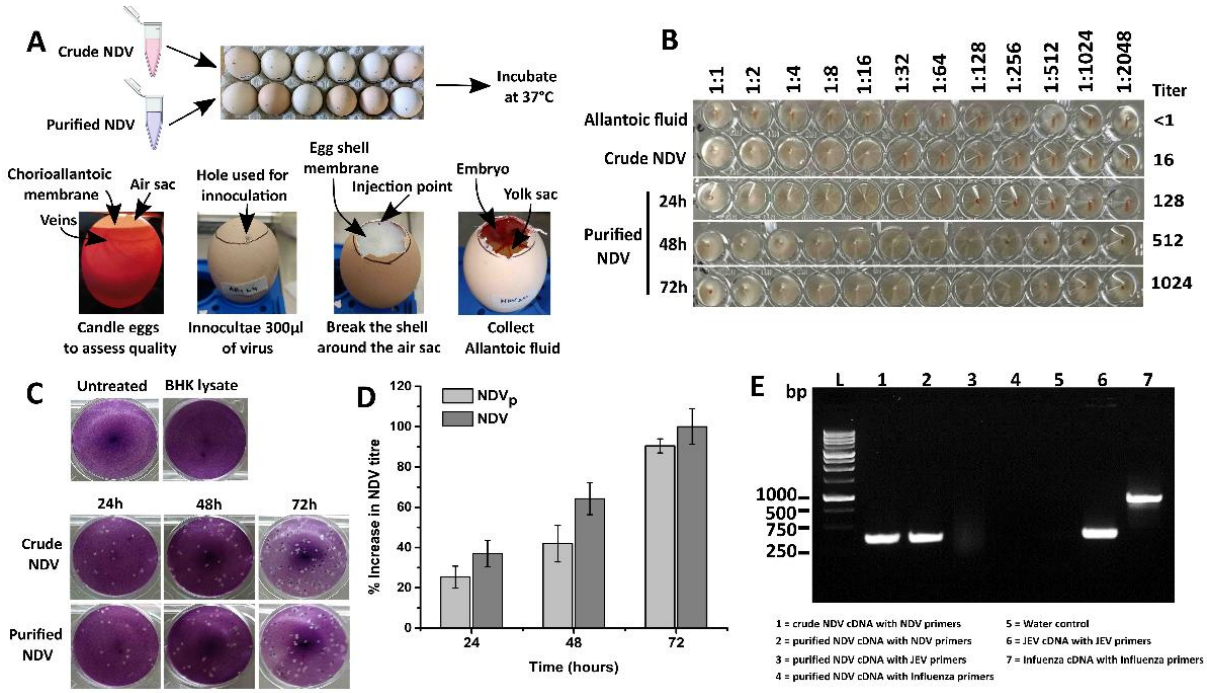

Figure 2.6: Anion exchange purified NDV can be used for downstream applications. (A) Propagation of crude and purified NDV in allantoic fluid. (B) HA of the allantoic fluid obtained from the eggs post-infection in 24, 48, and 72 h. (C and D) shows the plaque assay of both the purified and crude NDV derived from the allantoic fluid and the titers calculated from the assay in 24, 48, and 72 h. The 10^{-5} dilution was selected for counting the plaques. (E) A 423-bp fragment was amplified from the cDNA preparation of the virus particles for detecting the viral genome. L: Ladder, Lane 1: PCR product with NDV-specific primers using cDNA prepared from crude virus. Lane 2: PCR product with NDV-specific primers using cDNA prepared from the purified virus. Lane 3: PCR product with JEV-specific primers using cDNA from purified NDV. Lane 4: PCR product with Influenza-specific primers using cDNA from purified NDV. Lane 5: Water control. Lane 6: PCR product with JEV-specific primers using cDNA prepared from JEV. Lane 7: PCR product with Influenza-specific primers using cDNA prepared from Influenza virus.

Post-inoculation in the allantoic fluid, the HA of the purified NDV was observed at 24, 48, and 72 h. As evident from **Figure 2.6 B**, the HA titer of the purified NDV increased with time as the virus multiplied in the allantoic fluid. To compare the replicative potential of the purified NDV with the crude virus, we went directly for the plaque assay to determine the rate of increase in their titer (**Figure 2.6, C**). The NDV titers calculated from the plaque assay at three time points showed that the purified NDV retained its replicative potential and thus was able to multiply in the allantoic fluid. Quantitative estimation from the plaque assay showed that

the rate of increase in viral titers from 24 to 72 h was also similar in both purified and crude viruses, as shown in **Figure 2.6 D**.

Table 2.1: List of primers used in the current study.

Organism	Forward primer (5' → 3')	Reverse primer (5' → 3')	Amplicon size (bp)
NDV	GCAGCTGCAGGGATTGTGGT	GGATGTTGGCRGCATTYTGGTTGGC	423
JEV	GCAGAAAGCAAAACAAAAGAG	ACGGATCTCCTGCTTCGCTTG	450
Influenza (PR8)	TATTCGTCTCAGGGAGCAAAAGCAGGGTG	ATATCGTCTCGTATTAGTAGAAACAAGGGTGTTTT	900

The crude and purified NDV expanded in the allantoic fluid were used for cDNA preparation and subsequently probed with NDV-specific primers to amplify a 423-bp product. Lanes 1 and 2 show the 423-bp amplified product from the F gene of NDV with specific primers used to probe the cDNA of crude and purified NDV respectively (**Figure 2.6 E**). The cDNA from the purified NDV was also probed using JEV and influenza (PR8) primers to further confirm that the purified virus is NDV. Lanes 3 and 4 show that there is no amplification from the cDNA of the purified NDV with the JEV and influenza-specific primers. Thus, the results confirm that the purified virus is indeed NDV and there is no cross-contamination with other viruses. Lane 5 shows the water control. Lanes 6 and 7 depict the amplified product for JEV (450 bp, E gene) and influenza (900 bp, NS gene), with specific primers used with the cDNA of the respective species. Thus, it was confirmed that the anion exchange–purified virus was NDV and carried an intact genome.

2.4 Discussion

Anion exchange chromatography is a widely utilized method for purifying various viruses, either in combination with ultracentrifugation or as a standalone procedure [13, 14]. In previous studies on NDV, the application of a DEAE-cellulose column for purifying surface proteins from disrupted NDV particles was reported [15]. Another investigation utilized a prepacked strong anion exchange column to purify long helical capsids of NDV [16]. However, literature concerning the purification of intact NDV particles using ion exchange methods with traditional column chromatography is currently lacking. Alternative approaches for NDV purification have been explored in separate studies, which included the application of interference chromatography and a combination of depth filtration, tangential flow filtration

(TFF), and density gradient ultracentrifugation [17]. Interference chromatography involves the addition of citrate to the NDV stock before passing it through an anion exchange membrane, thereby reducing the binding of negatively charged host proteins and DNA onto the membrane and obtaining ultrapure virus particles. Membrane filtration techniques like TFF, often used for desalting, buffer exchange, and protein concentration, could potentially be applied for virus purification. However, removing cellular proteins with membrane filtration may be challenging and necessitates downstream processing with chromatography. Density gradient ultracentrifugation, while effective, is time-consuming and limited in sample size processing. Additionally, a considerable amount of medium may become a contaminant due to the equilibration of viral bands in the gradient zone. Subsequent steps typically involve the elimination of remnants of CsCl, sucrose, and others from the virus fraction using dialysis [18].

In our study, we employed a straightforward approach to obtain purified virus particles while minimizing the introduction of additional chemicals or steps. It was essential to develop such a procedure as we required NDV of very high purity, without any added contaminants, for the co-infection studies with the malaria parasite. Anion exchange chromatography offered a simple and efficient procedure to obtain NDV of high purity in significantly less time. It also has several advantages over membrane-assisted purification and ultracentrifugation, including ease of operation, scalability, and a reduced timeframe for isolating viruses from cellular contaminants. Furthermore, these columns are compatible with various protein purification systems and can be reused multiple times. Also, another potential benefit could be the co-elution of different viruses from biological sera with different biochemical characteristics, which might lead to the identification of previously undetected but associated viruses. Thus, it can potentially aid in our understanding of the disease pathology, particularly in cases of coinfection with different virus types.

2.5 References

1. Sun, W., et al., Newcastle disease virus (NDV) expressing the spike protein of SARS-CoV-2 as a live virus vaccine candidate. EBioMedicine, 2020. 62.

2. Burova, E. and E. Ioffe, Chromatographic purification of recombinant adenoviral and adeno-associated viral vectors: methods and implications. Gene therapy, 2005. 12(1): p. S5-S17.

3. Weigel, T., et al., Hydrophobic-interaction chromatography for purification of influenza A and B virus. Journal of Chromatography B, 2019. 1117: p. 103-117.

4. Li, H., et al., A hydrophobic interaction chromatography strategy for purification of inactivated foot-and-mouth disease virus. Protein Expression and Purification, 2015. 113: p. 23-29.

5. Taverne, J. and P. WILDY, Purification of herpes simplex virus by chromatography of calcium phosphate. Nature, 1959. 184(4699): p. 1655-1656.

6. Wolff, M.W., et al., Purification of cell culture-derived modified vaccinia ankara virus by pseudo-affinity membrane adsorbers and hydrophobic interaction chromatography. Biotechnology and bioengineering, 2010. 107(2): p. 312-320.

7. Kalbfuss, B., et al., Purification of cell culture-derived human influenza A virus by size-exclusion and anion-exchange chromatography. Biotechnology and Bioengineering, 2007. 96(5): p. 932-944.

8. Vajda, J., et al., Size distribution analysis of influenza virus particles using size exclusion chromatography. Journal of Chromatography a, 2016. 1465: p. 117-125.

9. Ganar, K., et al., Newcastle disease virus: current status and our understanding. Virus research, 2014. 184: p. 71-81.

10. Florman, A.L., Hemagglutination with Newcastle disease virus (NDV). Proceedings of the Society for Experimental Biology and Medicine, 1947. 64(4): p. 458-463.

11. Lomniczi, B., Plaque assay for avirulent (lentogenic) strains of Newcastle disease virus. Applied microbiology, 1974. 27(6): p. 1162-1163.

12. Shokeen, K., A. Srivathsan, and S. Kumar, Lithium chloride functions as Newcastle disease virus-induced ER-stress modulator and confers anti-viral effect. Virus Research, 2021. 292: p. 198223.

13. Okada, T., et al., Scalable purification of adeno-associated virus serotype 1 (AAV1) and AAV8 vectors, using dual ion-exchange adsorptive membranes. Human gene therapy, 2009. 20(9): p. 1013-1021.

14. Trilisky, E. and A. Lenhoff, Sorption processes in ion-exchange chromatography of viruses. Journal of Chromatography a, 2007. 1142(1): p. 2-12.

15. Seto, J., H. Becht, and R. Rott, Isolation and purification of surface antigens from disrupted paramyxoviruses. Medical Microbiology and Immunology, 1973. 159: p. 1-12.

16. Yap, C.F., et al., Purification of long helical capsid of newcastle disease virus from Escherichia coli using anion exchange chromatography. Biotechnology progress, 2013. 29(2): p. 564-567.

17. Santry, L.A., et al., Interference chromatography: A novel approach to optimizing chromatographic selectivity and separation performance for virus purification. BMC biotechnology, 2020. 20: p. 1-15.

18. Santry, L.A., et al., Production and purification of high-titer Newcastle disease virus for use in preclinical mouse models of cancer. Molecular Therapy Methods & Clinical Development, 2018. 9: p. 181-191.

Chapter 3

NDV displays an innate ability to disrupt the erythrocytic schizogony of the malaria parasite

*The contents of this chapter are partly published as "**Neog S, Vinjamuri SR, Vijayan K, Kumar S, Trivedi V. NDV targets the invasion pathway in malaria parasite through cell surface sialic acid interaction. FASEB J.** 2024 Aug 15;38(15):e23856. doi: 10.1096/fj.202400004RR. **PMID: 39092913.**

Summary

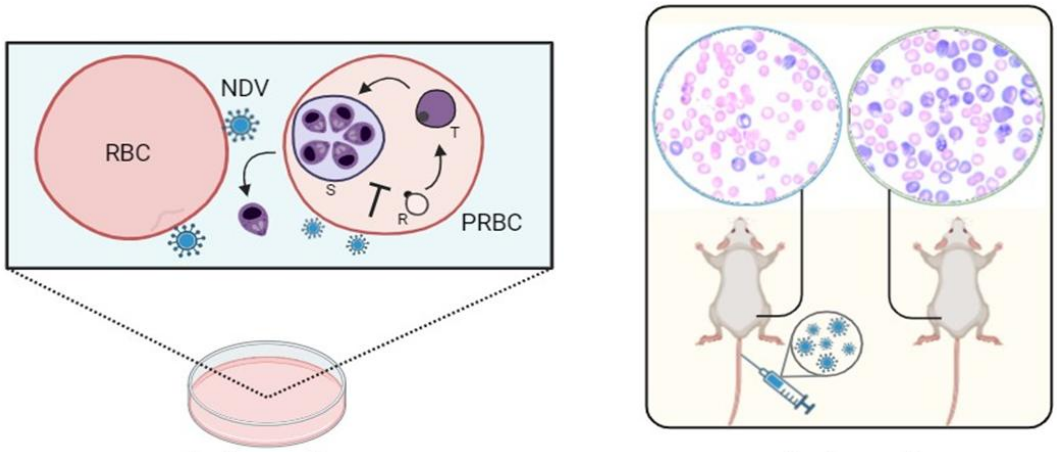

Merozoites are extracellular invasive form of the malaria parasite that exploits sialic acids present on the surface of RBCs for rapid adhesion and invasion. Notably, the Newcastle Disease Virus (NDV) also exhibit a pronounced affinity towards membrane-bound sialic acids which calls for an investigation into the effects of this interaction on the malaria parasite propagation. Incubation of NDV with the malaria parasites (*Plasmodium falciparum* 3D7) was found to dose-dependently reduce the cellular viability of the parasites. This anti-plasmodial activity of NDV was found to be specific, as no significant effect on parasite viability was observed upon incubation with other viruses such as JEV, DEV, IBV, and Influenza virus. Interestingly, pre-treating the host RBCs with NDV led to an 80% reduction in malaria parasite invasion, underscoring the potential role of NDV in perturbation of merozoite invasion. Evaluation of the effects of the virus on human RBCs revealed no agglutination of the cells and no impact on whole blood clotting, indicating its compatibility with human blood. The virus was also tested for any cytotoxic effects on the macrophages. Incubation of NDV with macrophages did not elicit any TNF-α release. The results indicate that the virus demonstrates an intrinsic ability to perturb the erythrocytic cycle of the malaria parasite and is safe for application in human blood. The virus was also tested against the murine parasite strain *P. yoelii* where NDV was able to restrict the parasite growth *in vivo*, both in pre-treatment and post-treatment scenarios. It suggests that the anti-plasmodial activity of NDV is a robust and pan-malaria phenomenon.

3.1 Introduction

The erythrocytic cycle of the malaria parasite is an excellent target for therapeutic intervention due to its central role in malaria pathogenesis [1, 2]. In the erythrocytic schizogony, the parasite exponentially multiplies in the RBCs, during which it undergoes distinct developmental stages. Erythrocytic schizogony begins when merozoites, an extracellular form of the malaria parasite, invade an uninfected RBC, leading to the development of the ring stage [3]. The rings mature into trophozoites and schizonts through continuous cell division. Upon maturation, the schizonts harbor numerous merozoites, which, after egress, invade new RBCs. The invasion of uninfected RBCs is crucial for parasite propagation and involves complex interactions, including adhesion, invasion, and evasion of the host immune system [4]. Merozoites display a diverse array of antigens on their surface that utilize sialic acids on the RBC surface for invasion. Additionally, parasite survival within the parasitized RBCs relies on essential signaling pathways involving cyclic nucleotides, ATP, and calcium, along with host cell-dependent pathways such as the MAPK pathway [5-8]. These pathways play crucial roles in sustaining parasite development, egress, and invasion. Thus, the disruption of these processes by an agent that potentially interacts with RBCs or parasitized RBCs could be detrimental to parasite survival.

Viruses such as Orthomyxoviruses, Paramyxoviruses, Adenoviruses, and Herpesviruses also exploit sialic acids as receptors for attachment and entry into host cells [9-12]. The majority of these viruses display dedicated lectins and hydrolases in their coat, such as Hemagglutinins, Hemagglutinin Neuraminidase (HN) and Neuraminidase (N) to target host cell surface sialic acids. These coat proteins also determine specificity for particular sialic acid linkages that influence viral tropism and host range, contributing to the variability of viral strains that affect humans, birds, and other animals [13-15]. In this regard, the Newcastle Disease Virus (NDV) classified within the avian orthoavulavirus 1 species, genus Orthoavulavirus, and family Paramyxoviridae exhibits a natural affinity for avian erythrocytes, particularly due to its spike protein HN, which facilitates cell recognition [16, 17]. The HN protein contains sialic acid binding sites for docking onto sialic acid-rich cell receptors, activating the other coat protein, called the Fusion or F protein, for membrane fusion and entry. This correlative interaction between NDV and the malaria parasite towards the sialic acid-rich RBC surface suggests that there could be potential implications in co-infection scenarios. Thus, we conducted this study to examine if NDV could have any impact on the erythrocytic schizogony of the malaria parasite.

In this chapter, the potential of NDV to disrupt the erythrocytic schizogony of the malaria parasite is investigated. We conducted in-vitro coinfection studies of the NDV with the malaria parasite to study the effect of the virus on the erythrocytic cycle of the parasite. For our initial co-infection studies, anion exchange purified NDV at an MOI of 10^3 was incubated with the malaria parasite for 96 hours and the parasite growth was monitored. The parasites were also treated with the BHK-lysate to negate the effects of any trace amounts of cellular contaminants that could hinder its growth. The initial results show that the virus possessed an innate ability to restrict the propagation of the parasite in human RBCs. Upon careful observation of the effects of NDV on parasite morphology, it was found that the virus also invokes severe cytopathy in the mature stages of the parasite. We also conducted dose-dependent studies where the parasite was incubated with different concentrations of NDV. It reveals that the virus was able to dose-dependently reduce the cellular viability of the malaria parasite. The influence of different incubation periods on the anti-plasmodial activity of NDV was also tested. Notably, the anti-plasmodial action of NDV was found to be rapid, as exposing the parasite to the virus for just 12 hours led to the disruption of the erythrocytic cycle.

Incubation of the parasite with other viruses such as Influenza, Japanese Encephalitis virus (JEV), Infectious Bronchitis virus (IBV) and Duck Enteritis virus (DEV) did not reduce parasite viability which suggests that the anti-plasmodial activity was unique to NDV. Furthermore, the mechanism of action of the virus was investigated, where we observed that it blocked the invasion of merozoites into uninfected RBCs, thereby disrupting the erythrocyte cycle. The impact of the virus on the human RBCs was also tested with the help of agglutination and clot retraction assays. NDV was able to cause high-order aggregation of chicken RBCs but did not cause any aggregation of human RBCs. Also, the clot retraction time of whole blood was not affected in the presence of the virus. To address the effects of NDV on the nucleated cells in the blood, the virus was incubated with macrophages at different concentrations and incubation periods while monitoring the levels of secreted TNF-α. The virus, even at very high concentrations, did not elicit any TNF- α response, suggesting that it was safe for application.

We also tested the virus against the murine parasite strain *P. yoelii*, where we found that a short treatment of the parasite with NDV, prior to its inoculation in mice, resulted in a substantial reduction of parasite growth. Additionally, mice infected with *P. yoleii* showed a marked decrease in parasitemia upon a single intravenous injection of NDV. Thus, the results indicate that the anti-plasmodial effect of NDV is a pan-malaria phenomenon and could prove to be an excellent platform for developing novel anti-malarial therapeutics.

3.2. Experimental procedures

3.2.1 Malaria parasite culture

Plasmodium falciparum (3D7) was cultured in RPMI 1640 medium as described previously [18]. Human blood group O+ was drawn from healthy volunteers. Subcultures were performed by diluting the parasites in fresh RBCs.

3.2.2 Virus strains and their propagation

NDV Lasota and R2B strains were propagated in baby hamster kidney (BHK-21) cells (NCCS, Pune, India), maintained in Dulbecco's modified Eagle's medium (DMEM, Himedia, India) supplemented with 10% fetal bovine serum (Gibco, USA). Virus titer was determined by HA and Plaque assay as described previously. Different virus concentrations were prepared from the stock in RPMI 1640 complete medium. In a few experiments, the virus from allantoic fluid was also used. The virus was propagated in the allantoic fluid of Day 9 SPF embryonated chicken eggs, purchased from Lotus Chicks' Hatchery, Guwahati, Assam, India [19].

3.2.3 Pf3D7 and NDV co-infection studies

Plasmodium falciparum (3D7) was grown up to 15-20% Parasitemia and synchronized using 5% D-sorbitol to obtain 6 to 8-hour ring-stage parasites. The Parasitemia was adjusted to the 1, 2 or 5% of rings or schizonts with fresh RBCs and incubated with NDV at different multiplicities of infection (MOI: 10, 10^2, 10^3, 10^4 and 10^5) prepared in RPMI1640 (Gibco, 23400-062) complete media for 72-96 hours. Post incubation thin smears were prepared at 24, 48, 72, and 96 hours and the parasitemia was monitored. To assess the impact of different viruses on malaria parasites, Influenza (PR8), Infectious Bronchitis virus (M14), Japanese Encephalitis virus (GIII), and Duck Enteritis virus along with NDV were prepared in RPMI1640 incomplete media and added to parasite cultures (1% parasitemia) at similar concentrations and the growth was monitored till 72 hours. The effect of viral concentration and incubation periods was investigated by administering increasing MOIs (10 to 10^5) of NDV to the parasites or incubating NDV with the parasite for different time periods (12, 24 and 48 hours). Growth was evaluated for 72 hours post incubation.

3.2.4 Parasite invasion assay

To examine the impact of NDV on invasion, uninfected RBCs were incubated with NDV at a MOI of 10^3 for 1 hour at 37°C and then washed and re-suspended in parasite culture media.

The schizonts were not treated with NDV to minimize any effect of the virus on egress of the merozoites as we wanted to observe the effects of the virus only on the invasion of the merozoites. Thus, a culture of homogenous schizonts was introduced into the virus-treated red cells at a final parasitemia of 5% and monitored for growth till 72 hours. The appearance of rings in subsequent time points was determined and a quantitative estimation of conversion of schizonts to rings was measured.

3.2.5 RBC agglutination test

NDV was incubated separately with 1% human and chicken RBC suspensions at an MOI of 10^3 for 1 hour at 37^0C in RPMI1640 complete media. The cells were washed three times with PBS followed by fixation with 0.5% Glutaraldehyde for 15 min at RT. Thin smears were prepared and stained with JSB staining solutions and viewed under 100x with a bright field microscope. Cells that appeared to be in triplets and higher aggregates were expressed as % RBC agglutination.

3.2.6 Clot retraction assay

The whole blood was separated into plasma and RBC fractions by centrifuging at 1500 rpm for 10 minutes. NDV was incubated with human RBCs at 0.5% hematocrit with an MOI of 500. The plasma was diluted in a 1:20 ratio with PBS and added to the NDV-treated RBCs. The clot retraction time was measured and compared between the NDV-treated and untreated RBCs.

3.2.7 Quantification of TNF-α in macrophages post-treatment with NDV

Macrophage cells (J774a.1) were seeded on a 96-well plate at a density of $1.5x10^5$ cells per well and allowed to set overnight for proper adhesion. The cells were treated with NDV at different MOIs for 1 hour and 12 hours. The cells were washed with PBS five times to remove the virus and incubated in incomplete media for 18 hours. The supernatant was collected from the wells and incubated with the capture antibody for 2 hours at room temperature (RT), pre-coated on a separate 96-well plate according to the manufacturer's instructions. The cells were washed and incubated in the detection antibody for 2 hours at RT followed by washing. The TMB substrate, H_2O_2 was added followed by treatment with 2N H_2SO_4 followed by collection of absorbance at 590 nm.

3.2.8 *In vivo* testing of NDV against murine malaria

NDV was incubated with *P. yoelii* at an MOI = 10^2 at 40% parasitemia for 3 hours at 37°C. Post-incubation, cells were washed with PBS to remove any unbound virus particles. Parasites with the same parasitemia were also incubated with heat-inactivated NDV at the same concentration and time period or treated with plain allantoic fluid (AF), without the virus, under similar conditions. Post-incubation, *P. yoelii-infected* blood from each treatment condition was injected intraperitoneally into 12-13 weeks-old mice. Tail snips were performed and smears were taken from day 0 to day 12 to monitor the growth of the parasite. In another experiment, *P. yoelii*-infected blood (40% parasitemia) was injected intraperitoneally in mice and allowed to grow. When the parasitemia reached to 3.28 ± 0.53, mice were injected with NDV from the allantoic fluid. Post-NDV challenge, the parasitemia was monitored till day 12 as described previously.

3.3 Results

3.3.1 NDV has an innate ability to disrupt the malaria parasite propagation:

The malaria parasite and the Newcastle disease virus (NDV) utilizes sialic acid rich cell surfaces for cell adhesion and entry. Consequently, both organisms display a strong affinity for the red blood cell, as the erythrocyte surface is rich in sialic acid. Hence, it was an intriguing question to investigate if the virus could affect the malaria parasite growth in human red blood cells. To answer this question, we conducted co-infection experiments of NDV with the parasite. The virus at a MOI = 10^3 was introduced to ring-synchronized malaria parasites of a parasitemia of 1%. In 48 hours, the parasitemia of the untreated culture increased exponentially from 1% to 5%, and it continued to grow for 72 hours. A comparison of the growth profile of the virus-treated and untreated cultures revealed that the NDV-treated parasites experienced a 40% reduction in parasitemia after 48 hours (**Figure 3.1 A**). After 48 hours, the untreated parasites were able to maintain parasitemia of roughly 5% till 96 hours, but the virus-treated cultures showed a 70% drop in parasitemia. Because the virus was propagated in BHK cells, we also investigated the impact of BHK lysate on parasite viability. The parasites were able to proliferate effectively in the presence of the lysate, following a similar growth pattern to the untreated culture. Thus, our initial results show that NDV has the inherent ability to restrict malaria parasite proliferation in human red cells and thus disrupt erythrocytic schizogony.

We further investigated the morphological changes in the PRBCs in the presence of NDV. The experimental samples from **Figure 3.1 A** were used to prepare thin smears to monitor the

morphological changes in the virus-treated parasites (**Figure 3.1 B**). The untreated parasites exhibited characteristic progression from rings to mature stages within red blood cells. The rings displayed a thin membrane with a darkly stained chromatin dot. The trophozoites showed an increase in cytoplasmic volume and density. Schizonts were significantly larger and often multinucleated in composition. It was observed that the ring stage of both the untreated and virus-treated parasite did not show any observable morphological aberration. However, trophozoites treated with the virus appeared to be smaller in size, while a few of them also displayed a defective membrane boundary. Additionally, compared to the untreated schizonts, the NDV-treated schizonts exhibited a substantial decrease in their cytoplasmic volume.

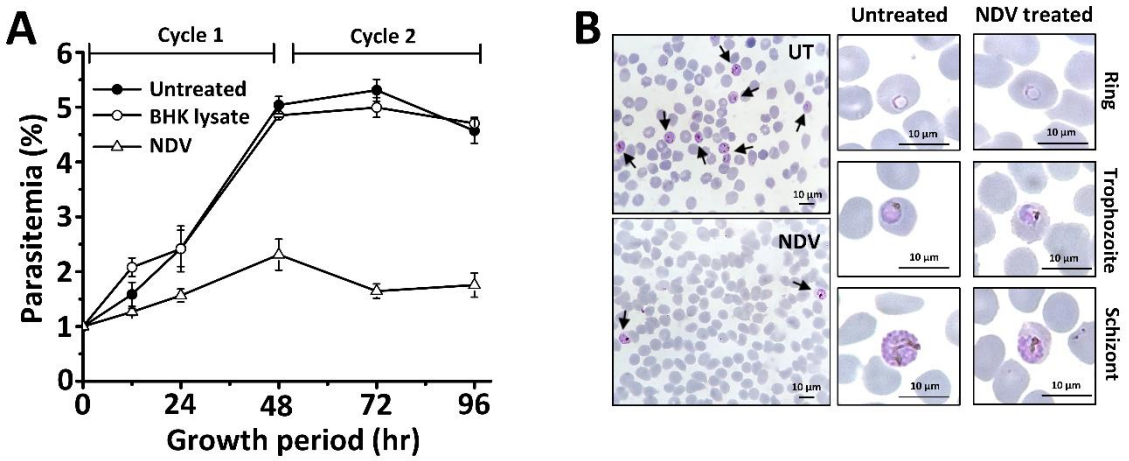

Figure 3.1: NDV disrupts the erythrocytic cycle of the malaria parasite in vitro studies. (A) NDV inhibits malaria parasite propagation. Growth curves of Pf3D7 with no treatment (untreated), treated with NDV propagated in BHK-21 cells or BHK-lysate (BHK lysate). Thin smears were taken every 24 hours, followed by JSB staining and calculation of parasitemia. Growth curves of the NDV-treated parasites were compared with parasites without any treatment or those treated with the BHK lysate. The mean ± standard deviation (n= 3) is shown for all the time points. (B) NDV induces cytopathy in the RBC stages of the parasite. Thin blood smears were prepared from the samples presented in (A) for morphological study of the different stages of the parasite under 100x magnification. Representative images from the 96-hour time-point of untreated (UT, top left panel) and NDV-treated (NDV, bottom left panel) reveal a global decrease of parasitemia in the NDV-treated culture compared to the control (UT). Progression of erythrocytic stages of the parasite during cycle 2; untreated and NDV-treated parasites show virus-induced cytopathy in different parasite stages.

They were considerably smaller and failed to demonstrate the same degree of maturity as the multinucleated schizonts of the untreated parasite culture. The non-parasitized RBCs of both the untreated and the NDV-treated cultures displayed no appreciable change in their structure and normal discoid morphology. Thus, it became evident that the virus induces cytopathy in PRBCs, which was severe as the parasites reached maturity.

3.3.2 The anti-parasitic action was unique to NDV:

We asked if the anti-parasitic action of NDV is unique to the virus or a phenomenon shared by any other virus species, given the similarities in their bimolecular composition and physical properties. Hence, we treated the malaria parasites at a multiplicity of infection (MOI) of 10^3 with several other virus strains, including Influenza (strain-PR8), Infectious Bronchitis virus (IBV, strain-M14), Japanese Encephalitis virus (JEV, strain-GIII), and Duck Enteritis virus (Netherlands). Upon examining the growth patterns, we observed that the untreated parasites multiplied rapidly, eventually attaining a parasitemia of 4% in the culture medium after 72 hours. The NDV-treated parasite culture exhibited a decline in parasite growth of over 80% when compared to the untreated culture after 72 hours (**Figure 3.2**). Upon examining the growth curves of the parasites treated with the other virus strains (Influenza, IBV, JEV, and DEV), we

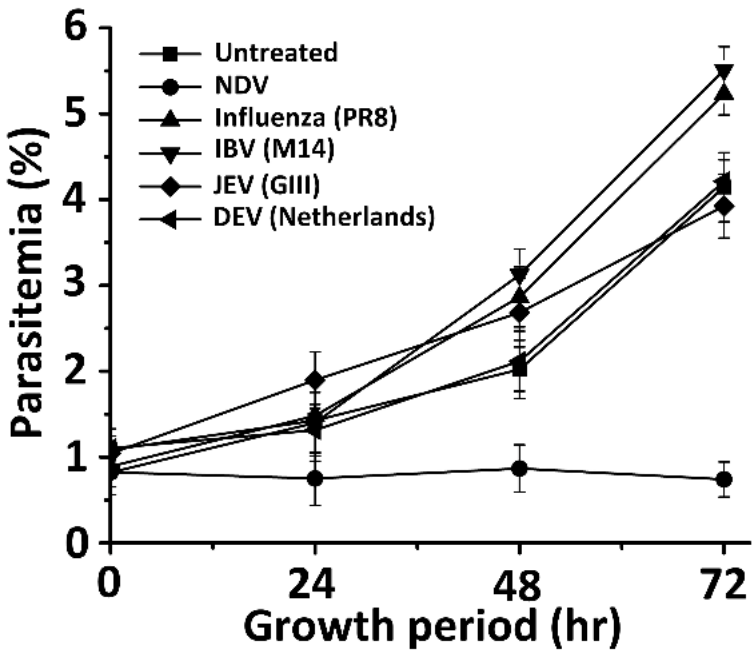

Figure 3.2: The anti-parasitic action of NDV is specific to the virus. Growth curves of Pf3D7 with no treatment (untreated) or treated with different virus strains such as NDV (Lasota strain), Influenza (PR8 strain), Infectious Bronchitis virus (IBV, M14 strain), Japanese Encephalitis virus (JEV, GIII strain) and Duck Enteritis virus (DEV, Netherlands strain). Thin blood smears were prepared every 24 hours, followed by JSB staining to monitor the growth of the parasite in different conditions. The parasitemia was calculated and presented as mean ± standard deviation (n= 3) for all the conditions.

observed that none of the other viruses were able to inhibit the malaria parasite growth. These cultures exhibited parasitemia levels of 4-5% at the end of 72 hours, which was equivalent to

the untreated parasite culture. However, it is important to note that all of the viral strains used in the study were of avian origin but only NDV inhibited the replication of the malaria parasite. Thus, NDV inhibits the malaria parasite growth and disrupts their cellular morphology, and these effects are unique to the virus.

3.3.3 The anti-parasitic effect of NDV is quick and dose-dependent:

Given that NDV inhibits the growth of the parasite we further investigated if these effects are dose-dependent and what could be the effect of different incubation periods on the anti-plasmodial effect of the virus. In order to address this, different NDV concentrations (MOI=10^1 to 10^5) were used to treat parasite cultures (1% parasitemia), and the growth of the cultures was tracked as described previously in materials and methods.

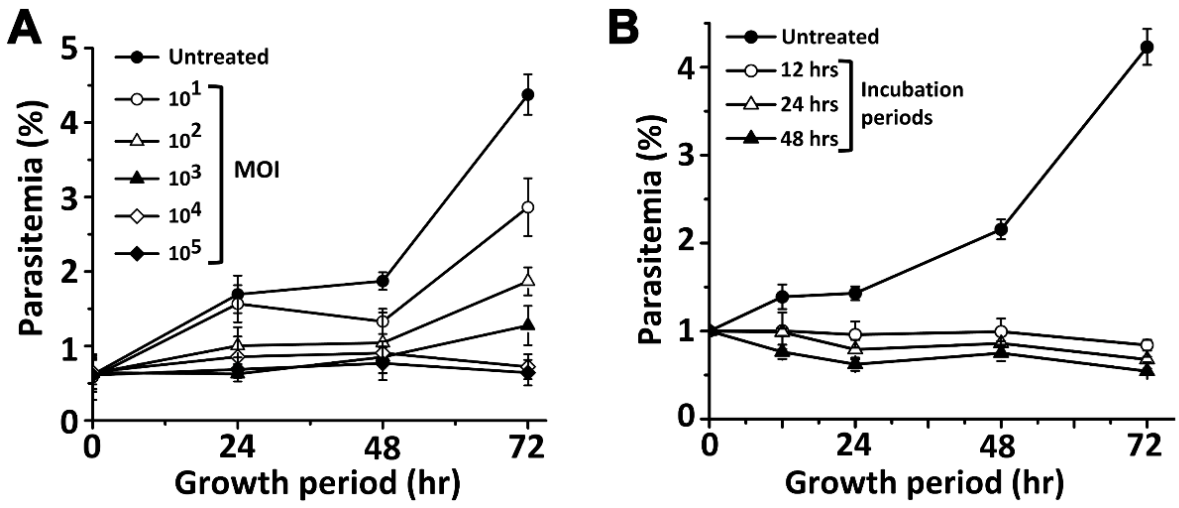

Figure 3.3: The anti-parasitic effect of NDV is dose-dependent. Growth curves of Pf3D7 incubated with NDV at different multiplicities of infection (MOI=10^1 to 10^5). Thin blood smears were prepared every 24 hours, followed by JSB staining to monitor the growth of the parasite. The growth of the NDV-treated parasites (MOI=10^1 to 10^5) was compared with the parasites without any treatment. The growth curves also display the mean ± standard deviation (n= 3). **(E) The NDV-mediated inhibition of malaria parasite growth needs brief exposure.** Growth curves of Pf3D7 incubated with NDV (MOI=10^3) for incubation periods (12, 24 and 48 hours). Post-incubation, the parasite cultures were washed, and new culture media without NDV was added to monitor the growth with the help of thin smears. Growth curves were presented as mean % parasitemia ± standard deviation (n= 3).

Treatment of the parasite culture with increasing virus concentration was found to inhibit parasite development in a dose-dependent manner. At a MOI = 10^1, the virus reduced parasite viability by 40% within 72 hours (**Figure 3.3 A**). At MOIs of 10^4 and 10^5, the parasitemia remained below 1%, resulting in a reduction of about 90% after 72 hours. Thus, it was evident

that the virus disrupted the viability of malaria parasites in a dose-dependent manner. During the erythrocytic schizogony, the malaria parasite multiplies rapidly within RBCs while progressing through several developmental stages. Thus, it is crucial to determine the minimum exposure duration required for NDV to exert its effects. To answer this question, we exposed the parasite culture to NDV (MOI = 10^3) over various exposure times (12-48 hours). Following incubation, the parasites were washed, and new culture media was added. The growth of the parasites was monitored for 72 hours (**Figure 3.3 B**). It was found that incubating the parasite culture with NDV for just a period of 12 hours prevents the parasite from growing, resulting in a greater than 90% decrease in parasitemia. It indicates that either the virus caused unrecoverable damage to the parasites by interacting with the PRBCs during the 12-hour incubation period, or that the NDV particles remained associated with the cells even after thorough washing, resulting in prolonged interruption of parasite growth. As a result, it became vital to explore the nature of the physical interactions between RBCs, PRBCs, and NDV, as well as identify the key molecular actors in this process responsible for the reported antimalarial effects.

Based on the data presented in **Figures 3.1 to 3.3**, a hypothetical model was proposed to explain the probable mechanism of the anti-plasmodial action of NDV (**Figure 3.4**).

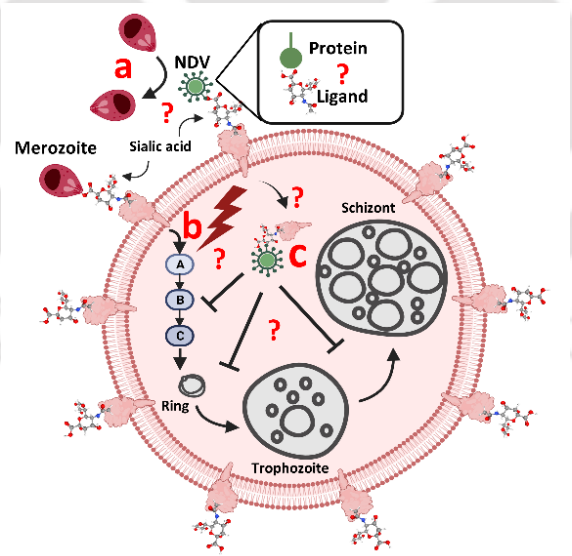

Figure 3.4: The proposed model to explain the anti-malarial action of NDV. A hypothetical model was proposed to explain the anti-malarial action of NDV. There are multiple possibilities: (a) NDV (green) could block the crucial cell surface receptors essential for the merozoites (dark red) to invade the RBC. (b) Also, the binding of the virus to these receptors might execute downstream signaling that could interfere with the crucial signaling pathways required for merozoite invasion. (c) NDV might enter the PRBC and interact directly with the parasite, thereby disrupting the development of the malaria parasite.

According to the proposed model:

(a) Merozoite invasion is linked to the receptor availability on the RBC surface. It is possible that the virus particles may be engaging similar receptors/ligands, which will result in competition between merozoites and NDV. If this is true, we expected the virus to disrupt parasite invasion/egress severely.

(b) Cell surface signaling is crucial for invasion/egress, and NDV interaction with cell-surface receptors could interfere with downstream signaling required for the invasion/egress of merozoites.

(c) The virus may enter the PRBC and disturb the progression of the parasite stages to complete erythrocytic schizogony. The questions raised in the hypothetical model are being explored in the subsequent investigations.

3.3.4 NDV blocks the invasion of the malaria parasite into RBCs

According to the hypothetical model shown in **Figure 3.4**, NDV could be interacting with vital receptors on the surface of RBCs to block merozoite entry into uninfected RBCs. If this hypothesis is accurate, allowing merozoites to infiltrate RBCs pre-treated with NDV should result in the reduction of invasion. In order to address this, we pre-treated red blood cells (RBCs) with NDV (MOI=10^3) for one hour, allowing the virus to engage with receptors on the RBC cell surface. The erythrocytic cycle was then triggered by incubating these cells with schizonts (5% parasitemia). We anticipated a reduction in the number of rings in the culture if NDV interfered with merozoite invasion. At the beginning of the experiment (time = 0 hours), the number of schizonts introduced in both untreated and NDV-treated RBCs was comparable, but the number of rings was insignificant (**Figure 3.5 A**). At 24 hours, it was evident that the rings in NDV-treated RBCs were more than 50% fewer in number than those in untreated RBCs. Also, the difference in the number of rings at the 24-hour time point was reflected 48 hours later, when the schizonts in the NDV-treated culture were reduced by 50%. When we examined the number of rings formed by these schizonts after 72 hours, we discovered that NDV-treated RBCs exhibited an 80% reduction in the number of rings compared to untreated RBCs (**Figure 3.5 A**).

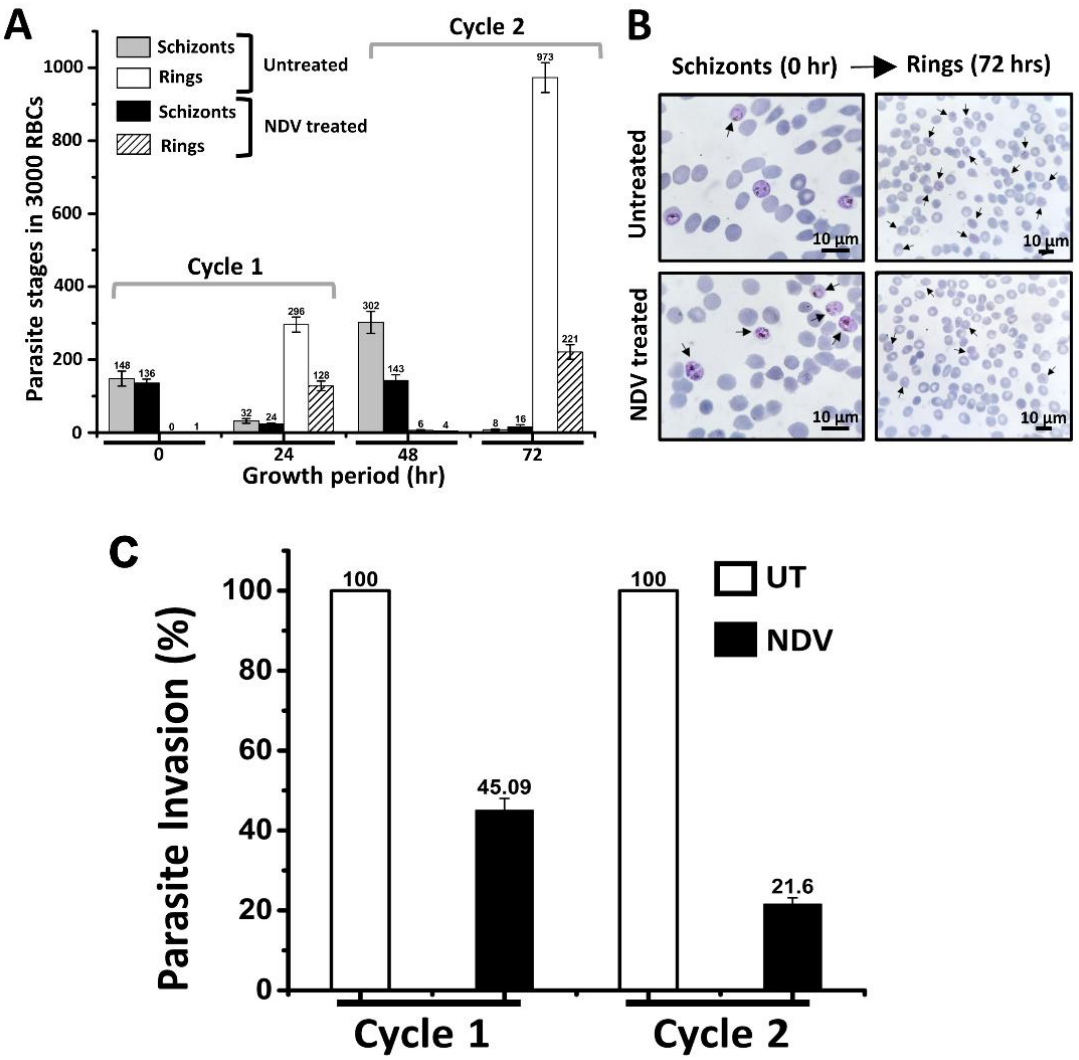

Figure 3.5: NDV blocks the invasion of merozoites into uninfected RBCs. Schizonts at a final parasitemia of 5% were incubated with fresh RBCs, either untreated or pre-treated with NDV (MOI=103) for 1 hour at 37°C. The parasite culture was monitored for the appearance of rings or schizonts at 24 hours and 72 hours in 3000 RBCs. (A) Schizonts introduced to untreated RBCs (grey) gave rise to twice the number of rings (white), while those introduced to NDV-treated RBCs (black) showed a significant reduction in the appearance of rings (bar with lines) at the end of the 72hours incubation. (B) Microscopic observation to monitor the conversion of schizonts to rings in cycle 2. The panels on the left show the representative images of schizonts at the start of the experiment (time = 0 hours), which were introduced either into the untreated RBCs (top) or NDV-treated RBCs (bottom). Panels on the right indicate a global reduction in the number of rings generated after 72 hours in the NDV-treated RBCs (bottom), compared to the untreated RBCs (top). The arrow denotes the schizonts (left panel) and rings (right panel) present in the images. (C) NDV reduces parasite invasion in the uninfected RBCs. The data from (A) was used to calculate the invasion (%) of merozoites into RBCs. Invasion in untreated RBCs in cycle 1 or 2 was considered as 100% (white bar) to express the % invasion of merozoites in NDV-treated RBCs (black bar).

We also studied the cells at high magnification in order to investigate the RBC stages in the NDV-treated and untreated RBCs further. In contrast to schizonts incubated with NDV-treated

RBCs, which formed fewer rings (**Figure 3.5 B**, bottom right panel), schizonts in the untreated culture (top left panel) had many rings with good morphology (**Figure 3.5 B**, top right panel). We quantitatively assessed the merozoite invasion of the RBCs after closely examining the number of rings that formed in the NDV-treated and untreated RBCs.

In cycle 1, the parasite invasion in the RBCs treated with NDV was less than 50%, while the invasion in the untreated RBCs was considered 100% (**Figure 3.5 C**). Approximately only 20% of the schizonts in cycle 2 were able to form rings, indicating a further decline in parasite invasion of about 80%. (**Figure 3.5 C**). This notable decline in invasion could be the major driver of the anti-plasmodial activity of NDV. Our findings indicate that NDV inhibits the growth of malaria parasites by blocking invasion. Thus, it becomes critical to explore any cognate receptor: ligand interaction which could drive the observed effects and potentially be responsible for the binding of NDV to the RBC or PRBCs. Hence, we conducted binding studies to investigate the nature of the NDV-RBC/PRBC interaction, specifically focusing on the involvement of any protein: protein or protein: ligand interaction, as discussed in later chapters.

3.3.5 NDV does not cause agglutination of human RBCs

NDV is known to induce higher-order agglutination in chicken RBCs. As we investigate NDV's potential against malaria parasites, it is critical to determine if the virus can promote higher-order aggregation in human RBCs. To investigate this, human or chicken RBCs were cultured with NDV (MOI=10^3) in the complete medium and visualized as indicated in the materials and methods. When we examined the cells at high magnification, we observed that the untreated avian or human RBCs were predominantly present as singlets (**Figure 3.6 A and B**).

It was found that the cells in the avian RBCs treated with NDV formed higher-order aggregates. Human RBCs treated with NDV, in contrast, exhibited little aggregation formation and were mostly seen as singlets, resembling untreated RBCs. Based on a quantitative evaluation of the data, the avian RBCs treated with NDV and those that were not were aggregated at 3.35 ± 0.56 and 93.42 ± 1.32%, respectively. In human red blood cells treated with NDV and those left untreated, the aggregation was 2.14 ± 0.36 and 2.38 ± 0.4%, respectively. The findings demonstrated that, at a multiplicity of infection (MOI) of 10^3, the virus could agglutinate avian red blood cells globally, but did not promote aggregation of human red blood cells.

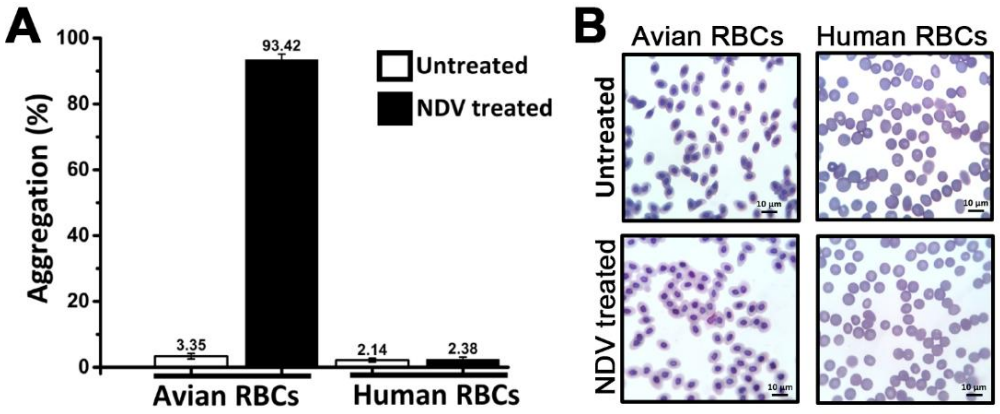

Figure 3.6: NDV does not agglutinate human RBCs. Chicken or human RBCs were treated with NDV (MOI=10^3), and the virus-induced aggregation was measured for both types of cells. Avian RBCs showed complete agglutination in the concentration of the virus used. Human RBCs did not show any agglutination with NDV at the same virus concentration.

3.3.6 Clot retraction assay

The clot retraction assay was used to assess the functionality of platelets, which are crucial components of blood involved in clotting. As the clot forms, platelets aggregate, and fibrinogen is converted to fibrin, forming a mesh that stabilizes the clot.

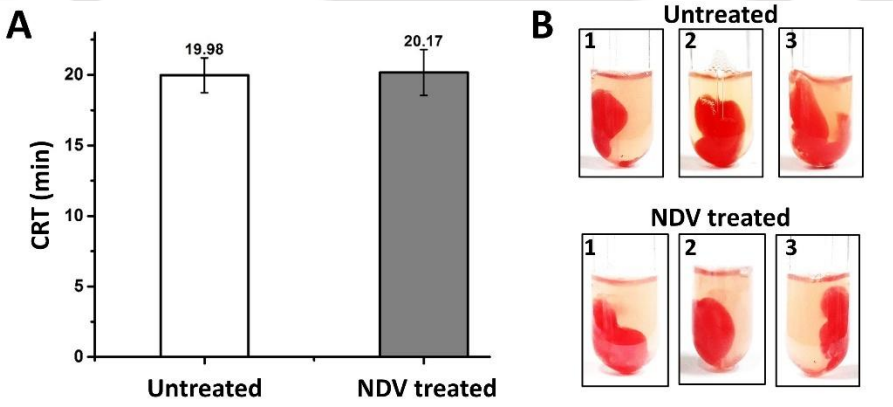

Figure 3.7: NDV does not affect the clotting of human blood. (A) The clot retraction time (CRT) in minutes was plotted in the Y-axis and compared for in the untreated and NDV treated whole blood. (B) Representative images showing clot retraction at the end of the experiment.

Over time, the clot contracts due to the activity of platelets and the interaction between fibrin fibres. Since the effects of NDV on the whole blood remains unreported, we tested if the virus could impact such basic functionality of blood. In our experiment we found that the average clot retraction time (CRT) was similar for the untreated (19.98 min) and NDV-treated (20.17 min) blood (**Figure 3.7**).

3.3.7 NDV does not activate murine macrophages

NDV was incubated with murine macrophages at different concentrations and for two different time periods, 1 hour and 12 hours. After the co-culture periods, the levels of tumor necrosis factor-alpha (TNF-α), a pro-inflammatory cytokine produced by activated macrophages, were quantified using enzyme-linked immunosorbent assay (ELISA). A graphical representation is shown where the J774A.1 cells in were treated with NDV (MOI = 10, 50, 100 and 200) for 1 hour or 12 hours or left untreated (**Figure3.8 A**). After 12 hours, the supernatant of the cells was collected and processed for ELISA as discussed in materials and methods. A standard curve was also generated, according to manufacturer's instructions to estimate the levels of TNF-α.

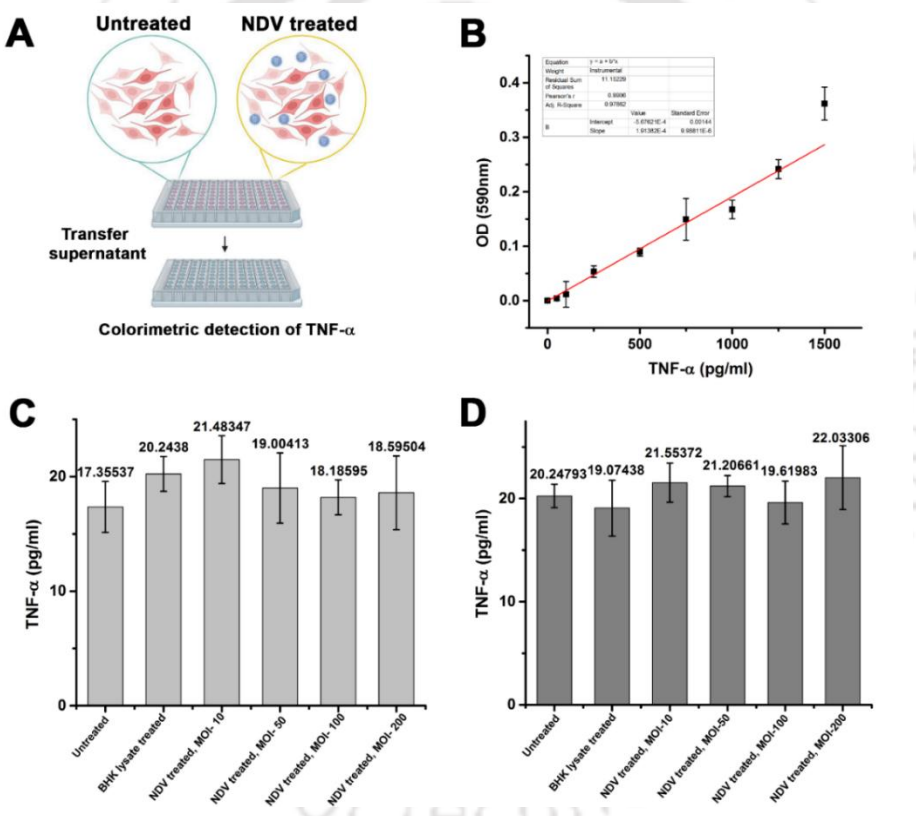

Figure 3.8: NDV does not activate macrophages. (A) Experimental procedure where J774A.1 cells were treated with an increasing MOI of NDV (10, 50, 100 and 200) for 1 hour and 12 hours. Post-incubations, supernatant was collected and processed for quantitative estimation of TNF-α with the help of ELISA. (B) Standard curve of TNF-α was generated according to manufacturer's instructions. (C, D) Levels of TNF-α of the untreated or NDV treated cells after 1 hour (C) and 12 hours (D) respectively.

The results, as depicted in **Figure 3.8 C and D** of the study, indicated that there was no significant correlation between the increasing concentration of NDV and the levels of TNF-α at both time points (1 hour and 12 hours). This lack of correlation suggests that NDV did not

induce stress signaling in the macrophages, as evidenced by the absence of a robust TNF-α response.

3.3.8 NDV restricts *P. yoelii* propagation in mice

We employed a dual approach for testing the anti-plasmodial activity of NDV against *P. yoelii*. In our first approach, *P. yoelii* (40% parasitemia) was incubated *in vitro* with NDV (MOI = 10^2) for 3 hours in an incubator at 37°C and 5% CO_2, before the parasites were injected into mice (**Figure 3.9 A, i**). This pre-treatment of the malaria parasite with the virus was performed to maximize the perturbation caused by the virus due to its interaction with the PRBCs and RBCs while minimizing the possible immunomodulatory effects of the virus *in vivo* in the mice. Parasites were also incubated with heat-inactivated NDV or with AF without the NDV and used as controls. Post-incubation, cells were washed with PBS to remove excess virus particles and injected to different groups as mice and parasitemia were monitored as described previously in materials and methods. The growth curves of *P. yoelii* from day 0 to day 12, under different experimental conditions were plotted as shown in **Figure 3.9 B**. Mice injected with AF-treated *P. yoelii*, parasites were detected earliest at day 4 with a parasitemia of 1.65 ± 0.28%. Mice injected with parasites pre-treated with heat-inactivated NDV also showed detectable parasitemia (0.84 ± 0.05%) at day 4. In contrast, mice injected with NDV-treated *P. yoelii* showed detectable parasites only on day 6 with a parasitemia of 0.61 ± 0.22%. This suggests that the virus delay the appearance of the parasites in peripheral blood circulation by 72 hours. Also, the parasite load was over 60% lower in NDV-treated *P. yoelii* compared to the untreated parasites. Monitoring the growth of the parasites indicate that the untreated parasites proliferated rapidly, reaching parasitemia of 48.73 ± 4.30% on day 12 whereas NDV-treated parasites showed a substantial decline in growth with 5.63 ± 1.69% parasitemia, revealing over 85% reduction in parasite load. *P. yoelii* treated with heat-inactivated NDV showed similar growth curves to the untreated. These results suggest that NDV could cause a substantial reduction in the proliferation of the murine malaria parasite in mice.

In the second approach (Post-treatment), mice were injected with the same amount of *P. yoelii* as in our first method, and the parasites were allowed to proliferate till the parasitemia of 3.28 ± 0.53% (**Figure 3.9 C**). After determining the parasitemia, mice were challenged with NDV (on day 6) and the parasitemia was monitored till day 12. 24 hours post-NDV challenge, we observed a substantial drop in parasitemia (0.61 ± 0.12%) with ~80% reduction in parasite

load compared to that of day 6. NDV was able to restrict the parasitemia below 1% which suggests that the anti-plasmodial effect of the virus was sustained.

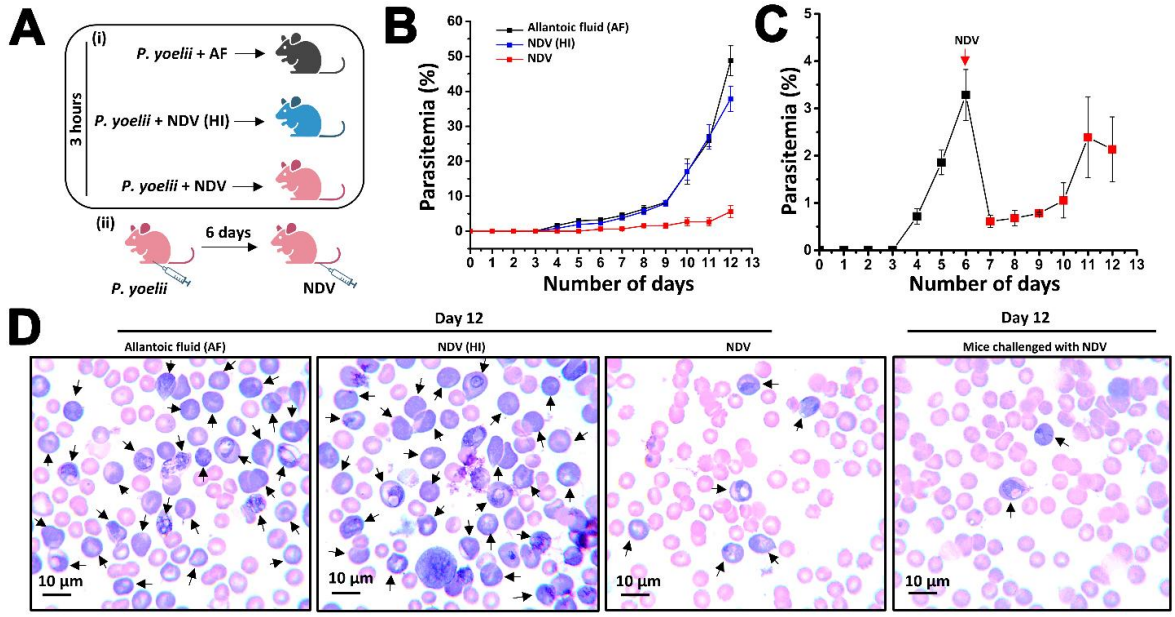

Figure 3.9: NDV displays anti-plasmodial activity against *P. yoelii* in mice. [A(i)] *P. yoelii* was incubated with allantoic fluid (AF) containing no virus, heat-inactivated (HI) NDV or NDV produced in allantoic fluid for 3 hours *in vitro*, followed by washing of the cells and injection into the peritoneum of mice. Thin smears were made from tail snips from day 0 to day 12, and stained by Giemsa for calculating parasitemia. [A(ii)] Untreated *P. yoelii* were injected in mice and allowed to grow for 6 days. On day 6, after the calculation of parasitemia, NDV from allantoic fluid was administered through the intravenous (IV) route, and parasitemia was monitored till day 12. (B) Growth curves of *P. yoelii* 17XNL treated with allantoic fluid (AF; black curve), HI-NDV (blue curve) and NDV (red curve). The mean ± standard deviation (n= 3) for parasitemia calculation from each mouse is shown for all the time points. **(C) Post-NDV challenge, *P. yoelii*-infected mice show a substantial reduction in parasite burden.** Growth curves of *P. yoelii* before administration of NDV (day 0 to day 6) and post-NDV challenge (day 6 to day 12). Red arrow indicates NDV administration at day 6 and red squares highlights the reduction in parasitemia, post-NDV challenge. **(D) (Left to right)** Representative images of Giemsa stained thin smears from day 12 of mice injected with AF-treated or HI-NDV treated or NDV treated *P. yoelii*. The last panel represents *P. yoelii*-infected mice challenged with NDV, post 6 days of infection. PRBCs are indicated by black arrows.

Representative images of Giemsa stained thin smears from day 12 are shown in **Figure 3.9 D**. As seen in the panel from left to right, pre-incubation of *P. yoelii* parasites with AF and NDV-HI showed a significant number of parasitized RBCs (marked by arrows) as compared to the NDV-treated *P. yoelii* and mice challenged with NDV. Thus, realizing the potent anti-plasmodial activity of NDV towards both human and murine malaria, we asked if the HN protein from the virus coat alone could display similar observations and also looked into the

differential engagement of the virus towards RBCs and PRBCs that could highlight its potential for targeted delivery as discussed in the later chapters.

3.4 Discussion

NDV is a versatile, multifunctional virus that has been extensively used as an oncolytic agent and a suitable vector for vaccine delivery against several viral, bacterial and protozoan infections [20-23]. The virus has an innate oncolytic ability as it preferentially selects tumor cells for replication and lysis [24]. It also displays potent immunostimulatory capabilities, which leads to the generation of robust anti-tumor, anti-bacterial and anti-viral immune responses. This versatile nature of the virus is primarily the result of its ability to target its host cells through its coat proteins selectively. The virus displays two spike proteins (HN and F) on its surface. The HN protein recognizes sialic acids on the host cell surface, which helps in virus attachment and is thus the major determinant of host cell recognition [25].

Interestingly, we have presented for the first time that NDV has the potential to be used as an anti-malarial agent against human malaria. Incubation of the virus with P. falciparum resulted in perturbation of the erythrocytic schizogony (**Figure 3.1, A and B**). NDV was also unique in its antagonistic relationship with the malaria parasite as the other virus strains investigated in our study did not affect the parasite propagation (**Figure 3.2**). The anti-plasmodial activity of NDV was quick and also dose-dependent (**Figure 3.3, A and B**). A closer inspection of the different virus strains reveals that although they were of similar biomolecular composition, they possessed vastly different surface chemistry. Influenza virus, which is a negative-sense, single-stranded RNA virus (Orthomyxoviridae family) has three envelope proteins (Hemagglutinin (HA), Neuraminidase (N), and M2). The hemagglutinin recognizes sialic acid receptors and facilitates membrane fusion [26, 27]. IBV is a gammacoronavirus (Coronaviridae family) with a single positive-sense RNA [28]. The spike protein (S) on its surface mediates receptor recognition and Hemagglutination [29]. Both the Influenza virus and IBV utilize sialic acid for binding with the host cells [30, 31]. However, they were found to be ineffective against the malaria parasite.

Viruses that utilize host sialic acid also exhibit specificity for the linkage with which the terminal sialic acid is bound to the immediate sugar, which is predominantly either α-2-3 or α-2,6 [11]. Influenza (PR8), which is an avian strain exclusively requires α-2,3 linked sialic acids for host-cell interaction [32]. Interestingly, it was a shift in linkage preference from α-2-3 to α-2,6 that allowed the influenza viruses (A/B) to adapt from animals to humans [33]. In

IBV, although the specific linkage type has not been well explored, the virus was reported to favor the α-2,3 linked sialic acids on the host cell surface [31]. In contrast, NDV could utilize both the α-2,3 and α-2,6 linked sialic acids on the host cell [16]. Human RBCs predominantly display α-2,6 linked sialic acids on the outer cell surface [34]. This could explain why NDV was able to engage strongly with the PRBCs and disrupt the parasite propagation. DEV and JEV do not utilize sialic acids on the host surface for attachment and were also found to be ineffective against the malaria parasite [35, 36]. Additionally, our results pertaining from the mechanism of action of NDV, we found that the blocking of invasion of the merozoites by the virus could be its major mode of its action (**Figure 3.5).** However, it is also evident that the virus at very low MOI of 10 and incubation period (12 hours) was also able to significantly reduce parasite viability (**Figure 3.3 A, B**). This indicates that the virus might also be involved in perturbation of signaling pathways crucial for the parasite survival. This indicates that NDV could be binding with the RBC or PRBC with the help of receptor: ligand interactions. To answer this, we investigated the interaction of NDV with human RBCs and PRBCs with the help of binding studies and decipher the involvement of any receptor: ligand interaction, which are discussed in the subsequent chapters.

NDV was also tested *in vivo* against the murine malaria strain *P. yoelii* (**Figure 3.9**). Although there is limited literature on the application of the virus against the malaria parasites, previous studies have demonstrated that NDV could inhibit the growth of *P. berghei* and *P. gallinaceum* in mouse and chicken models, respectively [37, 38]. In mice, NDV was found to be a potent inducer of interferons, protecting them from P. berghei infection in a dose-dependent manner. However, in the other study, NDV did not offer any in-ovo protection against P. gallinaceum infection but was able to limit the parasite growth in chicks by inducing interferons. Although in both studies, the interferon-inducing property of the virus was attributed to the observed effects, the possibility of NDV interacting directly with the malaria parasite was not investigated. The potential of the virus was explored in the limited context of its immunomodulatory role, similar to agents such as statolon and a double-stranded copolymer of polyriboinosinicacid and polyribocytidylic acid, which were also used in the study for inducing interferons. The virus was also not tested against human malaria in an in vitro system which could help to establish any innate anti-plasmodial activity that the virus may possess in the absence of its immunomodulatory effects. Thus, we asked whether NDV has any natural ability to restrict the erythrocytic schizogony of the malaria parasite, elucidate its mechanism of action and identify the key molecular players involved in the process.

In our study, we extensively showed that the virus could also act directly on the malaria parasite, thereby disrupting the erythrocytic schizogony of *P. falciparum*. Also, in our *in vivo* study, NDV disrupted the erythrocytic cycle of *P. yoelii*, although the virus was not able to completely restrict the parasite growth (**Figure 3.9 B and C**). This observation could be the result of the clearance of NDV-bound RBCs and PRBCs from blood circulation, resulting in new RBCs being available for the small fraction of parasites to invade, which initially survived the virus onslaught. However, it cannot be unruled that the immunomodulatory function of the virus was not active during this period. We speculate that in an *in vivo* system, both activities of the virus could act simultaneously on the parasite, resulting in the sustained anti-plasmodial activity observed in this study. Thus, a rigorous investigation pertaining to these questions is essential, particularly in an *in vivo* system.

3.5 References

1. Ashley, E.A. and A.P. Phyo, Drugs in development for malaria. Drugs, 2018. 78(9): p. 861-879.

2. Yahiya, S., et al., The antimalarial screening landscape—looking beyond the asexual blood stage. Current Opinion in Chemical Biology, 2019. 50: p. 1-9.

3. Cowman, A.F. and B.S. Crabb, Invasion of red blood cells by malaria parasites. Cell, 2006. 124(4): p. 755-766.

4. Gilson, P.R. and B.S. Crabb, Morphology and kinetics of the three distinct phases of red blood cell invasion by Plasmodium falciparum merozoites. International journal for parasitology, 2009. 39(1): p. 91-96.

5. Soni, R., et al., Signaling strategies of malaria parasite for its survival, proliferation, and infection during erythrocytic stage. Frontiers in immunology, 2017. 8: p. 349.

6. Adderley, J.D., et al., Analysis of erythrocyte signalling pathways during Plasmodium falciparum infection identifies targets for host-directed antimalarial intervention. Nature Communications, 2020. 11(1): p. 4015.

7. Singh, S. and C.E. Chitnis, Molecular signaling involved in entry and exit of malaria parasites from host erythrocytes. Cold Spring Harbor Perspectives in Medicine, 2017. 7(10): p. a026815.

8. Cowman, A.F., D. Berry, and J. Baum, The cellular and molecular basis for malaria parasite invasion of the human red blood cell. Journal of cell Biology, 2012. 198(6): p. 961-971.

9. Matrosovich, M., G. Herrler, and H.D. Klenk, Sialic acid receptors of viruses. Sialoglyco chemistry and biology II: tools and techniques to identify and capture sialoglycans, 2015: p. 1-28.

10. Neu, U., J. Bauer, and T. Stehle, Viruses and sialic acids: rules of engagement. Current opinion in structural biology, 2011. 21(5): p. 610-618.

11. Stencel-Baerenwald, J.E., et al., The sweet spot: defining virus–sialic acid interactions. Nature Reviews Microbiology, 2014. 12(11): p. 739-749.

12. Burzyńska, P., et al., Sialic acids as receptors for pathogens. Biomolecules, 2021. 11(6): p. 831.

13. Wasik, B.R., K.N. Barnard, and C.R. Parrish, Effects of sialic acid modifications on virus binding and infection. Trends in microbiology, 2016. 24(12): p. 991-1001.

14. Herrler, G., J. Hausmann, and H.-D. Klenk, Sialic acid as receptor determinant of ortho- and paramyxoviruses. Biology of the Sialic Acids, 1995: p. 315-336.

15. Zhao, C. and J. Pu, Influence of host sialic acid receptors structure on the host specificity of influenza viruses. Viruses, 2022. 14(10): p. 2141.

16. Sánchez-Felipe, L., E. Villar, and I. Muñoz-Barroso, α2-3-and α2-6-N-linked sialic acids allow efficient interaction of Newcastle Disease Virus with target cells. Glycoconjugate journal, 2012. 29: p. 539-549.

17. Connaris, H., et al., Probing the sialic acid binding site of the hemagglutinin-neuraminidase of Newcastle disease virus: identification of key amino acids involved in cell binding, catalysis, and fusion. Journal of virology, 2002. 76(4): p. 1816-1824.

18. Trivedi, V., et al., Clotrimazole inhibits hemo-peroxidase of P. falciparum and induces oxidative stress: proposed antimalarial mechanism of clotrimazole. Journal of Biological Chemistry, 2005.

19. Neog, S., S. Kumar, and V. Trivedi, Isolation and characterization of Newcastle disease virus from biological fluids using column chromatography. Biomedical Chromatography, 2023. 37(1): p. e5527.

20. Huang, Z., et al., Recombinant Newcastle disease virus as a vaccine vector. Poultry Science, 2003. 82(6): p. 899-906.

21. Vigil, A., et al., Recombinant Newcastle disease virus as a vaccine vector for cancer therapy. Molecular Therapy, 2008. 16(11): p. 1883-1890.

22. Duan, Z., et al., Recombinant Newcastle disease virus-vectored vaccines against human and animal infectious diseases. Future Microbiology, 2015. 10(8): p. 1307-1323.

23. Chu, K.-B. and F.-S. Quan, Virus-like particle vaccines against respiratory viruses and protozoan parasites. 2021.

24. Burman, B., G. Pesci, and D. Zamarin, Newcastle disease virus at the forefront of cancer immunotherapy. Cancers, 2020. 12(12): p. 3552.

25. Huang, Z., et al., The hemagglutinin-neuraminidase protein of Newcastle disease virus determines tropism and virulence. Journal of virology, 2004. 78(8): p. 4176-4184.

26. Lamb, R.A. and R.M. Krug, Orthomyxoviridae: the viruses and their replication. 2001.

27. Sriwilaijaroen, N. and Y. Suzuki, Molecular basis of the structure and function of H1 hemagglutinin of influenza virus. Proceedings of the Japan Academy, Series B, 2012. 88(6): p. 226-249.

28. Lin, S.-Y. and H.-W. Chen, Infectious bronchitis virus variants: molecular analysis and pathogenicity investigation. International journal of molecular sciences, 2017. 18(10): p. 2030.

29. Promkuntod, N., et al., Mapping of the receptor-binding domain and amino acids critical for attachment in the spike protein of avian coronavirus infectious bronchitis virus. Virology, 2014. 448: p. 26-32.

30. Tate, M.D., A.G. Brooks, and P.C. Reading, Correlation between sialic acid expression and infection of murine macrophages by different strains of influenza virus. Microbes and infection, 2011. 13(2): p. 202-207.

31. Rahman, S.A.E., et al., Comparative analysis of the sialic acid binding activity and the tropism for the respiratory epithelium of four different strains of avian infectious bronchitis virus. Avian Pathology, 2009. 38(1): p. 41-45.

32. Rogers, G.N. and J.C. Paulson, Receptor determinants of human and animal influenza virus isolates: differences in receptor specificity of the H3 hemagglutinin based on species of origin. Virology, 1983. 127(2): p. 361-373.

33. Rogers, G.N., et al., Differential sensitivity of human, avian, and equine influenza A viruses to a glycoprotein inhibitor of infection: selection of receptor specific variants. Virology, 1983. 131(2): p. 394-408.

34. Gagneux, P., et al., Human-specific regulation of α2–6-linked sialic acids. Journal of Biological Chemistry, 2003. 278(48): p. 48245-48250.

35. Unni, S.K., et al., Japanese encephalitis virus: from genome to infectome. Microbes and infection, 2011. 13(4): p. 312-321.

36. Dardiri, A., Duck viral enteritis (duck plague) characteristics and immune response of the host. American Journal of Veterinary Research, 1975. 36(4 Pt 2): p. 535-538.

37. Jahiel, R.I., et al., Anti-malarial effect of interferon inducers at different stages of development of Plasmodium berghei in the mouse. Nature, 1968. 220(5168): p. 710-711.

38. Herman, R., T. Shiroishi, and C.E. Buckler, Viral interference with exoerythrocytic forms of malaria (Plasmodium gallinaceum) in ovo. Journal of Infectious Diseases, 1973. 128(2): p. 148-155.

Chapter 4

The HN: sialic acid interaction mediates the anti-plasmodial activity of NDV

The contents of this chapter are partly published as "**Neog S, Vinjamuri SR, Vijayan K, Kumar S, Trivedi V. NDV targets the invasion pathway in malaria parasite through cell surface sialic acid interaction. FASEB J.** 2024 Aug 15;38(15):e23856. doi: 10.1096/fj.202400004RR. **PMID: 39092913.**

Summary

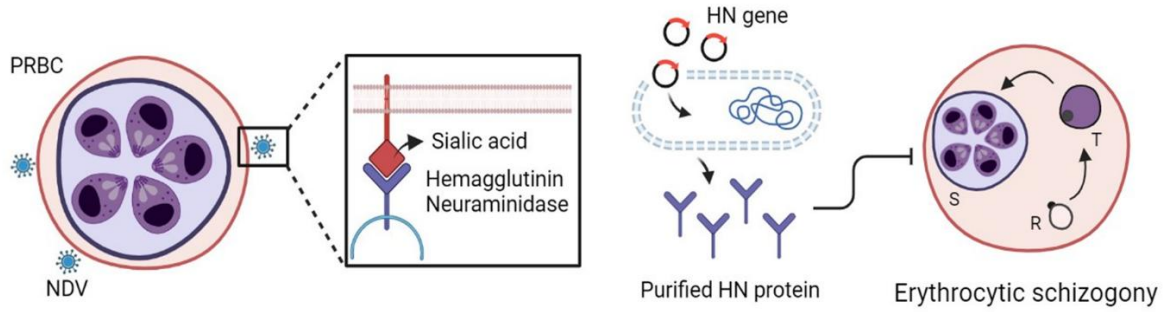

The Newcastle Disease Virus (NDV), known for its affinity to interact with avian red blood cells (RBCs), was investigated for its impact on the erythrocytic schizogony of *Plasmodium falciparum* (*Pf*3D7) and *Plasmodium yoelii*. Co-infection experiments demonstrated that NDV effectively disrupted the erythrocytic schizogony by preventing merozoite invasion into uninfected RBCs. Further investigations revealed that NDV binds rapidly and with higher affinity to RBCs infected with the malaria parasite (PRBCs) compared to uninfected RBCs in both human and murine malaria strains. This differential binding demonstrates potential application of the virus for targeted drug delivery. To elucidate the role of any protein: ligand interaction, various treatments including heat treatment, fixatives, and enzymatic processes were employed. Exposure of the virus to these conditions resulted in the loss of NDV binding. Particularly, removal of sialic acids from the erythrocyte surface significantly diminished NDV binding, emphasizing their essential role in virus-PRBC interaction. Blocking the active site of HN or using anti-HN antibodies abolished NDV binding to both RBCs and PRBCs and also resulted in a dose-dependent reduction in its anti-plasmodial activity. Thus, the interaction between the NDV spike glycoprotein HN and sialic acid was identified as a crucial component for the anti-plasmodial activity of the virus. Moreover, NDV HN protein was cloned, overexpressed and purified from the prokaryotic system. The purified HN protein also disrupts malaria parasite schizogony in a dose-dependent manner. This underscores the pivotal role of the HN protein in targeting sialic acid-containing receptors on RBCs and PRBCs, thereby disrupting malaria parasite proliferation in the blood.

4.1 Introduction

Sialic acids are nine-carbon sugars, typically found as terminal residues on glycoproteins and glycolipids on cell surfaces [1]. They act as important receptors for a myriad of human pathogens ranging from bacteria and viruses to protozoa [2-5]. Sialic acids play a pivotal role in the complex life cycle of human protozoan parasites, such as the malaria parasite [6, 7]. During the erythrocytic schizogony, the parasite selectively binds to the erythrocyte surface glycophorins, which are rich in sialic acids, to invade the uninfected RBCs. The merozoite surface displays a diverse group of antigens that utilize sialic acids containing receptors on the RBC surface for adhesion and entry. In the case of *P. falciparum*, the Erythrocytic Binding-Like (EBL) proteins facilitate the attachment of merozoites to human RBCs by targeting sialic acid-rich receptors, particularly the glycophorins, displayed on the red cell surface. Among the four homologs of EBLs characterized in *P. falciparum*, the EBA-175 merozoite antigen targets Glycophorin A (GPA), the EBA-140 recognizes Glycophorin C (GPC) and the EBL-1 binds to Glycophorin B (GPB). However, the erythrocyte receptor of EBA-181 remains elusive [8-11]. Although most field isolates of the malaria parasite are found to utilize the sialic acid-dependent invasion pathway, the parasites could also utilize the sialic acid-independent pathway for invasion [12]. In the sialic acid-independent pathway, a different set of molecular interactions, primarily mediated by the reticulocyte-binding protein homolog (Rh) family is employed by the parasite. Rh5 binds to basigin (BSG), a receptor on the erythrocyte surface [13]. Other Rh proteins, such as Rh2 and Rh4, also contribute to the invasion process. Rh2 has been shown to interact with an unknown receptor on the erythrocyte surface, while Rh4 can bind complement receptor 1 (CR1) [14, 15]. However, the exact roles and mechanisms of these interactions are still not fully elucidated.

Additionally, studies have shown that the sialic acid independent pathway is usually employed under certain experimental conditions, such as during enzymatic depletion of cell surface sialic acids [16, 17]. It shows that the malaria parasite utilizes a diverse set of receptors for invading new RBCs for the continuation of the erythrocytic schizogony. The Newcastle Disease Virus (NDV) exhibits a natural affinity for avian erythrocytes, particularly due to its coat protein hemagglutinin-neuraminidase (HN), which facilitates cell recognition [18, 19]. The HN coat protein of Newcastle Disease Virus (NDV) is a multifunctional glycoprotein critical for viral attachment, fusion, and release. The HN protein exhibits both receptor-binding (hemagglutinin) and receptor-destroying (neuraminidase) activities [20-22]. On the virus coat, the protein exists as a tetramer, each monomer consisting of an ectodomain or receptor binding

domain (RBD), a transmembrane domain, and a cytoplasmic tail [23]. The ectodomain harbors both the receptor-binding and neuraminidase sites. The receptor-binding site is responsible for recognizing and attaching to sialic acid moieties on host glycoproteins and glycolipids, initiating the infection process. The neuraminidase site, on the other hand, cleaves sialic acid residues, facilitating the release of progeny virions from the infected cell and preventing viral aggregation [24].

Our results from co-infection studies, as discussed in Chapter III, showed that the virus was able to dose-dependently disrupt the erythrocytic schizogony of the malaria parasite (*Pf*3D7) by blocking the invasion of merozoites into uninfected RBCs. Interestingly, NDV was also found to cause perturbation of the erythrocytic cycle of the murine malaria parasite *P. yoelii*. Given the central role of sialic acids in the pathogenesis of both organisms, we envisioned that the observed anti-plasmodial activity of the virus could be mediated by specific protein-ligand interaction. Thus, we began by asking whether NDV was able to engage with the human RBCs and PRBCs with the help of binding studies. Additionally, since the virus was also tested against *P. yoelii*, we checked the binding of the virus with both murine RBCs and PRBCs as well. Observations from the initial binding studies revealed that NDV was able to bind very rapidly with the vessel of the malaria parasite (RBCs) and also with the RBCs infected with the malaria parasite (PRBCs). Interestingly, we found a differential engagement of NDV with the RBCs and PRBCs. From our binding studies with flow cytometry and immunofluorescence imaging we found that the affinity of the virus towards the PRBCs was substantially higher as compared to the uninfected RBCs in both the human and murine malaria strains. It suggests that the virus might be actively targeting the PRBCs. It thus provides an excellent opportunity to explore the potential of NDV for targeted delivery of antimalarial drugs directly to the PRBCs.

To further elucidate the role of protein: ligand interaction, the binding of NDV with the erythrocytes was challenged with heat treatment, aldehyde fixatives and enzymatic treatment. Exposure of the virus to these conditions resulted in complete loss of binding. Also, the cleaving of erythrocyte surface proteins with protease or removal of the terminal sialic acids with neuraminidase resulted in a significant loss of NDV binding. It suggests that proteins from both the NDV coat and host cell surface were involved in the interaction. Also, the host surface sialic acids were indispensable for virus binding. In the case of NDV, the spike glycoprotein HN mediates the attachment of the virus with the cell surface by hijacking the host sialic acid receptors. Thus, to elucidate the role of the HN coat protein, we blocked its active site by pre-

treating the virus with an excess of extracellular sialic acid or employed specific anti-HN antibodies to hinder its activity. Notably, blocking of the HN protein not only resulted in the loss of binding of NDV with the RBCs and PRBCs but also led to a substantial decrease in the anti-plasmodial activity of the virus. This suggests that the binding of NDV to the PRBCs through the HN: sialic acid interaction is crucial for the virus to exert its anti-plasmodial action on the malaria parasite.

Hence, considering the central role of the NDV HN coat protein, we asked whether the protein alone could have any effect on the malaria parasite viability. To answer this, the HN gene from NDV was cloned into a prokaryotic expression vector and the protein was overexpressed and purified. The structural and functional activity of the purified protein was characterized with the help of circular dichroism (DM), Dynamic Light Scattering (DLS) and Plaque inhibition assay. Subsequently, the purified HN protein was tested against the malaria parasite, where we found that the single protein from NDV was able to dose-dependently inhibit the erythrocytic schizogony of the malaria parasite. Thus, it can be concluded that NDV, through its HN protein, targets sialic acid-containing receptors on the RBCs and PRBCs, leading to the disruption of the malaria parasite proliferation in blood.

4.2. Experimental procedures

4.2.1 Disrupting NDV proteome with an aldehyde fixative and heat inactivation

The binding of NDV with RBCs and PRBCs was examined using flow cytometry under various treatment conditions, as follows: The hemagglutinin-neuraminidase (HN) and Fusion (F) are the two spike proteins that protrude out from the NDV surface. The viral surface proteins were modified with the help of aldehyde fixative and heat treatment to check their involvement in NDV-RBC interaction. NDV was treated with 2% glutaraldehyde for 30 minutes at room temperature (RT). The unreacted glutaraldehyde in the virus sample was quenched with 2% glycine for 30 minutes and the virus preparation was incubated with RBCs for 1 hour at a MOI of 10^2. In another approach, we tested the affinity of heat-inactivated (HI) NDV towards RBCs. NDV was incubated at 60^0C for 1 hour in a water bath, followed by a brief incubation on ice, allowing the sample to cool down. Following the treatment, RBCs were incubated with heat-inactivated virus preparation (MOI=10^2) and processed for flow cytometry.

4.2.2 Enzymatic treatment to challenge NDV binding

Enzymatic removal of the NDV surface proteins was done by incubating the virus with Proteinase-K (0.4U/ml) for 1 hour at 37°C, followed by the inhibition of the protease with 1

mM PMSF. The virus preparation was incubated with RBCs for 1 hour at an MOI of 10^3. Proteins from the RBC surface were removed by treating the cells with Proteinase-K (0.4U/ml) for 1 hour at 37°C. Post-incubations the cells were washed and incubated with NDV at a MOI of 10^3. Sialic acids on the RBC surface were removed by treating the cells with neuraminidase (50 mU/ml) for 1 hour at 37°C. Post-incubations the cells were washed and incubated with NDV (MOI=10^3) and processed for flow cytometry.

4.2.3 Blocking of NDV HN protein with free sialic acid and specific antibody

To further elucidate the role of HN-sialic acid interaction in the binding of NDV with the PRBCs, NDV was treated with different concentrations of sialic acid (10, 100 and 200 µM) for 1 hour at 37°C. The virus preparations were incubated with malaria parasite culture (MOI=10^3) in complete media for 1 hour at 37°C and further processed for flow cytometry analysis. NDV was also incubated with an anti-HN antibody (~0.5µg in 0.5ml) overnight at 4°C under shaking conditions. Post-treatment the virus was incubated with parasite culture for 1 hour at 37°C and processed further as described below.

4.2.4 Flow cytometry analysis

Following the incubation of NDV with RBCs or PRBCs under different treatment conditions, the cells were washed with ice-cold PBS followed by fixation with 4% paraformaldehyde and 0.05% glutaraldehyde for 30 min at RT and permeabilized with 0.1% Triton X-100 for 10 min. Blocking was done with 5% BSA for 1 hour at RT followed by incubation with a chicken polyclonal anti-NDV antibody (1:2000)[25] or Mouse monoclonal anti-HN (1:2000) (Santa Cruz Biotechnology, HN14f, sc-53562) at RT for 1 hour. Cells were washed with PBS and probed with an appropriate FITC-conjugated secondary antibody. The PRBCs were counterstained with propidium iodide at a working concentration of 50 µg/ml for 20-30 min before analyzing the cells in a flow cytometer. A total of 50,000 events were recorded with a FACS caliber (Becton Dickinson). All flow cytometry data was analyzed with FCS Express version 5.

4.2.5 Scanning electron microscopy

NDV particles bound to the human erythrocyte cell surface were visualized with the help of scanning electron microscope. NDV was incubated with a MOI of 10 with RBCs for 30 min at RT followed by three washes with ice-cold PBS. The cells were adhered to Poly-L lysine-coated coverslips and fixed with 2% Glutaraldehyde for 15 min at RT. The adhered cells were washed four times with PBS and dried with a series of ethanol gradients and kept in the

desiccator until imaging. A single layer of gold coating was done before analysing with Gemini 500 FE-SEM.

4.2.6 Binding studies of NDV with *P. yoelii*-infected RBCs

Whole blood was collected in tubes with heparin from the tail vein of an anaesthetized mouse infected with the knobless parasite strain *Plasmodium yoelii* (17XNL). The parasitemia was calculated with thin blood smears stained with Giemsa, under 100x objective. Infected whole blood (100µl of 40% parasitemia) was incubated with NDV at an MOI = 10^3 for 1 hour at 37ºC, followed by washing the cells with ice-cold PBS. Cells were fixed with 4% paraformaldehyde and 0.05% v/v glutaraldehyde for 30 min at RT and permeabilized with 0.1% Triton X-100 for 10 min. Blocking was done with 5% BSA for 1 hour at RT. NDV was probed with a chicken polyclonal anti-NDV antibody (1:2000) for 1 hour at RT followed by an hour of incubation with an appropriate FITC-conjugated secondary antibody. *P. yoelii*-infected RBCs were segregated from uninfected RBCs with propidium iodide staining (50 µg/ml) for 20-30 min. A total of 50,000 events were recorded with a flow cytometer (BD FacsLyric), and data was analysed with FCS Express version 7.

4.2.7 Immunofluorescence imaging

NDV was incubated with Pf3D7 or *P. yoelii* infected RBCs at 37°C for 1 hour at an MOI of 10^3 and processed for immunofluorescence imaging. The cells were washed with ice-cold PBS to remove any unbound virus particles, fixed with 4% paraformaldehyde and 0.05% glutaraldehyde for 30 min at RT, followed by washing with ice-cold PBS to remove any unbound virus particles. Cells were permeabilized with 0.1% Triton X-100 for 10 min at (RT) and blocked with 5% BSA for 1 hour at RT. NDV was probed with a Chicken polyclonal anti-NDV antibody (1:500) and an appropriate FITC-conjugated secondary antibody. The cells were then washed and adhered on coverslips coated with Poly-L-lysine and mounted with Gold anti-fade DAPI mounting media. The samples were analyzed at 100x magnification under immersion oil with a fluorescence microscope (Nikon Eclipse T*i*-S, model: TI-FL) or a Confocal microscope (Olympus, FV-3000). During confocal imaging, fifteen optical sections of the cells were taken and z-stacking was performed using ImageJ software.

4.2.8 Cloning and construction of the expression plasmid with the HN gene

Genomic RNA extraction from NDV was adopted from a previous study[26]. The RNA isolated was used for cDNA synthesis using random hexamers. The cDNA was used to amplify the extravirion domain using the following primers: Forward (FW) -5'-

CGCGGATCCATGGGGGCTAGCACACCTAG-3' and Reverse (RV) -5'-CTCAAGCTTCTAGCCAGACCTGGCTTCTCT-3' with BamHI and HindIII restriction sites. The amplified product (1611 bp) was resolved in 1% agarose gel and visualized in the Bio-Rad chemiDoc system. The HN fragment was eluted from the gel with the help of a silica DNA extraction kit from Himedia (MB503-400PR) as per the manufacturer's instructions. The eluted product was ligated into a pMD20 T-vector from Takara (T-Vector pMD™20, 3270). The construct was subjected to restriction digestion with BamHI and HindIII and finally ligated into the expression vector pET-28a (+) (Novagen, EM69864-3). Successful ligation of the HN fragment in pET28a was confirmed with restriction digestion with BamHI and HindIII, followed by visualization of the released insert in an agarose gel. The resultant construct was used to transform *E. coli* Top 10 competent cells for maintenance and Rosetta (DE3) or BL-21(DE3) for protein expression. Positive colonies were selected with the help of colony PCR with primers described previously.

4.2.9 Heat shock protocol to obtain soluble expression of HN

Transformed colonies were initially screened with colony PCR and allowed to grow in 5 ml LB media with 50 µg/ml Kanamycin prior to expansion in 250 ml culture medium. A brief heat shock at 42°C was given for 15 min, followed by induction with 0.5 mM IPTG at 37°C for 3-4 hours. The cells were harvested, and suspended in buffer (50 mM sodium phosphate buffer, 500 mM NaCl, 20 mM Imidazole, pH 8) and lysed using a sonicator in the presence of PMSF (1 mM) as a protease inhibitor. The lysate was centrifuged at 13,000 rpm for 30 minutes at 4°C to obtain the soluble and the pellet (insoluble) fractions. The protein fractions were analyzed with SDS-PAGE and western blot.

4.2.10 Ni-NTA purification

The soluble fraction containing the HN protein was incubated with 1ml of equilibrated Ni-NTA slurry for 1 hour at 4°C, and the flow-through was collected. The slurry was washed with 10 Column volumes (CV) of binding buffer containing progressively higher concentrations of imidazole (20-50mM). The protein was eluted using 250 mM imidazole. All eluted fractions were analyzed with SDS-PAGE. The purified HN protein fractions were pooled together and concentrated using an Amicon Ultra 4mL concentrator with a 50 kDa cut-off, to a final volume of 500 µl. A further polishing step was performed to obtain pure HN protein fractions with a Superdex 200 increase 10/300 GL gel filtration column, connected to an FPLC system (AKTA pure, GE Healthcare, Chicago, IL, USA). The protein was finally obtained in the gel filtration

buffer (50 mM sodium phosphate buffer, 150 mM NaCl, pH 7.4). The concentration of the HN protein was estimated with a Bradford assay (Quick Start Bradford 1x Dye Reagent) according to the manufacturer's instructions and the purity was analyzed with SDS-PAGE.

4.2.11 Western blot analysis

All protein samples were separated in a 10% SDS-polyacrylamide gel and then transferred to a nitrocellulose membrane (Bio-Rad, 162-0112) on a Trans-Blot Turbo (Bio-Rad). The blots were blocked with 5% BSA for 2 hours at RT followed by incubation with mouse monoclonal anti-HN (1:8000) (Santa Cruz Biotechnology, HN14f, sc-53562) overnight at 4°C with constant shaking. Blots were washed with TBST and incubated with appropriate HRP-conjugated secondary antibodies for 1 hour at RT, washed, and developed with Bio-Rad Clarity Western ECL substrate kit. Chemiluminescence was captured in the Bio-Rad chemiDoc system.

4.2.12 Circular Dichroism Spectroscopy

The Circular dichroism (CD) spectrum of desalted HN protein was recorded on a Jasco J1500 spectropolarimeter and was analyzed with the CDSSTR program in DicroWeb [27].

4.2.13 Dynamic Light Scattering

The hydrodynamic size of the HN protein (0.1mg/ml) was calculated using a dynamic light scattering instrument, Zetasizer Nano ZS90 (Malvern Instruments, Malvern UK). The particle size was recorded by scattering light from a 632.8nm laser passing through the sample in a quartz cuvette, at an angle of 175°. The average value of 10 runs for each sample and the controls was calculated as the hydrodynamic size.

4.2.14 Plaque Inhibition Assay

Monolayers of BHK-21 cells were incubated with 0.4 ml of different concentrations of purified HN protein, diluted in plain DMEM for two hours in the incubator and gently rocked every 15 min. Cells were washed with plain DMEM, followed by incubation with 0.4 ml of NDV-R2B at a MOI of 0.01 in plain DMEM for 1 hour. The infection media was removed and the cells were washed three times and gently overlaid with pre-warmed solid medium (0.3% Agarose Plaque media). The cells were incubated at 37ºC and 5% CO2 for 48 hours and fixed with 10% PFA for 30 min by directly overlaying it in the solid media. The solid agarose layer was removed and the fixing solution was drained. The cells were washed with PBS and stained with

1% Crystal violet solution for 15 min. The excess stain was washed off and the wells were allowed to dry before counting the visible plaques.

4.2.15 Treatment of malaria parasite with purified HN protein

Malaria parasite cultures (*Pf*3D7) were synchronized with sorbitol to obtain a homogenous culture of schizonts at 1% Parasitemia, which was treated with increasing concentrations of the purified HN coat protein of NDV (1, 5 and 10 µM). Schizonts were also treated with BSA (10 µM) or NDV (MOI = 10^3) or left untreated and used as controls. Parasitemia of the HN protein treated and control parasites was monitored every 24 hours till the 96-hour time point. The morphology of the parasites was also studied under high magnification, as described before.

4.3 Results

4.3.1 NDV binds to human RBCs

The coinfection studies, as described in Chapter III, showed that NDV carries potent anti-plasmodial activity against both the human (*Pf*3D7) and murine (*Py*17XNL) malaria parasites. Both human and murine RBCs are known to have heavily sialylated cell surface glycoproteins that the malaria parasite targets during the erythrocytic schizogony. These sialic acid-rich cell surfaces could also be targeted by NDV, considering its known hemagglutinin activity against the avian erythrocytes. It was thus a curious question of whether the virus was able to bind with the human and murine uninfected RBCs or plasmodium-infected RBCs (PRBCs). To test this, we initially checked the binding of the virus with the human RBCs without the malaria parasite. NDV was briefly incubated with human RBCs followed by multiple steps of washing to remove any unbound virus particles as described in materials and methods. The cell surface bound NDV particles were probed with specific antibodies and virus bound erythrocytes were detected using flow cytometry. As shown in **Figure 4.1 A**, the NDV-treated RBCs showed a strong fluorescence signal (green curve) as compared to the untreated RBCs (black curve) and RBCs incubated with only the antibodies (red curve), which negates any possibility of the non-specific signal. It suggests that the virus was able to bind with human RBCs.

We also performed Scanning Electron Microscopy (SEM) for direct visualization of the virus particles bound on the surface of human RBCs. The electron micrographs were first taken at 30,000x magnification where the untreated RBCs showed the typical discoid morphology with a smooth surface (**Figure 4.1 B**). RBCs treated with NDV showed distinct virus particles attached to the red cell surface. Also, the dry state diameter of the cell surface bound particles

calculated at 30,000x and 100,000x were found to be in the range of 180 to 200 nm, which is typical for the NDV particles. Thus, it was confirmed that the virus was able to bind rapidly with human RBCs.

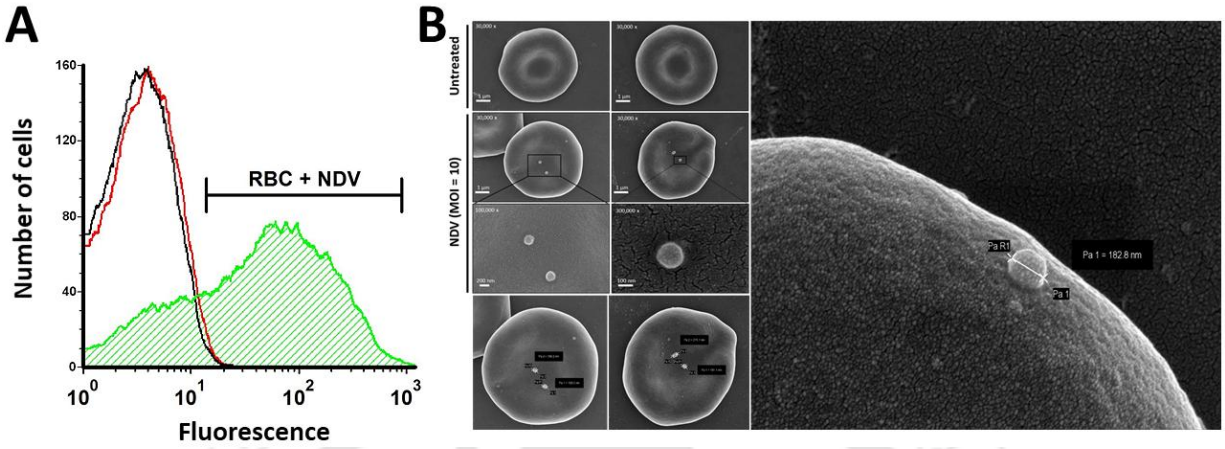

Figure 4.1: NDV binds to human RBCs. (A) Human RBCs were incubated with NDV (MOI = 10^3) for 1 hour and processed for flow cytometry as discussed in materials and methods. RBCs were kept untreated or incubated with only antibodies and used as controls. The number of cells (counts) was plotted on the Y-axis, and fluorescence from NDV-bound RBCs (green fluorescence) was plotted on the X-axis. The graph shows the population of untreated RBCs (black curve), RBCs incubated with antibodies (red curve), and RBCs incubated with NDV (green curve). (B) Direct visualization of NDV bound to the surface of human RBCs with the help of SEM. RBCs without the virus (untreated) showed normal discoid morphology with a smooth surface. RBCs treated with NDV (MOI = 10) showed distinct virus particles adhered to the cell surface. The particle size was also determined and found to be within the range of 180-200 nm in diameter.

4.3.2 NDV preferentially targets the *Pf*3D7 parasitized RBCs

Based on the binding studies of NDV with human RBCs we tested the binding of the virus with the parasitized RBCs as well. The affinity of the virus towards the PRBCs and uninfected RBCs was measured with the help of flow cytometry as described in the material and methods. Parasite cultures were treated with NDV at a MOI of 10^3 for 1 hour and then processed for flow cytometry as described in materials and methods. The PRBC population was segregated from the uninfected RBC population by staining the parasite DNA with propidium iodide (**Figure 4.2 A**). The dot blot analysis shows two distinct populations based on the PI signal, where the population gated in the red square represents the PRBCs or iRBCs, whereas the populations gated in the blue square denote the uninfected RBCs. Following the identification of the PRBC population, histograms from the NDV-bound RBCs and PRBCs were recorded. As shown in **Figure 4.2 B**, the fluorescence intensity from the PRBCs (blue curve) was significantly high compared to uninfected RBCs **(**red curve). Quantitative estimations from the histogram

analysis showed that the binding of NDV to the PRBC is 2.5-fold greater than that from the uninfected RBCs (**Figure 4.2 C**). This indicates that the virus particles were predominantly bound to PRBCs and, therefore might possess a stronger affinity for the plasmodium-infected RBCs.

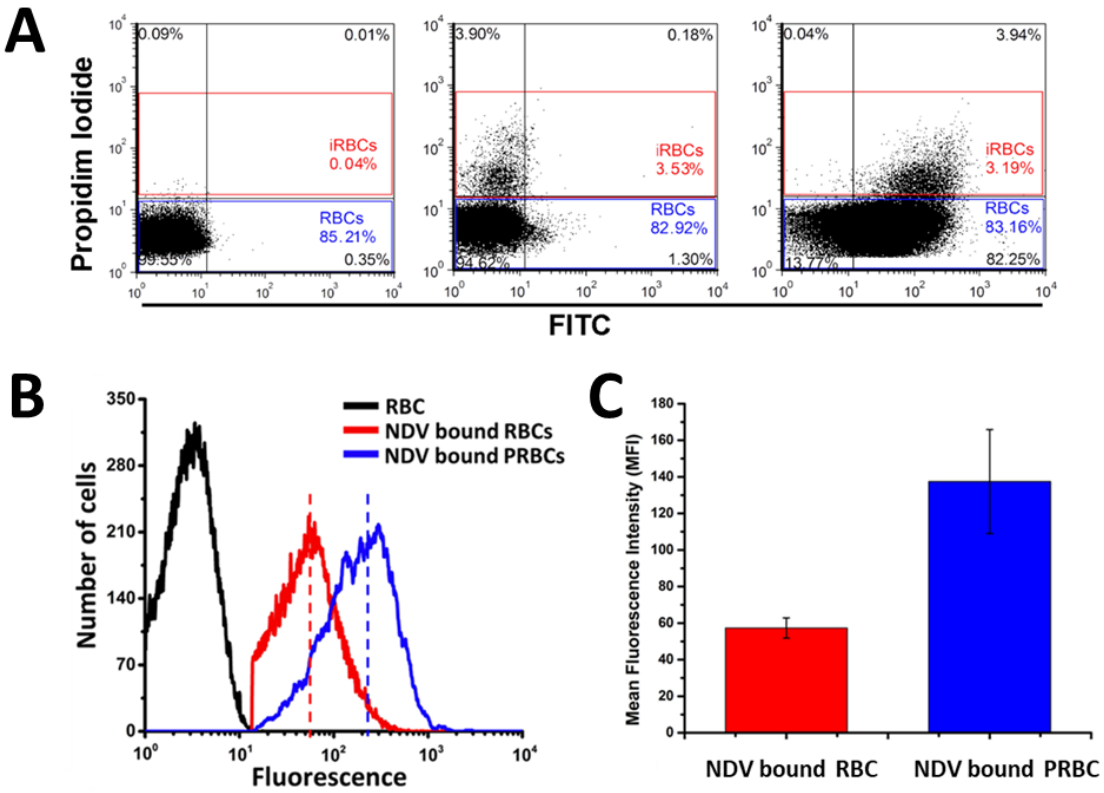

Figure 4.2: NDV preferentially targets the PRBCs. NDV (MOI=10^3) was incubated with synchronized rings and its binding affinity with the RBCs or PRBCs was analyzed with the help of flow cytometry. (A) NDV-bound PRBCs population was characterized with propidium iodide staining and separated from the NDV-bound uninfected RBCs. (B) The two cell populations were gated (RBCs: blue and PRBCs: red) followed by histogram analysis. Cell counts were plotted on the Y-axis, while fluorescence from untreated RBCs (black curve), NDV-bound RBCs (red curve) or NDV-bound PRBCs (blue curve) was plotted on the X-axis. (C) Mean Fluorescence Intensity (MFI) is plotted of NDV-bound RBC (red) and NDV-bound PRBC (blue).

4.3.3 Immunofluorescence imaging of NDV-bound *P. falciparum*-infected RBCs

To further confirm the higher affinity of NDV to PRBCs, we performed immune-localization studies using anti-NDV antibodies in conjugation with FITC-labelled secondary antibodies as described in the material and methods. DAPI was used for staining the nucleus of the malaria parasite. The virus-treated PRBCs showed a strong FITC signal (green fluorescence) localized with the cell membrane and a very weak signal inside the cells (**Figure 4.3**). In comparison,

uninfected RBCs showed very weak NDV signals (green fluorescence) on the cell surface. These observations agree with our previous results from binding studies with flow cytometry. The results confirmed that the NDV has a greater affinity for the PRBCs compared to uninfected RBCs and, therefore, are suitable for further application in anti-malarial drug delivery.

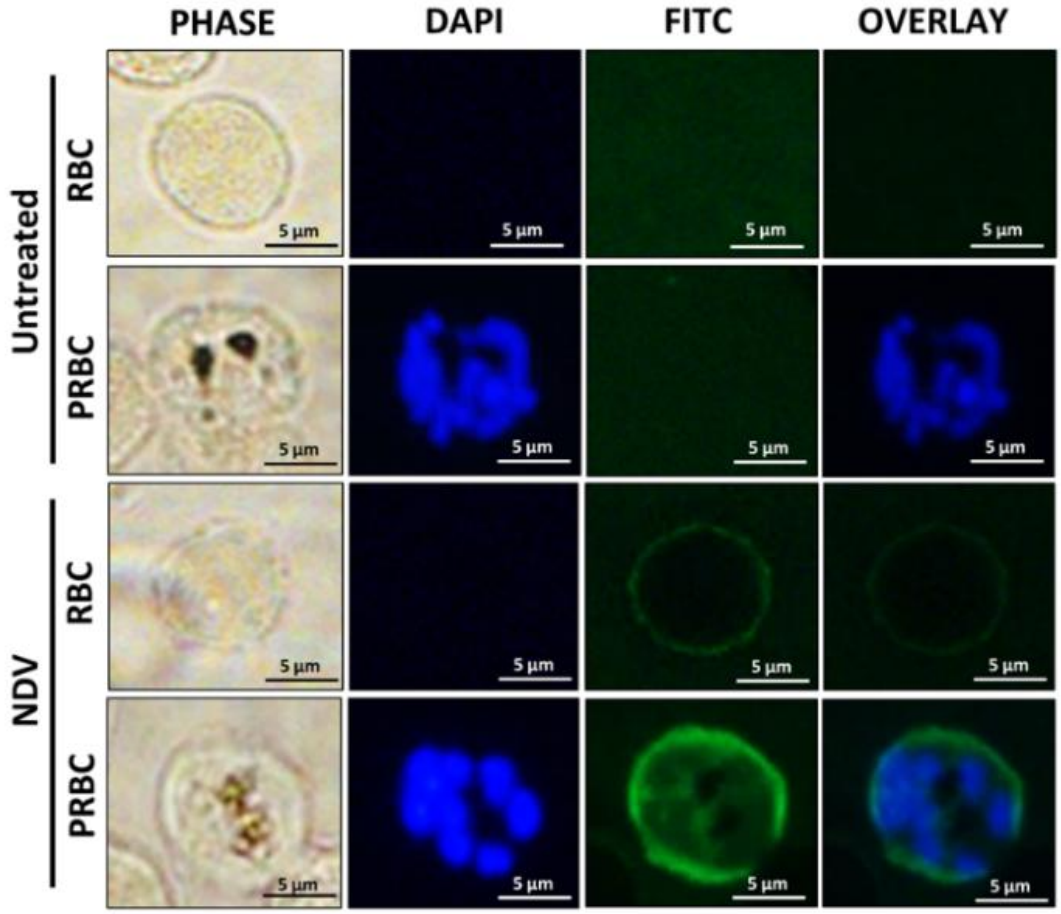

Figure 4.3: Immuno-localization of NDV on the PRBC and RBC. To visualize the virus bound with the RBCs and PRBCs, NDV was incubated with the malaria parasite for 1 hour and processed for immunolocalization as described in materials and methods. Parasite DNA was stained with DAPI (blue) and green fluorescence (FITC) corresponds to the NDV signal.

4.3.4 NDV preferentially targets the *P. yoelii*-infected RBCs

The binding studies of NDV with the human malaria parasite (Pf3D7) revealed that the virus has a greater affinity for the PRBCs compared to the RBCs. Thus, we asked whether this differential engagement of the virus could be observed in the case of *P. yoelii* as well. NDV was incubated with *P. yoelii* infected RBCs (40% parasitemia) at a MOI = 10^3 for 1 hour and

processed for flow cytometry as described in materials and methods. PRBCs were segregated from the uninfected RBC population with the help of Propidium Iodide (PI) staining.

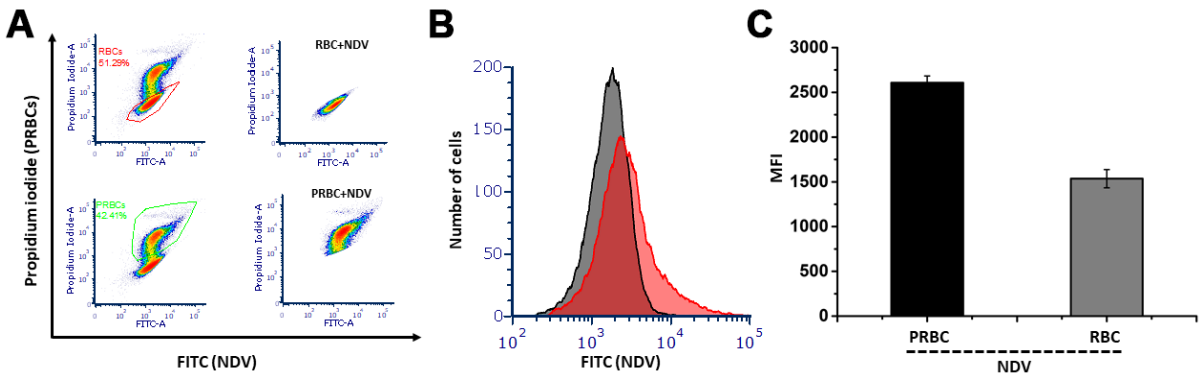

Figure 4.4: NDV preferentially targets the *P. yoelii*-infected RBCs (PRBCs). NDV at a MOI=10^3 was incubated with *P. yoelii* infected blood and its binding affinity with the RBCs or PRBCs was analyzed with the help of flow cytometry. (A) NDV-bound PRBCs population (green gating) was characterized with propidium iodide staining and distinguished from the NDV-bound uninfected RBCs (red gating). Y-axis: fluorescence from PI (PRBCs), X-axis: fluorescence from FITC (NDV). (B) Histogram analysis of the NDV-bound RBCs and PRBCs, where cell counts were plotted on the Y-axis, while fluorescence from NDV-bound RBCs (grey curve) or NDV-bound PRBCs (red curve) was plotted on the X-axis. (C) Mean Fluorescence Intensity (MFI) is plotted of NDV-bound RBC (grey) and NDV-bound PRBC (black).

A depiction of the gating of NDV-bound RBC (red gating) and NDV-bound PRBC (green gating), with the Y-axis representing PI fluorescence (PRBCs) and the X-axis representing FITC or green fluorescence from cell surface bound NDV was plotted (**Figure 4.4 A)**. The histograms of NDV-bound RBCs and PRBCs demonstrate that the fluorescence intensity of virus-bound PRBCs (red curve) is greater than that of virus-bound RBCs (grey curve**) (Figure 4.4 B).** Quantitative estimations from the histogram analysis showed that the binding of NDV to the PRBC is 1.7-fold greater than that from the uninfected RBCs (**Figure 4.4 C**). It demonstrates that the NDV particles preferentially target *P. yoelii*-infected RBCs, which is consistent with the results observed for the human malaria parasite *P. falciparum* (**Figure 30**).

4.3.5 Immunofluorescence imaging of NDV-bound *P. yoelii*-infected RBCs

Immunolocalization of NDV was performed to examine the binding NDV to Plasmodium yoelii-infected red blood cells (PRBCs). NDV was incubated with *P. yoelii*-infected RBCs at 37°C for 1 hour and processed for flow cytometry as described in materials and methods. DAPI staining was used to stain the Plasmodium yoelii parasite DNA within the red blood cells (blue fluorescence). NDV was probed with specific antibodies and detected with a FITC-conjugated secondary antibody (green fluorescence). In the untreated parasites, the parasite nucleus shows

strong DAPI fluorescence and no virus specific green fluorescence was observed (**Figure 4.5**). In the NDV-treated parasite culture, the co-localization of blue (DAPI) and green fluorescence (NDV), suggests that NDV binds to the PRBCs.

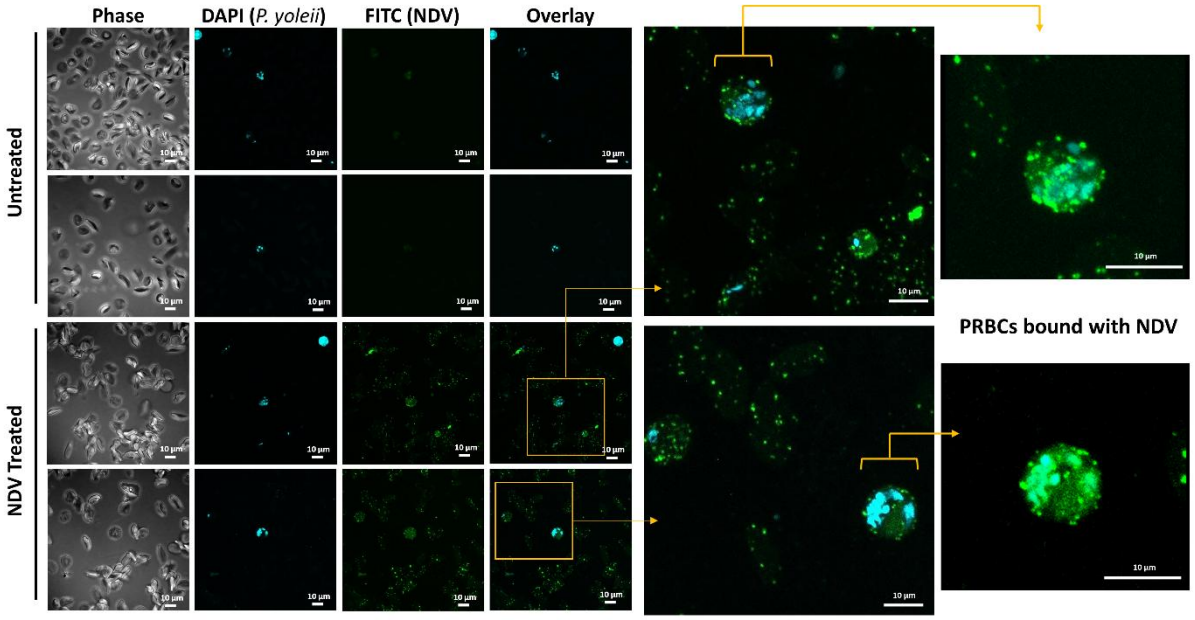

Figure 4.5: Immuno-localization of NDV bound to P. yoleii infected RBCs. To visualize the virus bound with the RBCs and PRBCs, NDV was incubated with the malaria parasite for 1 hour and processed for immunolocalization as described in materials and methods. Parasite DNA was stained with DAPI (blue) and green fluorescence (FITC), corresponding to the NDV signal.

On the right, snippets from the original images depict PRBCs with both blue (DAPI) and green (FITC) fluorescence, showing the binding of NDV to the PRBCs. A qualitative inspection of the images also shows that the localized green signals from NDV on the PRBCs are substantially higher compared to the RBCs.

4.3.6 The proteinaceous ligands present on RBC surface is crucial for NDV-RBC interaction

To study the involvement of the virus coat proteins in the NDV-RBC interaction, the binding of the virus with RBCs was tested under different experimental conditions. It was previously reported that heating of NDV particles at 60°C results in the complete loss of the activity of the HN protein due to its denaturation. We have explored an alternate strategy to physically disrupt the virus by heating. We incubated the virus at 60°C for 1 hour in a water bath followed by a brief incubation on ice to allow the sample to cool down. Following the treatment, RBCs were incubated with the heat-inactivated virus preparation (MOI=10^2) and binding was tested

using flow cytometry as described in material and methods. RBCs incubated with the heat-inactivated NDV give a fluorescence peak (blue curve), which corresponds to the fluorescence of RBCs without the virus (black curve) (**Figure 4.6 A**). This suggests that the capacity of the virus for binding to RBCs has been lost due to the heat treatment. The results show that the NDV surface proteins are crucial for binding with the human RBCs.

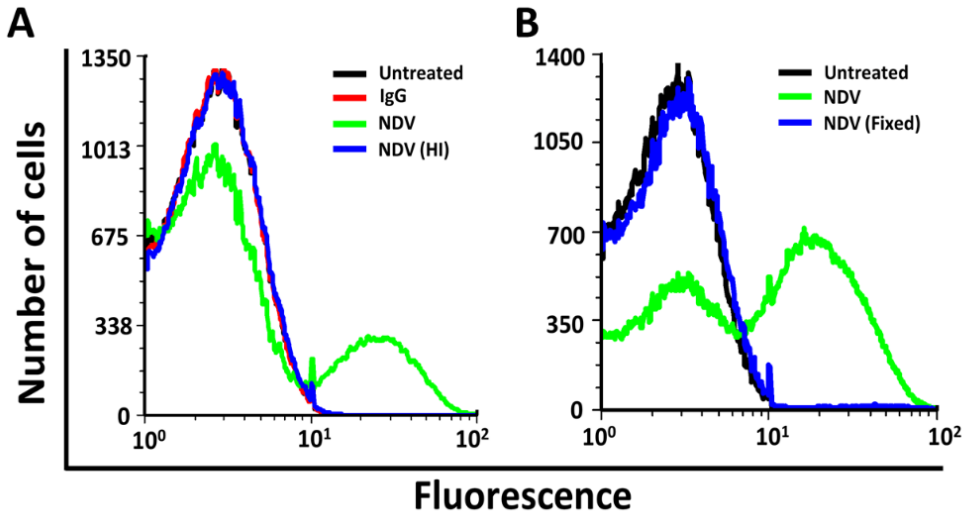

Figure 4.6: Physical disruption of the NDV coat proteins results in the loss of NDV-RBC interaction. The proteome of NDV was modified by treating the virus with 2% glutaraldehyde (30 minutes at RT) or a brief heat treatment at 60°C for 1 hr. Post-treatment, the ability of the virus to bind with RBCs was tested with the help of flow cytometry as described in materials and methods. (A) Number of cells (counts) were plotted on the Y-axis, and fluorescence from NDV-bound RBCs (green fluorescence) was plotted on the X-axis. The graph shows the population of untreated RBCs (black curve), RBCs incubated with antibodies (red curve), RBCs incubated with NDV (green curve), RBCs incubated with fixed NDV (blue curve). (B) Number of cells (counts) were plotted on the Y-axis, and fluorescence from NDV-bound RBCs (green fluorescence) was plotted on the X-axis. The graph shows the population of untreated RBCs (black curve), RBCs incubated with NDV (green curve), and RBCs incubated with fixed NDV (blue curve).

Additionally, protein cross-linking agents, such as aldehydes were previously shown to inactivate the surface proteins of NDV, preventing the attachment of the virus to its host cells. For our investigation, we treated NDV with glutaraldehyde. The virus preparation was incubated with RBCs and the binding was analyzed with flow cytometry as described in materials and methods. The untreated NDV showed robust interaction with the RBCs (green curve), confirming that the virus was able to physically bind with the human RBCs (**Figure 4.6 B**). RBCs incubated with the aldehyde-fixed NDV showed the fluorescence peak (blue curve) corresponding to the RBCs fluorescence (black curve) indicating that the fixation has disrupted the interaction between NDV and RBCs (**Figure 4.6 B**).

4.3.7 The surface proteins of RBCs are crucial for NDV-RBC interaction

Our previous results have shown that physical disruption of the viral proteins results in abrogation of NDV-RBC binding. Further confirmation of the involvement of protein-protein interaction would require the testing of NDV-RBC binding where the red cell surface has been modified. To achieve this, RBCs were treated with Proteinase-K (100 µg/ml) for 1 hour at 37ºC, washed and incubated with NDV at an MOI of 10^3, followed by analysis in flow cytometry as described in materials and methods. As shown in **Figure 4.7 A**, NDV was able to strongly interact with the untreated RBCs to give strong fluorescence (green curve). However, the enzymatic removal of the cell surface proteins from RBCs resulted in a significant loss in virus binding, as indicated by the binding curve (cyan curve). To confirm that the proteolysis activity of Proteinase-K was responsible for loss in NDV binding, we also incubated RBCs with heat-inactivated Proteinase-K. NDV was able to bind strongly with RBCs treated with heat-inactivated Proteinase-K (blue curve). Therefore, crucial proteins on the surface of RBCs must be acting as ligands for NDV.

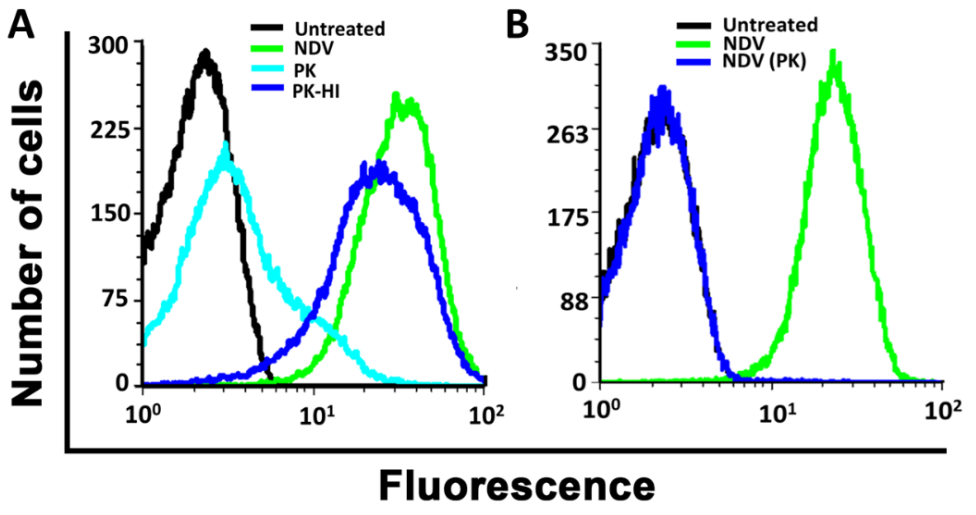

Figure 4.7: RBC contributes to NDV-RBC interaction through cell surface proteins. (A) To test whether the surface proteins on RBCs were potential ligands for NDV, the cells were treated with Proteinase-K (0.4 U/ml) to remove the surface proteins. The binding of NDV with these cells was analyzed with flow cytometry as described in materials and methods. Cell counts were plotted on the Y-axis, while fluorescence from NDV-bound RBCs was plotted on the X-axis. The graphs show the population of untreated RBCs (black curve), RBCs incubated with NDV (green curve), RBCs treated with Proteinase-K and incubated with NDV (cyan curve), RBCs treated with heat-inactivated Proteinase-K (B) In another experiment, NDV was also treated with Proteinase-K to remove spike proteins present in the virus coat and NDV binding to RBC was analyzed as described in the material and methods. The graphs show the population of untreated RBCs (black curve), RBCs incubated with NDV (green curve) and RBCs incubated with NDV that was pre-treated with Proteinase-K (blue curve).

Since physical or chemical disruption is a non-specific approach to address the role of proteins present in the NDV coat to facilitate the interaction with the RBCs, NDV was pre-treated with Proteinase-K to further verify the involvement of NDV coat proteins in the binding. NDV was incubated with Proteinase-K (0.4U/ml) for 1 hour at 37°C, followed by the inhibition of the protease with 1 mM PMSF. The virus preparation was incubated with RBCs for 1 hour at a MOI of 10^3 and the binding was analyzed with flow cytometry (**Figure 4.7 B**). The treatment of NDV with the protease completely abolished the ability of NDV to bind with the RBCs (blue curve). It is, however, unclear whether the incubation of the virus with the protease would result in the removal of only the surface spike proteins or induce a globalized effect on the virus proteome. Nevertheless, the results showed that the binding of the NDV with human RBC was mediated by protein-protein or protein-ligand interactions.

4.3.8 NDV utilizes the hemagglutinin-neuraminidase on its coat for binding with PRBCs

From our initial binding studies, it was clear that proteins on both the RBC cell surface and NDV are involved in their interaction. It is known that the HN spike protein of NDV is the primary determinant of host cell recognition. The HN protein recognizes the sialic acids on the cell surface and helps in virus attachment. Since, the RBC and PRBC surface is rich in sialic acid, we envisioned that the virus could be utilizing these sialic acids for binding. Thus, we employed two approaches to explore the role of the sialic acid and HN spike protein in the binding of the virus with the RBCs and PRBCs: (i) Removal of sialic acid from the RBC cell surface with neuraminidase. (ii) Treating the virus with extracellular sialic acid or with antibodies against the HN protein to disrupt its function (**Figure 4.8 A**).

For our first approach, the sialic acids from the cell surface were enzymatically removed with the help of neuraminidase. RBCs were treated with neuraminidase (50 mU/ml) for 1 hour at 37°C and binding of NDV was analyzed with flow cytometry as described in material and methods. It was observed that there was a significant reduction in the binding of NDV with the neuraminidase-treated RBCs (**Figure 4.8 B, blue curve**) when compared with untreated (**Figure 4.8 B, green curve**) RBCs. In our second approach, ring synchronized PRBCs were treated with NDV pre-incubated with different concentrations of sialic acid (10, 100, and 200 µM) and virus binding was measured by flow cytometry as described in material and methods. Contour plots describe the uninfected RBC and PRBC population distinguished by staining of parasite DNA with Propidium iodide, and the binding of NDV with the PRBCs was analyzed [**Figure 4.8 C (i)**]. The PRBCs incubated with NDV in a complete medium give

a strong signal, as seen in **Figure 4.8 C (ii)**. In comparison, NDV pre-incubated with sialic acid showed a gradual decrease in the virus-bound PRBC population with the increase in sialic acid concentration [**Figure 4.8 C (iii, iv, v)**].

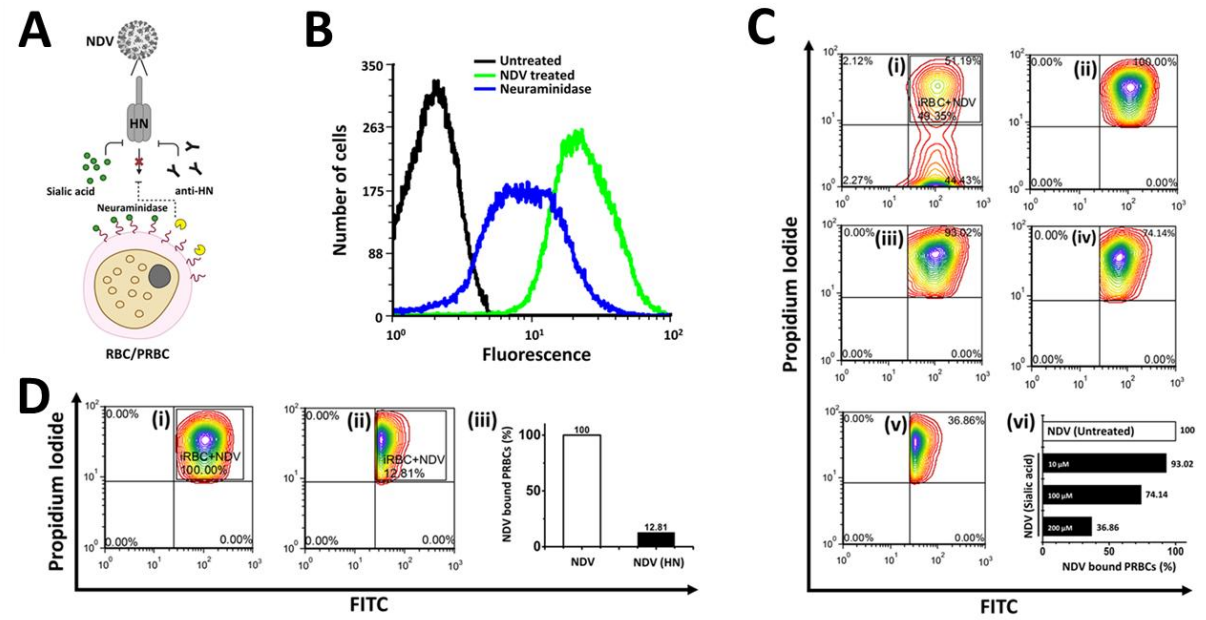

Figure 4.8: HN-sialic acid interaction is crucial for NDV-PRBC binding and mediates the anti-malarial action of NDV. (A) A graphical illustration of the approaches used to investigate the role of the HN-sialic acid interaction in the anti-malarial action of NDV. **(B) NDV binds weakly with neuraminidase-treated RBCs**. RBCs were treated with neuraminidase to remove surface sialic acids. NDV binding to sialic acid-depleted RBCs was assessed using flow cytometry. Cell counts were plotted on the Y-axis, while fluorescence from NDV-bound RBCs was plotted on the X-axis. The graph shows binding curves of untreated RBCs (black curve), RBCs incubated with NDV (green curve), and Neuraminidase treated RBCs incubated with NDV (blue curve). **(C) Pre-incubation of NDV with sialic acid reduces its binding with the PRBCs.** NDV was pre-incubated with different concentrations of sialic acid (10, 100, and 200 µM) and virus binding to PRBCs was analyzed by flow cytometry. (i) RBC and PRBC populations were distinguished by staining the parasite DNA with Propidium iodide. Contour plots represent the NDV-bound RBCs and NDV-bound PRBCs as two separate populations. (ii) Characterization of the NDV-bound PRBCs based on PI and FITC fluorescence signal. (iii-v) NDV-bound PRBCs where the virus was pre-incubated with 10, 100, and 200 µM sialic acid. (vi) The percentage of NDV-bound PRBCs in the parasite cultures incubated with NDV or different concentrations of sialic acid (10-200 µM) treated NDV. **(D) The treatment of NDV with an anti-HN antibody inhibits the virus from binding to the PRBCs.** NDV was pre-incubated with the anti-HN antibody (~0.5 µg in 0.5 ml), and the binding of the virus to PRBCs was analyzed by flow cytometry. (i) Contour plots display the NDV-bound PRBCs population. (ii) PRBCs incubated with NDV pre-treated with anti-HN antibody. (iii) Percentage of NDV-bound PRBCs in parasite cultures incubated with untreated NDV (white bar) or NDV treated with anti-HN antibodies (black bar).

Quantitative estimation of NDV binding indicates gradual loss of NDV affinity towards PRBC. Considering the binding of NDV to untreated PRBC as 100%, sialic acid pre-incubated NDV loses its binding affinity with almost 70% reduction in NDV bound population at 200 µM (**Figure 4.8 C, vi**). Thus, the recognition of cell surface sialic acid through the HN spike protein of NDV is crucial for binding of the virus to the PRBCs. To further confirm the role of HN-sialic acid interaction, NDV was pre-incubated with a monoclonal anti-HN antibody to block HN present on the virus and its ability to bind the ring synchronized PRBCs was determined by flow cytometry as described in material and methods. The treatment of the virus with an anti-HN antibody resulted in a pronounced reduction in the NDV-bound PRBC population (**Figure 4.8 D, (ii)**) when compared to PRBCs incubated with untreated NDV (**Figure 4.8 D, (i)**). Quantitative estimation of the NDV-bound PRBC population indicates more than 80% loss of NDV binding to the PRBC in the presence of anti-HN antibodies (**Figure 4.8 D, (iii)**).

4.3.9 NDV exploits RBC surface sialic acid to exhibit its anti-plasmodial activity

The binding assays of NDV with the PRBC suggested that the HN present on the virus coat and sialic acid present on the RBC surface are indispensable for the NDV interaction with the PRBC. To elucidate whether the loss in the HN-mediated binding of the virus with the PRBC could abrogate the anti-parasitic activity, the virus was pre-incubated with different concentrations of sialic acid (0, 10, 100, and 200 µM) and anti-malarial activity was measured as described in material and methods. As expected, NDV was able to block the proliferation of the malaria parasite, whereas NDV pre-incubated with sialic acid (10 µM) abolishes its activity by 50% (**Figure 4.9 A**). As we increased the concentration of sialic acid, it was observed that the anti-malarial activity of NDV reduced in a dose-dependent manner, and there was a complete reversal at 100 µM. To further verify the role of the HN protein in the process, the virus was pre-incubated with a monoclonal anti-HN antibody (~0.5µg in 0.5ml) to block the HN protein, and its anti-plasmodial activity was measured as described in material and methods. NDV pre-incubated with anti-HN antibodies abolished the anti-malarial activity of NDV. The parasites incubated with anti-HN treated NDV only showed around a 30% decrease in parasite viability at 96 hours (Figure 4.9 B). On the other hand, untreated NDV successfully restricted the growth of the parasites with about an 80% decrease in parasitemia. The results suggested that the blocking of the HN protein severely reduced the ability of NDV to restrict the parasite growth and that the NDV-PRBC interaction through sialic acid is crucial for the anti-parasitic activity of the virus.

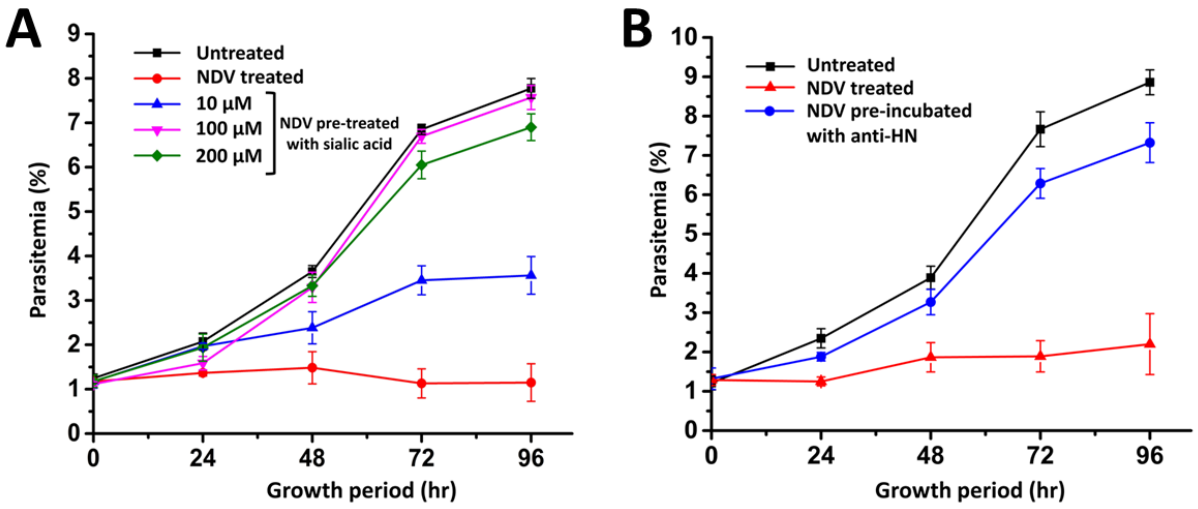

Figure 4.9: Blocking of NDV HN protein with extracellular sialic acid and anti-HN antibody renders the virus ineffective against the malaria parasite. (A) Pre-incubation of NDV with sialic acid eliminates the anti-parasitic effect of NDV. NDV was treated with different concentrations of sialic acid (10, 100, or 200µM) followed by incubation with Pf3D7 (MOI=10^3) and parasite growth was monitored for 96 hrs. Growth curves of the parasites treated with NDV and sialic acid-treated NDV are shown with their mean ± standard deviation (n= 3). Growth curves of the parasites without any treatment (black curve) and parasites incubated with sialic acid-treated NDV; 10µM (blue curve), 100µM (pink curve), 200µM (green curve) show a dose-d1ependent reduction in the anti-malarial action of NDV when compared with the untreated NDV (red curve). (B) Treatment of NDV with anti-HN antibody inhibits its anti-parasitic action. NDV was pre-incubated with a monoclonal anti-HN antibody (0.5µg in 0.5ml) and its anti-plasmodial activity was assessed. Growth curves of the parasites without any treatment (black curve) and parasites incubated with NDV (red curve) or NDV pre-treated with anti-HN antibody (blue curve).

4.3.10 Cloning of NDV_HN protein in prokaryotic expression vector

The extravirion domain or Receptor Binding Domain (RBD) was amplified through RT-PCR using specifically designed primers as described in materials and methods. Subsequently, the amplified fragment was extracted from the agarose gel and cloned into a T/A cloning vector. Verification of the HN gene fragment in the pMD20 vector was carried out by enzymatic digestion with Bam HI and Hind III and also specific amplification from the vector with PCR, which confirmed the insert of 1.6 kb (**Figure 4.10 A, Lane 2 and 3**). Following the successful T/A cloning, the HN gene fragment was sub-cloned into the pET-28a (+) expression vector pre-digested with Bam HI and Hind III (**Figure 4.10 A, Lane 5**). The successful cloning of HN_RBD into pET-28a (+) was confirmed with restriction digestion, where the release of the 1.6 kb gene fragment was observed as shown in **Figure 4.10 B, Lane 2**.

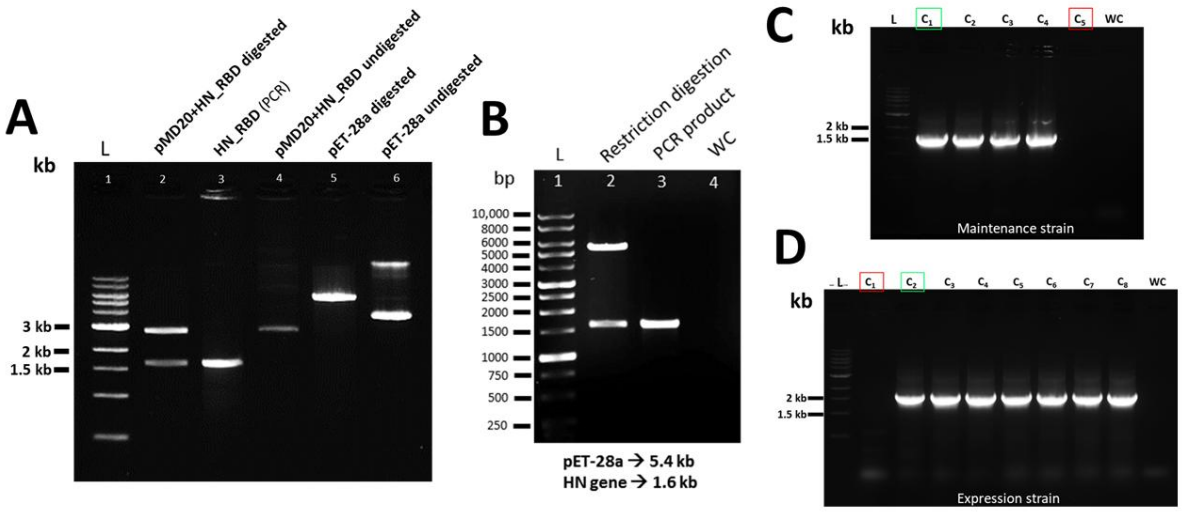

Figure 4.10: Cloning of NDV_RBD into a prokaryotic expression vector. (A) The 1.6 kb HN_RBD gene was amplified from cDNA preparations of the NDV R_2B strain. The gene segment was initially ligated into the PMD20 vector by Topo TA cloning and sub-cloned into the pET-28a (+) expression vector. Lane 1: DNA ladder, Lane 2: Restriction digestion of recombinant PMD20 vector showing the release of 1.6 kb insert. Lane 3: PCR amplification of HN_RBD gene from recombinant PMD20. Lane 4: Undigested PMD20 vector with insert. Lane 5: Empty pET-28a (+) vector digested with BamHI and HindIII. Lane 6: Undigested pET-28a vector. (B) Restriction digestion of pET-28a showing the release of 1.6 kb insert. Lane 1: DNA ladder. Lane 2: Restriction digestion with BamHI and HindIII. Lane 3: PCR amplification of HN_RBD gene from recombinant pET-28a. (C, D) Colony PCR to confirm the positive colonies containing the recombinant pET28a-HN_RBD.

The ligated products were used to transform the Top 10 bacterial strain (maintenance strain), and positive colonies were screened with the help of colony PCR (**Figure 4.10 C**). Positive colonies were expanded in a 5 ml LB medium with appropriate antibiotics and used for amplification of the recombinant pET-28a-HN vector. Isolation of the recombinant vector with the HN gene was done and used to transform *E. coli* expression strains, such as Rosetta (DE3) and BL21(DE3). Positive clones were selected with colony PCR using the cloning primers as described previously (**Figure 4.10 D**).

Positive colonies were expanded in 5 or 250 ml LB for overexpression studies and protein purification. By analyzing the nucleotide sequence of the HN gene, an open reading frame (ORF) of 1611 base pairs was identified, which encodes a protein consisting of 536 amino acids. It should be noted that when considering the N-terminal tags and elements of the vector, the total length of the HN protein was calculated to be 564 amino acids. The molecular mass of the recombinant protein was predicted to be 61.64 kDa, with a theoretical isoelectric point (pI) of 8.14 calculated with the help of the ExPASy server (https://web.expasy.org/cgi-bin/compute_pi/pi_tool).

4.3.11 Expression and purification of HN protein in prokaryotic system

The recombinant pET-30a vector, harboring the HN gene was used to transform competent BL21 (DE3) and Rosetta (DE3) *E. coli* expression strains. The transformed cells were induced with 0.5 mM IPTG at 37^0C for 4 hours. Analysis of the uninduced and induced culture fractions through SDS-PAGE and Coomassie blue staining showed a prominent overexpressed protein band with an approximate molecular weight of 60 kDa between the 75 and 50 kDa markers in the pellet fraction in both BL21 and Rosetta (**Figure 4.11 A and B**). However, it was observed that the expression of the protein in Rosetta (DE3) was significantly higher than in BL-21 (DE3). Western blot analysis was also performed to confirm that the overexpressed protein was HN_RBD. Following the transfer of proteins onto nitrocellulose membranes, the blot was probed with a monoclonal anti-HN antibody. The antibody specifically detected the overexpressed protein band, as depicted in **Figures 4.11 A and B**. However, in BL21 (DE3) a prominent truncated version of the protein was observed just above the 37 kDa marker. It is highly probable that the corresponding band was a truncated version of the protein, not detected in the transformed Rosetta strain. Consequently, the Rosetta (DE3) strain was selected for further optimization of the overexpression and, subsequently, purification of the protein from larger culture volumes. It was further observed that the overexpressed HN protein was localized in the insoluble fraction or the pellet. Thus, a heat shock protocol was employed to obtain soluble expression of the HN protein with high yield.

Previous studies have suggested that subjecting a recombinant bacterial culture to a brief period of heat shock at 42°C before induction could enhance the yield of recombinant protein in the soluble fraction. In the case of the HN protein, it was observed that a brief heat shock at 42°C for 20 minutes prior to induction led to a significant increase in the amount of soluble protein. Two 5 ml cultures of transformed Rosetta with the pET-28a-HN construct were induced with 0.5 mM IPTG at 37^0C for 4 hours. As shown in **Figure 4.11 C**, one of the cultures was given a heat shock before induction (right) while the other was not (left). The supernatant fractions of both cultures were incubated with 100 µl of charged Ni-NTA beads to observe the binding of the HN protein to the beads, if present. A thick protein band could be observed in the fractions eluted with 250 mM imidazole in the supernatant from the heat shock bacterial cells and is absent in the supernatant of other bacterial cultures. The soluble HN protein was also probed with the monoclonal anti-HN antibody which specifically recognized the HN protein in the supernatant fraction as shown in the **Figure 4.11 C**.

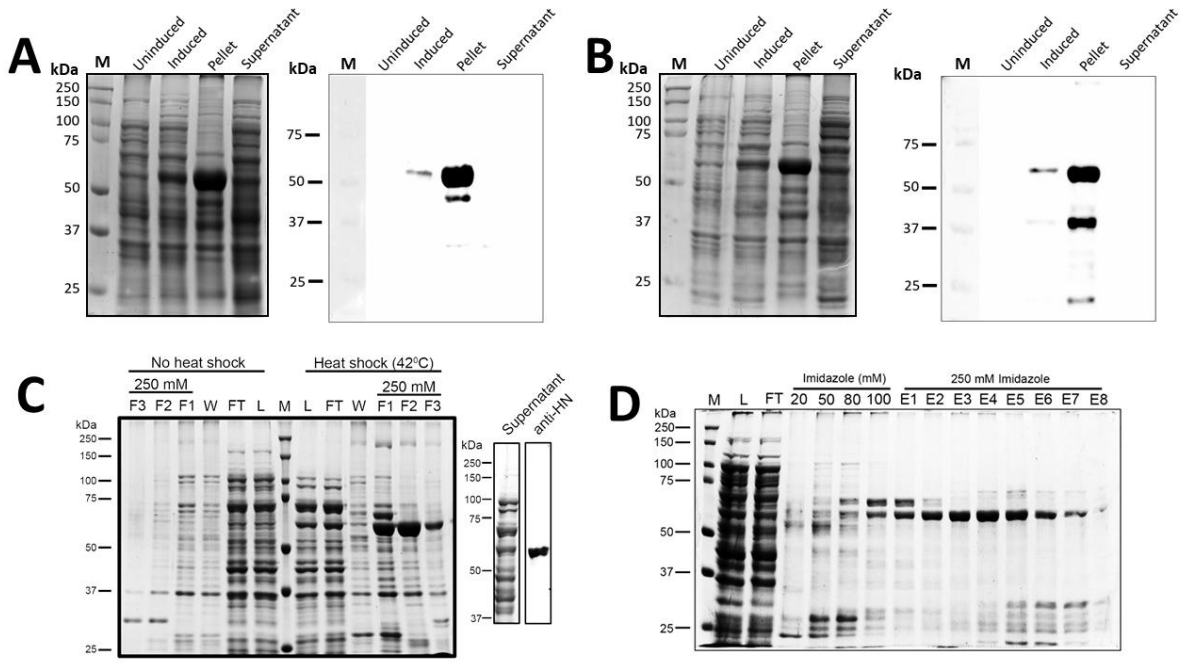

Figure 4.11: Overexpression and western blot analysis of the HN protein. (A) Overexpression of HN protein in BL21 (DE3). Left: SDS-PAGE analysis. M: protein ladder, Lane 1: uninduced, Lane 2: induced, Lane 3: pellet, Lane 4: supernatant. Induction was done with 0.5 mM IPTG. Right: Western blot analysis where the overexpressed HN protein was probed with a monoclonal anti-HN antibody. Lane 1: uninduced, Lane 2: induced, Lane 3: pellet, Lane 4: supernatant. (B) Overexpression of HN protein in Rosetta (DE3). Left: SDS-PAGE analysis. M: protein ladder, Lane 1: uninduced, Lane 2: induced, Lane 3: pellet, Lane 4: supernatant. Induction was done with 0.5 mM IPTG. Right: Western blot analysis with monoclonal anti-HN antibody. Lane 1: uninduced, Lane 2: induced, Lane 3: pellet, Lane 4: supernatant. (C) Heat shock method and soluble expression of HN protein. Left: SDS-PAGE analysis. M: protein ladder, L: Load, FT: Flow-through, W: wash with 50 mM imidazole, F1, F2 and F3: eluted fractions with 250 mM imidazole. Right: Western blot detection of soluble HN protein with monoclonal anti-HN antibody. (D) Ni-NTA purification of HN. M: protein ladder, Lane 1: Load, Lane 2: Flow through, Lane 3: 20 mM imidazole, Lane 4: 50 mM, Lane 5: 80 mM, Lane 6: 100 mM, Lane 7-14: 250 mM elution fractions.

The HN protein in the supernatant obtained from a 250 ml induced Rosetta culture was subjected to Ni-NTA purification under native conditions. As shown in **Figure 4.11 D**, it was observed that the protein was successfully bound to the column. During the washing step with 20-100 mM imidazole (**Lanes 3-6**), several non-specific proteins, including a small amount of the HN protein, were eluted. The fractions collected from the elution with 250 mM imidazole contained the majority of the HN protein.

4.3.12 Purified HN protein from the prokaryotic system is functionally active

To achieve a higher level of purity of the HN protein, a subsequent polishing step was performed using a gel filtration column, after Ni-NTA purification. The eluted fractions

obtained with 250 mM imidazole were pooled together and concentrated to a final volume of 500 µl and loaded in a gel filtration column. Analysis of the size exclusion chromatogram revealed that the HN protein eluted as a single peak (**Figure 4.12 A**).

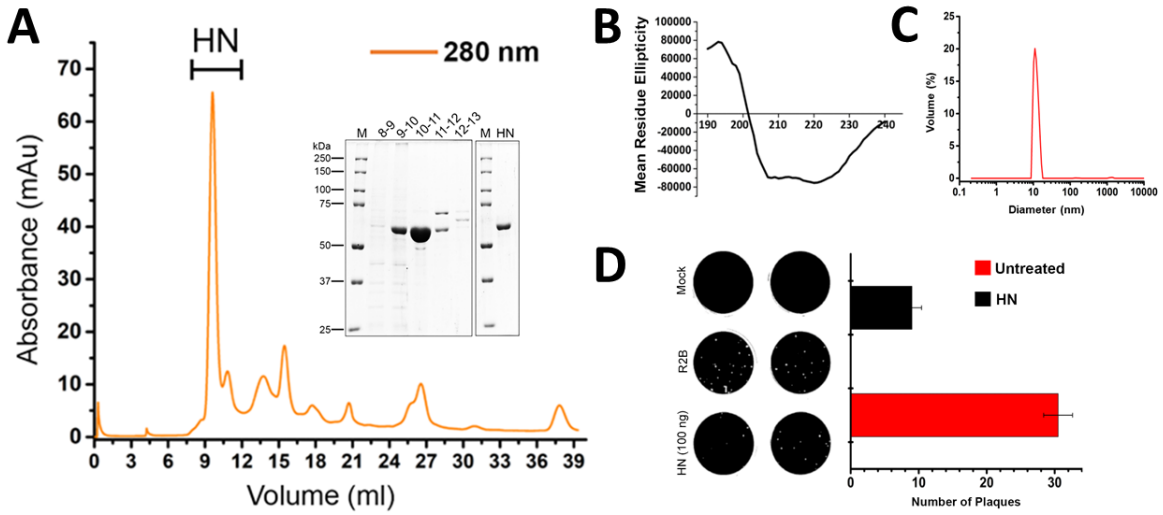

Figure 4.12: Characterization of the purified HN protein. (A) Size exclusion profile of concentrated HN protein after Ni-NTA purification. (C) Left: SDS-PAGE gel stained with Coomassie, showing the protein fractions from 8-13 ml collected during gel filtration. M: protein ladder, Lane 1: 8-9 ml, Lane 2: 9-10 ml, Lane 3: 10-11 ml, Lane 4: 11-12 ml, Lane 5: 12-13 ml. Right: SDS-PAGE analysis of the purified HN protein. M: protein ladder, Lane 1: Purified HN showing a single protein band. (D) CD spectra of HN. (E) DLS of HN showing a single peak at corresponding to 10 nm particle size. (F) Plaque inhibition assay showing a 3-fold reduction in the number of plaques in cells pre-treated with the purified HN protein.

SDS-PAGE analysis of the eluted fractions (from 8-13 ml) showed that a single protein band corresponding to the HN protein was successfully obtained in a final volume of 1 ml (**Figure 4.12 A**). The HN protein from the fraction was run in an SDS-PAGE to confirm a single protein band (**Figure 4.12 A**). The concentration of the protein was estimated with the Bradford assay and was found to be in the average of 600 µg/ml. Thus, with the pET28a-HN construct through the heat shock protocol, a high yield of purified HN protein was achieved with an average concentration of 600-700 ng/µl from 250 ml cultures, which is significantly higher than previously reported, as discussed in section 4. The secondary structure of the purified protein was analyzed with the help of CD spectroscopy as shown in **Figure 4.12 B**. In our analysis, the HN protein was found to possess 45 % α-helix, followed by 30% β-sheets and 25% loops confirming that the secondary structure of the protein was conserved. The hydrodynamic size of the purified HN was also determined with DLS analysis and was found to be 10 nm, which is also consistent with previous findings (**Figure 4.12 C**).

In order to verify that the purified HN protein was active, we conducted a plaque inhibition test. Monolayers of BHK-21 cells were incubated with the HN protein before giving an infection with the NDV (MOI = 0.01). We hypothesized that an active HN protein could cleave the sialic acid residues on the cell surface through its neuraminidase activity, resulting in a reduction in subsequent infection with the ND virus. Also, a fraction of the HN protein could remain bound with the cell surface resulting in the blocking of crucial sialic acid receptors needed for NDV to establish an infection. Consequently, a reduction in the number of plaques observed in the HN-treated cells would serve as confirmation of the protein's activity. The plaque inhibition test showed that there was a 3-fold reduction in the number of plaques in the cells that were pre-treated with the HN protein (**Figure 4.12 D**). Thus, it can be concluded that the recombinant HN protein showed structural integrity and was functionally active.

4.3.13 The HN protein from the NDV coat exerts anti-parasitic activity

Following the characterization of the purified HN protein, synchronized schizonts at a parasitemia of 1% were incubated with increasing concentrations of HN (1, 5, and 10 µM) for 96 hours and parasite viability was monitored as described in materials and methods. During the course of the experiment, the parasites multiplied exponentially, reaching a maximum parasitemia of around 8% in 96 hours (**Figure 4.13 A**). The HN protein at 5 and 10 µM concentrations showed a substantial reduction in parasitemia. We also treated the parasites with BSA (10 µM) to negate any non-specific action on the parasite due to the presence of another protein (**Figure 4.13 A**). Upon analysis of the parasitemia at the end of the experiment (96 hours), the HN protein-treated parasites show a dose-dependent reduction in parasite growth with more than 50% reduction in parasitemia at 10 µM, which was the highest concentration of HN used in our experiment (**Figure 4.13 B**). At 1 µM and 5 µM of HN protein concentration, the parasitemia was reduced by 10% and 30% respectively.

Under a similar assay setup, NDV was found to induce more than an 80% reduction in parasitemia, which coincided with our previous experimental results (**Figure 4.13 A**). The observed differences could be either due to the higher affinity of virus-bound HN towards sialic acid or a localized concentration of the protein in the viral coat. Black arrows indicate the addition of the purified HN protein into the parasite culture. Thin smears showing rings from the 96-hour time-period of untreated (UT), HN-treated (10 µM) and NDV-treated (NDV) are shown in **Figure 4.13 C**. Representative images of untreated or HN-treated (10 µM) rings,

trophozoite and schizonts from **Figure 4.13 D** clearly indicate cellular damage and perturbation of parasite erythrocytic schizogony. The results demonstrated that with a single protein from the virus, the proliferation of the malaria parasite could be severely disrupted. The concentration of the HN protein could be a crucial factor in achieving complete inhibition of parasite growth. Additionally, the stability of the purified HN protein in complete media remains unclear. Nevertheless, the HN spike protein, even at a much lower concentration, was found to elicit significant anti-plasmodial activity.

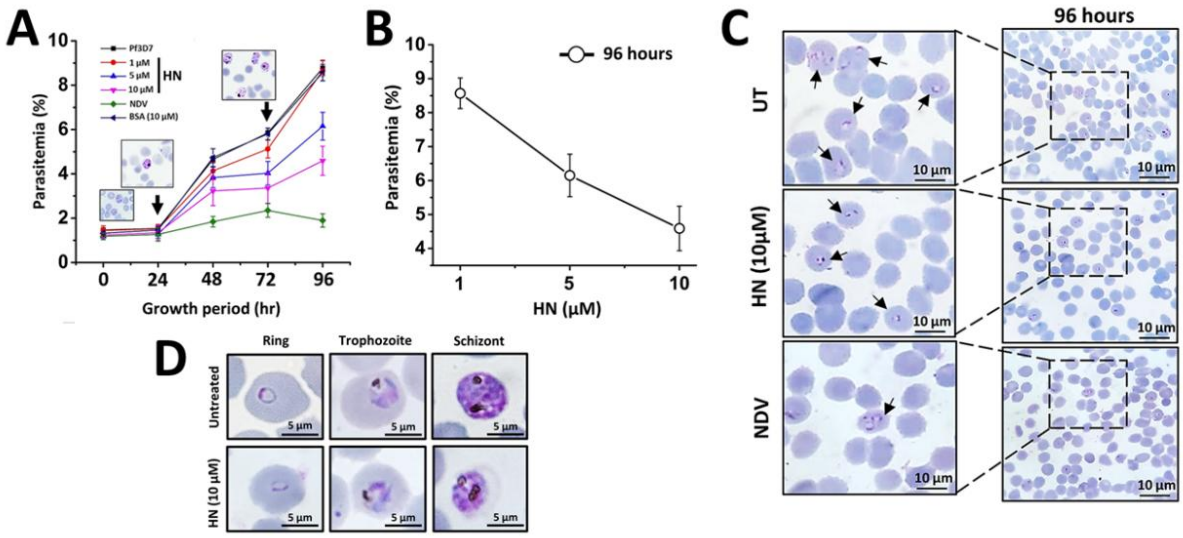

Figure 4.13: Purified HN protein restricts malaria parasite growth. (A) The HN protein dose-dependently reduces parasite propagation in RBCs. Schizonts at a final parasitemia of 1% were incubated with increasing concentrations of pure HN protein (1, 5, or 10µM) for 96 hours, and parasite growth was monitored as described in the material and methods. Black arrows represent the introduction of the HN protein in the parasite culture. Culture media was replenished at 72 hours. (B) 96-hour Parasitemia of the HN treated cultures (1, 5 and 10 µM) was plotted, which shows a dose-dependent inhibition of the malaria parasite growth. (C) Representative thin smears at 96-hours of untreated parasites (UT), parasites treated with HN (10 µM) and parasites treated with NDV (MOI = 10^3). (D) Purified HN protein induces cytopathy in the RBC stages of the parasite. Thin smears of the parasite culture treated with 10µM of HN protein were used to study cellular morphology. The HN protein also induced morphological aberrations in different parasite stages.\

4.4 Discussion

Our binding studies of NDV with RBCs and PRBCs reveal that a brief exposure to the virus is enough for it to interact with the uninfected RBCs or parasitized human RBCs (PRBCs) (**Figures 4.1 and 4.2)**. Interestingly, in the case of both human and murine malaria, NDV was found to have a greater affinity for the PRBCs compared to the uninfected RBCs, which could have potential implications for targeted delivery of antimalarial drugs directly to the PRBC (**Figures**

4.2 to 4.5). We also demonstrated that the interaction between NDV and human RBCs/ PRBCs could be mediated by specific protein: protein or protein: ligand interactions (**Figures 4.6 and 4.7)**. Upon further investigation, it was revealed that the virus utilizes its HN receptor for high-affinity interaction with sialic acids present on the RBC and PRBC as blocking the activity of this capsid protein with an excess of free sialic acid and specific antibodies abrogates the binding of the virus (**Figure 4.8**). However, it should be noted that a complete reversal in virus binding was not observed when we removed the sialic acids present on the RBC surface with the help of neuraminidase (**Figure 4.8 B**). There is a possibility that the neuraminidase treatment was inadequate for the removal of all the sialic acid from the cell surface. However, a quantitative estimation of the residual sialic acid on the RBCs was beyond the scope of this study. Alternatively, the virus could also be using some other ligand/receptor for interacting with the RBCs. Also, the specificity of HN towards sialic acid is unclear as the virus may recognize other terminal sugars for binding with the RBC surface.

Furthermore, the blocking of the HN coat protein of NDV resulted in a substantial reduction of its anti-plasmodial activity (**Figure 4.8**). Our results demonstrated that the HN-sialic acid interaction was crucial for NDV to exert its anti-parasitic effect by binding with both the RBC and PRBC. To test whether the HN protein alone could have similar effects on the parasite, the viral surface protein was cloned into a prokaryotic expression vector (**Figures 4.10 to 4.12**). The HN protein alone could also restrict the parasite propagation in a dose-dependent manner (**Figure 4.13**). We demonstrated that a high yield of functionally active HN protein could be produced in the bacterial expression system. It could have potential applications, such as in vaccine development, where the protein could be used to immunize avian species and challenge NDV infection. We also intend to use this protein to further study its biochemical and biophysical properties. Some of the potential applications of this study could be to exploit NDV or its HN spike protein for developing efficient anti-malarial drug delivery platforms. Classical drug delivery vehicles such as liposomes or PEGylated liposomes have been used for passive drug delivery of several drugs including Artemisinin, Dihydroartemisinin, and Artesunate [28]. Active drug delivery vehicles with better efficacies made use of various receptors that could target specific ligands on the PRBC surface. Tagami and group developed the Phosphatidylserine (PS) specific peptide-conjugated liposomes (PSP-liposomes) to target specifically the PRBCs. Although the nanocarriers could deliver a higher dose of drugs to the PRBC, they were found to cause RBC eryptosis [29]. In another study, antibodies against Glycophorin A were decorated on the surface of liposomes and PEG liposomes for targeting

the RBCs. However, the antibodies could not distinguish between the RBC and PRBC [30, 31]. In this regard, Nano-carriers coupled with the NDV-HN spike protein could be developed for specifically targeting the PRBCs. Also, the whole virus in the form of NDV-VLPs could be used as Nano-carriers, possibly without the need for any surface modifications to test and compare their capacity for targeted delivery of antimalarial drugs into the PRBCs [32]. This could result in the reduction of dosage while also improving their efficacy.

Another application may include the development of novel anti-malaria peptides from the NDV-HN protein. Although viruses are not known to produce antimicrobial peptides naturally within their host cells, active peptides could be derived from their functional proteins. This was illustrated in a study by Bianchin et al. where they described the screening of antimalarial peptides from the plasmodium and human proteome to derive peptides that could block the invasion of RBCs by merozoites [33]. Specifically, peptides that were derived from proteins actively involved in the invasion from both the parasite and human counterparts were the most effective. In our study we have demonstrated that the HN protein was functionally active and was able to inhibit the growth of the malaria parasite (**Figure 4.13**). Thus, the active HN protein could be an excellent source of antimalarial peptides that could potentially be produced in a good yield in the prokaryotic system. In conclusion, the study demonstrates that NDV is a potent antimalarial agent and a viable platform for targeted antimalarial drugs using NDV-VLPs or HN-conjugated nanocarriers. This dual role of the virus might offer significant therapeutic promise against malaria.

4.5 References

1. Varki, A., R.L. Schnaar, and R. Schauer, Sialic acids and other nonulosonic acids. 2017.

2. Burzyńska, P., et al., Sialic acids as receptors for pathogens. Biomolecules, 2021. 11(6): p. 831.

3. Severi, E., D.W. Hood, and G.H. Thomas, Sialic acid utilization by bacterial pathogens. Microbiology, 2007. 153(9): p. 2817-2822.

4. Wasik, B.R., K.N. Barnard, and C.R. Parrish, Effects of sialic acid modifications on virus binding and infection. Trends in microbiology, 2016. 24(12): p. 991-1001.

5. Ghosh, S., Sialic acid and biology of life: An introduction. Sialic acids and sialoglycoconjugates in the biology of life, health and disease, 2020: p. 1.

6. DeLuca, G.M., et al., Plasmodium falciparum Merozoite Adhesion Is Mediated by Sialic Acid. Biochemical and biophysical research communications, 1996. 225(3): p. 726-732.

7. Friedrich, N., S. Matthews, and D. Soldati-Favre, Sialic acids: key determinants for invasion by the Apicomplexa. International journal for parasitology, 2010. 40(10): p. 1145-1154.

8. Duraisingh, M.T., et al., Erythrocyte-binding antigen 175 mediates invasion in Plasmodium falciparum utilizing sialic acid-dependent and-independent pathways. Proceedings of the National Academy of Sciences, 2003. 100(8): p. 4796-4801.

9. Adams, J.H., et al., A family of erythrocyte binding proteins of malaria parasites. Proceedings of the National Academy of Sciences, 1992. 89(15): p. 7085-7089.

10. Brown, A. and M.K. Higgins, Carbohydrate binding molecules in malaria pathology. Current opinion in structural biology, 2010. 20(5): p. 560-566.

11. Berzins, K., Merozoite antigens involved in invasion. Malaria immunology, 2002. 80: p. 125-143.

12. Okoyeh, J.N., C. Pillai, and C.E. Chitnis, Plasmodium falciparum field isolates commonly use erythrocyte invasion pathways that are independent of sialic acid residues of glycophorin A. Infection and immunity, 1999. 67(11): p. 5784-5791.

13. Rodriguez, M., et al., PfRH5: a novel reticulocyte-binding family homolog of Plasmodium falciparum that binds to the erythrocyte, and an investigation of its receptor. PloS one, 2008. 3(10): p. e3300.

14. Spadafora, C., et al., Complement receptor 1 is a sialic acid-independent erythrocyte receptor of Plasmodium falciparum. PLoS pathogens, 2010. 6(6): p. e1000968.

15. Sahar, T., et al., Plasmodium falciparum reticulocyte binding-like homologue protein 2 (PfRH2) is a key adhesive molecule involved in erythrocyte invasion. PloS one, 2011. 6(2): p. e17102.

16. Ord, R.L., et al., Targeting sialic acid dependent and independent pathways of invasion in Plasmodium falciparum. PloS one, 2012. 7(1): p. e30251.

17. Soubes, S.C., et al., Search for the Sialic Acid-Independent Receptor on Red Blood Cells for Invasion by Plasmodium falciparum. Vox sanguinis, 1999. 76(2): p. 107-114.

18. Ganar, K., et al., Newcastle disease virus: current status and our understanding. Virus research, 2014. 184: p. 71-81.

19. Connaris, H., et al., Probing the sialic acid binding site of the hemagglutinin-neuraminidase of Newcastle disease virus: identification of key amino acids involved in cell binding, catalysis, and fusion. Journal of virology, 2002. 76(4): p. 1816-1824.

20. Huang, Z., et al., The hemagglutinin-neuraminidase protein of Newcastle disease virus determines tropism and virulence. Journal of virology, 2004. 78(8): p. 4176-4184.

21. Ke, G.M., et al., Analysis of sequence and haemagglutinin activity of the HN glycoprotein of Newcastle disease virus. Avian Pathology, 2010. 39(3): p. 235-244.

22. Iorio, R.M., et al., Structural and functional relationship between the receptor recognition and neuraminidase activities of the Newcastle disease virus hemagglutinin-

neuraminidase protein: receptor recognition is dependent on neuraminidase activity. Journal of virology, 2001. 75(4): p. 1918-1927.

23. Yuan, P., et al., Structure of the Newcastle disease virus hemagglutinin-neuraminidase (HN) ectodomain reveals a four-helix bundle stalk. Proceedings of the National Academy of Sciences, 2011. 108(36): p. 14920-14925.

24. Takimoto, T., et al., Role of the hemagglutinin-neuraminidase protein in the mechanism of paramyxovirus-cell membrane fusion. Journal of virology, 2002. 76(24): p. 13028-13033.

25. Shokeen, K., A. Srivathsan, and S. Kumar, Lithium chloride functions as Newcastle disease virus-induced ER-stress modulator and confers anti-viral effect. Virus Research, 2021. 292: p. 198223.

26. Neog, S., S. Kumar, and V. Trivedi, Isolation and characterization of Newcastle disease virus from biological fluids using column chromatography. Biomedical Chromatography, 2023. 37(1): p. e5527.

27. Trivedi, V., et al., Purification and biochemical characterization of a heme containing peroxidase from the human parasite P. falciparum. Protein expression and purification, 2005. 41(1): p. 154-161.

28. Jha, S., R. Deshmukh, and V. Trivedi, Approaches and molecular tools for targeted drug delivery in malaria infected red blood cells, in Combination drug delivery approach as an effective therapy for various diseases. 2022, Elsevier. p. 149-172.

29. Tagami, T., et al., Evaluation of phosphatidylserine-specific peptide-conjugated liposomes using a model system of malaria-infected erythrocytes. Biological and Pharmaceutical Bulletin, 2015. 38(10): p. 1649-1651.

30. Biosca, A., et al., An immunoPEGliposome for targeted antimalarial combination therapy at the nanoscale. Pharmaceutics, 2019. 11(7): p. 341.

31. Moles, E., et al., ImmunoPEGliposomes for the targeted delivery of novel lipophilic drugs to red blood cells in a falciparum malaria murine model. Biomaterials, 2017. 145: p. 178-191.

32. McGinnes, L.W. and T.G. Morrison, Newcastle disease virus-like particles: preparation, purification, quantification, and incorporation of foreign glycoproteins. Current protocols in microbiology, 2013. 30(1): p. 18.2. 1-18.2. 21.

33. Bianchin, A., et al., Design and evaluation of antimalarial peptides derived from prediction of short linear motifs in proteins related to erythrocyte invasion. PLoS One, 2015. 10(6): p. e0127383.

Chapter 5

Understanding and exploitation of sialic acid biophore to improve anti-malarial potentials of NDV-HN

Summary

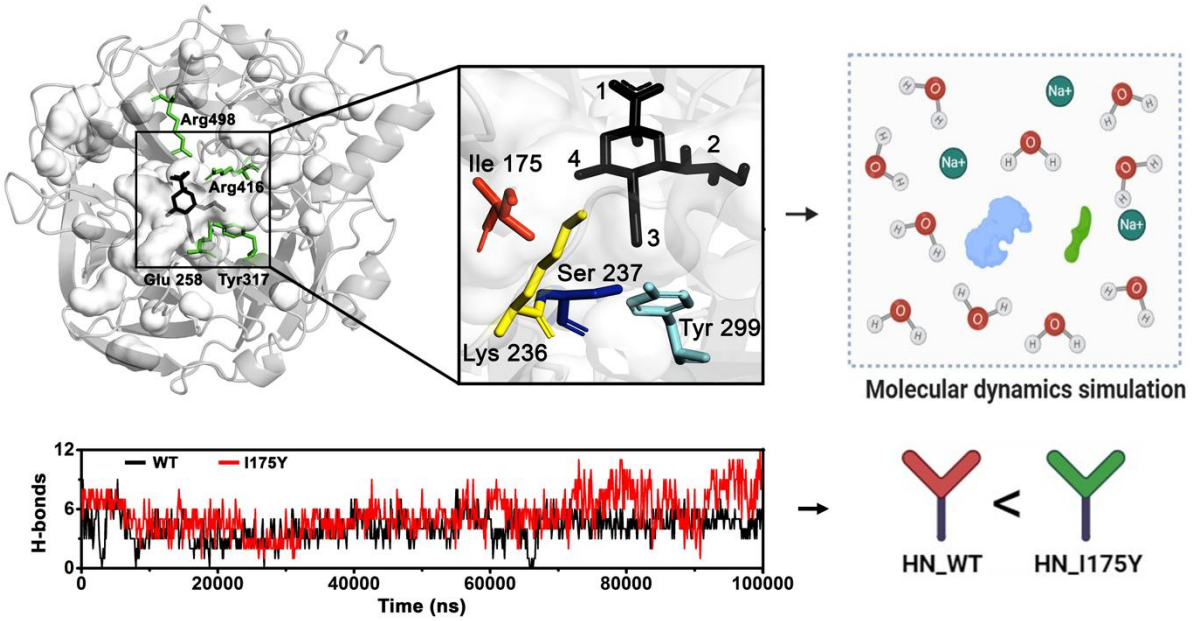

Sialic acids are nine-carbon sugars found at the terminal position of glycan chains on glycoproteins and glycolipids in mammalian cells, playing a critical role in viral attachment and entry into host cells. Various pathogenic viruses use viral lectins, such as Hemagglutinin (HA), Neuraminidase (NA), and Hemagglutinin Neuraminidase (HN) to target host cell-surface sialic acids. The HA protein of influenza viruses binds to sialic acid residues, while NA cleaves these residues to facilitate the release of progeny virions and prevent viral particle aggregation. In contrast, the HN protein of Newcastle Disease Virus (NDV), a clinically significant member of the Paramyxoviridae family, combines receptor binding and neuraminidase activity in a single protein. The HN protein of NDV has been shown to target sialic acids on malaria parasitized red blood cells (PRBCs), leading to reduced parasite viability. Comparative structural analyses revealed that HN has a Type-IV sialic acid-binding module, characterized by fewer interactions with sialic acid functional groups compared to the Type-I module found in NA. A specific mutation (I175Y) in HN was designed to enhance sialic acid interaction, transforming the binding module from Type-IV to Type-I and resulting in a 2.8-fold increase in binding affinity. The mutant exhibited significantly greater plaque inhibition and viral blocking activities, as well as a 30% increase in anti-plasmodial activity at specific concentrations compared to the wild type. These findings suggest that targeted mutations in HN can enhance its sialic acid binding affinity and biological activity, offering potential for improved therapeutic strategies.

5.1 Introduction

Complex carbohydrates, often found as glycoproteins or glycolipids on cell surfaces, are crucial for cell-cell recognition due to their diverse and specific sugar moieties. These terminal carbohydrates serve as recognition sites for lectins, which are sugar-binding proteins that mediate cell-cell interactions [1-3]. However, they can also act as important ligands for a myriad of pathogenic organisms. Among the various sugar moieties, sialic acids are particularly recognized for their involvement in various infectious diseases [4-6]. These terminal sugars are a family of nine-carbon sugars located at the terminal position of glycan chains on glycoproteins and glycolipids in mammalian cells [6]. In the case of viruses, they play a crucial role in viral attachment and subsequent entry into the host cells. Several pathogenic viruses from diverse families, such as the Orthomyxoviruses, Paramyxoviruses, Adenoviruses, and Herpesviruses display dedicated lectins and hydrolases in their coat to target host cell-surface sialic acids [7-9]. The Hemagglutinins (HA), Neuraminidase (NA) and Hemagglutinin Neuraminidase (HN) are major sialic acid-binding lectins employed by these viruses [5, 9-11]. Among these viral lectins, the HA coat protein from the Influenza viruses is responsible for recognizing and binding to sialic acid residues on the surface of host cells. Neuraminidase (NA), the other coat protein, is primarily involved in cleaving sialic acid residues from the host cell surface and newly synthesized viral glycoproteins. The neuraminidase activity facilitates the release of progeny virions from the infected cell and prevents aggregation of viral particles. This role of NAs in sialic acid removal complements HA's binding function [12, 13]. In contrast, the Hemagglutinin Neuraminidase (HN), from the Newcastle Disease Virus (NDV) and other members of the Paramyxoviridae family, display [14] both receptor binding and neuraminidase activity in a single protein.

The Newcastle Disease Virus (NDV) is a clinically significant member of the Paramyxoviridae family as it is a well-studied oncolytic virus and has been used extensively as a platform for vaccine delivery [15-18]. Although in the context of protozoan diseases, the clinical relevance of NDV is minimally explored, few studies have highlighted its potential to be used as an immunomodulatory agent in the case of murine and avian malaria [19, 20]. Interestingly, our group have shown for the first time that the virus has an innate potential to restrict human malaria parasite growth as well [14]. One of our major findings highlights the central role of HN in disrupting malaria parasite propagation. Results show that the virus through its HN protein targets sialic acids present on the malaria parasitized RBCs (PRBCs), leading to the loss of parasite viability. This HN: sialic acid interaction is essential for the anti-

plasmodial activity of the virus. Additionally, NDV displays a stronger affinity for the PRBCs compared to the uninfected RBCs, which provides an excellent opportunity for targeted delivery. Thus, realizing the crucial role of the NDV-HN coat protein we undertook further investigations to gain a thorough understanding of the molecular intricacies involved in its sialic acid recognition. Additionally, we asked whether the sialic acid binding pocket of HN could be modulated to augment its affinity for its ligand.

Comparative structural analyses of the hemagglutinin-neuraminidase (HN) and neuraminidase (NA) coat proteins from different virus species elucidated a conserved six-bladed β-propeller architecture across both protein families. Although both HN and NA share a conserved fold, the sialic acid-binding pockets in both the families differ significantly. The NAs were found to have a Type-I sialic acid binding module while the HNs possessed a Type-IV binding module, which is characterized by lesser number of interactions with the different functional groups of sialic acid. Independent studies regarding the affinity of H9N and NAs towards sialic acids have shown that the NAs possessed significantly higher binding affinities and thus showed greater Hemagglutination activity. This could be the result of multiples interactions of amino acid residues, within the biophore of NAs, with all the available functional groups of sialic acid. Conversely, in the sialic acid binding biophore of HN, the hydroxyl group at C_4 and the acetamido group at C_5 of sialic acid remains free. This raises an interesting question regarding the potential of specific mutations in the binding site of HN to engage all the functional groups of sialic acid. Such modifications could enhance the affinity of HN towards its ligand by potentially altering the type of sialic acid binding module.

To address this, we identified key sites for mutagenesis, located spatially within 5 Å from the free hydroxyl and acetamido group of sialic acid. Initial screening of mutants using in-silico tools such as Docking and Molecular Dynamics (MD) simulation revealed that a substitution of Isoleucine (I) to Tyrosine (Y) at 175 position led to a significant increase in the binding affinity. Further analysis showed over 1.5-fold increase in the number of average hydrogen bonds (H-bonds), while 2-D residue interaction analysis revealed its transformation from a Type-IV to Type-I sialic acid binding module. Following the in-silico results, we performed site directed mutagenesis to generate the I175Y mutant of HN. Both the wild type and mutant, were overexpressed and purified successfully from the prokaryotic expression system. Isothermal Titration Calorimetric (ITC) measurements with 6-sialolactose showed a 2.8-fold decrease in K_d value of the I175Y mutant compared to the wild type, indicating a much stronger binding. The biological activity of the mutant and wild type HN was also compared

with the help of Plaque Inhibition Assay (PIA), cell-based assays and in-ovo studies. At equivalent protein concentrations, the I175Y mutant exhibited approximately 25% greater Plaque Inhibition activity compared to the wild type. Similar results were also obtained when NDV was allowed to infect monolayers of cells, pre-treated with the HN-WT and HN-I175Y, where the mutant displayed around 30% and 20% greater potential to block the virus infection based on western blot and real time PCR quantification respectively.

In in-ovo studies, both the wild type and I175Y mutant showed significant ability to hinder the replication of NDV in allantoic fluid. Pre-inoculation of the mutant in the allantoic fluid yielded a 10 % lesser titer of NDV compared to the wild type which indicates that the rationale driven mutagenesis of the HN protein could indeed show enhanced biological activity. Furthermore, both the wild type and the I175Y mutant of HN were tested for their anti-plasmodial activity against the malaria parasite. The HN proteins dose-dependently reduced the malaria parasite viability. Upon comparing the anti-plasmodial potential of the HN-WT and HN-I175Y, we observed that both the proteins exhibit significant anti-plasmodial activity across different concentrations. However, at 5 µM protein concentration, the I175Y mutant showed about 30% more reduction in parasite viability compared to the wild type HN. Also, quantitative estimation of the IC_{50} values for both the proteins suggests that the I175Y mutant shows better anti-plasmodial activity against the malaria parasite. In summary, our results demonstrate that the sialic acid binding affinity of HN could be augmented by specific mutations that alters the binding module type of the protein.

5.2 Experimental Procedures

5.2.1 Comparative analysis of sialic acid binding pocket

A data set consisting of the crystal structures of sialic acid bound neuraminidase (12) and hemagglutinin-neuraminidase (11) from different virus species was generated. The sialic acid binding pocket of the proteins was analyzed using Discovery Studio Visualizer to determine the spatial arrangement of key residues interacting with the ligand. Finally, the 2-D residue interaction maps were generated to determine the amino acid residues involved in hydrogen bond formation with different functional groups of sialic acid.

5.2.2 Receptor and Ligand preparation

Sialic acid was downloaded from PubChem in SDF format which were later converted into Mol2 format after their energy minimization in Chem3D pro software. The suitable PDB files

for the protein targets obtained were downloaded from RCSB PDB (https://www.rcsb.org/) and listed in Table 5.3. All the protein PDB files were subjected to energy minimization in Swiss-PDB viewer.

5.2.3 Molecular Docking

The amino acid residues I175, K236, S237 and Y299 were mutated with Chimera X software followed by energy minimization and addressing of any unfavorable contacts due to the mutations. The β-anomer of sialic acid was chosen as the ligand and also energy minimized with spdv software. Docking of the ligand was performed in the sialic acid binding pocket of HN-protein (wild type and mutants) with the help of Autodock 4.2 [21]. The rank 1 with maximum cluster number was chosen as the best fit and used for binding energy derivation and 2D-interaction plot analysis with Discovery studio.

5.2.4 Molecular Dynamics (MD) simulation

The molecular dynamics simulation of the HN proteins in complex with sialic acid were performed using GROMACS 2018.1. The topology files were generated using CHARMM-GUI server(https://charmm-gui.org/) and the force fields were generated using CHARMM36. The system was neutralized with sodium and chloride ions wherever necessary and the energy minimization was done with Lincs algorithm [22]. Solvation of the complexes was done in a dodecahedron box with a 1 nm distance from the edges of the resultant solvated box. The temperature and the pressure of the system were set to 300 K and 1 atmospheric pressure. The vanderwaals distance cut off was set to 1.2 nm. Hydrogen bonds, electrostatic interactions, and Vander Waals interactions were each constrained using the LINCS algorithm, particle-mesh Ewald (PME), and Verlet algorithms, respectively. The 100 ns MD simulation run was performed with integration step of 2fs under NVT thermal equilibration conditions followed by isothermal-isobaric (NPT equilibrations) equilibrations under same temperature conditions. The quality and stability of molecular dynamics (MD) simulations were assessed using commonly employed MD simulation parameters. Radius of gyration (Rg) indicated protein compactness, while root mean square deviation (RMSD) measured structural deviation from a reference structure (protein backbone). Root mean square fluctuation (RMSF) determined residue flexibility, and hydrogen bond count evaluated stability. GROMACS software facilitated these analyses, providing insights into simulation dynamics and protein-ligand interactions. The results obtained were analyzed and the images were developed Origin Pro 9.

5.2.5 Site directed mutagenesis (SDM)

SDM was performed with the help of mega primer method involving two PCR reactions [22]. The first PCR was used to generate the mega primer using the cloning forward and the mutated reverse primer using the wild type pET-HN construct as a template. The amplified product was run in a 1% Agarose slab and gel eluted. The purified mega primer was used in the second PCR reaction with the reverse cloning primer to generate full length mutated HN gene. The full-length mutated gene was gel extracted, purified and digested with BamHI and HindIII, followed by ligation with pET-28a. Confirmation of mutants was done by restriction digestion with KpnI. Primers used for mutagenesis are shown below:

Table 5.1: Sequence of the primers used for site directed mutagenesis in the I175 position of NDV-HN protein. KpnI site was inserted into the primers for verification of the mutants.

Mutation	Primers (5'→3')	%GC	Tm (°C)	Length	Restriction site
I175Y_FW	CTGCACTCGGTACCCCTCGTTCG	61	62.5	23	KpnI (GGTACC)
I175Y_RV	CGAACGAGGGGTACCGAGTGCAG	61	62.5	23	KpnI (GGTACC)

5.2.6 Overexpression and Western blot analysis

Transformed CD41 (DE3) colonies were initially screened with colony PCR and allowed to grow in 5 ml LB media with 50 µg/ml Kanamycin prior to expansion in 250 ml culture medium. It was followed by induction with 0.2 mM IPTG at 37°C for 3-4 hours. The cells were harvested, and suspended in buffer (50 mM sodium phosphate buffer, 500 mM NaCl, 20 mM Imidazole, pH 8) and lysed using a sonicator in the presence of PMSF (1 mM) as a protease inhibitor. The lysate was centrifuged at 13,000 rpm for 30 minutes at 4°C to obtain the soluble and the pellet (insoluble) fractions. The protein fractions were analyzed with SDS-PAGE and western blot. All protein samples were separated in a 10% SDS-polyacrylamide gel and then transferred to a nitrocellulose membrane (Bio-Rad, 162-0112) on a Trans-Blot Turbo (Bio-Rad). The blots were blocked with 5% BSA for 2 hours at RT followed by incubation with mouse monoclonal anti-HN (Santa Cruz Biotechnology, HN14f, sc-53562), NDV polyclonal or anti-His antibody (Bio Bharati Life Science, Cat# BB-AB0010S) overnight at 4°C with constant shaking. Blots were washed with TBST and incubated with appropriate HRP-conjugated secondary antibodies for 1 hour at RT, washed, and developed with Bio-Rad Clarity Western ECL substrate kit. Chemiluminescence was captured in the Bio-Rad chemiDoc system.

5.2.7 Ni-NTA purification

The soluble fraction containing the HN protein was incubated with 1ml of equilibrated Ni-NTA slurry for 1 hour at 4°C, and the flow-through was collected. The slurry was washed with 10 Column volumes (CV) of binding buffer containing progressively higher concentrations of imidazole (20-50mM). The protein was eluted using 250 mM imidazole. All eluted fractions were analyzed with SDS-PAGE. The purified HN protein fractions were pooled together and concentrated using an Amicon Ultra 4mL concentrator with a 50 kDa cut-off, to a final volume of 500 µl. A further polishing step was performed to obtain pure HN protein fractions with a Superdex 200 increase 10/300 GL gel filtration column, connected to an FPLC system (AKTA pure, GE Healthcare, Chicago, IL, USA). The protein was finally obtained in the gel filtration buffer (50 mM sodium phosphate buffer, 150 mM NaCl, pH 7.4). The concentration of the HN protein was estimated with a Bradford assay (Quick Start Bradford 1x Dye Reagent) according to the manufacturer's instructions and the purity was analyzed with SDS-PAGE.

5.2.8 Characterization of wild type HN and mutants

After purification of both the wild type and I175Y-mutant of HN with affinity chromatography, we performed analytical gel filtration with a Superdex 200 (16/600) column in order to determine the molecular weight, oligomeric status and proper folding of the proteins.

Table 5.2: List of standards used for analytical gel filtration.

Standards	Molecular weight (kDa)	Concentration (mg/ml)	Injection volume (µl)
1. Blue dextran	2000	0.8	500
2. B-Amylase (sweet potato)	200	0.5	500
3. Alcohol dehydrogenase (Yeast)	150	0.6	500
4. Bovine Serum Albumin (BSA)	66	5.25	500
5. Cytochrome c (Horse)	12.4	0.3	500

The protein standards used for the experiment are listed in Table 5.2. Following gel filtration chromatography of the standards, 500 µl (1 mg/ml) of HN proteins, wild type or mutant, was loaded into the column and the chromatograms were generated. The elution volumes of both the wild type and mutant HN was calculated and used for molecular weight determination with the help of the standard plot.

5.2.9 Isothermal Titration Calorimetry

The binding of HN (wild type and mutant) with 6-sialolactose was analyzed with the help of ITC. Proteins were kept in the sample cell and the ligand was loaded in the syringe. The reference power was set to 5 µW, and 19 injections with 2 µl injection volume, 180-sec initial delay, and 150-sec time spacing were injected at a stirring speed of 1000 rpm. The obtained isotherms were analyzed in the instrument software and the dissociation constants were determined. Control experiments, including protein-buffer and ligand-buffer titrations, were also performed and subtracted before the binding was analyzed.

5.2.10 Virus Titration and Infection

The NDV (strain R2B) stock was prepared by inoculating it in nine-day-old specific-pathogen-free embryonated chicken eggs. Allantoic fluid containing NDV was collected 48 hours post-inoculation, and its presence was confirmed by Hemagglutination assay using 1 % chicken RBC. The virus titer was determined by plaque assay as per the standard procedure. The recombinant NDV expressing GFP available in the laboratory was used for the fluorescent-based study.

5.2.11 Plaque inhibition assay

A monolayer of BHK 21 cells was used for plaque assay as described previously [14]. Briefly, BHK-21 cells were seeded on a 12-well cell culture plate at a 70-80% confluency and kept overnight for adhesion. The cells were incubated with 0.4 ml of different concentrations of purified HN protein diluted in plain DMEM for two hours in the incubator and gently rocked every 15 min. Following the incubation, the excess protein was removed by three washes with media, followed by incubation with 0.2 ml of NDV-R2B at an MOI of 0.01 in plain DMEM for 1 hour. The infection media was removed, and the cells were washed three times with media and gently overlaid with a pre-warmed methylcellulose medium. After removing the overlaying media, the cells were incubated at 37°C and 5% CO_2 for 48 hours and fixed with methanol for 30 min. The cells were washed with PBS and stained with 1% Crystal violet solution for 15 min. The excess stain was washed off, and the wells were allowed to dry before the visible plaques were counted.

5.2.12 Cell-based assays

To study the effects of the HN protein on NDV replication, monolayers of BHK-21 cells at around 80% confluency were incubated with either wild type or mutant HN protein at a concentration of 100 nM, followed by a washing step to remove unbound protein. Following

the treatment, NDV at an MOI of 0.01 was incubated for 1 hour at 37°C for virus adsorption. The unbound virus particles were removed by washing the cells monolayer with PBS twice. Infection was allowed to proceed over a 72-hour period in Dulbecco's Modified Eagle Medium (DMEM) supplemented with 2% fetal bovine serum (FBS) to support viral replication while limiting cell overgrowth. Virus titration assays were conducted to quantify viral replication, while virus reduction studies were performed using Western blotting to assess viral protein expression levels. Quantitative PCR (qPCR) was also employed to measure viral RNA levels.

5.2.13 Gene expression analysis

Total cellular RNA was extracted 72 hours post-infection using TRIzol reagent (Invitrogen, USA) following the manufacturer's instructions. For cDNA synthesis, 1 µg of purified RNA was reverse transcribed using a high-capacity cDNA reverse transcription kit (Thermo Scientific, USA). The gene expression was studied from cDNA by qPCR using PowerUp SYBR Green Master Mix (Applied Biosystems, USA). The gene expression study was done using host and NDV gene-specific primers (Sequences of primers are available upon request). The relative mRNA expression levels in treated versus untreated samples were calculated by the 2^(−ΔΔCt) method using GAPDH as an internal control for normalization [23].

5.2.14 Protein Expression Analysis

The NDV-infected BHK-21 cells were lysed with Laemmli buffer and subjected to protein estimation with the help of TCA analysis. An equal quantity of proteins was loaded in SDS-PAGE gels and transferred to a nitrocellulose membrane. Membranes were blocked with 5% BSA and NDV proteins were probed with the chicken NDV polyclonal antibody available in the laboratory, anti-β-actin antibody and subsequently with the appropriate horseradish peroxidase (HRP)-conjugated secondary antibodies (Invitrogen, USA). The blots were developed using the ECL reagent (BioRad, USA). The density of the bands was analyzed by ImageJ software (NIH).

5.2.15. *In ovo* studies

Nine-day-old specific-pathogen-free embryonated chicken eggs were used in the study, where the wild type or the I175Y-HN proteins, each at 1µM concentration, were injected into the allantoic fluid 1 hour prior to NDV inoculation. After inoculation with NDV, the eggs were incubated at 37°C for 48 hours. The allantoic fluid from each group was collected, and the NDV was titrated by HA and plaque assay. The allantoic fluid from each group was also subjected to western blot analysis for protein expression studies as described earlier. The

embryo tissue samples were also collected from the respective groups and used for gene expression studies with the help of Quantitative PCR as described earlier.

5.2.16 SYBR green assay

To investigate the anti-plasmodial effects of the wild type HN protein and its I175Y mutant, synchronized schizonts at a parasitemia of 1% were treated with increasing concentrations of the proteins, ranging from 1 to 50 µM. After a 48-hour incubation period, parasite viability was assessed using the SYBR green assay. Media was not replenished during the incubation. After incubation of 48 hours, 100 µl sample containing parasites was mixed with 100µl of Lysis buffer (20mM Tris pH 7.5, 5Mm EDTA, 0.008%-gram Saponin, 0.08% ml TritonX-100) and SYBR green dye at a dilution of 1: 10,000 and incubated in dark at room temperature for 3 hours. Following the incubation, fluorescence intensity was measured at 485 nm excitation and 528 nm emission using a microplate reader.

5.2.17 Statistical analysis

All the statistical analyses in the study were performed using the one-way ANOVA with Tukey's HSD. The significant differences among the different groups were indicated as *, **, and *** when $p < 0.05$, $p < 0.01$, $p < 0.001$, respectively.

5.3 Results

5.3.1 Comparative analysis of sialic acid binding pocket in viral coat proteins

The HN coat protein of NDV is a sialic acid binding lectin employed by the virus to target sialic acid-rich host cell surface for initial binding and subsequent entry. Previous studies have suggested that the protein has a central sialic acid binding domain that shows both hemagglutinin (sialic acid binding) and neuraminidase (sialic acid cleaving) activities. To gain further insight into the sialic acid biophore of the protein, we did a comparative analysis of HN from different viral species and also the NAs, which are a closely related class of proteins. Our analysis of HNs and NAs from different virus species elucidated a conserved six-bladed β-propeller architecture across both protein families. The β-propeller structure, characterized by six radially arranged β-sheets, forms a toroidal configuration that serves as a fundamental scaffold supporting the sialic acid binding pocket of these glycoproteins (**Figure 5.1 A**). Despite the shared three-dimensional fold, significant differences are evident in the configuration of the sialic acid-binding pockets within HN and NA proteins.

Table 5.3: List of available crustal structure of viral lectins complexed with sialic acid was used for comparative analysis of the sialic acid biophore between the HN and NA.

S.N.	Organism	PDB ID	Functional family	Structural Domains
1	Human respirovirus 3	1V3D	Hemagglutinin-neuraminidase	6-beta propeller
2	Human respirovirus 3	1V3C	Hemagglutinin-neuraminidase	6-beta propeller
3	Mammalian orthorubulavirus 5	1Z4X	Hemagglutinin-neuraminidase	6-beta propeller
4	Mammalian orthorubulavirus 5	1Z4Z	Hemagglutinin-neuraminidase	6-beta propeller
5	avian paramyxovirus 1	1USR	Hemagglutinin-neuraminidase	6-beta propeller
6	avian paramyxovirus 1	1USX	Hemagglutinin-neuraminidase	6-beta propeller
7	avian paramyxovirus 1	1E8U	Hemagglutinin-neuraminidase	6-beta propeller
8	avian paramyxovirus 1	1E8V	Hemagglutinin-neuraminidase	6-beta propeller
9	Mumps orthorubulavirus	5B2D	Hemagglutinin-neuraminidase	6-beta propeller
10	Mumps orthorubulavirus	6JJM	Hemagglutinin-neuraminidase	6-beta propeller
11	Mumps orthorubulavirus	6JJN	Hemagglutinin-neuraminidase	6-beta propeller
12	Influenza A virus (A/Tokyo/3/1967(H2N2))	2BAT	Neuraminidase (N2)	6-beta propeller
13	Influenza A virus (A/Moscow/10/1999(H3N2))	8DWB	Neuraminidase (N2)	6-beta propeller
14	Influenza A virus H3N2 subtype	4GZQ	Neuraminidase (N2)	6-beta propeller
15	Influenza A virus H3N2 subtype	4GZX	Neuraminidase (N2)	6-beta propeller
16	Influenza A virus H3N2 subtype	4GZW	Neuraminidase (N2)	6-beta propeller
17	Influenza A virus (A/RI/5+/1957(H2N2))	4H53	Neuraminidase (N2)	6-beta propeller
18	Influenza A virus	1W20	Neuraminidase (N6)	6-beta propeller
19	Influenza A virus	1MWE	Neuraminidase (N9)	6-beta propeller
20	Influenza A virus	2QWB	Neuraminidase (N9)	6-beta propeller
21	Influenza A virus (A/Shanghai/02/2013(H7N9))	5L18	Neuraminidase (N9)	6-beta propeller
22	Influenza A virus	2C4A	Neuraminidase (N9)	6-beta propeller
23	Influenza B virus (STRAIN B/BEIJING/1/87)	1NSC	Neuraminidase	6-beta propeller

The predominant form of sialic acid in humans is N-acetylneuraminic acid (Neu5Ac), which features a carboxyl group (-COOH) at C_1, a hydroxyl group (-OH) at C_4, an acetamido group at C_5, and a three-carbon chain at C_6 with hydroxyl groups (-OH) at C_7, C_8, and C_9 [24]. In hemagglutinin-neuraminidases (HN), Arginine forms H-bonds with the carboxyl group at C_1, while Glutamate, Tyrosine, or Arginine engage with the hydroxyl groups at C_7, C_8, and C_9 (**Figure 5.1 B**). The hydroxyl group at C_4 and the acetamido group at C_5 of sialic acid remains free. Conversely, in neuraminidases (NAs), the sialic acid binding pocket primarily consists of Arginine and Glutamate residues which interacts with all the functional groups of sialic acid at C_1, C_4, C_5, and $C_{7\text{-}9}$ through hydrogen bonds (**Figure 5.1 C**).

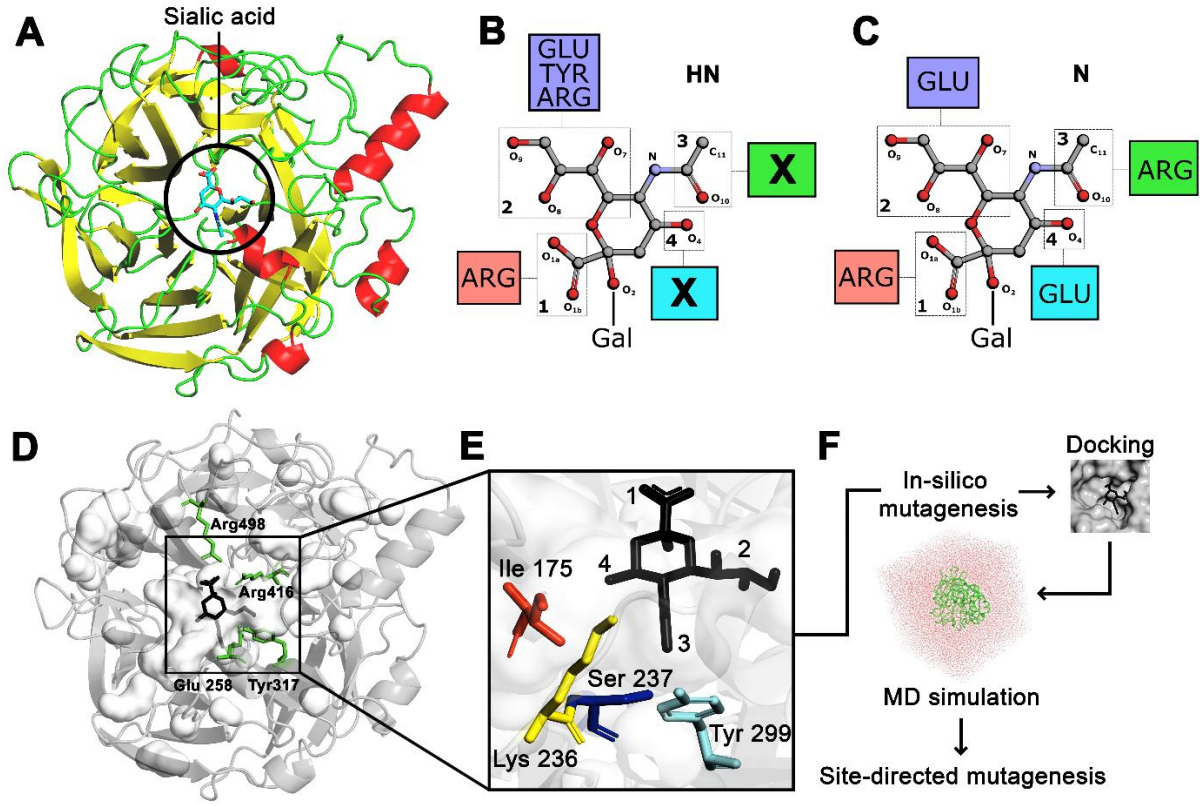

Figure 5.1: The NDV-HN protein has a Type-IV sialic acid binding module. (A) The Neuraminidases (NAs) and the Hemagglutinin-Neuraminidases (HNs) share a conserved six-bladed β-propeller fold. The receptor binding and catalytic site of the protein is shown in a black circle. (B) 2-D residue interaction analysis of the HN protein showing key residues interacting with different functional groups of sialic acid (grey). Arginine residues (red) stabilizes the carboxyl group at C_1 while Glutamate, Tyrosine and Arginine (blue) forms H-bonds with the hydroxyl groups at C_7, C_8 and C_9. No residues from the sialic acid biophore interacts with the Hydroxyl group at C_4 and the acetoamide group at C_5. (C) 2-D residue interaction analysis of the NA protein showing key residues forming H-bonds with different functional groups of sialic acid (grey). Similar to the HN biophore, arginine residues (red) stabilizes the carboxyl group at C_1 while Glutamate engages with the hydroxyl groups at C_7, C_8 and C_9. Glutamate (cyan) forms H-bonds with the hydroxyl group at C_4 and Arginine (green) stabilizes the acetoamide group at C_5. Multiple residues from the NA biophore interacts with all the functional groups of sialic acid. (D and E) Residues selected for mutagenesis (F) In-silico studies involving docking and MD simulation.

While there is currently no comprehensive study in the literature that examines sialic acid binding across different viral lectins, using standard biochemical techniques such as Isothermal Titration Calorimetry (ITC) or Surface Plasmon Resonance (SPR), it is conceivable that Neuraminidases (NAs) might exhibit a stronger affinity for sialic acid compared to Hemagglutinin-Neuraminidases (HNs). This potential difference in binding affinity could be the results of the extensive interactions that NAs have with sialic acid, as opposed to the relatively fewer interactions observed in HNs (**Figure 5.1 B and C**). Thus, we asked if specific

mutations could be carried out in the active site of HN to accommodate the free groups of sialic acid, potentially leading to an increased number of interactions that could result in a greater affinity for sialic acid. To achieve this, we identified key sites for mutagenesis, located spatially within 5 Å from the free hydroxyl and acetamido group of sialic acid in the sialic acid binding biophore of HN (**Figure 5.1 D and E**). In-silico mutagenesis of the selected amino acid residues Ile 175, Lys 236, Ser 237 and Tyr 299 to Arg, Glu, Asp, Lys, Tyr, Asn, Gln and His was performed. The binding of the wild type HN and respective mutants to sialic acid was analyzed with the help of docking and MD simulation (**Figures 5.2 and 5.3**). Following the in-silico analysis, mutants that showed greater affinity towards sialic acid were selected for further analysis.

5.3.2 In-silico mutagenesis of key amino acid residues showed greater affinity for sialic acid

Based on our analysis of the sialic acid binding biophore within the NDV-HN protein, we hypothesized that altering specific residues in the binding module could enhance the binding affinity of HN for sialic acid. To test this hypothesis, we performed in-silico site-directed mutagenesis on four key residues: I175, K236, S237, and Y299. Each residue was mutated to one of the following amino acids: R, D, E, K, Y, Q, N, or H based on our comparative analysis. We used the Autodock suite to conduct molecular docking simulations and evaluate the binding energies of these mutants with sialic acid. Validation of the docking protocol was established by superimposing the sialic acid from the crystal structure and docking, which yielded an RMSD of 0.81 (**Figure 5.2 A**). The wild type HN protein exhibited a binding energy of -3.98 kcal/mol with sialic acid, which served as our reference point (**Figure 5.2 B**). Among the mutants, the I175Y substitution demonstrated the most significant improvement, resulting in a binding energy of -4.31 kcal/mol. This suggests a stronger interaction between the mutant protein and sialic acid compared to the wild type. Similarly, the I175D mutant also exhibited enhanced binding affinity, with a binding energy of -4.23 kcal/mol. Other notable mutations included K236N and K236H, both of which showed binding energies of -4.13 kcal/mol, and the S237D mutant, which yielded a binding energy of -4.15 kcal/mol. These results indicate that these specific mutations may confer subtle improvements in binding affinity. However, it is important to note that mutations at the Y299 position did not result in any favorable changes in binding energy, suggesting that this residue may be less responsive to modifications that enhance sialic acid binding. Overall, our findings indicate that targeted mutations, particularly at the I175 position, can significantly improve the binding affinity of HN for sialic acid. Thus,

based on these initial results, we tested the binding of the mutants to sialic acid under dynamic conditions with the help of MD simulation.

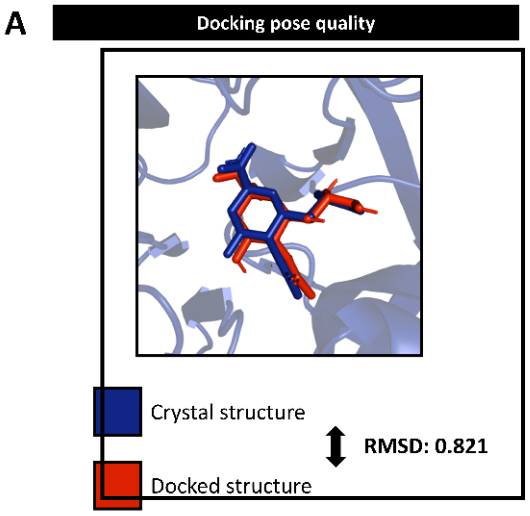

B

Docking results

Residue	Rotamers	Binding energy	KI (mM)	Residue	Rotamers	Binding energy	KI (mM)
WT	--	-3.98	1.2	WT	--	-3.98	1.2
I_{175}	R	-3.8	1.64	K_{236}	R	-4.00	1.16
	D	-4.23	0.795		D	3.96	1.24
	E	-3.79	1.67		E	-4.06	1.05
	K	-3.99	1.18		K	--	--
	Y	-4.31	0.691		Y	-3.56	2.45
	Q	-4.02	1.14		Q	-4.03	1.11
	N	-3.89	1.4		N	-4.13	0.936
	H	-3.7	1.95		H	-4.13	0.936
Residue	Rotamers	Binding energy	KI (mM)	Residue	Rotamers	Binding energy	KI (mM)
WT	--	-3.98	1.2	WT	--	-3.98	1.2
S_{237}	R	-2.71	10.25	Y_{299}	R	-3.91	4.58
	D	-4.15	0.905		D	-3.86	1.49
	E	-3.18	4.67		E	-2.96	6.81
	K	-3.24	4.19		K	-3.2	4.5
	Y	-2.91	7.33		Y	--	--
	Q	-3.84	1.53		Q	-3.1	5.33
	N	-3.84	1.54		N	-3.83	1.53
	H	-2.54	13.71		H	3.85	1.5

Figure 5.2: Docking of the NDV-HN and its mutants with sialic acid. (A) Superimposition of sialic acid from the crystal structure (blue) and docking (red) shows that post-docking the ligand was bound in the correct orientation in the pocket. (B) The binding energy of the wild type HN and its mutants. Red squares represent the mutants showing better binding with sialic acid and hence selected for further analysis with Molecular Dynamics Simulation studies.

5.3.3 The substitution of I175 with Y resulted in a greater affinity for sialic acid

Molecular dynamics (MD) simulations were conducted to assess the stability of sialic acid binding in both the wild type and mutant HN proteins over a 100 ns timeframe. These simulations aimed to validate the docking predictions and further explore the dynamic behavior of the protein-ligand interactions. Ligand-bound structures were extracted at 0, 25, 50, 75, and 100 ns, as illustrated in **Figure 5.3 A**. Among the five mutants predicted from the docking studies, only two demonstrated stable binding to sialic acid throughout the 100 ns simulation. Contrary to initial docking predictions, the I175D mutant (depicted in green), which initially showed promising binding affinity, was found to form an unstable complex with sialic acid during the MD simulation. Similarly, the K236H (dark grey) and K236N (orange) mutants also exhibited unstable binding, as confirmed by the 3D structural analysis of the binding pocket and the pair distance analysis (**Figure 5.3 A and B**). In contrast, the I175Y (blue) and S237D (cyan) mutants maintained stable binding of sialic acid, with pair distance graphs closely resembling those of the wild type protein.

A more detailed analysis of hydrogen-bonded residues (marked in red) and residues involved in van der Waals interactions (marked in yellow) revealed a greater degree of interactions between sialic acid and the binding pocket in the I175Y and S237D mutants compared to the wild type (light grey) (**Figure 5.3 A**). However, it is important to note that in the S237D mutant, the pair distance analysis indicated an abrupt dissociation of the ligand-receptor complex at around 70 ns, as evidenced by spikes in the graph (**Figure 5.3 B, iv**). This instability suggests potential challenges in maintaining a stable interaction over time. Based on these findings, the I175Y mutant emerged as the most promising candidate for further investigation, given its stable binding profile and enhanced interaction with sialic acid compared to the wild type protein.

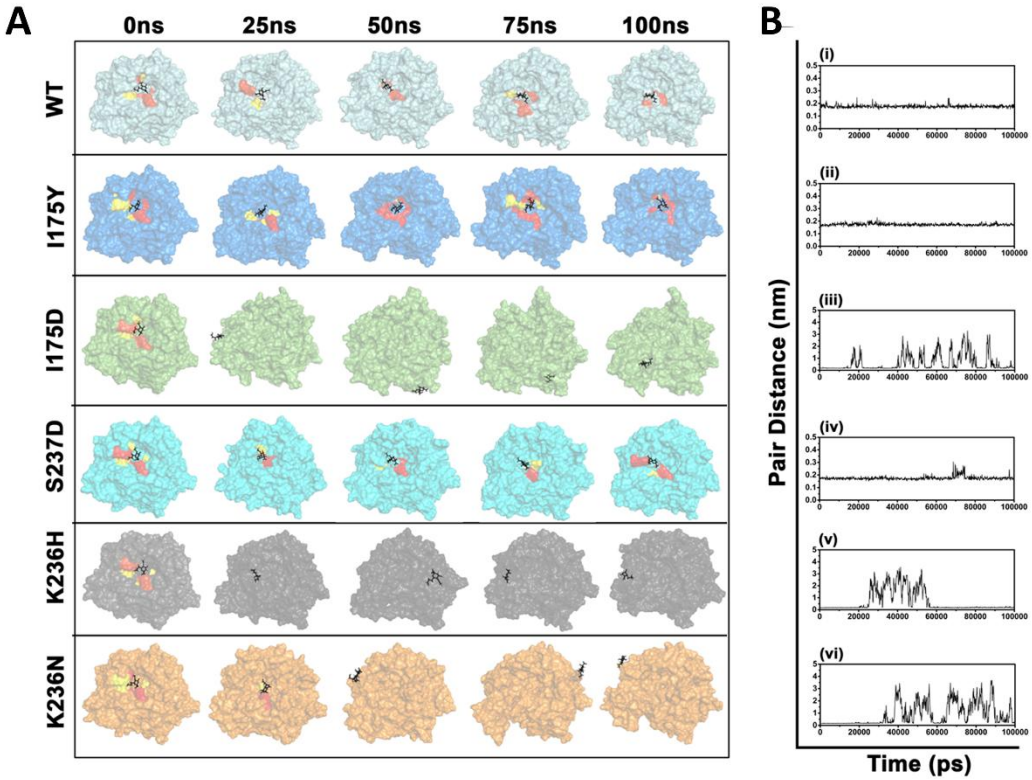

Figure 5.3: Molecular Dynamics (MD) Simulation of wild type HN and its mutants with sialic acid reveals the I175Y mutant to be the most promising candidate. (A) Ligand bound structures were extracted at 0, 25, 50, 75 and 100 ns. Residues interacting with sialic acid through H-bonds are colored in red while those involved with hydrophobic interactions are colored in yellow. (B) Pair distance (PD) graph showing the distance between the protein and ligand in nanometers (nm). X-axis: MD simulation period in picoseconds (ps), Y-axis: distance in nm.

We also assessed key parameters such as Root Mean Square Deviation (RMSD) and Radius of Gyration (Rg) for both the wild type and mutant proteins. The analysis revealed no significant

variations in RMSD and Rg between the wild type and mutant structures (**Figure 5.4 A and B**), indicating that the mutations introduced did not compromise the overall structural stability of the proteins. Further analysis focused on the Root Mean Square Fluctuation (RMSF) of the sialic acid-bound complexes, which provided insights into the flexibility of individual residues within the proteins. The RMSF comparison between the wild type and the I175Y mutant revealed notable differences, particularly in two regions: residues 340-350 and 450-460. In the I175Y mutant, these residues exhibited significantly higher fluctuations from their mean positions (**Figure 5.4 C**). This increased flexibility suggests that the I175Y mutation may induce altered dynamics in these regions, potentially leading to a shift in the overall protein conformation. Such a conformational change could affect the configuration of the sialic acid binding site, potentially enhancing or modifying its interaction with the ligand. Hydrogen bonding (H-bonding) analysis further supported the distinction between the wild type and I175Y mutant.

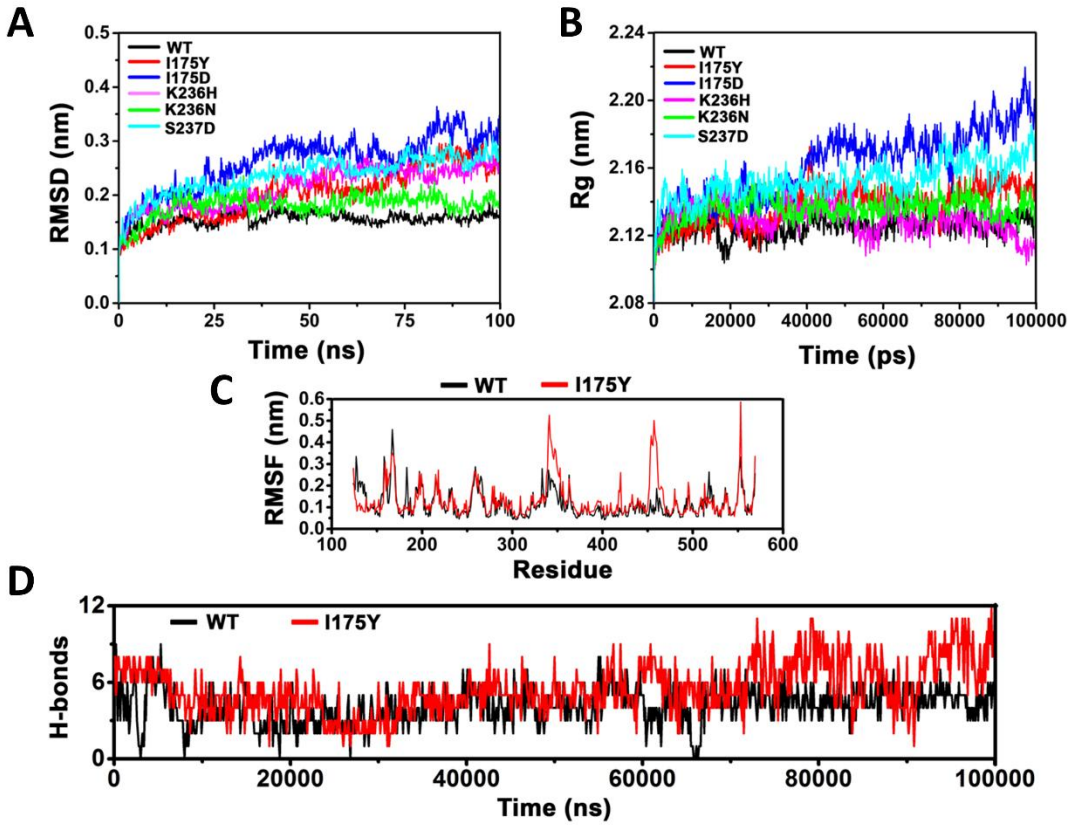

Figure 5.4: The HN-I175Y mutant showed greater number of average hydrogen bonds with sialic acid compared to the wild-type protein. (A) Root Mean Square Deviation (RMSD) of wild type and different mutants HN. X-axis: MD simulation period in ns, Y-axis: RMSD in nm (B) Radius of gyration (Rg) of wild type HN and its mutants. X-axis: MD simulation period in ps, Y-axis: Rg in nm. (C) Root Mean Square Fluctuation (RMSF)

of the residues in wild type HN (black curve) and the I175Y mutant (red curve). X-axis: Residue number, Y-axis: RMSF in nm. (D) Hydrogen bonds (H-bonds) between sialic acid and amino acid residues in the binding pocket throughout the MD simulation. H-bonds formed by the wild type HN is depicted in black while those by the I175Y mutant in red.

The average number of H-bonds in the wild type complex was found to be 4.174, while the I175Y mutant exhibited higher average of 6.515, respectively (**Figure 5.4 D**). The I175Y mutant consistently maintained a higher number of H-bonds with sialic acid throughout the simulation, suggesting a more stable and stronger interaction. Given the consistent higher H-bonding observed in the I175Y mutant, we selected this variant for further 2-D residue interaction analysis to gain deeper insights into the nature of its interaction with sialic acid. This analysis could help elucidate the specific interactions and potential structural alterations that contribute to the enhanced binding affinity observed in the I175Y mutant, making it a promising candidate for further study.

5.3.4 The I175Y mutation induces a transition from a Type-IV to a Type-I sialic acid binding module, resulting in enhanced affinity for sialic acid

The 2-D residue interaction analysis was conducted to identify the key amino acid residues involved in hydrogen bonding with the different functional groups of sialic acid during the 100 ns molecular dynamics simulation. This analysis provided insights into the dynamic interactions between the HN protein and sialic acid in both the wild type and the I175Y mutant. The amino acid interaction timeline, illustrated in **Figure 5.5 (A and B)**, displays the temporal interaction of critical residues with sialic acid. The depth of the orange hue represents the intensity of these interactions, highlighting the multiple contact points that certain residues maintain with the ligand. In the wild type HN (**Figure 5.5 A and C**), residues R498 and R416 exhibit persistent interactions with sialic acid, engaging with the carboxyl group at the C_1 position of approximately 85% and 83% of the time, respectively. Additionally, residues T467, G468 and S452 residues interacts with the multiple hydroxyl (-OH) groups of C_7, C_8 and C_9 approximately 54%, 37% and 35% of the time, while the hydroxyl group at C_4 and the acetamido group at C_5 remained free. It agrees with the results obtained from our comparative analysis which suggested a Type-IV sialic acid binding module in NDV-HN (**Figure 5.1 B**). This indicates that in the wild type HN, certain functional groups of sialic acid are not occupied, potentially limiting the overall binding affinity of the protein for its ligand. It is also important to note that the I175 residue is not involved in any interaction with the sialic acid in the wild type HN protein.

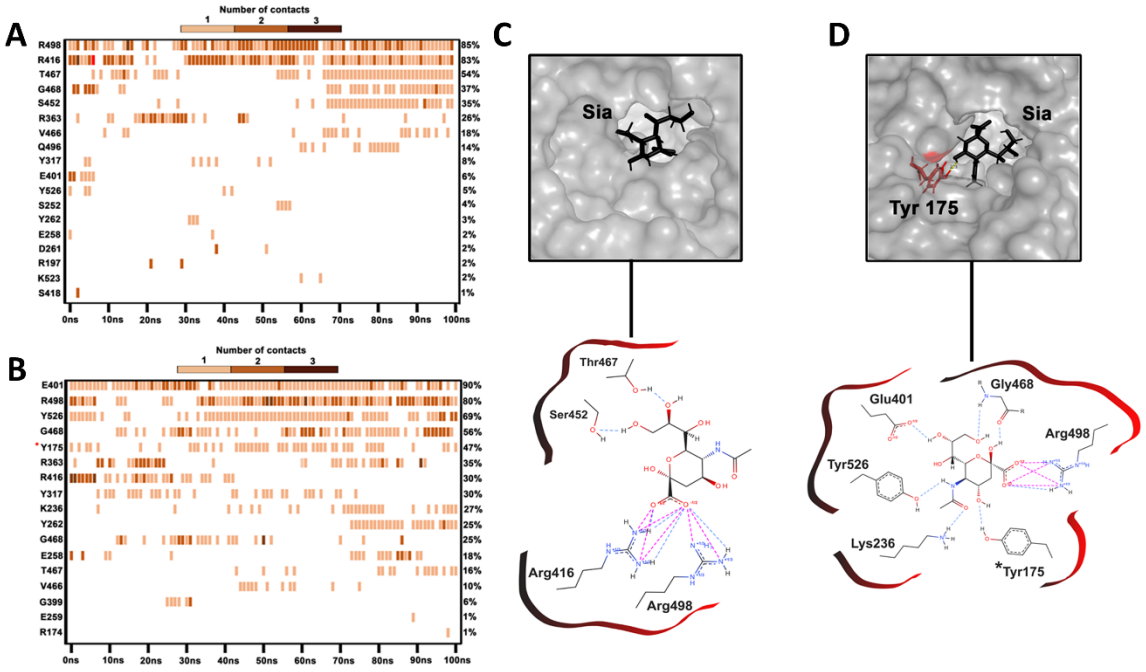

Figure 5.5: The 2-D residue interaction analysis reveals an altered binding module in mutant HN sialic acid binding module. (A and B) Amino acid interaction timeline during the 100 ns MD simulation. Positive interactions are depicted by a vertical line, while a gradient of orange depicts the number of interactions made by the residue with sialic acid. (C and D) 2-D residue interaction map depicting the most prominent residues involved in H-bonding in the wild type (C) and I175Y mutant (D). Analysis show a transition of the binding module from Type-IV to Type-I in the I175Y mutant.

The amino acid interaction timeline of the I175Y mutant of HN reveals a significantly altered interaction profile compared to the wild type. In this mutant, residue R498 continues to maintain persistent interactions with the carboxyl group at the C_1 position of sialic acid approximately 80% of the time, similar to the wild type protein (**Figure 5.5 B and D**). This consistency underscores the importance of R498 in anchoring the sialic acid molecule to the HN protein. However, notable differences arise in the interactions of other residues with the functional groups of sialic acid. In the mutant, residue E401 interacts with the hydroxyl groups at positions C_7, C_8, and C_9 approximately 90% of the time, while G468 engages with these groups around 56% of the time. These interactions suggest an enhanced stabilization of the hydroxyl groups compared to the wild type. More importantly, the mutant introduces new and critical interactions that were absent in the wild type HN. Residues Y526 and the substituted residue Y175 engage with the acetamido group at C_5 and the hydroxyl group at C_4 approximately 69% and 47% of the time, respectively. This marks a significant shift from the wild type, where these functional groups remained free. The substitution of isoleucine at

position 175 with tyrosine not only altered the interaction profile but also expanded the range of stabilizing contacts between the protein and sialic acid, thus transforming the binding module to a Type-I from a Type-IV.

5.3.5 Site-directed mutagenesis, overexpression and purification of HN protein

Based on the in-silico predictions indicating enhanced binding affinity and altered interaction profiles of the I175Y mutant of HN, we proceeded to generate this mutant using site-directed mutagenesis. The I175Y mutation was introduced using the megaprimer method, which involves a two-step PCR process. Complementary pairs of mutagenesis primers were designed to specifically introduce the I175Y substitution into the HN gene (Table 5.1). The pET-28-HN construct, containing the wild type HN gene, served as the template for mutagenesis.

The presence of the wild type HN gene, approximately 1.6 kb in size, was confirmed through restriction digestion and PCR analysis (**Figure 5.6 A**). This confirmation ensured that the template was suitable for subsequent mutagenesis steps. To generate the mutant megaprimer, a 403 bp fragment containing the I175Y mutation was amplified using the cloning forward primer and the mutated reverse primer in a gradient PCR (**Figure 5.6 B**). Following PCR amplification, the mutant megaprimer was purified through gel elution. This purified megaprimer was then used as a template in a second round of PCR to amplify the full-length mutated HN gene (**Figure 5.6 C**). The resulting full-length I175Y HN gene was subsequently ligated into the pET-28a expression vector. The recombinant pET-28a-HN-I175Y construct was then transformed into Top10 and later into the C41(DE3) strain for protein expression. Both the wild type and I175Y-HN proteins were overexpressed in transformed C41(DE3) by induction with 0.2 mM IPTG at 37°C for 4 hours. The soluble expression of these proteins was assessed using SDS-PAGE and western blot analysis. As shown in **Figure 5.6 G**, analysis of uninduced and induced fractions by SDS-PAGE revealed a prominent protein band corresponding to the overexpressed HN protein, with a molecular weight of 60 kDa in the soluble fraction. To further confirm the identity of the overexpressed proteins, they were transferred onto a nitrocellulose membrane and probed with specific antibodies (NDV polyclonal, anti-HN and anti-His), as described in the materials and methods section.

The western blot analysis confirmed the presence of the HN protein by detecting the overexpressed band specifically, validating the expression of the protein (**Figure 5.6 G**). Following confirmation of expression, the HN proteins were purified using Ni-NTA affinity chromatography under native conditions. During the purification process, it was observed that

the HN proteins effectively bound to the Ni-NTA column, as shown in **Figure 5.6 H and I**. In the washing step with 50 mM and 80 mM imidazole (**Figure 5.6, H and I, Lanes 4 and 5**), several non-specific proteins were eluted. The majority of the HN protein was successfully eluted in fractions collected with 250 mM imidazole (**Figure 5.6, H and I, Lanes 6 to 11**). The purified protein fractions were pooled together and subjected to dialysis for removing the imidazole and concentrated with a protein concentrator of 50 kDa cut-off and further polishing step was performed with gel filtration. Analytical gel filtration was carried out to check the molecular weight, oligomeric status and proper folding of the HN protein. Both the wild type and mutant HN proteins were first purified using Ni-NTA affinity chromatography, ensuring that the samples were of high purity and suitable for SEC analysis. The purified proteins were then subjected to analytical gel filtration on a calibrated SEC column, pre-equilibrated with an appropriate buffer to maintain native conditions. The column was calibrated using a series of molecular weight standards (**Figure 5.6 J**), which provided reference elution volumes corresponding to proteins of known molecular weights.

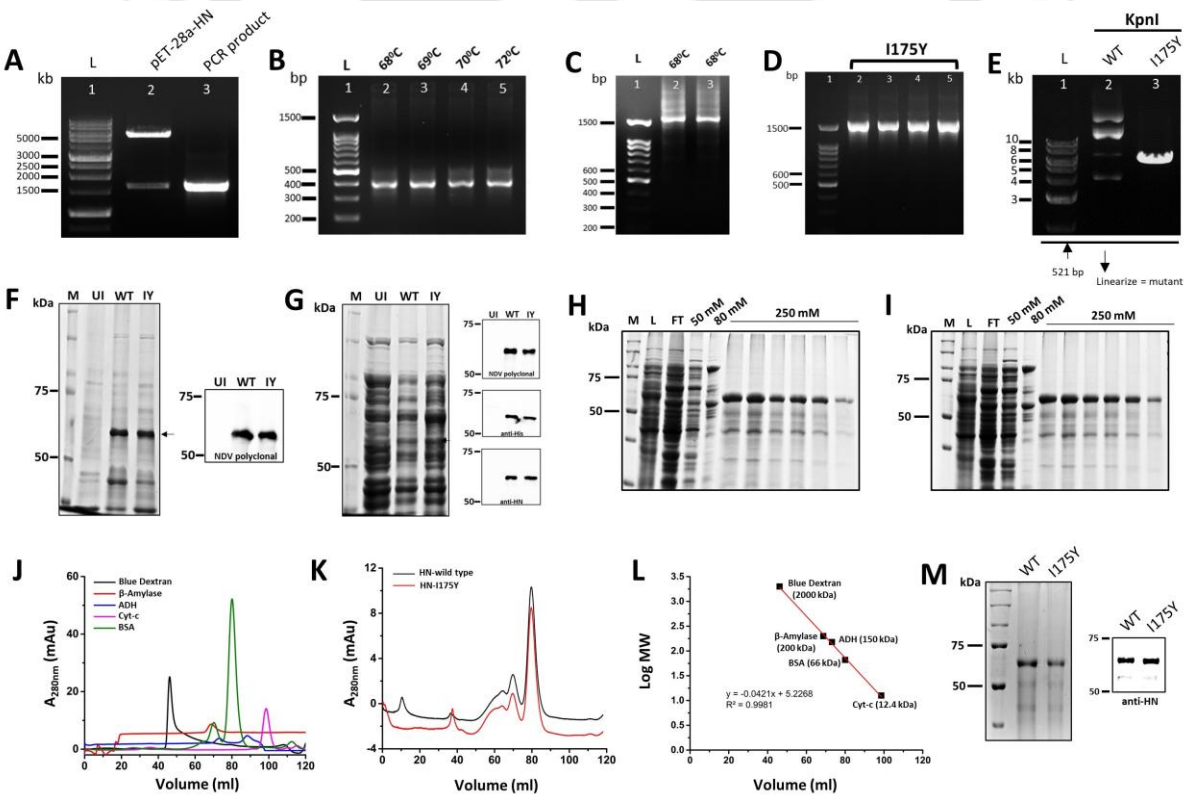

Figure 5.6: The I175Y mutant of HN was generated by the megaprimer method followed by its overexpression and purification. (A) Restriction digestion of the pET28a-HN construct to confirm the presence of insert along with amplification of the cloned fragment with PCR. Lane 1: Ladder, Lane2: Restriction digestion with BamHI and HindIII showing the release of 1.6 kb insert, Lane3: PCR amplification of the 1.6 kb HN fragment with cloning forward and reverse primers. (B) First PCR reaction of the megaprimer method for the generation of

the 403 bp long megaprimer containing the mutant fragment. The cloning forward and the mutated reverse primers were used to amplify the megaprimer with pET28a-HN construct as a template. Lane 1: Ladder, Lane 2 to 5: Gradient PCR for synthesizing the megaprimer (C) Second PCR reaction to generate full length mutated HN gene. The cloning reverse and the megaprimer (403 bp) generated from the first PCR reaction was used. Lane 1: ladder, Lane 2 and 3: Two PCR reactions generating the full length I175Y mutant gene. The mutated gene was digested with BamHI and HindIII and ligated into an empty pET-28a digested with the same enzymes. The product of the ligation reaction was used to transform Top10 cells for plasmid confirmation and expansion. (D) Colony PCR confirming the presence of the pET-28-HN (I175Y) construct. Lane 1: Ladder, Lane 2-5: colony PCR product showing the amplified HN-I175Y mutant gene fragment. (E) Digestion of the pET-28-HN (I175Y) construct with KpnI to confirm the presence of the I175Y mutation. Lane 1: Ladder, Lane 2: pET28-HN (wild type) digested with KpnI shows no enzymatic activity, Lane 3: KpnI digestion linearizes the mutant plasmid. (F and G) Overexpression of wild type HN and mutated protein in C41(DE3) shows that the overexpressed proteins were present both in the insoluble (F) and soluble (G) fractions. Western blot analysis was done to confirm that the overexpressed protein was NDV-HN with NDV polyclonal, anti-HN and anti-His antibodies. (H and I) Purification of the wild type (H) and mutated (I) proteins with the help of Ni-NTA chromatography. (J) Chromatograms of the standards used for analytical gel filtration. (K) Chromatograms of wild type HN (black) and I175Y mutant (red). (L) Standard curve was plotted with the help of the standards and the equation obtained was solved for ‘‘y’’ to obtain the molecular weight of the HN proteins. (M) Purity of the wild type HN and I175Y mutant was confirmed with SDS-PAGE analysis along with western blot analysis with anti-HN antibodies.

For both the wild type and I175Y mutant proteins, the elution profile revealed a distinct peak corresponding to the major protein species in solution (**Figure 5.6 K**). By comparing the elution volumes with the calibration curve generated from the molecular weight standards, the approximate molecular weight of the both the wild type and mutant HN was calculated to be around 60 kDa (**Figure 5.6 L**).

Table 5.4: Table showing the elution volumes obtained for each standard after gel filtration and the Log of their molecular weight, which were used for obtaining the standard plot.

Standards	Molecular weight (kDa)	Log of Molecular weight	Elution volume (ml)
1. Blue dextran	2000	3.3	46.2
2. B-Amylase (sweet potato)	200	2.3	68.7
3. Alcohol dehydrogenase (Yeast)	150	2.18	73.2
4. Bovine Serum Albumin (BSA)	66	1.82	80
5. Cytochrome c (Horse)	12.4	1.1	98.6

This indicated that the HN proteins existed primarily as monomers in the solution and were properly folded. The eluted proteins were further concentrated and checked for their purity with

the help of SDS-PAGE and western blot analysis with anti-HN antibody (**Figure 5.6 M**). Following the biochemical characterization of the proteins, the binding of the wild type and I175Y mutant was checked with sialic acid with the help of Isothermal Titration Calorimetric (ITC) and the biological activity of the protein was also evaluated with standard assays.

5.3.6 ITC analysis reveals a stronger affinity of HN-I175Y with 6-sialolactose

In an isothermal titration calorimetry (ITC) study, the binding affinities of the wild-type hemagglutinin-neuraminidase (HN) protein and its I175Y mutant to the ligand 6-sialolactose were quantitatively analyzed. The ITC results indicated that the I175Y mutant demonstrated a significantly enhanced binding affinity, with a dissociation constant (K_d) of 53.9 µM, compared to the wild-type HN protein, which had a K_d of 155 µM (**Figure 5.7 A**). This 2.8-fold reduction in the K_d value signifies a more robust interaction between the I175Y mutant and 6-sialolactose, indicates that the mutation strengthens the binding of the protein to the ligand. The enhanced binding affinity observed in the I175Y mutant can be attributed to a change in the structural characteristics of the binding module within the protein. Specifically, the I175Y mutation alters the binding module from a Type-IV to a Type-I conformation as observed in our computational studies. Thus, given that the I175Y mutant showed greater affinity for sialic acid, we did additional experiments to determine the consequences of this mutation on the biological activity of the protein.

5.3.7 The HN-I175Y mutant displays enhanced biological activity compared to HN-WT

The sialic acid binding and neuraminidase activity of the HN protein depends on the degree of interactions between the amino acid residues of the central active site of the protein and the functional groups of sialic acid. Interestingly, the neuraminidase activity of the HN protein involves cleaving the glycosidic bond between sialic acid and the adjacent sugar in glycoproteins and glycolipids. For efficient catalysis, sialic acid must undergo a conformational change from its stable chair form to a distorted form, such as a boat or skew-boat. Amino acid residues in the active site of the HN protein facilitates this distortion, stabilizing the transition state and lowering the activation energy needed for bond cleavage. Therefore, an increased number of interactions towards sialic acid could help elevate both the sialic acid binding and neuraminidase activity of the protein. To address this, we initially tested the ability of the wild type and I175Y-HN protein to inhibit plaque formation by NDV on monolayers of cells. The cells were pre-incubated with either the wild-type or mutant HN protein at varying concentrations, allowing the proteins to interact with sialic acid residues on the cell surface.

This interaction potentially blocks the sialic acids from being recognized by NDV, thereby preventing viral attachment and entry. Additionally, the neuraminidase activity of HN could cleave terminal sialic acids, further reducing the availability of viral receptors on the cell surface. Quantitative analysis of plaque formation by NDV revealed that both the wild-type and I175Y mutant HN proteins significantly reduced the number of plaques, indicating effective inhibition of viral infection (**Figure 5.7 C**). Specifically, the wild-type HN protein at a concentration of 100 nM reduced plaque formation by over 50%, and at 500 nM, plaques were nearly undetectable (**Figure 5.7 C**). In comparison, the I175Y mutant demonstrated enhanced inhibitory activity, with over a 75% reduction in plaque formation at 100 nM and a complete absence of plaques at 500 nM. These results indicate that the I175Y mutant possessed greater affinity for sialic acid thereby delivering approximately 25% greater plaque inhibition than the wild-type protein at equivalent concentrations. This enhanced activity may be attributed to the increased affinity of the mutant for sialic acid residues or altered neuraminidase activity, leading to more effective blocking and cleavage of sialic acids on the cell surface.

In a subsequent experiment, monolayers of cells were incubated with either wild type or mutant HN protein at a concentration of 100 nM, followed by a washing step to remove unbound protein. Following the treatment, NDV at an MOI of 0.01 was used for infecting the cells. Post-infection at 72 hours, cells were processed for quantitative estimation of NDV infection with the help of western blot analysis and real time PCR. Brightfield images of cells at 72 hours post infection are shown in **Figure 5.7 D**, where robust infection of NDV could be seen in the untreated cells based on the observed cytopathic effects. Cells treated with the wild type or the I175Y mutant HN protein showed a marked decrease in NDV-induced cytopathy. The control cells without any protein treatment or NDV infection appeared to be of normal morphology. To track the level of infection with NDV, we probed the HN protein of the virus with the help of western blotting (**Figure 5.7 E**). Quantitative estimation from the blots showed a 50% decrease (0.5-fold) in the levels of NDV-N protein in the cells treated with wild type HN (Figure 5.5 F). On the contrary, in the cells treated with the I175Y mutant, an 80% decrease (0.8 fold) in NDV-N protein was observed. To verify the results, we also did quantitative PCR for estimation of the Ct values in the untreated and HN treated cells. Similar to the results from western blotting, NDV-N protein showed over 90% reduction in the RNA level in the cells treated with the HN protein (Figure 5.5 G). Furthermore, between the wild type and I175Y-HN treated cells, a difference of 10% was observed in the RNA levels of NDV-N protein.

A similar experimental set up was used to directly visualize NDV infection post-treatment with the proteins with the help of an NDV-GFP construct. As shown in **Figure 5.7 H**, NDV was able to infect the untreated cells efficiently, as evident from the fluorescence from GFP, which directly correlates with the expression of the viral genomic cassette. The cells treated with 100 nM of wild type HN showed a marked decrease in GFP expression, which suggests that the protein was able to reduce NDV infection substantially. A comparison between the GFP expression in the cells treated with the wild type HN and I175Y mutant shows that the mutant protein in equivalent concentration was able to further impede the NDV replication in the cells, suggesting enhanced ability to restrict infection of the virus. Thus, it was clear that the I175Y mutant of the HN protein showed enhanced biological activity compared to the wild type protein.

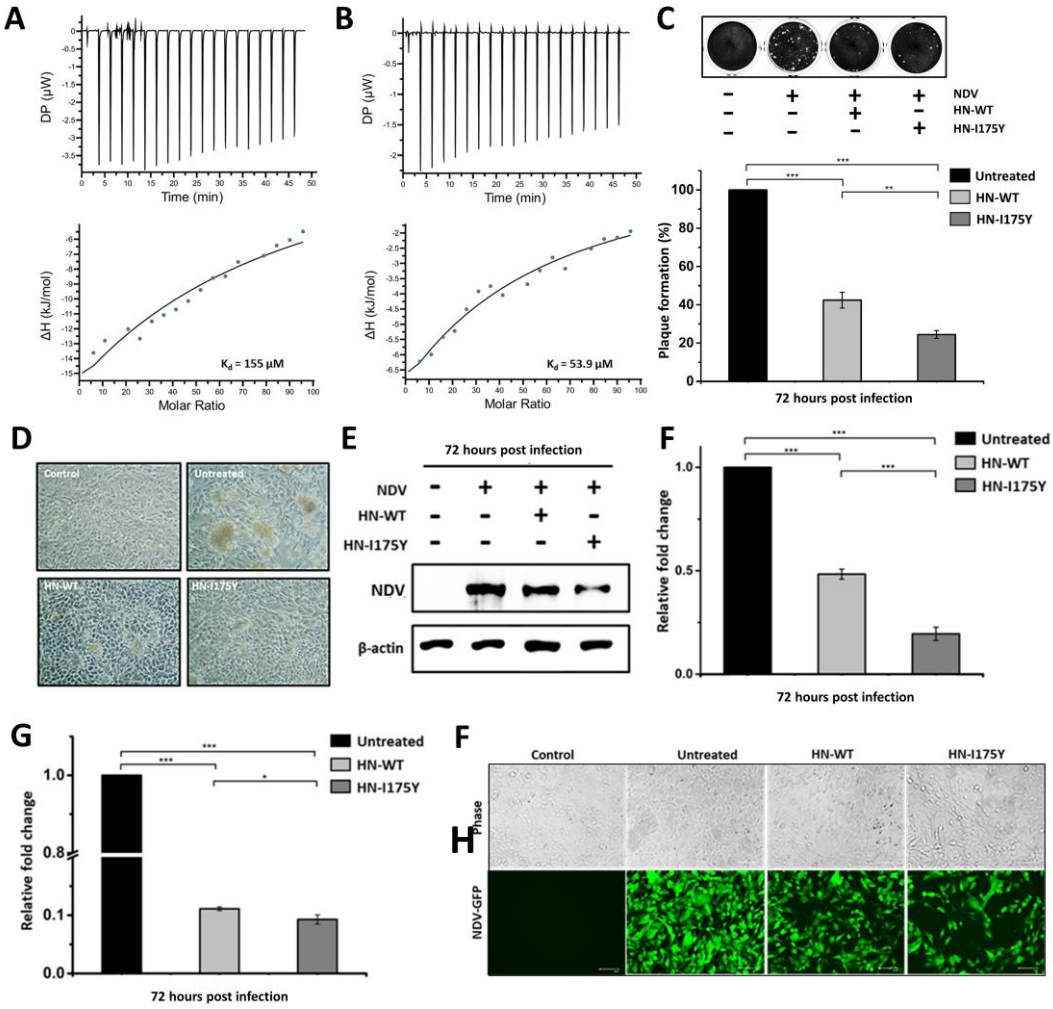

Figure 5.7: The I175Y mutant of HN shows greater affinity for its ligand and also displays higher biological activity compared to the wild type protein. (A) Isothermal Titration Calorimetry of wild type and (B) mutant HN with 6-sialilactose. (Upper) Raw titration data, (Lower) Integration plot of the titration data. (C) Plaque

inhibition assay (PIA). (Upper) Visible plaques post-72 hours used for viral titer calculation. (Lower) Number of plaques were calculated for each group. Considering the untreated (NDV) as 100%, percentage of plaques formed in the protein treated samples was calculated. (D) Brightfield images of BHK-21 cells without any treatment or NDV infection (Control), without any treatment but incubated with NDV (Untreated), treatment with wild type HN prior to NDV infection (HN-WT) and treatment with mutant HN before NDV infection (HN-I175Y). (E) Western blot analysis of the cell lysates to quantify the NDV infection. (F) Densitometry analysis of the bands and fold-change in expression of the HN protein between different groups. (G) Quantification of viral RNA in different treatment groups and expressed as relative fold-change. (F) Recombinant NDV-GFP virus was used to directly visualize its replication in the wild type HN treated and I175Y mutant treated cells. Levels of GFP expression correlates positively with NDV infection.

5.3.8 *In ovo* studies highlight the protective role of HN protein against NDV infection

We evaluated the protective effects of the I175Y mutant of hemagglutinin-neuraminidase (HN) protein, compared to the wild-type HN, against Newcastle disease virus (NDV) infection using an *in ovo* model. Following promising results from our cell-based assays, where the I175Y mutant exhibited enhanced activity against NDV infection, we proceeded to test these proteins in embryonated chicken eggs. Equivalent concentration (1µM) of the wild type or I175Y-HN were injected into the allantoic fluid (AF) of Day-9 SPF eggs and incubated for 1 hour. Post-treatment, 100 µl of plain NDV was injected into the allantoic fluid and the virus was allowed to replicate for 48 hours. The allantoic fluid from each group was collected and the virus titer was determined with the help of plaque assay. Embryos that were infected with NDV but received no HN treatment exhibited severe hemorrhaging and were non-viable at the 48-hour time point (**Figure 5.8 A**). In contrast, embryos treated with either wild-type or I175Y-HN proteins were viable and demonstrated significantly reduced hemorrhaging. Quantitative analysis revealed a 2.51-fold reduction in NDV titer in the wild type HN-treated group, whereas the I175Y-HN treated group exhibited an even greater reduction, with a 3.71-fold decrease in viral titer (**Figure 5.8 B**). To further validate the results, allantoic fluid from different groups was used from western blot analysis. Quantitative estimation from the blots showed a 20% decrease in the levels of NDV-N protein in the AF treated with wild type HN (**Figure 5.8 C**). On the contrary, in the embryos treated with the I175Y mutant, a 40% decrease in NDV-N protein was observed.

Additionally, tissue samples from the embryos were collected for RNA isolation, followed by cDNA synthesis and quantitative PCR to assess the NDV-N gene mRNA expression. The mRNA levels in both the wild-type and I175Y-HN-treated groups showed an approximately 80% reduction compared to the untreated control group (**Figure 5.8 D**). While a further

reduction of around 17% in NDV-N mRNA levels was observed in the I175Y-HN-treated group compared to the wild-type HN, this difference was not statistically significant. These results collectively suggest that the I175Y mutant of the HN protein confers greater protective effects against NDV infection compared to the wild type protein. Thus, given the enhanced biological activity of the mutant, we next tested its anti-plasmodial activity against the malaria parasite and compared it with the wild type HN protein.

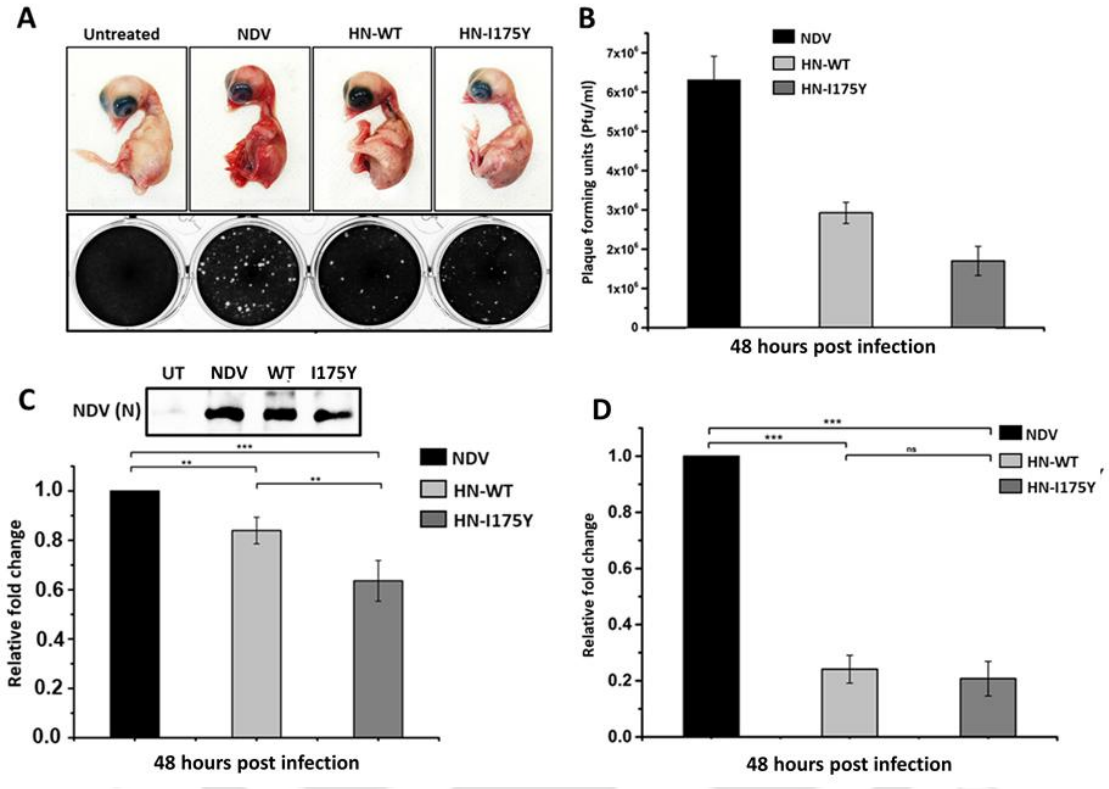

Figure 5.8: The I175Y mutant of HN shows a greater protective effect against NDV in chicken embryo. (A) Proteins (wild type and I175Y HN) at equal concentration (1 µM) were injected into the allantoic fluid (AF), 1 hour prior to injection of NDV into the AF. Untreated: No protein treatment or injection of NDV. NDV: No protein treatment but injected with NDV. HN-WT: Treated with wild type HN prior to NDV injection. HN-I175Y: Treated with mutant HN prior to NDV injection. (Upper) Images of chicken embryos after termination of the experiment at 48-hour time point. (Lower) Plaque assay for NDV quantification in AF. (B) NDV titer in the untreated (NDV), HN-WT treated and HN-I175Y treated groups are expressed as plaque forming units (pfu) per ml. (C) (Upper) Western blot analysis of the AF to quantify the NDV infection. (Lower) Densitometry analysis of the bands and fold-change in expression of the NP protein between different groups. (D) Quantification of viral RNA in tissues obtained from the embryos in different treatment groups and expressed as relative fold-change.

5.3.9 The anti-plasmodial activity of HN-I175Y is higher compared to HN-WT

Building on our previous findings that the hemagglutinin-neuraminidase (HN) protein from Newcastle disease virus (NDV) could disrupt the erythrocytic schizogony of the malaria

parasite (**Chapter IV, Figure 4.**), we explored the therapeutic potential of this viral coat protein. Given its potential for targeted delivery for malaria, we sought to determine whether the biological activity of the HN protein could be modulated to enhance its efficacy. This led to the development of the I175Y mutant of the NDV-HN protein, designed with the hypothesis that specific mutations could enhance its biological activity. Our preliminary investigations revealed that the I175Y mutant indeed exhibited greater biological activity compared to the wild-type HN protein. To further understand the potential of this mutant, we first assessed the binding affinity of both the wild-type and I175Y mutant proteins to human red blood cells (RBCs) and parasitized red blood cells (PRBCs). This binding study was crucial to confirm that the mutation did not adversely affect the ability of the protein to interact with red cell surface, a key factor in its anti-plasmodial activity. Following these binding studies, we evaluated the anti-plasmodial activity of both the wild-type and I175Y mutant HN proteins using the standard SYBR Green assay.

The binding of the wild type and I175Y-HN with human RBCs and PRBCs was checked with the help of flow cytometry. Briefly, malaria parasite cultures were incubated with wild type HN or I175Y-HN at a concentration of 1 µM for 1 hour and processed for flow cytometry. HN- bound PRBCs were segregated from the RBCs with the help of propidium iodide staining as discussed before (**Chapter IV, Figure 4.**). **Figure 5.9 A** shows the HN-bound RBC gated in blue and HN-bound PRBC population gated in red. Subsequent analysis focused on the HN-bound PRBC population, using histogram analysis to compare the binding affinities of the wild-type and I175Y-HN proteins (**Figure 5.9 B**). A total of 50,000 events were recorded during the flow cytometry experiments, and the resulting histograms are presented in **Figure 5.9 C**. Analysis of the binding curves reveals that the I175Y-HN mutant at equivalent concentration shows substantially higher binding with the PRBCs compared to the wild type HN protein.

Given that the binding of HN to sialic acid residues on the host cell surface is a critical step for its anti-plasmodial activity, we hypothesized that the enhanced binding observed with the I175Y-HN mutant might correlate with increased anti-plasmodial efficacy. To test this hypothesis, we conducted a dose-response study to evaluate and compare the anti-plasmodial activity of both the wild-type and mutant HN proteins against the malaria parasite. To further investigate the anti-plasmodial effects of the wild-type HN protein and its I175Y mutant, synchronized schizonts at a parasitemia of 1% were treated with increasing concentrations of HN, ranging from 1 to 50 µM. After a 48-hour incubation period, parasite viability was

assessed using the SYBR green assay. The results showed a dose-dependent reduction in parasite viability for both the wild-type and I175Y-HN proteins (**Figure 5.9 D and E**). Interestingly, the I175Y mutant consistently exhibited greater anti-plasmodial activity across all the tested concentrations. Specifically, at a concentration of 10 µM, the wild-type HN protein induced approximately a 20% reduction in parasite viability, while the I175Y mutant achieved a 50% reduction, indicating a 30% enhancement in its activity over the wild-type protein. However, at higher concentrations, the difference in anti-plasmodial activity between the wild-type and mutant proteins became less pronounced. To quantify the comparative efficacy, the IC_{50} values were calculated for both proteins. The I175Y mutant HN gave an IC_{50} value of 4.16 µM, whereas the wild-type HN protein exhibited an IC_{50} of approximately 6.9 µM. The lower IC_{50} value of the I175Y-HN mutant signifies enhanced anti-plasmodial activity compared to the wild-type protein. This highlights the potential of this mutation to enhance the therapeutic efficacy of HN against malaria parasites and provides an additional variant of the protein that could be used for targeted drug delivery.

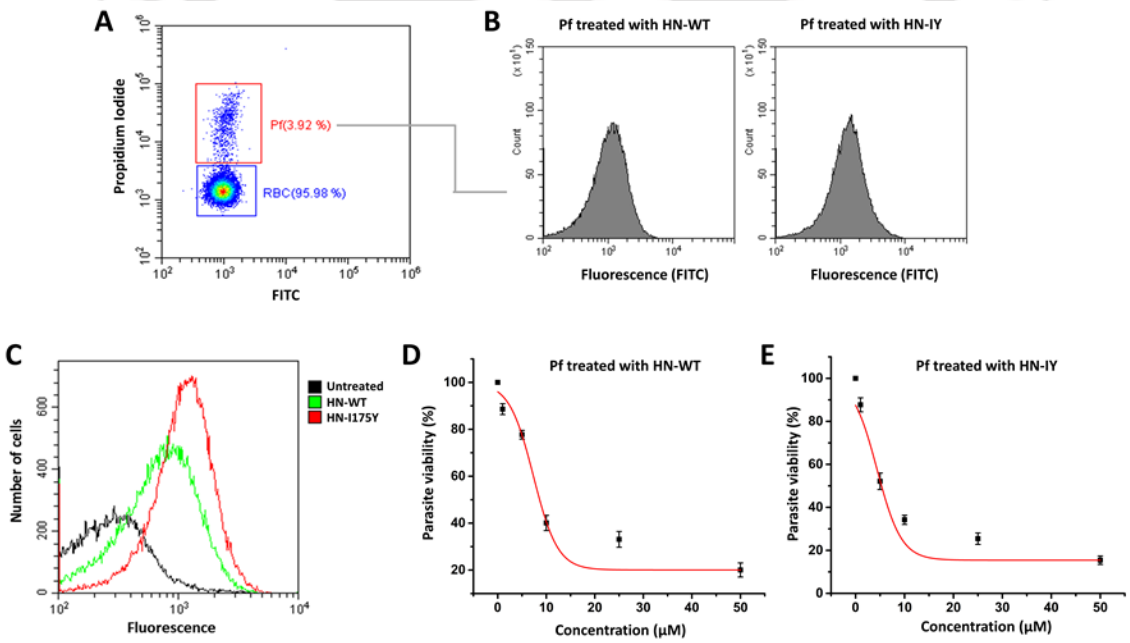

Figure 5.9: The anti-plasmodial activity of the I175Y-HN is greater than the wild type protein. (A) Flow cytometry analysis was done to check the binding of both the wild type and mutant HN with the PRBCs. Dot plot showing the HN-bound malaria culture where the protein-bound PRBCs are gated in red and protein-bound RBCs in blue. PRBCs were segregated from the RBCs with Propidium Iodide (PI) staining. (B) Histograms were obtained from the HN-WT and HN-I175Y bound PRBCs. X-axis: Fluorescence (FITC) signal from the HN protein (wild type or mutant), Y-axis: Counts or number of cells. (C) Overlay of histograms showing the fluorescence curve of wild type HN bound PRBCs (green) and I175Y-HN bound PRBCs (red). Untreated PRBCs did not show any signal (black). (D and E) SYBR green assay was performed to determine the anti-plasmodial activity of the

wild type and I175Y mutant HN protein at increasing concentrations (1, 10, 20, 30, 40 and 50 µM) respectively. IC_{50} was calculated by fitting the graphs in Origin 9 software.

5.4. Discussion

The HN protein of NDV uniquely combines receptor binding and neuraminidase activity, targeting sialic acids on malaria-parasitized red blood cells (PRBCs) and reducing parasite viability. A mutation (I175Y) in HN, designed to enhance sialic acid interaction, transformed its binding module, increasing its affinity for sialic acid which resulted in enhanced anti-plasmodial and viral inhibition activities. Our comparative studies on the HN protein across different members from the Paramyxoviridae family shows that residues constituting the sialic acid biophore are highly conserved (**Figure 5.1 B and C**). A previous report dealing with an in-depth analysis of an exhaustive list of sialic acid binding proteins from various organisms have shown that majority of the lectins could be grouped into six different categories based on the composition of key residues in the binding pocket. Upon analysis of the sialic acid biophore of HN, we found that it belongs to the Type-IV binding module (**Figure 5.1 B**).

Crystallographic studies of the NDV HN protein by independent groups have shown that the R416, E401 and Y526 appeared to be the most important residues for sialic acid binding [25, 26]. Other notable residues important for receptor binding included the R498, E258, Y317 and K236. The R416 and R498 were found to be the most crucial residues that forms hydrogen bonds with the carboxyl group at C_1 of sialic acid, tethering the molecule in the active site. Residues Y526, Y317 and E401 were shown to stabilize the three-carbon arm, comprising of C_7, C_8 and C_9, by forming H-bonds with the hydroxyl (-OH) groups of these carbons. In our study, we obtained similar results where the wild type HN protein, through the 100 ns simulation utilized R498 and R416 extensively (**Figure 5.5 A and C**). However, in the wild type protein, E401, Y526, E258 were found to minimally engage with sialic acid. Moreover, similar to our in-silico analysis, the hydroxyl group at C_4 and the acetamido group at C_5 of sialic acid remains unoccupied. In the I175Y mutant of HN, apart from E258 which was engaged with the receptor for only 18% of the time, other crucial residues such as E401, R498, Y526, R416 and Y317 were involved for 90%, 80%, 69%, 30% and 27% of the time, forming H-bonds with specific functional groups of sialic acid (**Figure 5.5 B and D**). Apart from these known residues, G468 and R363 represent novel additions that interacted with sialic acid for 56% and 35% during the simulation period. This shows that a single mutation could potentially increase the number of residues interacting with all the functional groups of sialic acid. It

further validates our analysis that the modification of the biding module from a Type-IV to Type-I could drastically alter the architecture of the sialic acid biophore.

To modulate the binding of sialic acid by the HN protein, it was important to understand the effect of mutations on different amino acid residues that constitute the binding pocket. Several studies have reported the effect of mutations on the key residues of the sialic acid biophore. In particular, the study by Connaris and group wherein they have mutated 10 important residues from the binding pocket of HN, led to the identification of the key residues mentioned earlier [25]. Results indicate that the triarginyl cluster comprising of R174, R416, and R498 were the most sensitive to mutations, and hence most important. The next most deleterious mutations appeared to be in the positions E401, E258, Y317 and K236. On the contrary, mutations of the I175 position appeared to be the least disruptive. According to their structural analysis, Isoleucine at 175 performs a cushioning role for the Tyrosine at 526. Mutagenesis of I175 to Leucine did not affect the neuraminidase (NA) activity of the protein but the hemadsorption (HAd) activity was reduced to 50%. Substitution of I175 to Glutamate resulted in a significant increase in NA activity but the HAd activity was merely 10-30% of the wild type. Mutation to a Threonine had no significant effect on either NA or Had activity. Despite these differences, none of the I175 mutations appeared to have significantly affected the expression levels and overall biological activity of the mutant viruses. Another study that reported the effect of mutation of an Isoleucine dealt with the I192 position, where the I192M in a mutant showed a lesser NA activity [27]. The mutant virus, however, was able to cause infection without any decline in infectivity and replicative potential. Other notable mutations reported for the HN protein delve into substitution in residues that, although they are not in the active site of the protein, result in altered activities. Substitution of A430 to Threonine resulted in weak HAd activity but the NA activity remained unaffected [28]. Mutagenesis of A89 to Asparagine and L94 to Alanine resulted in a little over 50% reduction in HAd activity, while P93 to Alanine resulted in an over 80% decrease in NA activity [29]. Substitution of S315 to Phenylalanine and I369 to Valine resulted in higher HAd and F-activity and also increased the thermostability of the HN protein [30]. Interestingly, the I175Y mutation in the NDV-HN protein, discussed in this study, represents a novel alteration that has not been previously reported.

The central core of the 6-bladded beta propeller scaffold that gives rise to the sialic acid binding pocket of HN is not the only site through which the protein interacts with sialic acid. Although previous studies have proposed the central catalytic site, in the globular head of HN, to be solely responsible for sialic acid binding and hydrolysis, few studies have stated

otherwise. It is now well-recognized that the NDV-HN protein has two sialic acid binding sites [26]. Site-I is the classical central biophore that is involved in receptor engagement via sialic acid. It triggers the interaction of the HN protein to the Fusion (F) protein, initiating the fusion of the NDV and host cell membrane. Site-II for sialic acid binding is located in the interface between two dimers and helps to maintain high avidity receptor binding during the fusion process [31]. We focused on the modulation of the Site-I of sialic acid binding as it is the initial and primary site of contact with host cell surface sialic acid and carries both HAd and NA activities. Moreover, our biochemical characterization of the prokaryotically expressed HN protein revealed that the proteins existed mostly as monomers in soluble form and thus Site-II, which is located at the dimer interface, might not exist in this scenario.

Generating a virus harboring the I175Y mutation could provide critical insights into the altered biological activity that a single amino acid substitution might induce. By characterizing the I175Y variant, we can better understand how this mutation impacts the overall infectivity and pathogenicity of the whole virus. Another aspect would be to characterize the effects of this mutation separately on the Neuraminidase (NA) and Hemadsorption (HAd) activities of the protein. Furthermore, while it is established that the HN protein of NDV interacts with both 3-sialolactose and 6-sialolactose, the precise differences in its binding affinity toward these ligands remain poorly characterized. In our study, we were able to compare the wild-type and I175Y-HN proteins based on their binding only with one of the ligands, 6-sialolactose. Thus, it would be essential to perform a comparative analysis between the wild type and mutant based on their binding with 3-sialolactose as well.

Mutations such as the I175Y of the HN protein, associated with increased biological activity, must also be handled with care, particularly in the scenario of generating whole virus mutants. Nevertheless, few studies have shown that such alternative forms of the HN protein could also be of significant therapeutic value. For instance, mutation of S519 to Glycine in the NDV-HN protein was found to increase the specificity of the mutant virus towards the colorectal cancer cells (HCT116), thereby increasing the oncolytic selectivity of the mutant virus [32]. For our application, we envision that both the wild type HN and the I175Y mutant could be explored further in the context of targeted delivery against the malaria parasite and other protozoan diseases.

5.5. References

1. Sharon, N., Lectins: carbohydrate-specific reagents and biological recognition molecules. Journal of Biological Chemistry, 2007. 282(5): p. 2753-2764.

2. Sharon, N. and H. Lis, Carbohydrates in cell recognition. Scientific American, 1993. 268(1): p. 82-89.

3. Blaese, R.M., et al., The role of cell surface lectin–carbohydrate interactions in cellular recognition, cooperation, and regulation. Journal of Pediatric Hematology/Oncology, 1983. 5(2): p. 199-206.

4. Burzyńska, P., et al., Sialic acids as receptors for pathogens. Biomolecules, 2021. 11(6): p. 831.

5. Matrosovich, M., G. Herrler, and H.D. Klenk, Sialic acid receptors of viruses. Sialoglyco chemistry and biology II: tools and techniques to identify and capture sialoglycans, 2015: p. 1-28.

6. Varki, A., R.L. Schnaar, and R. Schauer, Sialic acids and other nonulosonic acids. 2017.

7. Neu, U., J. Bauer, and T. Stehle, Viruses and sialic acids: rules of engagement. Current opinion in structural biology, 2011. 21(5): p. 610-618.

8. Stencel-Baerenwald, J.E., et al., The sweet spot: defining virus–sialic acid interactions. Nature Reviews Microbiology, 2014. 12(11): p. 739-749.

9. Herrler, G., J. Hausmann, and H.-D. Klenk, Sialic acid as receptor determinant of ortho- and paramyxoviruses. Biology of the Sialic Acids, 1995: p. 315-336.

10. Kumlin, U., et al., Sialic acid tissue distribution and influenza virus tropism. Influenza and other respiratory viruses, 2008. 2(5): p. 147-154.

11. Varghese, J.N., et al., The structure of the complex between influenza virus neuraminidase and sialic acid, the viral receptor. Proteins: Structure, Function, and Bioinformatics, 1992. 14(3): p. 327-332.

12. Wagner, R., M. Matrosovich, and H.D. Klenk, Functional balance between haemagglutinin and neuraminidase in influenza virus infections. Reviews in medical virology, 2002. 12(3): p. 159-166.

13. Mitnaul, L.J., et al., Balanced hemagglutinin and neuraminidase activities are critical for efficient replication of influenza A virus. Journal of virology, 2000. 74(13): p. 6015-6020.

14. Neog, S., et al., NDV targets the invasion pathway in malaria parasite through cell surface sialic acid interaction. The FASEB Journal, 2024. 38(15): p. e23856.

15. Ravindra, P., et al., Newcastle disease virus as an oncolytic agent. Indian Journal of Medical Research, 2009. 130(5): p. 507-513.

16. Bello, M.B., et al., Exploring the prospects of engineered Newcastle disease virus in modern vaccinology. Viruses, 2020. 12(4): p. 451.

17. Choi, K.-S., Newcastle disease virus vectored vaccines as bivalent or antigen delivery vaccines. Clinical and Experimental Vaccine Research, 2017. 6(2): p. 72-82.

18. Zamarin, D. and P. Palese, Oncolytic Newcastle disease virus for cancer therapy: old challenges and new directions. Future microbiology, 2012. 7(3): p. 347-367.

19. Herman, R., T. Shiroishi, and C.E. Buckler, Viral interference with exoerythrocytic forms of malaria (Plasmodium gallinaceum) in ovo. Journal of Infectious Diseases, 1973. 128(2): p. 148-155.

20. Jahiel, R.I., et al., Anti-malarial effect of interferon inducers at different stages of development of Plasmodium berghei in the mouse. Nature, 1968. 220(5168): p. 710-711.

21. Morris, G.M., R. Huey, and A.J. Olson, Using autodock for ligand-receptor docking. Current protocols in bioinformatics, 2008. 24(1): p. 8.14. 1-8.14. 40.

22. Barik, S., Site-directed mutagenesis by double polymerase chain reaction: megaprimer method. PCR Protocols: Current Methods and Applications, 1993: p. 277-286.

23. Rao, X., et al., An improvement of the 2ˆ (–delta delta CT) method for quantitative real-time polymerase chain reaction data analysis. Biostatistics, bioinformatics and biomathematics, 2013. 3(3): p. 71.

24. Varki, A., Diversity in the sialic acids. Glycobiology, 1992. 2(1): p. 25.

25. Connaris, H., et al., Probing the sialic acid binding site of the hemagglutinin-neuraminidase of Newcastle disease virus: identification of key amino acids involved in cell binding, catalysis, and fusion. Journal of virology, 2002. 76(4): p. 1816-1824.

26. Zaitsev, V., et al., Second sialic acid binding site in Newcastle disease virus hemagglutinin-neuraminidase: implications for fusion. Journal of virology, 2004. 78(7): p. 3733-3741.

27. Estevez, C., et al., A single amino acid substitution in the haemagglutinin–neuraminidase protein of Newcastle disease virus results in increased fusion promotion and decreased neuraminidase activities without changes in virus pathotype. Journal of general virology, 2011. 92(3): p. 544-551.

28. Chen, X., et al., Identification of a new amino acid mutation in the HN protein of NDV involved in pathogenicity. Veterinary Research, 2021. 52: p. 1-10.

29. Liu, B., et al., Two single amino acid substitutions in the intervening region of Newcastle disease virus HN protein attenuate viral replication and pathogenicity. Scientific reports, 2015. 5(1): p. 13038.

30. Ruan, B., et al., Residues 315 and 369 in HN protein contribute to the thermostability of Newcastle disease virus. Frontiers in Microbiology, 2020. 11: p. 560482.

31. Mahon, P.J., A.M. Mirza, and R.M. Iorio, Role of the two sialic acid binding sites on the newcastle disease virus HN protein in triggering the interaction with the F protein required for the promotion of fusion. Journal of virology, 2011. 85(22): p. 12079-12082.

32. Jung, B.-K., et al., The artificial amino acid change in the sialic acid-binding domain of the hemagglutinin neuraminidase of newcastle disease virus increases its specificity to HCT 116 colorectal cancer cells and tumor suppression effect. Virology Journal, 2024. 21(1): p. 7.

Chapter 6

Conclusions and Future Directions

6.1 Conclusions

From our co-infection studies, investigation into the anti-plasmodial potential of Newcastle Disease Virus (NDV) reveals compelling evidence of its effectiveness in disrupting the erythrocytic schizogony of malaria parasites. The *in vitro* co-infection studies, where NDV was incubated with malaria parasites showed significant restriction of parasite growth in human RBCs. Initial results demonstrated that NDV not only restricted parasite propagation but also induced severe cytopathic effects, particularly in the mature stages of the parasite. The dose-dependent studies further confirmed that NDV reduces parasite viability in a concentration-dependent manner, with notable anti-plasmodial activity observed after just 12 hours of exposure. These findings suggest that NDV rapidly affects the erythrocytic cycle of the malaria parasite.

Moreover, when compared to other viruses such as Influenza, Japanese Encephalitis Virus (JEV), Infectious Bronchitis Virus (IBV), and Duck Enteritis Virus (DEV), NDV was uniquely effective in reducing parasite viability, underscoring its specific anti-plasmodial activity. NDV was also observed to block the invasion of merozoites into uninfected RBCs, disrupting the erythrocyte cycle and preventing parasite proliferation. Agglutination and clot retraction assays indicated that while NDV caused high-order aggregation of chicken RBCs, it did not affect human RBC aggregation or clot retraction times, suggesting minimal adverse effects on normal blood components. Furthermore, testing the virus against the murine malaria strain *P. yoelii* demonstrated that pre-treatment with NDV or intravenous administration post-parasite inoculation significantly reduced the parasitemia. These comprehensive findings highlight the broad-spectrum anti-malarial activity of the virus.

From our molecular studies, we found that the Newcastle Disease Virus (NDV) exhibits a rapid and preferential binding to parasitized red blood cells (PRBCs) compared to uninfected red blood cells (RBCs) in both human and murine malaria strains. This differential engagement indicates that NDV may specifically target PRBCs, presenting a promising opportunity for targeted delivery of anti-malarial drugs. Binding studies using flow cytometry and immunofluorescence imaging demonstrated that affinity of the virus for PRBCs is significantly higher, suggesting a specific interaction with the malaria-infected RBCs/ PRBCs. Further investigations into the binding mechanism showed that heat treatment, aldehyde fixatives, and enzymatic treatments completely abolished NDV binding, indicating the involvement of both viral and host cell surface proteins, with host sialic acids being crucial for interaction. The spike

glycoprotein HN of NDV was identified as a key mediator in binding, as blocking its active site or using anti-HN antibodies led to a loss of virus binding and a substantial decrease in anti-plasmodial activity. This highlights the critical role of the HN protein in the anti-malarial action of the virus. To explore the potential of the HN protein alone, we cloned and overexpressed it, and found that the purified HN protein could dose-dependently inhibit the erythrocytic schizogony of the malaria parasite. These results confirm that NDV targets sialic acid-containing receptors on RBCs and PRBCs through its HN protein, leading to effective disruption of malaria parasite proliferation. Overall, the NDV-HN protein holds significant promise for developing targeted anti-malarial therapies, emphasizing the potential of the virus as a valuable tool in malaria therapeutics.

Furthermore, our investigation into the Newcastle Disease Virus (NDV) hemagglutinin-neuraminidase (HN) coat protein reveals significant insights into its sialic acid binding mechanisms and the impact of targeted mutations. Structural comparisons of HN and neuraminidase (NA) proteins from various virus species identified a conserved six-bladed β-propeller fold but distinct sialic acid-binding modules, with HN exhibiting a Type-IV module and NA a Type-I module. The Type-IV module of HN interacts less extensively with the functional groups of sialic acid compared to the Type-I module of NA, which contributes to higher binding affinity and hemagglutination activity.

To enhance the binding affinity of HN, we focused on specific mutations, identifying the I175Y mutation as a promising candidate. In silico analyses showed that this mutation significantly increased binding affinity by altering the binding module from Type-IV to Type-I, as evidenced by a 1.5-fold increase in hydrogen bonds. Experimental validation of the I175Y mutant through Isothermal Titration Calorimetry (ITC) revealed a 2.8-fold decrease in the Kd value compared to the wild type, indicating stronger binding to sialic acid. Biological assays demonstrated that the I175Y mutant exhibited approximately 25% greater plaque inhibition activity and showed enhanced efficacy in blocking NDV infection in cell monolayers, with a 10% reduction in viral titer in *in ovo* studies. Additionally, the I175Y mutant displayed superior anti-plasmodial activity, with a 30% greater reduction in malaria parasite viability at 5 µM protein concentration compared to the wild type. These findings underscore that specific mutations in HN can effectively augment its sialic acid binding affinity, enhancing its biological and therapeutic potential.

6.2 Future directions

The outcome of this thesis could be extended into future investigations such as:

1. *In Vivo* Validation: To conduct extensive in vivo studies to confirm the efficacy of NDV and the HN-I175Y mutant in animal models of malaria. This would provide deeper insights into the therapeutic potential and safety of NDV-based treatments.

2. Mechanistic Studies: To investigate the detailed molecular mechanisms underlying the interaction of with PRBCs and its anti-plasmodial effects though possible modulation of signaling pathways and cellular processes disrupted by NDV.

3. Optimization of HN Mutants: To further explore additional mutations in the HN protein to enhance its binding affinity and anti-plasmodial activity. Systematic mutagenesis studies could identify other key residues that improve the efficacy of the HN protein.

4. Combination Therapies: To evaluate the potential of combining NDV or the HN-I175Y mutant with existing anti-malarial drugs to assess synergistic effects and improve therapeutic outcomes.

5. Targeted Drug Delivery: To develop and test NDV-based delivery systems for targeted delivery of anti-malarial drugs to PRBCs, leveraging NDV's natural tropism for these cells.

6. Broader Pathogen Testing: To access the anti-pathogenic activity of NDV and the HN-I175Y mutant against other protozoan parasites or pathogens to explore their broader therapeutic potential.

7. Structural Studies: To perform high-resolution structural analyses of NDV-HN in complex with sialic acid and other ligands to gain a more detailed understanding of the binding interactions and refine the design of enhanced variants.

8. Human Cell Line Studies: To conduct studies in human cell lines to evaluate the safety and efficacy of NDV and HN proteins, addressing potential differences in response compared to murine or avian models.

9. Clinical Translation: To initiate preclinical and clinical trials to evaluate the safety, efficacy, and pharmacokinetics of NDV-based therapies in humans, aiming for eventual clinical application.

10. Immunogenicity Assessment: To investigate the immunogenicity of NDV and its mutant proteins to understand potential immune responses and address any adverse effects in therapeutic contexts.

11. Other viruses: To conduct similar studies including other strains of viruses and explore its effects on the malaria parasite in both *in vitro* and *in vivo* experimental settings.

List of Publications:

1. **Neog S,** Vinjamuri SR, Vijayan K, Kumar S, Trivedi V. **NDV targets the invasion pathway in malaria parasite through cell surface sialic acid interaction**. FASEB J. 2024 Aug 15;38(15):e23856. doi: 10.1096/fj.202400004RR. PMID: 39092913.

2. **Neog, S.,** Kumar, S., & Trivedi, V. (2023). **Isolation and characterization of Newcastle disease virus from biological fluids using column chromatography**. Biomedical Chromatography, 37(1), e5527.

3. **Neog, S.,** & Trivedi, V. (2022). **Approaches and methods to study cell signaling: Linguistics of cellular communication.** In Advances in Protein Molecular and Structural Biology Methods (pp. 589-623). Academic Press.

4. **UNDER REVIEW in Journal of Virology:** Neog, Siddharth, Sachin Kumar, and Vishal Trivedi. "**Sialic acid biophore directed design of enhanced affinity HN protein from Newcastle Disease Virus.**" (2025) (ID: JVI00425-25)

Conferences:

1. Oral presentation in International Conference on "**Mechanistic and Therapeutic Approaches in Human and Animal Health**", 6th to 8th December, 2021 at Department of Zoology, Cooch Behar Panchanan Barma University, West Bengal.

Received: 3 January 2024 | Revised: 1 July 2024 | Accepted: 21 July 2024

DOI: 10.1096/fj.202400004RR

RESEARCH ARTICLE

The FASEB Journal

NDV targets the invasion pathway in malaria parasite through cell surface sialic acid interaction

Siddharth Neog[1] | **Sandeep Reddy Vinjamuri**[2] | **Kamalakannan Vijayan**[2] | **Sachin Kumar**[3] | **Vishal Trivedi**[1]

[1]Malaria Research Group, Department of Biosciences and Bioengineering, Indian Institute of Technology-Guwahati, Guwahati, India

[2]School of Biology, Indian Institute of Science Education and Research Thiruvananthapuram, Thiruvananthapuram, India

[3]Viral Immunology Laboratory, Department of Biosciences and Bioengineering, Indian Institute of Technology-Guwahati, Guwahati, India

Correspondence
Vishal Trivedi, Malaria Research Group, Department of Biosciences and Bioengineering, Indian Institute of Technology-Guwahati, Guwahati 781039, Assam, India.
Email: vtrivedi@iitg.ernet.in

Abstract

Merozoites utilize sialic acids on the red blood cell (RBC) cell surface to rapidly adhere to and invade the RBCs. Newcastle disease virus (NDV) displays a strong affinity toward membrane-bound sialic acids. Incubation of NDV with the malaria parasites dose-dependently reduces its cellular viability. The antiplasmodial activity of NDV is specific, as incubation with Japanese encephalitis virus, duck enteritis virus, infectious bronchitis virus, and influenza virus did not affect the parasite propagation. Interestingly, NDV is reducing more than 80% invasion when RBCs are pretreated with the virus. Removal of the RBC surface proteins or the NDV coat proteins results in disruption of the virus binding to RBC. It suggests the involvement of specific protein: ligand interaction in virus binding. We established that the virus engages with the parasitized RBCs (PRBCs) through its hemagglutinin neuraminidase (HN) protein by recognizing sialic acid-containing glycoproteins on the cell surface. Blocking of the HN protein with free sialic acid or anti-HN antibodies abolished the virus binding as well as its ability to reduce parasite growth. Interestingly, the purified HN from the virus alone could inhibit the parasite's growth in a dose-dependent manner. NDV binds strongly to knobless murine parasite strain *Plasmodium yoelii* and restricted the parasite growth in mice. Furthermore, the virus was found to preferentially target the PRBCs compared to normal erythrocytes. Immunolocalization studies reveal that NDV is localized on the plasma membrane as well as weakly inside the PRBC. NDV causes neither any infection nor aggregation of the human RBCs. Our findings suggest that NDV is a potential candidate for developing targeted drug delivery platforms for the *Plasmodium*-infected RBCs.

Abbreviations: ACTs, Artemisinin Combination Therapies; AEs, Adverse Effects; AF, Allantoic Fluid; ATP, Adenosine Triphosphate; BHK-21, Baby Hamster Kidney-21; BSA, Bovine Serum Albumin; CD, Circular Dichrotsm; CNS, Central Nervous System; CV, Column Volumes; DEV, Duck Enteritis Virus; DMEM, Dulbecco's Modified Eagle's Medium; EBAs, Erythrocyte Binding Antigens; FACS, Fluorescence-Activated Cell Sorting; FITC, Fluorescein Isothiocyanate; HA, Hemagglutination Assay; HN, Hemagglutinin Neuraminidase; IBV, Infectious Bronchitis Virus; IPTG, Isopropyl β-D-1-thiogalactopyranoside; JEV, Japanese Encephalitis Virus; MAPK, Mitogen-Activated Protein Kinase; MOI, Multiplicity of Infection; NDV, Newcastle Disease Virus; PBS, Phosphate-Buffered Saline; Pf3D7, Plasmodium falciparum 3D7 strain; PMSF, Phenylmethylsulfonyl Fluoride; PRBCs, Parasitized Red Blood Cells; RBCs, Red Blood Cells; RBD, Receptor Binding Domain; RBPs, Reticulocyte-Binding Proteins; RT, Room Temperature; SDS-PAGE, Sodium Dodecyl Sulfate–Polyacrylamide Gel Electrophoresis; SPF, Specific Pathogen-Free; VLP, Virus-Like Particles.

Received: 19 August 2022 | Revised: 13 October 2022 | Accepted: 13 October 2022
DOI: 10.1002/bmc.5527

RESEARCH ARTICLE

Biomedical Chromatography WILEY

Isolation and characterization of Newcastle disease virus from biological fluids using column chromatography

Siddharth Neog[1] | **Sachin Kumar**[2] | **Vishal Trivedi**[1]

[1]Malaria Research Group, Department of Biosciences and Bioengineering, Indian Institute of Technology-Guwahati, Guwahati, India
[2]Viral Immunology Laboratory, Department of Biosciences and Bioengineering, Indian Institute of Technology-Guwahati, Guwahati, India

Correspondence
Vishal Trivedi, Malaria Research Group, Department of Biosciences and Bioengineering, Indian Institute of Technology-Guwahati, Guwahati 781039, India.
Email: vtrivedi@iitg.ernet.in and vishalash_1999@yahoo.com

Abstract

Newcastle disease virus (NDV), belonging to the species avian orthoavulavirus 1, genus *Orthoavulavirus*, and family Paramyxoviridae, is responsible for Newcastle disease in poultry and other avian species. It has shown significant potential as an oncolytic virus and as a vector for vaccine delivery. NDV from infected biological serum is usually isolated or purified using density gradient ultracentrifugation. However, it has many disadvantages, including the fact that it is time consuming and can process only a limited quantity of sample at one time. In our study, native agarose gel electrophoresis and dynamic light scattering (DLS) analysis showed that NDV carried a net negative surface charge. Thus, we purified the virus using a HiTrap Q Sepharose Fast Flow anion exchange column with salt elution. Hemagglutination assay and plaque assay showed that the procedure yielded high-purity NDV particles with a recovery of more than 80%, and the process was fast and simple. The purity of the virus was confirmed using sodium dodecyl sulfate-polyacrylamide gel electrophoresis (SDS-PAGE) and Western blot analysis. The hydrodynamic volume and 'dry state' diameter of the purified NDV were analyzed using dynamic light scattering and transmission electron microscopy and were to be in the range of 200–300 nm. The viruses did not exhibit any deviation from their known physical properties. The genome of the virus was also detected by amplifying a 423-bp region using reverse transcription-polymerase chain reaction. Our study confirmed that NDV could be effectively purified using an anion exchange column. In addition, the procedure could be easily upscaled or downscaled based on the experimental requirements.

KEYWORDS
anion exchange chromatography, NDV purification, Newcastle disease virus, viral purification

1 | INTRODUCTION

Newcastle disease is an economically significant disease in poultry caused by the Newcastle disease virus (NDV). The virus packages a negatively sensed RNA as its genetic material and belongs to the species avian orthoavulavirus 1, genus *Orthoavulavirus*, and family Paramyxoviridae (Dimitrov et al., 2019). Accumulating evidence in the past decade has shown that NDV possesses significant therapeutic potential as an oncolytic virus and as a suitable vector for vaccine delivery (Duan et al., 2015; Zakay-Rones et al., 2015). The virus possesses an innate oncolytic ability as it preferentially selects tumor cells for replication and lysis (Yurchenko et al., 2018). In addition, it exhibits strong immunostimulatory properties that help in generating potent antitumor immune responses (Fournier et al., 2012). In humans, the virus exhibits minimal side effects, which is evident from various clinical trials (Lam et al., 2011). It also has a high safety profile as it replicates only in the cytoplasm and is not programmed to integrate its genetic material into the host genome (Duan et al., 2019). Considering its

ACADEMIC PRESS

Advances in Protein Molecular and Structural Biology Methods

2022, Pages 589-623

Chapter 36 - Approaches and methods to study cell signaling: Linguistics of cellular communication

Siddharth Neog, Vishal Trivedi

https://doi.org/10.1016/B978-0-323-90264-9.00036-2

Abstract

All living cells are dynamic systems capable of responding to internal and external stimuli or signals. The majority of cell signaling pathways are cascades of biomolecular reactions where the receptor, upon binding with its ligand, often undergoes a conformational change. The ligand-bound receptor then activates cascades of intracellular protein networks that help the signal to be internalized. Depending on the signal received, the cells may reorganize their metabolic activities, divide, migrate, or even undergo apoptosis. The functions of these signaling proteins can be studied with the help of classical biochemical approaches, such as western blotting, pull-down assays, and immunoprecipitation. They are often combined with modern platforms, enabling the study of these signaling molecules directly in live cells or analyze hundreds and thousands of proteins and their posttranslational modifications simultaneously. In this chapter, some of the classical signaling pathways are described, followed by the experimental approaches routinely used to study these pathways.